INTEGRATING GRAVITY AND SEISMIC METHODS WITH PETROLEUM SYSTEM MODELLING TO ASSESS EXPLORATION RISK FACTORS IN OFFSHORE LAMU BASIN, KENYA

DENNIS OMBATI

DOCTOR OF PHILOSOPHY

(Applied Geophysics)

JOMO KENYATTA UNIVERSITY

OF

AGRICULTURE AND TECHNOLOGY

2024

Integrating Gravity and Seismic Methods with Petroleum System Modelling to Assess Exploration Risk Factors in Offshore Lamu Basin, Kenya

Dennis Ombati

A Thesis Submitted in Partial Fulfillment of the Requirement for the Degree of Doctor of Philosophy in Applied Geophysics at the Jomo Kenyatta University of Agriculture and Technology

2024

DECLARATION

This thesis is my original work and has not been presented for a degree in any other University.

Signature ……. Date …….

Dennis Ombati

This thesis has been submitted for examination with our approval as University Supervisors.

Signature ……. Date …….

Prof. John Githiri, PhD.
JKUAT, Kenya

Signature ……. Date …….

Dr. Maurice K'Orowe, PhD.
JKUAT, Kenya

DEDICATION

I dedicate this work, especially to my family. My wife: Ann Wanjiku, Daughters: Gloria, Shirleen, Verusha, and Gabriella. God has used them in supporting me in all spheres besides offering constant encouragement through earnest prayers. Receive God's blessing in Jesus' name.

ACKNOWLEDGEMENT

I solemnly thank my gracious Father above for His faithfulness thus far. He has granted me travelling mercies, good health, physical and mental strength, and financial breakthroughs in the course of my PhD program.

I am greatly indebted to the fine team of my university supervisors, Prof. John Githiri and Dr. Maurice K'Orowe. They have honestly held my hand on every step of the walk in this academic journey. Their professional guidance, correction, motivation, and devotion to this study have largely contributed to my success. May God richly reward my role models in the years of their service. I also appreciate Dr. Munyithya for the occasions of the fruitful consultations that we had and the rest of the entire Department of Physics, Jomo Kenyatta University of Agriculture and Technology, for their challenge, advice, suggestions, and general support that made this program a success, I say thank you.

I am grateful to the International Gravity Bureau (BGI) for providing the gravity data and the National Oil Corporation of Kenya for the gravity information, well logs, seismic data, geochemical data, and related information and for granting me an opportunity to use the needed software in their work stations. I wish to also recognize and appreciate my friends in the industry for their introduction, encouragement, and support: Godfrey Osukuku, Abiud Masinde, Kathleen Asena, Mary Mugambi, Ayan Omar, and Josphat Kioko (NOCK-Kenya), and Joseph Gichira (GDC). God bless you friends for your kindheartedness.

Finally, I register my heartfelt gratitude to my family for their overwhelming support financially, socially, emotionally, and spiritually. My wife and daughters, each in their turn of prayer, remembered to whisper requests over my studies. My mum and my sisters always wished me well and encouraged me all way. I thank my parents-in-law who practically prayed for me constantly for I could feel the power of their prayers. Dr. Alex and Maggy many blessings for housing me during my many visits to Nairobi in

pursuit of my studies. I also give cognizance to the ESWA family, colleagues at Kisii University Physics Department and my friends at large for their encouragement and motivation during my studies. God bless you all.

TABLE OF CONTENTS

LIST OF TABLES

LIST OF FIGURES

LIST OF APPENDICES

LIST OF ABBREVIATIONS AND ACRONYMS

API	American Petroleum Institute
AVO	Amplitude versus Offset
BGI	International Gravity Bureau
BHT	Bottom Hole Temperature
BPSM	Basin and Petroleum System Modelling
CBA	Complete Bouguer Anomaly
CSV	Comma Separated Value
DHI	Direct Hydrocarbon Indicator
DST	Drill Stem Test
DW-FTB	Deep Water Fold and Thrust Belt
DWFZ	Davie Walu Fracture Zone
DWR	Davie Walu Ridge
EGM	Earth Geopotential Model
ETOPO	Earth Topography
FE	Formation evaluation
FHD	First Horizontal Derivative
GM-SYS	Geosoft Modelling System

GRACE Gravity Recovery and Climate Experiment

HF Heat Flow

HGM Horizontal Gradient Magnitude

HI Hydrogen Index

LWD Logging While Drilling

NOCK National Oil Corporation of Kenya

PETROMOD Petroleum Systems Modelling Software

PSM Petroleum System Modelling

PWD Paleo Water Depth

QC Quality Check

RAPS Radially Averaged Power Spectrum

RMS Root Mean Square

SESA Strategic Environmental and Social Assessment

SWIT Sediment-Water Interface Temperature

TCF One Trillion Cubic Feet

TOC Total Organic Carbon

ABSTRACT

Lamu basin is located in South Eastern Kenya and covers onshore (about 85 000 km^2) and offshore (about 170 000 km^2) with a total area of about 255 000 km^2. Carbonates, shales, and sandstones constitute the sediments of the area. Tectonic movements, which brought about Gondwana's breaking up, control the region's geology. East Africa's potential for hydrocarbon is indicated by the significant oil and gas discoveries in Mozambique and Tanzania and the heavy oil deposits in Madagascar's conjugate margin. Unfortunately, many of the drilled wells in the Lamu Basin turned dry save for gas and oil shows from a few of the Lamu Basin's twenty (20) drilled exploration wells. This study, therefore, assessed exploration risk factors of the Lamu shallow offshore by evaluating the basin's evolution and analyzing the development of the petroleum system using one dimension petroleum system modelling integrated with gravity and seismic geophysical methods. Major and minor subsurface structural features have been delineated through filtering, processing, and regionally interpreting gravity Isostacy data. The features like the ridges, troughs, and faults mainly trending in the North West-South East direction are discernable from the regional anomaly map. The developed models show the basement highs and lows with a possibility of anticlinal and synclinal structures and thick sedimentary successions likely to represent good hydrocarbon source kitchens. Appropriate seismic attributes have been leveraged to extract subsurface properties from the seismic data and have guided the interpretation to delineate closed structures and potential subsurface traps. Reservoir zones delineated through petrophysics and rock physics analyses were characterized. The resulting petrophysical properties indicate a good range of reservoir characteristics: low shale volume (0.07-0.26), low water saturation (0.23-0.56), high effective porosity (0.12-0.25), and a net thickness (18.95 m- 43.224 m). The rock physics cross-plot models delineated the reservoir lithology and discriminated the fluid content. The probable zones discriminated include the hydrocarbon-bearing zone with low water saturation, gamma radiation, and high porosity compared to brine-saturated sand and shale zones. Gassmann fluid substitution was used to calculate the fluid effect on elastic rock properties from the rock frame properties. The behaviour of clean reservoir zone saturation scenarios resulting from the brine, oil, and gas fluid substitution models was measured. The values indicate that fluid substitution has a greater effect on compressional velocity than on shear velocity and density (ρ) significantly decreased when hydrocarbons replaced water saturation in the wells. Shear wave velocity (V_s) indicated a slight change in all the wells. Petroleum system modelling was applied to evaluate the geological conditions necessary for a successful charge by reconstructing the burial, thermal, and maturity histories. The models were calibrated using geochemical analysis's measured Vitrinite Reflectance and generative properties. Calculations from the simulated models were correlated with the measured values, from which inferences were made. From the upper cretaceous maturity maps, the results seem to favour near coastal regions where average total organic carbon is about 1.4 wt%, Vitrinite reflectance is more than 0.5%, transformation ratio is more than 10%, and temperatures range from 80 ^{0}c to 160 ^{0}c. Greater uncertainty rests on the source rock's

presence and viability tending toward the deep offshore. Combining gravity and seismic methods for regional structural interpretation, petrophysics and rock physics for reservoir delineation and characterization, and petroleum system modelling for source rock characterization improved the understanding of the occurrence of the petroleum system elements and processes necessary for hydrocarbon accumulation. Appropriate points where wells may be drilled with reduced exploration risk have been suggested.

CHAPTER ONE

INTRODUCTION

1.1 Background to the Study

The new industry's focus on East Africa's offshore since 2010 follows the discovery of approximately 140 trillion cubic feet (Tcf) of gas in the deep-water section in Mozambique and Tanzania (Al-Hajeri *et al.*, 2009). East Africa's potential for hydrocarbon is indicated by the significant oil and gas discoveries in Mozambique and Tanzania and the heavy oil deposits in Madagascar's conjugate margin (Osicki *et al.*, 2015). South-Eastern Kenya's Lamu basin forms part of the passive continental margin of Kenya, covering both the onshore and offshore (Figure 1.1).

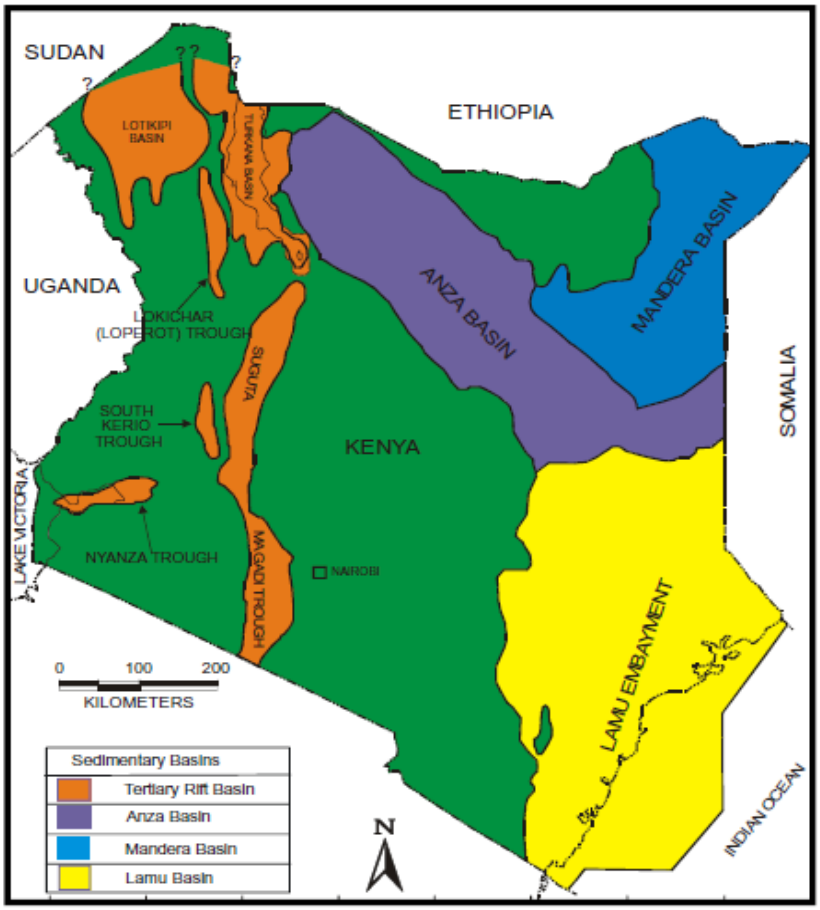

Figure 1.1: Simplified Map of Kenya's Sedimentary Basins.

Source: Nyaberi and Rop (2014).

It relates to the continents like Australia, America, India, Antarctica, Africa, and Madagascar that separated during the Jurassic rifting (Coffin & Rabinowitz, 1987). The basin extends to an area of about 256 000 km^2 where the thickness of the sediments ranges from 3 km to 10 km onshore and 12 km near the coastline to less than 3 km offshore, thinning towards the deep Indian Ocean (Beicip-Franlab, 2020). Carbonates, shales, and marine sandstones constitute the sediments of the area.

Following the worldwide scale for exploration status and success rate, computed according to the number of drilled exploration wells per 5000 km^2, the exploration status in Kenya remains very low (i.e., grade 1 to grade 2), and the success rate at category 3 (Tables 1.1 and 1.2) (Beicip-Franlab, 2020).

Table 1. 1: Distribution of Basinal Wells in Kenyan Basins(NOCK, 2009)

Basin	No. Of wells	Wells with Shows	Dry wells
Lamu	20	(10) 4 Discoveries (2G & 2O)	6
Anza	17	(9) 1 Discovery (G)	7
Mandera	3	(0) One oil SEEP	2
Tertiary Rift	36	(4) 10 Exploration Discoveries (20 including appraisal wells with Oil, 1 O & 1G)	

Table 1.1 shows the statistics of the wells drilled in the various Kenyan basins as contained in the strategic environmental and social assessment (SESA) report sourced from the Ministry of Energy and Petroleum report of 2016. The statistics capture the number of drilled wells, wells with hydrocarbon shows, discovery wells, and dry wells.

Table 1.2: World Wide Scale for Exploration Status, Success Rate, and Exploration Potential with Scores from Kenyan Basins (Beicip-Franlab, 2020)

	1	2	3	4	5
Exploration status	<1 Well/ 5000km^2	1-2 Wells/ 5000km^2	2-5 Wells/ 5000km^2	5-10 Wells/ 5000km^2	>2 Wells/ 1000km^2
Success ratio	None	<10%	10-20%	20-30%	>30%

Basin	**Area(Km^2)**	**Wells**	**Exploration status**	**Category**
Lamu	256000	20	0.39	1
Anza-Mandera	131000	20	0.76	1
Tertiary Rift	78000	26	1.67	2

Basin	**wells**	**Discoveries**	**Success rate (%)**	**Category**
Lamu	20	4	20	3
Anza-Mandera	20	2	10	2
Tertiary Rift	26	10	38	5

Basin	**Exploration Potential (%)**
Lamu	51
Anza-Mandera	14
Tertiary Rift	23

Table 1.2 shows the Kenyan basins' statistics and scores of the exploration status, success ratio and exploration potential by the year 2020.

Since the prospective offshore Lamu basin of Kenya has received much interest in hydrocarbon exploration, the exploration potential defined by the ratio of success rate to exploration status stands fair (51%) compared to other basins in Kenya (Figure 1.1). Several gas and oil shows are evidenced from the drilled twenty (20) exploration wells (see Table 1.1). However, most of the drilled wells are dry. This study focuses on an integrated approach of combining gravity and seismic geophysical methods, well log analysis, and one dimension (1D) petroleum system modelling to delineate necessary structures and evaluate related geological conditions required for a possible hydrocarbon accumulation in the shallow offshore Lamu basin, Kenya (Figures 1.2 and 1.3).

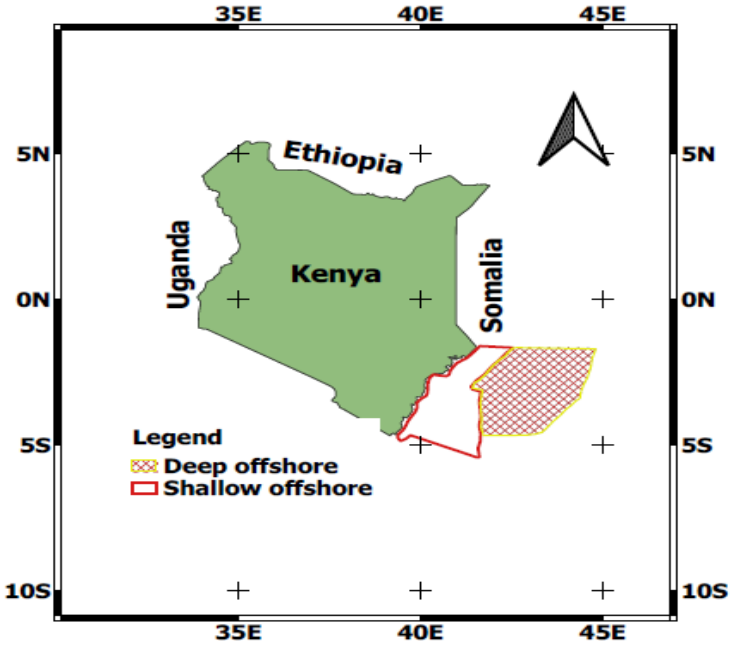

Figure 1. 2: Map of Kenya Showing the Area of Study Outlined in Red

(Modified from NOCK Library)

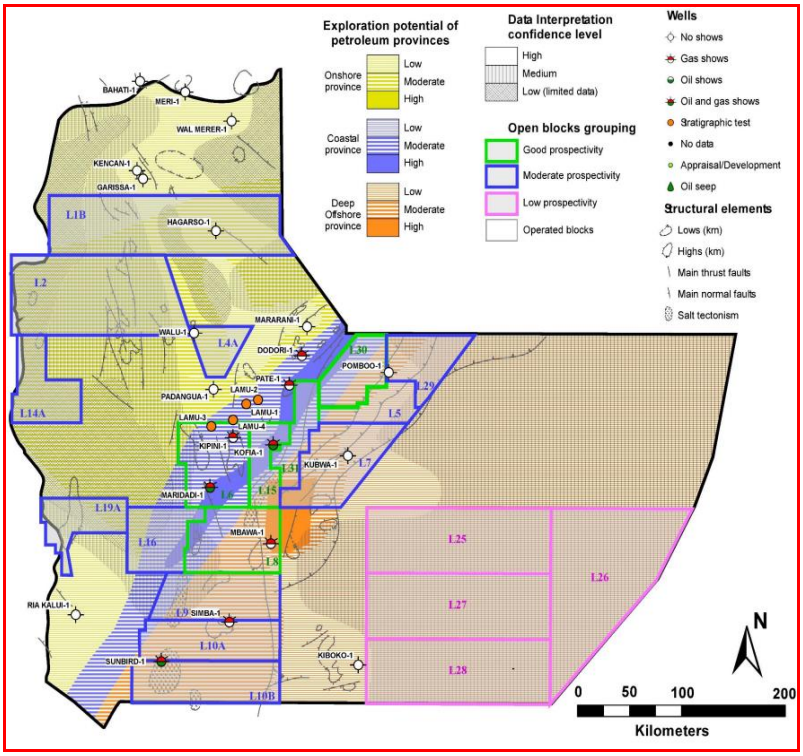

Figure 1. 3: Distribution of the Drilled Wells Considered in the Current Study

(Beicip-Franlab, 2020)

The gravity method is preferred in hydrocarbon exploration because it shows stratigraphic and structural features. In this method, the subsurface geology is examined based on the variation of rock density giving rise to different earth's gravitational fields. Gravity interpretation techniques such as spectral analysis and first horizontal derivative were applied to the reduced gravity data to delineate and model structures (Ombati, Githiri, K'Orowe, & Nyakundi, 2022).

In hydrocarbon exploration, the seismic method is most widely applied because of its capability to image small to large-scale subsurface features. In this method, acquired data is processed, data reduction is made, anomaly maps are drawn, and seismic sections are translated to geological structures. Seismic methods involve estimating the shapes and physical properties of Earth's subsurface layers from the returns of sound waves propagated through the Earth (Bjorlykke, 2010). Seismic interpretation is the last step in the seismic method and involves telling the geologic story in the seismic data. Seismic attributes such as envelop, sweetness, variance edge, Root Mean square (RMS) amplitude, and relative acoustic impedance were applied to the two dimension (2D) seismic data from part of the study area alongside the interpreted horizons and faults to enhance the visualization of the subsurface features.

Integrating petrophysics and rock physics models can be a great tool in subsurface modelling to describe reservoir lithology and fluid content accurately and minimize exploration risks (Rasaq, Igwenagu, & Onifade, 2015). Following a study carried out in the Lamu basin, it was concluded that the location of the drilled wells along the reservoirs appears to be characterized by faults (structural lead features) and geothermal highs (sub-surface stratigraphic elements), moreover, there is a need to embrace an integrated approach that will improve reservoir characterization and, thus, appropriately locate wells before drilling (Nyaberi & Rop, 2014). Petrophysical analysis and rock physics models have been used in this study to delineate lithologies, characterize the identified reservoirs to obtain the petrophysical properties and discriminate the fluid content.

A petroleum system is a geologic system that encompasses the hydrocarbon source rocks and all related oil and gas and includes all of the geologic elements and

processes essential if a hydrocarbon accumulation is to exist (Figure 1.4) (Magoon & Dow, 1994).

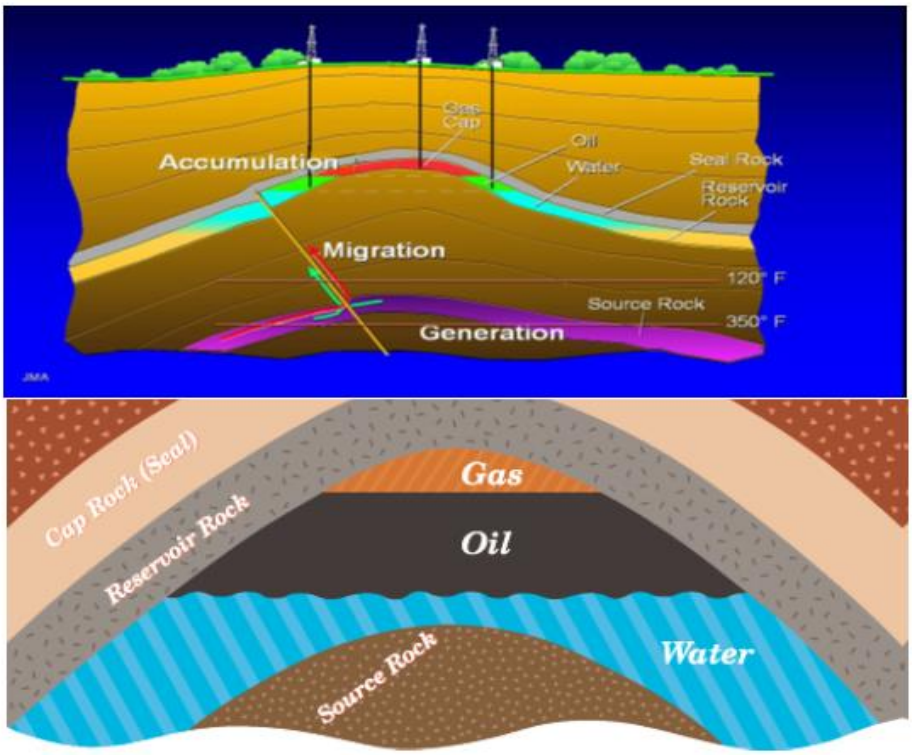

Figure 1.4: Images Showing Source Rock, Reservoir Rock, and Cap Rock

(Adapted from http://www.ngridenergyworld.com/ngsw/html/kids1b.html)

Petroleum Systems Modelling (PSM) is a vital component of exploration risk assessment and is applicable during all stages of exploration, from frontier basins with no well control to well-explored areas. Petroleum system models require geochemical and petrophysical characterization of the sedimentary formations in conjunction with boundary conditions (paleo-water depth, sediment-water interface temperature, and basal heat flow) (Busanello, Del Ben, & Pipan, 2017). The three major stages involved in this model building include the basin modelling stage, the numerical simulation stage, and the calibration stage (Ben-Awuah, Adda, Mijinyawa, Andriamihaja, & Siddiqui, 2013).

1.2 Geology of Lamu Basin

1.2.1 Regional Geology

Gondwana break up resulting from tectonism control the area geology. As shown in Figure 1.1, the Sedimentary basins of Kenya comprise of Mandera basin trending in the North-South orientation, the Anza basin in the Northwest-Southeast direction, the tertiary rift basin in the North-South direction, and the Lamu basin extending into the Indian Ocean passive margin. They are characterized by intrabasinal faults and crustal depressions, which are fault-bounded, resulting from a failed continental rift system. Full graben, as well as half-graben systems with basin infill controlled by faults, characterize most of the sedimentary basins (NOCK, 1995).

The Lamu basin consists of carbonates, marine shales, fluvial-deltaic sandstones, and sandstone sediments. The depo-centre (offshore) has a 12 km to 13 km sedimentary column thickness (Nyagah, 1995). Lamu Basin is the tri-radial rift system's failed arm (Reeves *et al.*, 1987), having passively developed due to the drifting, from the East African coast, of Madagascar (Bosellini, 1986). There is a very close relationship between the basin's Southern part passive margin, Madagascar's pre-drift position, and the Indian Ocean basin's formation during the Mesozoic.

Offshore Kenya is subdivided into the Northern and Southern Lamu Basins, separated by a North-South trending structural high called the Davy-Walu High. Onshore, the dominant structural feature is the East-West trending Anza Graben. While the Northern and Southern Lamu Basins have a similar stratigraphic fill, they have very different structure styles. The Southern Lamu Basin is a predominantly extensional basin that has undergone a period of inversion. The Northern Lamu Basin is characterized by thin-skin gravity-driven tectonics resulting in up-dip extension coupled with down-dip contraction, giving rise to a deep water fold and thrust belt)NOCK, 1995(.

The N-S trending Davie Fracture Zone, with a more than 2000 km length, connects Somali and Mozambique Basins. At the northern edge of the Davie Fracture Zone, a broad gravity high represents Davy-Walu Ridge (DWR), a prominent basement high,

uplifted since the mid-Cretaceous. Passive-margin fold-and-thrust belts (DW-FTBs) are geological features of considerable economic interest since many oil and gas fields have been discovered in traps associated with these systems (Fiduk *et al.*, 1999);(Roy *et al.*, 2008).

Recently, a prolific hydrocarbon fairway has been proven to exist in the offshore Rovuma Basin (NE Mozambique), trapped in a system of gravity-driven, Extensional-compressional deepwater DW-FTBs (Mahanjane & Franke, 2014). This discovery has dramatically increased interest in the underexplored continental passive margin of East Africa (Cruciani & Barchi, 2016). The history of the basin is dominated by the break-up of Kenya from Madagascar and can be divided into pre-rift (late Proterozoic to Triassic), syn-rift (Triassic to Late Jurassic), and post-rift phases (Late Jurassic to Holocene) (Osicki, Schenk, & Kornpihl, 2015). The edges of the Davie Walu fracture ridge (DWFR) have large-sharp negative anomalies, which indicate a large vertical displacement due to adjacent faults along the fracture zone. The displacements brought by these faults have created gravity-negative depocentres such as the happy valley (Masinde, 2019). For a successful exploration of the wildcat, the elements of a petroleum system, such as trap and seal, reservoir rock, source rock, and migration pathways, should be in place and have their proper arrangement and timing.

1.2.2 Source Rocks, Reservoir Rocks, Seal, and Trap Configuration

A source rock is rich in organic matter, which, if heated sufficiently, will generate oil or gas. Typical source rocks, usually shales or limestones, contain about 1% organic matter and at least 0.5% total organic carbon (TOC), although a rich source rock might have as much as 10% organic matter. The quantity of organic matter is commonly assessed by a measure of the TOC contained in a rock. Quality is measured by determining the types of Kerogen in the organic matter. Thermal maturity is most often estimated using Vitrinite reflectance measurements and data from pyrolysis analyses (Waples, 1994).

The Lamu Basin has potential source rocks ranging from type I to type III Kerogen (NOCK, 1995). These include Jurassic Oolitic Limestone and Lacustrine shales, with

an average TOC of 1.4%. Type III Kerogen is the most dominant Kerogen type, and gas occurrences are the most frequent hydrocarbon encountered in the Lamu Basin (Ngechu, 2012). Jurassic to Cretaceous source rocks is widely distributed with good quality and is the primary source rocks in the east coast of Africa. Tertiary source rocks have a lower thermal evolution degree and are considered ineffective source rocks in all basins except Somali Basin. Lamu Basin has bad source rock conditions, which is inferred to may have two sets of source rocks and to lack high-quality source rock (Zongying, Ye, Shujun, & Wenlong, 2013). The maturity and nature of source rocks in the Lamu Basin remain crucial (Osicki et al., 2015). The critical risk for deep offshore Lamu Basin is the charge, primarily source presence, and there is no definitive evidence of deep-water marine source rock in the Basin. As the presence of source rock is unproven, the stratigraphic interval that may contain source potential is also uncertain (Osukuku et al., 2022) (Appendix V).

Reservoirs correspond to deltaic prograding sandstones (Kipini formation) and local carbonate build-ups. The central Lamu embayment deposits constitute suitable reservoirs devoid of source potential, comprising shaley interbedded limestones and anhydrite intercalations, gradually becoming calcareous and terminating as evaporitic sequences (Nyaberi & Rop, 2014).

The presence of limestones in the Lamu basin (onshore) renders it a potential reservoir. The prospectively suitable reservoirs consist of Oligocene deltaic Clastics and shelf carbonate facies. The potential targets for the reservoir are the Lamu reefs off-shore and near-shore. 3.1 mcf/d of gas was recovered in the Dodori-1 Well, while in Pandagua-1 Well, 12.7 mcf/d of gas was recovered during Drill Stem Test (DST) in about half an hour. The reservoir in the Dodori-1 well is 40m thick Paleocene Sands (see appendices I and II) (NOCK, 2009).

The seal is an impermeable rock (usually claystone or shale) that prevents the passage of hydrocarbons. Walu shales may act as regional seals in the upper cretaceous play offshore. In the Eo-Oligocene play, regional Kipini formation shales may provide the regional seals, and in the Miocene play, transgressive marine shales may act as seals and possibly source rocks. The sealing potential is adequately provided by the abundant presence of the thick shale sequences (NOCK, 1995).

Faulted blocks characterize the trapping potential and anticlinal structures in the North and South (NOCK, 2009).

1.2.3 Stratigraphy

Based on the geological and geophysical well data and outcrop studies, the stratigraphic section was divided into four significant sequences, which range from Triassic through to the Tertiary age)Nyagah, 1995(.

Megasequence I (Karoo Group)

This group represents the oldest sedimentary units of Lamu Basin, comprising sandstones. The sandstones include; Upper Mazeras sandstones, Mazeras sandstones, Mariakani sandstones, Maji ya Chumvi limestones, and Taru grits. Megasequence I Comprise strata deposited during the Permo-Carboniferous to Early Jurassic Karoo extension and the subsequent Jurassic rifting, which separated Madagascar from Africa. They are from the Permian to the Triassic. Karroo rocks in Lamu Basin are typically sequences of terrigenous clastic sediments associated with long periods of continental intracratonic sedimentation. The late Jurassic unconformity separates Megasequence I and II (Figure 1.5) (NOCK, 1995).

Megasequence II (Sabaki Group)

It is formed by lithostratigraphic assemblages ranging in age from Early Cretaceous to Early Paleocene. The assemblages formed from two marine regressions and one transgression. The second regression phase was coeval with the Late Cretaceous tectonic uplift which promoted increased inputs of deltaic sands (Kofia Sands) deposited above an erosional unconformity of regional extent. They include the Ewaso Sands, the Walu Shale, the Hagarso Limestone, the Frere Limestone, and the Kofia Sands (Nyagah, 1995). In this group, we have the early and late cretaceous plays and an event of tectonic quiescence covered by a carbonate shelf. The Paleocene unconformity separates Megasequence II and III.

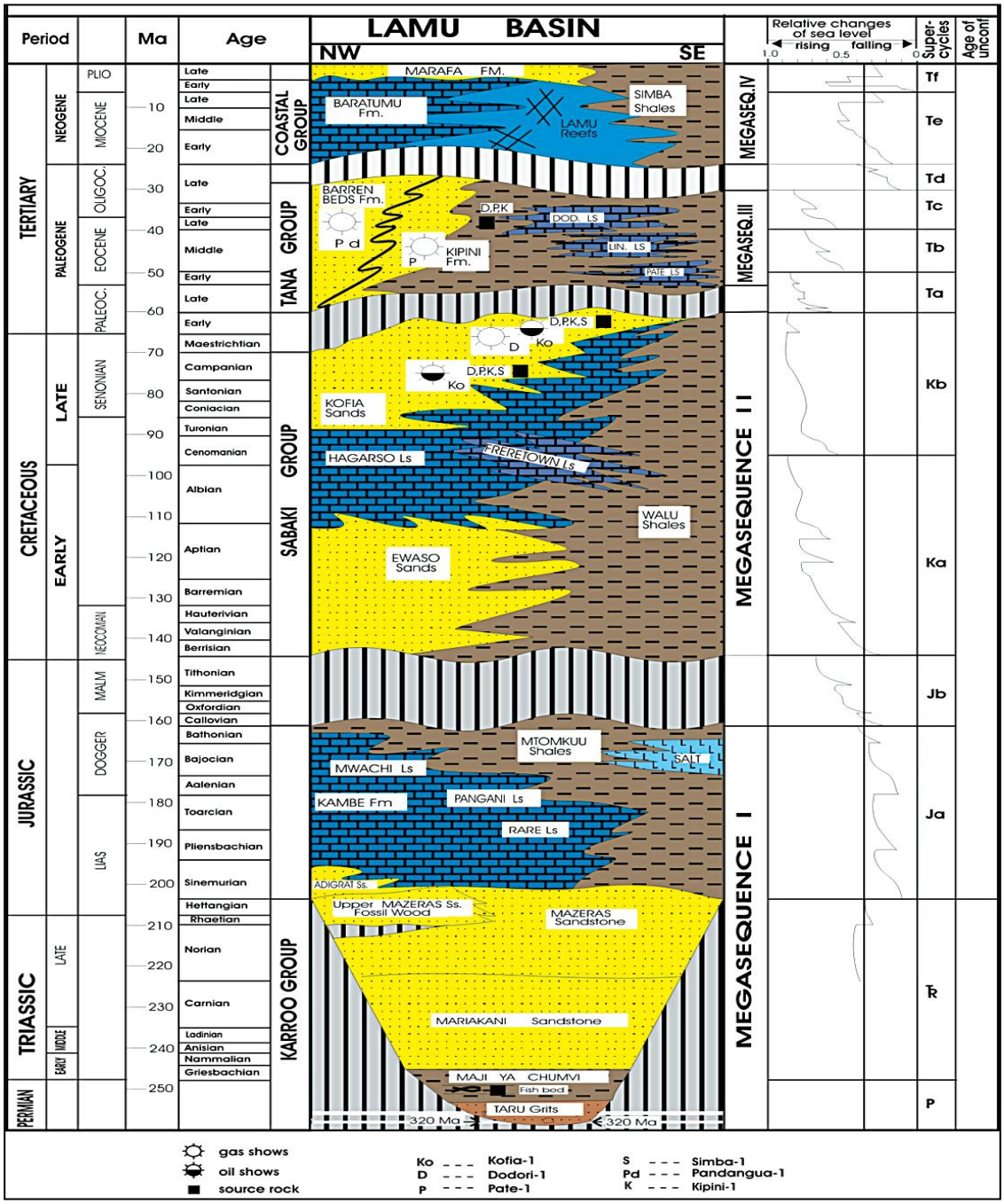

Figure 1.5: Chronostratigraphic Chart Showing Lamu Basin Events from Triassic Through to Tertiary (Nyagah, 1995).

Megasequence III (Tana Group)

It consists of Eocene to Oligocene rocks deposited in three phases of sea level rise and a single regressive phase of deposition. This lithostratigraphic assemblage

comprises shelf-carbonate and fluviodeltaic facies (Kipini Formation) deposited by a Paleo Tana River distributary system. The rock units of the Tana Group are the Kipini Formation, comprising Pate Limestone, Linderia Limestone, and Dodori Limestone Members, and the Barren Beds Formation *(NOCK, 1995)*. Eocene play is found in this Megasequence III which is separated from Megasequence IV by the Oligocene unconformity.

Megasequence IV (Coastal Group)

It is made of carbonate sequences associated with marine shales and overlying siliciclastic sequences. This succession comprises carbonate units associated with marine shales and an overlying siliciclastic sequence (Marafa Formation), synchronous with the main Pliocene uplift phase of the Kenya Rift Valley. The lithostratigraphic units of the Coastal Group were deposited during three major sea-level cycles: the Baratumu Formation, the Lamu Reefs, the Simba Shales, and the Marafa Formation)NOCK, 1995(.

1.4 Statement of Research Problem

The exploration of hydrocarbons in rather extreme and adverse areas, such as areas with geological complexity, is driven by the increasing demand for oil and gas today. Geological complex areas pose a high exploration risk. Kenya's Lamu basin is hitherto underexplored even though there have been notable discoveries along the margin of East Africa. Many of the drilled wells in the Lamu Basin turned dry save for gas and oil shows from a few of the Lamu Basin's twenty (20) drilled exploration wells. Related previous studies on the region have cited possible reasons for dry wells including poor well site and immature source rock, all these being petroleum system element challenges. This study, therefore, delineated major and minor structures using gravity method whereby techniques like spectral analysis, first horizontal derivative and gravity modelling within the Oasis Montaj software enhanced the visualization of the structures. Seismic method was employed to map possible closed structures within the study area. The method used seismic to well tie, seismic surface slicing, and seismic attribute analysis within the Schlumberger’s

Petrel software platform in enhancing structure visibility. The structures delineated using gravity and seismic methods represent the trap, being the first petroleum system element assessed. The second element is the hydrocarbon reservoir that was assessed using petrophysics and rock physics techniques. The petrophysical properties and the rock physics models obtained from the well log data analyzed within the Schlumberger's Techlog software suggest presence of good reservoirs. Petroleum system modelling was utilized in characterizing the source rock (the third petroleum system element). The maturity maps developed by the Petrel software indicate regions with mature source rocks and can therefore be used to suggest suitable well locations for possible drilling. Generally, the integrated approach employed gravity and seismic geophysical methods to delineate the structures necessary for hydrocarbon accumulation and preservation. Petrophysics and rock physics modelling was leveraged in reservoir characterization and petroleum system modelling was utilized in source rock evaluation. The utilization of the results of this study will tremendously minimize the high investment risks. The focus of the study is on the Lamu Basin shallow offshore.

1.5 Justification of the Study

This study assessed the exploration risk factors including the structural traps, reservoirs and source rocks. The sedimentary basin dynamics and fluids associated with it were examined by integrating petroleum system modelling with gravity and seismic geophysical methods, and petrophysical and rock physics analysis techniques to verify if the conditions favoured the generation, migration, accumulation, and preservation of hydrocarbons. The integrated approach covered the limitation of individual methods like the seismic method which is a powerful tool for subsurface imaging but limited to predicting trap content reliably. The results from the combination were utilized in delineating necessary structures, characterizing the reservoirs and determining source rock properties hence guiding the proper well drilling location which will consequently minimize the number of dry wells drilled. Therefore, the integrated study increased the confidence of the findings since the required structures were delineated, possible reservoirs characterized, and potential source rocks evaluated. Ascertaining hydrocarbons' presence, types, and volumes

before drilling is a sure way to reduce investment risk. The hope of drilling discovery wells will go a long way to profiting both the investors and the country at large since most of the industries still depend on hydrocarbon fuels.

1.6 Hypothesis

a) Most of the exploration wells are dry because of poor siting of the wells.

1.7 Objectives

1.7.1 General Objective

To assess exploration risk factors of the Lamu shallow offshore basin using gravity and seismic methods together with petroleum system modelling.

1.7.2 Specific Objectives

1. To determine the overall regional interpretation of the minor and major structures within the basin by processing gravity Isostatic data.
2. To delineate closed structures and potential subsurface traps through seismic interpretation of Lamu offshore.
3. To characterize the reservoirs by identifying and evaluating potential zones utilizing well log data.
4. To apply petroleum system modelling in evaluating geological conditions necessary for a successful charge.

1.8 Research Questions

1. What are the main subsurface structures that impact the hydrocarbon potential?

2. Are closed structures that would support the petroleum system available?

3. What are the properties of the potential reservoir zones?

4. Where are the conditions necessary for a successful charge favourable?

CHAPTER TWO

LITERATURE REVIEW

2.1 Introduction

This chapter captures some of the regions where geophysical methods and techniques have been successfully applied in the exploration of hydrocarbons. This study also discusses the scientific theory of the geophysical methods, techniques, and the basin and petroleum system modelling workflow.

2.2 Previous Studies

A study on the petroleum prospects of the Lamu basin was carried out. Though suitable structures for hydrocarbon exploration were visualized from the 2D seismic interpretation and the existing well results, the result of the sub-surface studies on sedimentology and stratigraphy indicated a more pelagic tendency of the Cretaceous sediments of Lamu embayment towards deep offshore. Developed geophysical models indicated mature upper Cretaceous sediments available in the Walu–Kipini–Pate Dodori wells. This study found out the presence of Overmature lower Cretaceous sediments except the near coast shore proximity where they may be mature at depths ranging between 3,300 m – 4,700 m. It was concluded that the location of the drilled wells along the reservoirs appears to be characterized by faults (structural lead features) and geothermal highs (sub-surface stratigraphic elements). The study, therefore, recommended that a model that will integrate transient pressure, petrophysical, and seismic data yields be developed to improve the characterization of the reservoir besides informing the decision to drill wells at appropriate reservoir points, away from high thermal gradient zones and major fault zones (Nyaberi & Rop, 2014).

In another study focusing on the deep Lamu offshore basin, it was recommended that an update of all interpretations in light of the additional information provided by the broadband survey be done. In this study, 2D seismic data was interpreted to analyze the regional basin stratigraphy. Attribute analysis highlighted possible and potential

reservoir and source intervals, contributing to plays ranging from Jurassic syn-rift fault blocks through Cretaceous basin floor fans to Tertiary channels, reefs, and turbidites. The modelled cretaceous marine shales in the deep offshore was found to lie in the oil window while the Eocene Kipini and Pate source rocks were delineated as immature. The petroleum systems study also indicates that the elements of the systems formed in the correct order for hydrocarbon accumulation to occur. The study recommended a three dimension (3D) petroleum system modelling with lateral facies variation informed by attribute analysis to understand how petroleum system elements vary over the basin. The study also recommended gravity modelling to understand the position of the continent-ocean boundary. The continent-ocean boundary is significant for hydrocarbon exploration as it is very unlikely to discover commercial quantities on the oceanic crust. This is because the oceanic crust lacks source rocks, has low heat flow, lacks reservoirs, and has deep water exploration constraints. Finally, the study recommended AVO attribute analysis and 3D seismic acquisition in the most prospective areas (Osicki et al., 2015).

Identifying and delineating possible hydrocarbon traps and prospective areas in the Lokichar basin, five lines of 2D seismic data were interpreted by picking horizons and tracing faults of interest. The interpretation results confirmed the existence of the Lokichar fault, which could control the deposition of sediments in the basin. Structure controlled hydrocarbon accumulation and trapping were delineated. Various structures have been delineated from the study as shown in figure 2.1. The structures include the fold anticlines and fault closures which could be forming the target areas for hydrocarbon prospecting (Anabwani, 2012).

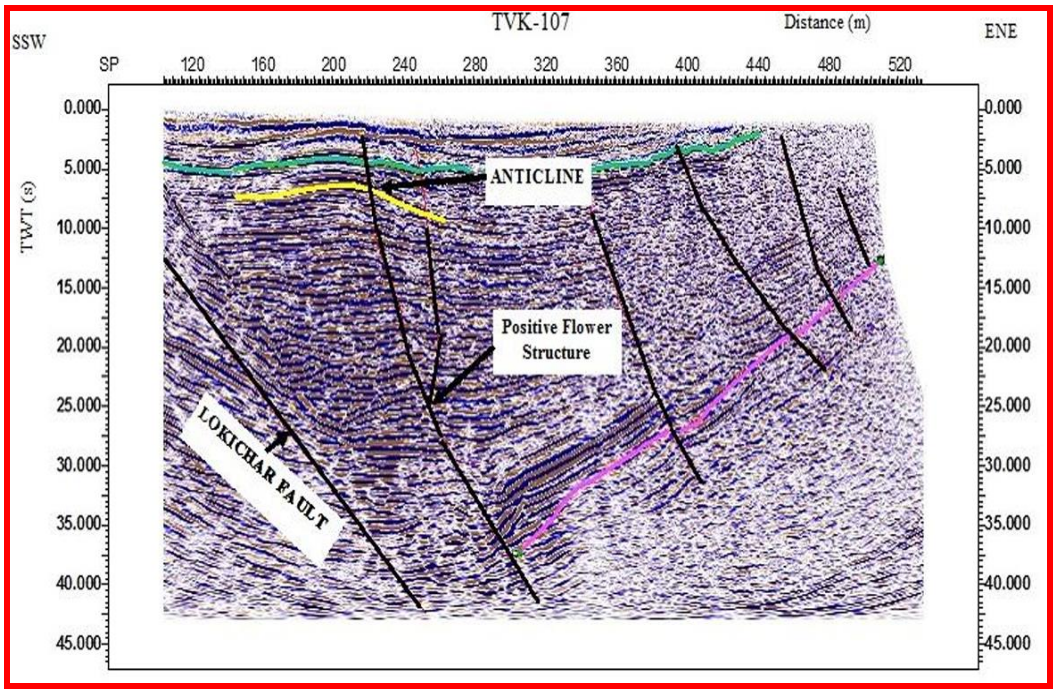

Figure 2.1: Interpreted Vertical Seismic Display Showing Structures

(Anabwani, 2012).

A study assessing hydrocarbon generation potential and thermal maturity of the deep offshore Lamu Basin using 2D petroleum system modelling indicates that the Rock-Eval pyrolysis and the calibrated models result favour, in terms of Vitrinite reflectance and temperature, near coastal region in the Upper Cretaceous. Despite the drilled deep offshore wells penetrating good quality seal and reservoir rock units, the presence and maturity of definitive deep marine source rocks remain a critical play risk (Osukuku et al., 2022).

A detailed deep water fold and thrust belt interpretation along the eastern Africa passive margin was successfully made using a 2D seismic structural and stratigraphic interpretation (Cruciani & Barchi, 2016). A structural framework composed of hydrocarbon potential and structural and stratigraphic traps resulted from interpreting 2D seismic reflection data in the Davie Fracture Zone and the adjacent Nacala and Angoche basins (Mahanjane, 2014).

Characterization of complex sand reservoirs in the deepwater of the Niger Delta was carried out through petrophysical and rock physics evaluation of well log data from three wells. Petrophysical analysis was performed to determine clay volume, porosity, lithologies, and hydrocarbon saturation. Rock physics was studied in the velocity-porosity plane to analyze the influence of depositional and diagenetic features on the reservoirs. The results provided a model that increased the possibility of finding reservoir sand while mitigating the risk involved in finding hydrocarbons (Oladele, Salami, & Adeyemi, 2019).

Petrophysical analysis of some of the Lower Cretaceous Alam ElBueib reservoir units was carried out using wireline logs from four wells representing two fields (Geb and Apries) located in the western part of the Shushan Basin, north Western Desert. The most prospective reservoir intervals are found in the upper and middle reservoir units and are recommended for future exploration and development (Othman, Abdeldayem, Soliman, & El-Qady, 2022).

The Monagas fold and Venezuela thrust belt study demonstrate improved modelling by integrating petroleum system modelling and structural restoration in assessing seal integrity and charge risk within a tectonically compressive sub-thrust prospect. The temporal evolution of the salt tectonics and surrounding deformation in the offshore Essaouira salt basin was described through the development of the salt restoration workflow involving decoupled sub-salt and salt-overburden restoration with salt-area balancing (Neumaier, 2016).

In the investigation of the North Adriatic Sea's deep Mesozoic basin, the basin and petroleum system modelling (BPSM) technique was employed, and the results of the unproven thermogenic hydrocarbon were correlated with the proven petroleum systems of the Croatian and Italian offshore areas. The results from the modelling simulation and the scenarios evaluated during the sensitivity tests confirmed that the basin might present all the requirements for the successful generation, migration, and accumulation of hydrocarbons. The turbiditic slope sediments on the flank of the carbonate platforms may have the proper porosity to host the accumulation of hydrocarbon. The results further indicated that the system could eventually generate

oil and gas, as shown by the time extraction diagrams of hydrocarbon generation through time and the accumulations can preferentially occur in stratigraphic closures owing to the presence of low-permeable calcareous sealing formations. From the sensitivity tests performed on the properties of the faults, it is possible to infer that the faults worked to conduct oil and gas into the upper stratigraphic units where it was trapped below the Cretaceous marly intervals (Busanello *et al.*, 2017).

In Myanmar, modelling Petroleum systems will guide subsequent exploration if knowledge about petroleum systems is leveraged. In 2009, an integrated exploration potential evaluation was done by building geological models (3D). Seismic data from deeper parts of the basin was tied with well data from the shallower parts. The well data achieved the depth conversion of seismic data and the eight horizons' interpretation. The combination of the geological model and the geochemical data aided in building a 3D petroleum system model of the area. The model was then consequently applied to predicting the amount and location of yet-to-be-discovered hydrocarbon accumulations (Bryant *et al.*, 2013).

In the Hammerfest basin in Norway, a study was carried out to understand the Triassic play within and to demonstrate the use of basin modelling and analysis of the petroleum system to reduce exploration risk (Ben-Awuah *et al.*, 2013). In the Soviet waters, a total of 250,000 km of seismic was acquired, and 423,000 km was done in the Norwegian waters. As parts of the Barents Sea, 22 exploration wells were drilled in the Soviet and 45 in Norwegian by 1990 (Johansen *et al.*, 1993). The seal integrity in the Hammerfest basin has been significantly compromised due to uplifts and erosion leading to hydrocarbon leakage. This explains the reason for many dry wells hence increasing exploration risk. The local cessation of hydrocarbon generation is caused by temperature reduction due to erosion in uplifted areas. Finally, The Hammerfest Basin is representative of a province rich in petroleum with many play characteristics. Therefore, the recommendation is to carry out advanced BPSM to understand the petroleum system better and delineate the episodic uplifts within the basin (Ben-Awuah *et al.*, 2013).

According to Al-Hajeri *et al.* (2009), most companies keep basin and petroleum systems modelling achievement stories secret because of the sensitivity associated with such results. For instance, such success was reported in Indonesia, given that the operator was looking for a partner to drill with. Makassar Slope and Mahakam Delta would likely produce oil, although, at the time, there was a common belief that source rocks were postmature thermally and were prone to gas (Al-Hajeri *et al.*, 2009). The permitted stratigraphic-geochemical model showed the source rocks' restriction to shelfal regions that were up-dip. On the other hand, reservoir rocks of similar age on the outer part of the shelf were taken to have lost good reservoir quality since they were too deeply buried. However, Mobil geologists applying BPSM gave predictions that indicated that the area of interest's Miocene source rock was within the present oil window and was effective and active. The success of BPSM resulted in a great discovery by Unocal and Mobil whereby some wells could yield up to 10,000 bbl/d [which is equivalent to 1,600 m^3/d] of oil from some wells within the Makassar straits' deep-water which had been otherwise abandoned. The view of the industry concerning deep-water deltaic systems the world over was then changed through the findings of the study. More than the historical application of BPSM to assess hydrocarbon charge risk in basin analysis, it is now widely being applied in explaining the genesis of fluid complexities in fields that are producing (Al-Hajeri *et al.*, 2009).

Four rock units from the Sayun-Masilah basin were evaluated qualitatively and quantitatively in a petroleum source rock characterization study through the geophysical and geochemical approaches. Rock-Eval pyrolysis data, hydrogen index (HI) and TOC, were used as input to one-dimensional basin modelling and measured Vitrinite reflectance and borehole temperature to calibrate the created models. The models indicate that the paleo-heat flow was highest during the upper Jurassic; the early oil generation window occurred during the upper Cretaceous, and the main oil window in the early Eocene. Therefore the Sayun-Masilah basin has generative source rock potential in the prospective area (Al-Areeq, 2018).

2.3 Geophysical Methods and Techniques

This section highlights the theories and concepts of gravity and seismic geophysical methods and the interpretation of resultant processed data, well log analysis techniques and basin and petroleum system modelling procedures.

2.3.1 Gravity Studies

Despite being masked by seismology, the gravity method has remained a crucial constraint in some exploration areas. In hydrocarbon exploration, it was the first geophysical technique to be used and is particularly applicable in targets that lie below high-velocity zones, regions of salt, underexplored basins, and overthrust and foothills belts (Nabighian *et al.*, 2005). The under-utilization of the gravity method as one of the potential field data methods in hydrocarbon exploration is due to the deadline pressures whereby explorers choose to give only seismic results. However, in more complex areas and those covered by basaltic rocks, it is paramount to use the gravity geophysical method since in such areas seismic method has limited use (Lowrie & Fichtner, 2019).

The gravity method is preferred in hydrocarbon exploration because of its ability to show both the stratigraphic and structural features. In this method, the geology of the sub-surface is examined based on the variation of density of the rocks giving rise to the different gravitational field of the earth. The conceptual idea is that the body that brings about the varying gravity of the earth is a unit of rock whose density is relatively different from other rocks in the vicinity. This body whose density is different from the rest possesses a different mass as well which results in a perturbed gravity region commonly known as a gravity anomaly (Watts, 2001).

As far as gravity data is concerned, a geological anomaly is defined as any lateral change occurring in the subsurface geology of the area. This can happen as a result of either change in the density of a horizontal layer or a change in the horizontality of a constant-density layer (Figure 2.2). In either case, such a geological anomaly would create the corresponding disturbance in the gravity field, known as the gravity anomaly. It is called regional gravity anomaly when it describes large-scale

geological changes and residual anomaly when the changes are of localized nature. Due to imminent ambiguity in gravity interpretation and given that an anomalous body produces a non-unique gravity anomaly; it is, therefore, paramount to apply constraints to increase solution certainty. The amplitude of the anomaly is the function of both the density difference (density contrast) and the depth of the responsible geological structure (Alsadi & Baban, 2014).

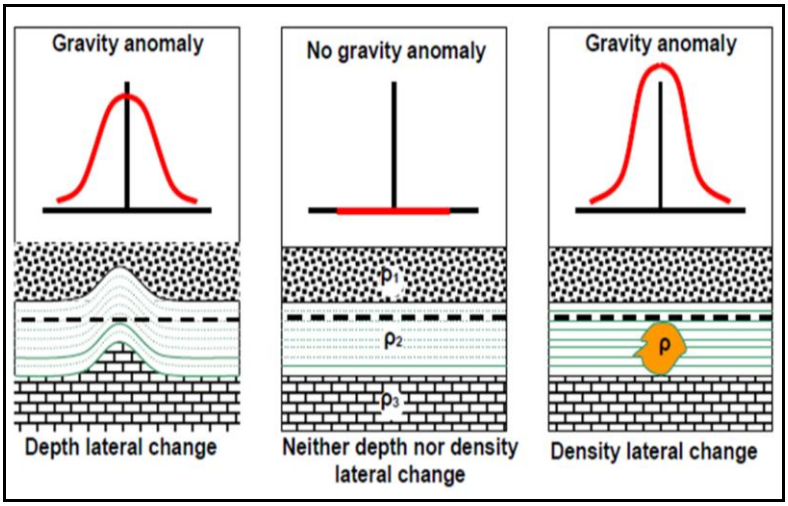

Figure 2.2: Gravity Anomaly Created by Local Geological Anomaly with Lateral Changes in Depth or Density or with Both

(Alsadi & Baban, 2014)

The gravity method has been underutilized in hydrocarbon exploration despite its existence in the field for quite a while. This is partly because of pressure by companies to get results within a limited time and therefore explorers choose to give only seismic results. The gravity method is paramount in impossible or difficult situations where the seismic method cannot apply. For instance in sub-salt play exploration and areas covered with basalt where imaging becomes difficult because of the presence of high-velocity rocks (Lowrie & Fichtner, 2019).

The seismic technique can effectively be used to image the top of the salt but cannot be utilized to image underneath the salt because of increased velocities. Potential field methods, magnetics, and gravity have had extensive applications in exploring basalt-covered regions in integrating seismic data and beneath-the-salt imaging. The

approach is vital in Africa's frontier areas and given that it takes a short time, large areas can be covered cheaply and quickly (Geotechnologies).

In the application of potential field data in hydrocarbon exploration, the gravity method is more popular than magnetics. This is because gravity can show various geological features such as salt domes and anticlines/synclines. The variation in the gravitational field of the earth resulting from subsurface rock density variations makes subsurface geology investigation possible. The concept behind the investigation is a causative body with density contrast which represents a zone of anomalous mass causing the gravitational field to be perturbed to produce a gravity anomaly (Saibi *et al.*, 2006).

Free-air anomaly, Bouguer anomaly, and Isostatic anomaly maps constitute the three types of anomalies. In geology, Isostacy means the lithospheric and asthenospheric gravitational equilibrium in which the tectonic plates are suspended at a level depending on their density and thickness. Isostatic adjustment is suggested in the principle of Isostacy whereby changes in the surface of the earth's mass cause the earth's crust to adjust. Due to the earth's surface mass changes, the earth's crust responds through either subsidence or rebound. Three Isostatic models are normally employed. They include The Pratt-Hayford Model, The Vening Meinesz (Flexural Model), and The Airy-Heiskanen Model (Watts, 2001)

Correction of gravity results is necessary before interpretation to eliminate variations not resulting from density contrasts of the rocks. This is what is described as reducing gravity data. Gravity reduction is achieved through Eötvös correction, Drift correction, Elevation corrections (Free air, Bouguer, and Terrain), Latitude correction, and Tidal correction (Murray & Tracey, 2001). Free air correction reduces the effects of elevation differences between the measuring points (Ekinci & Yiğitbaş, 2015). In the Bouguer anomaly map, bathymetry-sourced anomalies have been removed but still, the Moho-sourced anomalies remain a challenge (Close, 2010);(Green, Fairhead, & Maus, 1998). The Isostacy anomaly map represents data free of the Moho effects and the water effects in the offshore setting (Ombati et al., 2022).

Interpretation of gravity anomalies is easy. For instance, if you have gravity high (positive gravity anomaly), the body represented is denser. An integrated interpretation is useful and therefore Watson's technology toolkit which includes Geosoft is very helpful since it provides the necessary packages. Key to seismic interpretation is the production of depth surfaces and this results from the integration of good data and seismic with the help of Geosoft modelling system (GM-SYS) software. The software provides a platform where visualization of both seismic and gravity data is effectively possible. This, therefore, makes it possible to come up with a model that satisfies both data sets within the same software. GM-SYS software can run on top of the Oasis Montaj platform being the primary platform before integration (Abdul Fattah *et al.*, 2013).

2.3.2.1 Spectral Analysis of Gravity Data

In regions of limited crustal structure information, the power spectral analysis technique can be used to yield potential density contrast depths in the crust. The power spectral decay curve shape is affected by the factors of the source ensemble like the thickness, widths, and depths. The distinguishing feature of the logarithmic decay of the energy curve shows the rapid decrease of the curve at low wavenumbers (deep sources), and a gentler decline of the remainder of the curve (shallow sources) (Ombati et al., 2022).

A typical energy spectrum may consist of three parts namely; a deep source component, a shallow source component, and a noise component. The depth to the source ensemble H ($\hat{h}$, q) is the main factor that controls the shape of the energy spectral decay curve as is expressed in equation 2.1 (Likkason, 2011).

$$H(\hat{h}, q) = e^{-2\hat{h}q} \qquad 2.1$$

The decay slopes of the power spectral curve describe the various depths of a source ensemble. Deep source ensemble is described at a lower frequency (low wavenumber) and shallow source ensemble at a higher frequency (high wavenumber). The depth of

a source ensemble can be computed from the slope of a tangent fitted to any linear segment of the curve (Saibi *et al.*, 2006)

The power spectrum method is used for depth estimation and for designing filters to separate regional and residual fields (or deeper from shallower sources) (Spector & Grant, 1970). A plot of log power versus Wavenumber, figure 4(a), gives a straight line whose slope equals -4πh (for k = 1/λ) from equation 2.2,

$$\log S^2(k) = \log B - 4\pi hk \qquad 2.2$$

i.e. slope is proportional to depth to source since in equation 2.3;

$$h = -\frac{s}{4\pi} \qquad 2.3$$

Information about the earth's subsurface can be determined through the gravity method. This is achievable through a qualitative examination of the grid of gravity values, contour maps or gravity profiles to determine the lateral location of any gravity variations. In quantifying the nature of the subsurface anomaly causative object in terms of depth, density and geometry, more detailed analysis and modelling are done (Mariita, 2007).

2.3.2 Seismic Studies

In hydrocarbon exploration, the method that is most widely applied is seismic, primarily because it is capable of detecting large-scale to small-scale subsurface features. In the seismic method, acquired data is processed, data reduction is done, anomaly maps are drawn, and translation of seismic sections to geological structures is done. Seismic methods involve the estimation of the shapes and physical properties of Earth's subsurface layers from the returns of sound waves that are propagated through the Earth (Bjorlykke, 2010).

Seismic technology had been used since the early 1900s to measure water depths and detect icebergs, and by 1924, Seismic data were first used in the discovery of a

Texan oil field (Milligan, 2004). This method uses acoustic waves (sound) to image the subsurface. The seismic source generates a wavefront, Wavefront represented by the seismic wavelet. The two main techniques that can be employed in the seismic method include the refraction and the reflection methods (Alsadi, 2017). Reflection seismic is the most widely used technique in hydrocarbon exploration. Seismic pulses for exploration surveys are generated as follows; air-gun (2000-5000 psi) for marine surveys whereas for land seismic surveys vibrators (5-100 Hz) and dynamite (3000-10000 m/s) are used. These seismic sources generate surface waves (Rayleigh and love waves) and body waves (P- waves, and S-waves). Since surface waves propagate almost parallel to the earth's surface, they are not as significant in hydrocarbon exploration as the body waves which are capable to propagate through the interior of the earth (Yilmaz, 2001). Seismic reflection profiling is an echo-sounding technique. A controlled sound pulse is issued into the Earth and the recording system listens for a fixed time for energy reflected from interfaces within the Earth. The interface is often a geological boundary, for example, the change of sandstone to limestone. However, there are other seismic reflections out there that may not be stratigraphic in origin; would be due to fluid contacts, fault planes, and multiples. Equation 2.4 is used in the determination of the reflection coefficient (RC) at the interface.

$$RC = \frac{AI_2 - AI_1}{AI_2 + AI_1} \qquad 2.4$$

Where RC, is the reflection coefficient and AI, is the acoustic impedance.

Knowing the travel time to the reflectors and the velocity of propagation, the geometry of the reflecting interfaces can be reconstructed and interpreted in terms of geological structure in depth. The principal purpose of seismic surveying is to help understand geological structure and stratigraphy at depth and in the oil industry is ultimately used to reduce the risk of drilling dry wells. The amplitude and polarity of the reflection are proportional to the acoustic impedance (product of velocity and

density) change across an interface. The arrival of energy at the receiver is termed a seismic event (Simm, Bacon, & Bacon, 2014).

The most commonly used form of seismic wave is the P (primary)-wave which travels as a series of compressions and rarefactions through the earth, the particle motion being in the direction of wave travel. The propagation of P-waves can be represented as a series of wave fronts (lines of equal phase) that describe circles for a point source in a homogeneous media (similar to when a stone is dropped vertically onto a calm water surface). As the wavefront expands the energy is spread over a wider area and the amplitude decays with distance from the source (Gadallah & Fisher, 2009).

This decay is called spherical or geometric divergence and is usually compensated for in seismic processing. Rays are normal to the wave fronts and diagrammatically indicate the direction of wave propagation. Usually, the shortest ray path is the direction of interest and is chosen for clarity. Secondary or S waves travel at up to 70% of the velocity of P-waves and do not travel through fluids because fluids lack shearing capacity. The particle motion for an S-wave is perpendicular to its direction of propagation (shear stresses are introduced) and the motion is usually resolved into a horizontal component (S_H waves) and a vertical component (S_V waves). The amount of the energy reflected depends on the impedance contrast (see equation 2.4). The higher the contrast, the stronger the reflection (Mondol, 2010). The possible candidates for reflection include lithology, porosity, pore fluid, degree of saturation, and diagenesis.

2.3.2.1 Marine Data Seismic Acquisition

In marine acquisition, large ships are used to trail one or multiple air-gun arrays for source and hydrophone arrays for receivers in either a swatch or patch design. In 2D marine data acquisition, a single streamer is trailed whereas in 3D acquisition, multiple streamers are deployed (Figure 2.3). The incident waves from the source are reflected at different interfaces, ranging from the water-sediment interface to the sedimentary layers, due to varying acoustic impedance (Figure 2.4). Hydrophones are designed to detect seismic energy in the form of pressure changes in water with

the aid of the piezoelectric material which generates a voltage upon deformation. The reflected acoustic energy is converted into an electric signal and displayed as a seismic trace being a convolution of the seismic signal and the reflectivity sequence of the earth plus noise (Mondol, 2010).

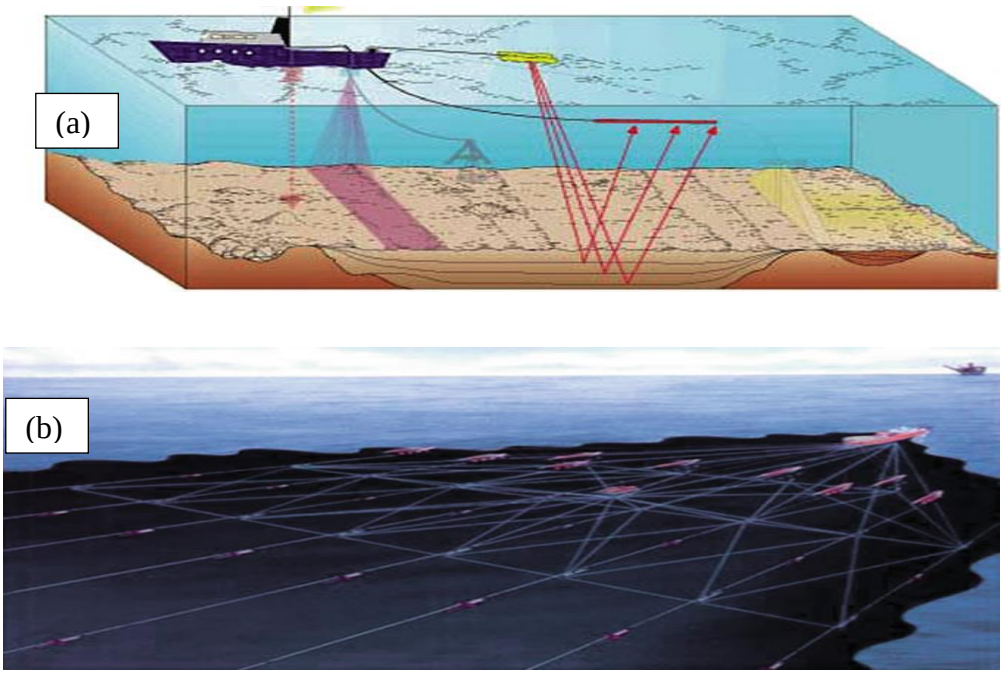

Figure 2.3: (a) A 2D Marine Seismic Acquisition (b) A Towed Streamer for 3D Seismic Acquisition (Mondol, 2010)

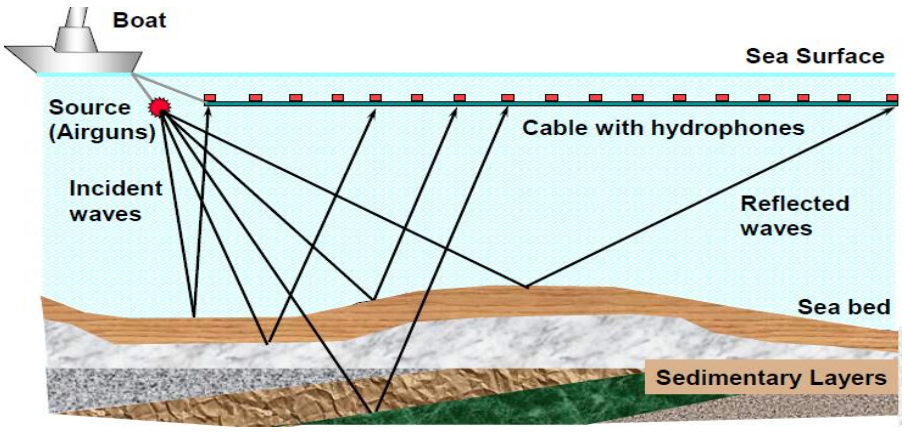

Figure 2.4: Seismic data Acquisition Array Showing Different Refection Points (interfaces) (Mondol, 2010)

What is recorded at the acquisition stage is called raw seismic data which contains real signals, noise, and multiples. There is a need, therefore, to optimize the data by enhancing the signal and suppressing the coherent and non-coherent noises and multiples.

2.3.2.2. Marine Data Seismic Processing

Processing consists of the application of a series of computer routines to the acquired data guided by the hand of the processing geophysicist. The purpose of seismic processing is to manipulate the acquired data into an image that can be used to infer the sub-surface structure. From the tape, a wiggle is obtained which is a vibration of the ground as a function of time. A series of wiggles are used in building a seismic section as a representation of the underlying geologic section. Processing, therefore, makes a seismic section as close as possible to a geologic section by removing all the unwanted artefacts of the seismic method, all noise, and the distortions introduced along the path of a seismic wave (Gadallah & Fisher, 2009).

There is no single "correct" processing sequence for a given volume of data. At several stages judgments or interpretations have to be made which are often subjective and rely on the processor's experience or bias. The interpreter should be involved at all stages to check that processing decisions do not radically alter the interpretability of the results detrimentally. It is worth noting, at this point, that even though optimization of data through signal enhancement and noise reduction is made possible during data acquisition and processing, it is only in the field that the signal-to-noise ratio can be improved without sacrifice by applying multiple coverage (Alsadi, 2017).

Processing routines generally fall into one of the following categories: enhancing signal at the expense of noise, providing velocity information, collapsing diffractions and placing dipping events in their true subsurface locations (migration), and increasing resolution (wavelet processing). The unwanted signals (noise) due to direct waves, refraction, and ground roll are attenuated by normal moveout, muting, stacking, filtering, and migration (Mondol, 2010).

2.3.2.3 Seismic Data Interpretation

Seismic interpretation is the last step in the seismic method as depicted in the workflow below. It involves the transformation of seismic data presented on seismic sections into geological information. Seismic interpretation involves correlating two types of surfaces: horizons and faults (Figure 2.5). A horizon is a surface separating two rock layers that give rise to a seismic reflection according to the acoustic impedance contrast whereas a fault is a displacement of rocks along a shear zone)Sheriff, 2002(. Horizons are correlated by recognizing and tracking continuous or changing patterns of reflections. Faults are based on recognizing discontinuous patterns or offsets. However, faults sometimes form a continuous reflector along the fault plane. A series of horizons and faults that leads to a geological framework is developed. Structural interpretation includes the structural analysis of faults, folds, diapirs, and detached faults. On the other hand, stratigraphic interpretation includes the stratigraphic analysis of terminations (onlap and erosional), reflection geometries, and horizon amplitude (Simm *et al.*, 2014).

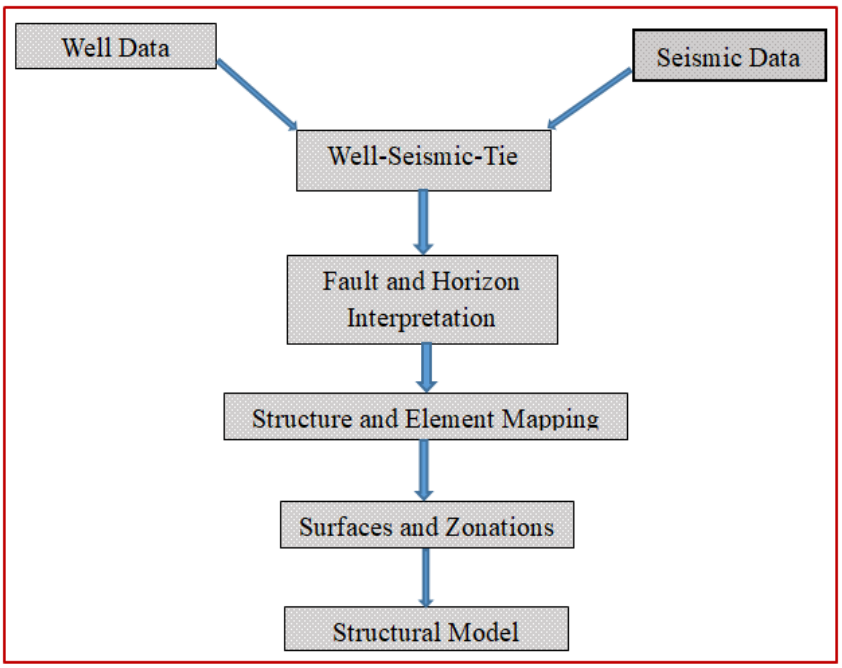

Figure 2.5: Seismic Interpretation Workflow

Stratigraphic and tectonic development of the much underexplored Lamu basin is understood better through the seismic interpretation results. Seismic structures will

be very useful in the evaluation of reservoir properties, fluid migration, fluid flow channels, and permeable zones. The seismic method is limited to resolving a given thickness of the bed (vertical resolution) and a given extension of the bed (horizontal resolution). Seismic resolution refers to the minimum distance between features where they can be distinguishable as two discreet features. The minimum area of the bed that can be resolved is known as the Fresnel zone. The Fresnel zone is a frequency and range-dependent area of a reflector from which most of the energy of a reflection is returned and arrival time differs by less than half a period from the first break. Seismic waves cannot detect any geological features less than the Fresnel zone (Mondol, 2010).

Horizontal resolution can be improved by reducing the size of the Fresnel zone through migration. Vertical resolution can be described by the tuning thickness which is approximately 1/4 of the wavelength. At the tuning thickness, the interpretation criteria change. Deconvolution can improve vertical resolution by producing a broad bandwidth with high frequencies and a relatively compressed wavelet. Typically the recorded seismic frequencies are in the range of 5-100Hz. High frequency and short wavelengths provide better seismic resolution. However, very high frequencies are attenuated faster than lower frequencies (Bjorlykke, 2010).

To be interpreted include the composition of rocks, fluid content, extent, and geometry of rocks. The interpretation is based on the integrated use of seismic inlines, seismic crosslines, time slices, and horizon attributes (Dalley *et al.*, 1989), (Hesthammer *et al.*, 2001).

The interpretation can either be qualitative or quantitative. Qualitative seismic interpretation (also known as conventional seismic technique) implies picking and tracking laterally consistent seismic horizons to map geological structures, stratigraphy, and reservoir architecture. Its goal is to determine hydrocarbon traps that might be structural or stratigraphic, delineate their lateral extent and calculate the volume in the reservoir rock. Quantitative seismic interpretation, on the other hand, considers the physical variations of the amplitudes and how they can be used to predict hydrocarbon accumulation. The most important quantitative seismic

interpretation techniques include; post stack amplitude analysis (bright and dim spots), AVO (offset-dependent amplitude analysis), acoustic and elastic impedance inversion, and forward seismic modelling (Simm *et al.*, 2014). The seismic amplitude not only represents the contrast in elastic parameters of individual layers but also contains information on lithology, porosity, geofluid type, saturation levels, and pore pressure (Avseth *et al.*, 2010).

It is good to check the polarity of the data before interpreting to avoid wrong geology interpretation where one can interpret shallow gas sand as a volcanic intrusion and vice versa. There are two main seismic polarity conventions: Positive standard polarity (American) where a hard kick is a peak and Negative standard polarity (European) where a hard kick is a trough. For the marine data set, polarity can be determined from the data itself because the interface between the sea and the sea bed is always a hard kick since the change is from water with lower acoustic impedance. For non-marine data set polarity can be determined from the well data or the information of the processor (Simm *et al.*, 2014).

The interpretation, in the absence of geologic data from either nearby wells or outcrops, may be more geophysical in nature but offers useful information about the depth of the basement and its configuration, basement paleo-highs, lows, and faults. The deepest event (horizon) seen on a seismic section is usually considered the basement reflection. This reflection is generally characterized by low amplitude and low frequency is often discontinuous and may be punctuated by several faults. This horizon sometimes is termed a technical or acoustic basement by the interpreter where the fundamental Precambrian basement (Archaeozoic) is believed to be deeper but not seen in seismic. Reflections, or horizons, that are continuous and present over a wide area and can be easily correlated by their excellent character are known as seismic “markers”, analogous to a geologic marker bed (Nanda, 2016).

2.3.2.4 Seismic-to-Well Tie

The purpose of Well-seismic ties is to allow well data, measured in units of depth, to be compared to seismic data, measured in units of time. Figure 2.6 below shows the seismic-well tie workflow.

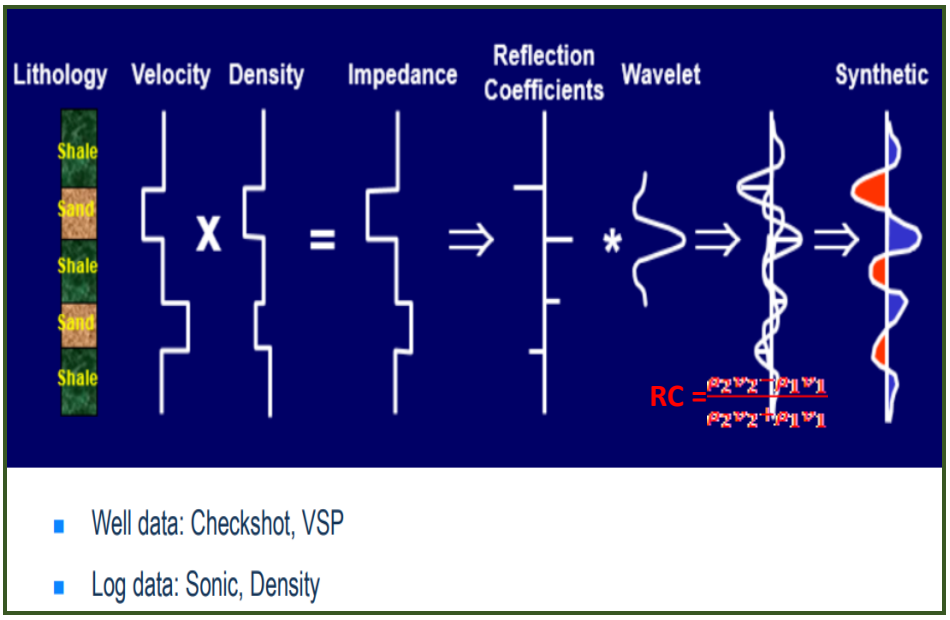

Figure 2.6: Seismic-Well Tie Workflow

(Liner & McGilvery, 2019)

This allows us to relate horizon tops identified in a well with specific reflections on the seismic section. We use sonic and density well logs to generate a synthetic seismic trace within the Petrel software (Figure 2.6). The synthetic trace is compared to the real seismic data collected near the well location. A synthetic seismogram is a bridge between geological information (well data in depth) and geophysical information (seismic data in time).

2.3.2.5 Seismic Attributes

The seismic attribute can be defined as any measure of seismic data that helps us better visualize or quantify features of interpretation interest. It is the component of the seismic data obtained from measurement, computation, and other methods from the seismic data and used to enhance the information that is otherwise subtle in the conventional seismic section (Farfour, Yoon, & Kim, 2015). Seismic attributes aid the geoscientist in seismic interpretation for risk analysis and reservoir characterization. The envelope attribute's importance is detecting bright spots caused by gas accumulations, and detecting major lithological changes that are caused by strong energy reflections and sequence boundaries. The attribute delineates

lithological changes and phase differences that could be subtle in conventional seismic data. The envelope attribute is also known as instantaneous amplitude, magnitude, or reflection strength. It is determined using equation 2.5,

$$\text{Env} = \sqrt{f^2 + g^2} \qquad 2.5$$

Where f is the original seismic trace sample component (real part) and g is the Hilbert transform sample component (imaginary part). The Variance edge attribute is used as a stratigraphic attribute and in isolating edges from the input data set consequently delineating discontinuities in the horizontal continuity of amplitude. RMS Amplitude computes root mean squares on instantaneous trace samples over a specified window. The attribute is quite effective for channel detection and characterization of gas-charged bearing sand units. Sweetness is the implementation of two combined attributes (Envelope and Instantaneous Frequency) and is used for the identification of features where the overall energy signatures change in the seismic data. Sweetness is defined by the formula (Equation 2.6):

$$\text{Sweetness} = \frac{\text{Envelop}}{\sqrt{\text{Instantaneous frequency}}} \qquad 2.6$$

Fault signatures are enhanced by calculating the variance within the seismic data volume with an edge enhancement option. Maximum curvature and coherence attributes can delineate small-throw faults within formations and instantaneous phase attributes show the lateral continuity of the fault networks. RMS amplitude attribute can correlate strongly with formation porosity and/or liquid saturation (Adero, Masinde, & Osukuku, 2017) ; (Oyeyemi & Aizebeokhai, 2015). Some seismic attributes are best suited for reservoir characterization and a cluster of others are associated with either stratigraphic or hydrocarbon anomalies (Oumarou et al., 2021);(Chopra & Marfurt, 2007).

2.3.3 Well Logs

Geophysical well logs are produced when a record of geophysical parameters is continuously taken as a borehole is being drilled. Measurements obtained at each

level versus depth are then used in continuous plotting. This process is very vital for oil and gas reservoirs to be developed successfully. The purpose of well-log measurements is to give information on the likely type and amount of available hydrocarbon in the geological environment (Tong, 2016). Well Logging is the technique of making petrophysical measurements in the sub-surface earth formations through the drilled borehole to determine both the physical and chemical properties of rocks and the fluids they contain. Well Logging Measurements are carried out through the drilled borehole. The drilled borehole may be either an Open Hole or a Cased Hole

2.3.3.1 Types of Well Logs

The well logs record physical properties of the borehole which must then be petrophysically interpreted to obtain the associated rock and fluid properties of the well. Classification of Logs depends on their operation principle and the logging tools. They include lithology (Spontaneous potential, Gamma-ray), fluid identification (resistivity; Laterolog and induction), petrophysical (porosity; neutron, density, and sonic), Auxiliary (caliper), and Nuclear magnetic resonance (NMR). The minimum logging suite required is the triple combo which includes gamma-ray (GR), resistivity (RT), density (RHOB), and neutron (PHI), or the quad combo which includes the triple combo list plus the sonic (Vp) logs. A detailed discussion of the logging suite follows in the subsequent sections (Baker, 1992) (Munyithya, Ehirim, & Dagogo, 2020).

2.3.3.2 Gamma Ray (GR) Log

In sedimentary formations, the GR log reflects the clay or shale content. Clean formations, such as sandstones or limestones, usually have a very low level of radioactivity. Sedimentary rocks have typically low radioactivity levels, but apparently, the radioactivity increases with shale content. The radioactivity is measured in the American Petroleum Institute (API) units by a calibrated detector (Table 2.1). In general, the lower the Gamma Ray reading, the cleaner the sand (Figure 2.6). Gamma Ray logs can be run in cased holes, but the data will be

suppressed. The volume of shale, as shown in equation 2.7, within the target zone, V_{Shale}, is estimated as

$$V_{Shale} = \frac{GR - GR_{Matrix}}{GR_{Shale} - GR_{Matrix}} \quad 2.7$$

Where V_{Shale} is the shale volume (%), GR is the response at a given depth, GR_{Matrix} is the response for a clean reservoir (having no shale) and GR_{Shale} is the response for 100% shale (Rider, 1986). Figure 2.7 shows the typical gamma ray responses as the measuring tool is pulled through various media including shale, shaly sand, and clean sand lithologies. The highest response is seen at the shale lithology while the lowest at the clean sand lithology.

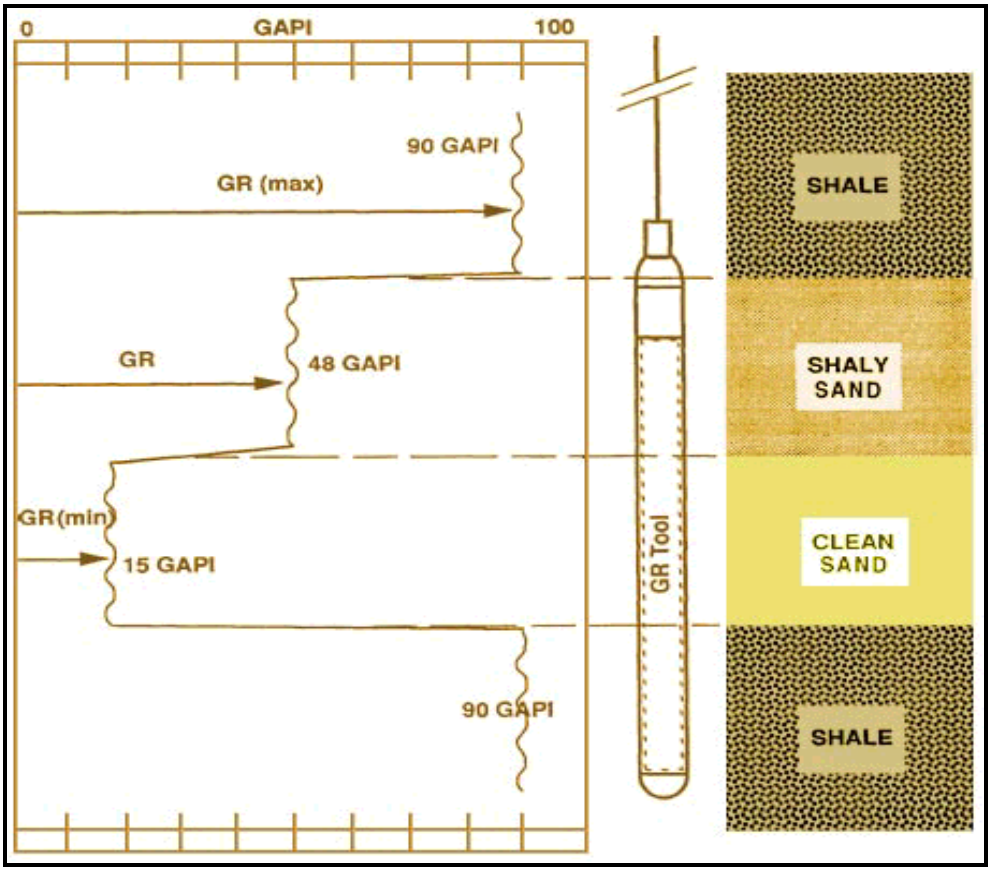

Figure 2.7: Typical Gamma-Ray Responses (Ellis & Singer, 2007)

Table 2.1 shows the various lithologies with their corresponding gamma-ray responses in API units. The highest response is seen in the Sylvite lithology and the least response is from anhydrite and halite. Sandstone, limestone, and dolomite register almost the same GR response range since they all make good reservoirs.

Table 2.1: Lithological Gamma-Ray Responses (AAPG, 2022)

Lithology	GR Values (API units)
Sandstone (quartz)	15–30 (rarely to 200)
Limestone	10–40
Dolomite	15–40 (rarely to 200)
Shale	60–150
Organic-rich shale	100–250
Anhydrite, halite	8–15
Sylvite (KCI)	350–500
Coal	15–150 (any value possible)

2.3.3.3 Resistivity (RT) Log

Resistivity is the physical property of a formation that impedes the flow of electric current. It is based on Induction or Latero-log (current focus) principle. Induction Tools are run in nonconductive or low-conductivity muds while Latero-log Tools are run in highly conductive muds (salt-based). The Resistivity of the salt water is low (highly conductive) compared to the resistivity of the Oil which is high (poor conductor). Dry, nonmetallic minerals (rock matrix) have a very high resistivity. The resistivity of a rock is a measurement of the resistivity of the rock matrix as well as the resistivity of the fluid within the porous volume of the rock (Table 2.2). Resistivity decreases with an increase in the moisture content and for rock with low moisture content resistivity is determined by the component minerals (Ijasan, Torres-Verdín, & Preeg, 2013). Lock, 1999 gave the resistivity values of common formations found in oil fields as summarized in table 2.2.

Table 2.2: Resistivity Values of Common Formation Found in Oil Fields (Modified after (Loke, 1999)

Formation	Resistivity (Ωm)
Limestones	50 – 400
Sandstones	8 – 4000
Shales	20 – 2000
Dolomite	100 – 10000
Sand	1 – 1000
Clay	1 – 100
Seawater	0.2 or less
Ground Water (Fresh)	10-100

2.3.3.4 Density (RHOB) Log

Formation Bulk Density is measured by the Density Logging Tool. The Tool uses a high-energy gamma-ray source (Cesium 137, 1.5 Curie) to allow the interaction of gamma rays with formation atoms (Figure 2.8). By measuring the number of gamma rays and their energy levels at a given distance from the source, the electron density of the formation can be predicted (Table 2.3). Applications of the density logs include determining accurate formation porosity, identifying lithology, delineating thin beds, and indicating gas points when used in combination with a neutron log.

Generally, the measured bulk density (ρ_b) depends on lithology, porosity, and pore

fluid density. It can be determined through equation 2.8,

$$\rho_b = \underbrace{\rho_{ma}(1-\emptyset)}_{\text{Matrix}} + \underbrace{\rho_f \emptyset}_{\text{Fluid}} \qquad 2.8$$

The Porosity ($\emptyset$) equation is given as in equation 2.9,

$$\emptyset = \frac{\rho_{ma} - \rho_b}{\rho_{ma} - \rho_f} \qquad 2.9$$

Where ρ_{ma} is the matrix density, ρ_f is pore fluid density and ρ_b the density log reading, at the target depth.

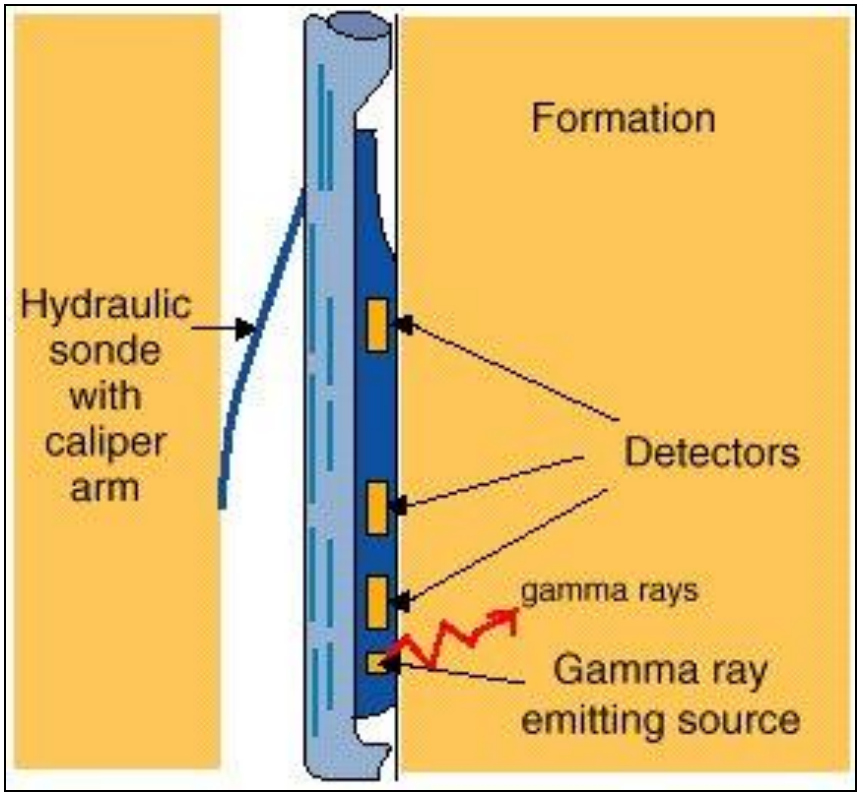

Figure 2.8: Density Measurement (Ijasan et al., 2013)

Density varies inversely with porosity as seen in equation 2.10.

$$\text{Density } \alpha \frac{1}{\text{Porosity}} \qquad 2.10$$

Table 2.3: Typical Density Values of Pore Fluid and Rock Matrix of Hydrocarbon Formations (Liu, 2017)

Substance	Density (g/cm^3)
Hydrocarbon gas (at low pressure)	0.05
Oil	0.8 - < 1
Fresh Water	1.0
Saline Water	1.1
Sandstone	2.65
Limestone	2.71
Dolomite	2.87

2.3.3.5 Neutron (NPH) Log

Porosity can be estimated from a variety of "porosity logs" (sonic, density, neutron, or magnetic resonance log). Neutron porosity logging is a nuclear technique based on neutron-nuclei interactions in the borehole environment. High energy neutrons are emitted into the formation from either a chemical source or a neutron generator device (minitron) (AmBe 241, 18.5 Curie) mounted on the tool and the response of the neutrons is measured as they interact with the formation (Figure 2.9). It is applied in conjunction with the density logs to measure the total porosity of formation for saturation calculation and gas detection. Neutron-Density logs are used in determining various lithologies such as clay at the point where the GR reading is maximum, sandstone, limestone, and dolomite where the GR reading is minimum, and applying the separation of the neutron and density logs (Figure 2.10). Figure 2.9 shows the neutron tool in use for estimating the formation porosity. Figure 2.10 shows the resulting logs (density and neutron porosity) plotted on the same track and the way they are varying in the different lithologies.

The neutron porosity log is used to determine the fluid type (gas, oil, or brine) present in a given formation signalled by low GR reading and high resistivity reading as seen in Figure 2.11.

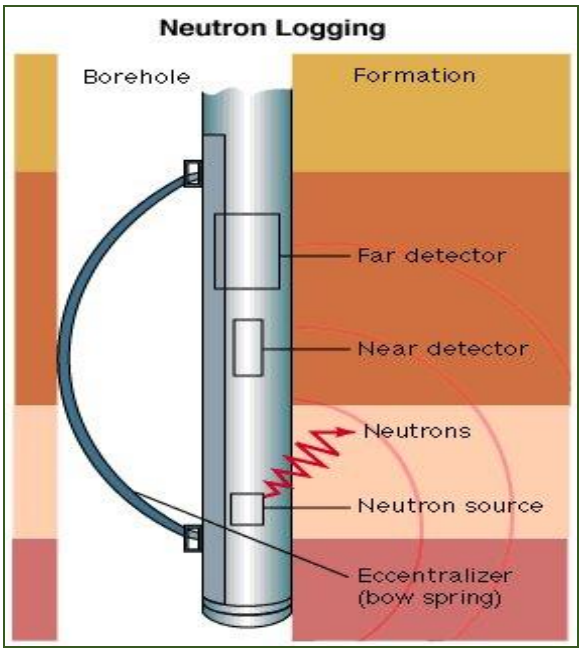

Figure 2.9: Neutron Logging (Ellis & Singer, 2007).

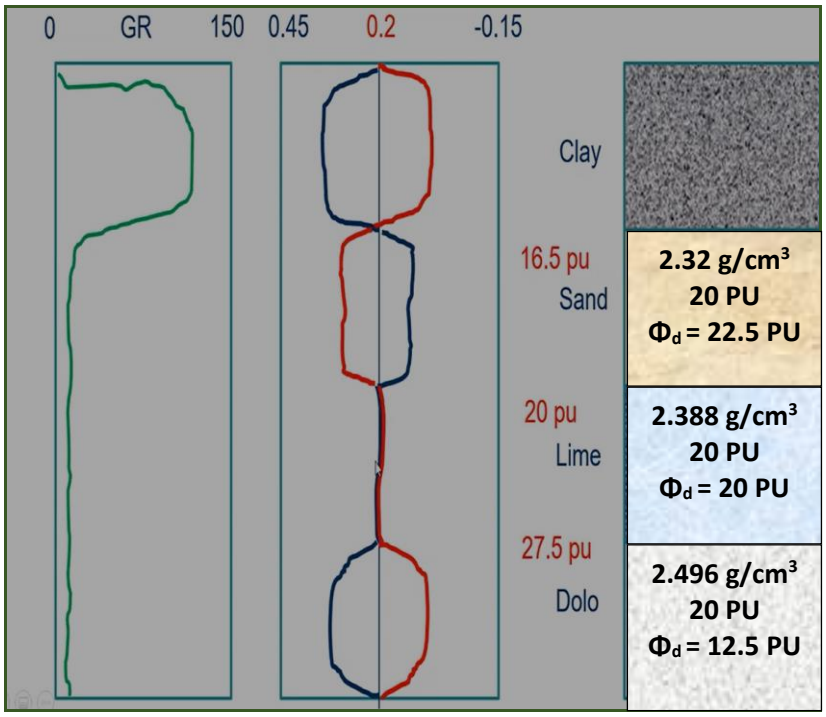

Figure 2.10: Neutron-Density Log (Oraby, 2021).

Shale volume calculation from the neutron log can be estimated using the formula in equation 2.11.

$$V_{sh} = \frac{\Omega_{log} - \Omega_{sand}}{\Omega_{sh} - \Omega_{sand}} \qquad 2.11$$

Where V_{sh} is the volume of the shale, Ω_{log} is gamma-ray reading, Ω_{sh} is maximum gamma ray reading, and Ω_{sand} is minimum gamma ray reading.

Hydrocarbon gas has a low hydrogen index resulting from its low density, and its presence will give rise to underestimations in porosity

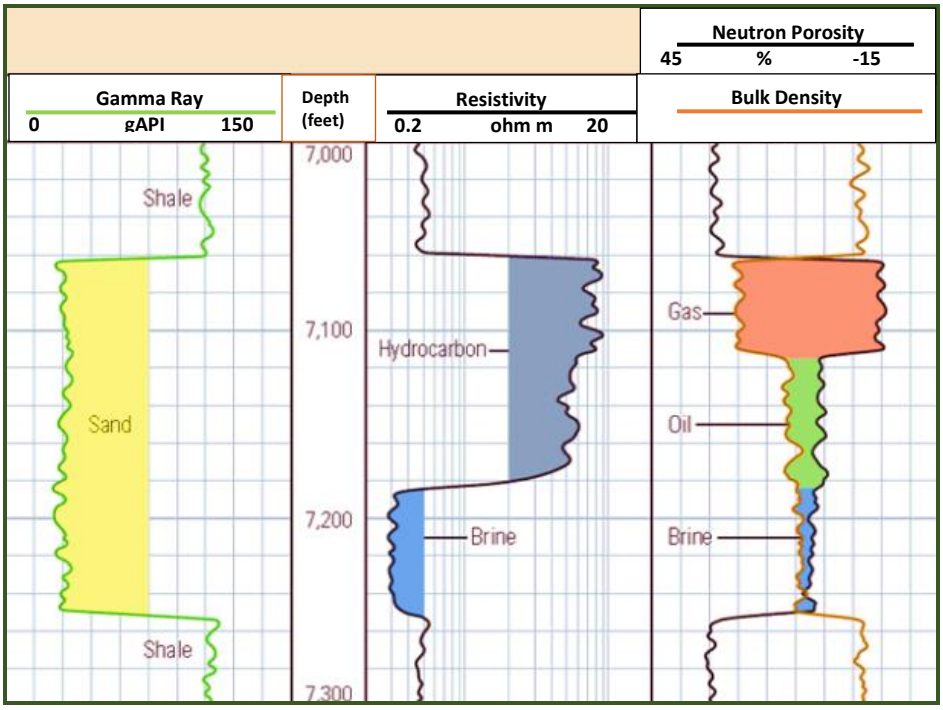

Figure 2.11: Neutron Porosity Log (Ellis, Case, & Chiaramonte, 2003)

2.3.3.6 Acoustic (Sonic) Logging

The Sonic or acoustic log is a measure of the time taken for a sound wave to travel through 1 foot of the formation. The travel time of the sound wave (Δt or DT, normally measured in micro-seconds per foot, μs/ft) depends on the lithology, porosity, and saturating fluids of the formation. Interval travel or transit time is the reciprocal of the velocity of a sound wave. Therefore, if lithology and fluid type are known then the sonic log can be used as another estimate of porosity (Figure 2.11). This technique is based on the propagation of sound waves in the reservoir rock matrix and fluid-filled pores. Sonic tools measure several formation sonic parameters like compressional & shear velocities and travel time using both monopole and dipole transmitters & receivers. It is used to: Find porosity, identify lithology, gas detection, study rock mechanical properties, anisotropy analysis, seismic correlation & AVO study, and Hydro-fracture evaluation. Typically, high porosity formations correspond to high transit times, and low porosity formations correspond to low transit times. Table 2.4 provides examples of *P*-wave transit time and velocity in a selection of reservoir rock types (Tang, Zheng, & Patterson, 2007).

Table 2.4: Typical Values of the Interval Transit Time of Hydrocarbon Reservoir Formation (Albakr, Abd, Hasan, & Al‐Sharaa, 2022)

Rock Type (no porosity)	Velocity(ft/sec)	Transit time(μsec/ft)
Sandstone	18,000-19,500	56-51
Limestone	21,000-23,000	48-44
Dolomite	23,000	44
Anhydrite	15,000	50
Salt	17,500	66
Shale	5,880-16,660	170-60

The measurement of compressional and shear wave slowness can help us estimate the Primary porosity, Lithology, and Presence of natural gas. Wyllie developed a relationship between porosity and *P*-wave transit time for clean unconsolidated

formations with uniformly distributed small pores, referred to as the Wyllie (Equation 2.12) (Saleh & Castagna, 2004).

$$t_{log} = t_{ma}(1 - \emptyset) + t_f\emptyset \qquad 2.12$$

The Wyllie linear time-averaged equation approximated porosity ($\emptyset$) as given in equation 2.13

$$\emptyset = \frac{t_{log} - t_{ma}}{t_f - t_{ma}} \qquad 2.13$$

Where (t_{log}) is sonic response interval transit time, (t_{ma}) is the response for the rock matrix, and (t_f) is the response for the fluid.

Figure 2.12 shows many logs including the sonic log that can also be applied in estimating porosity of the formation.

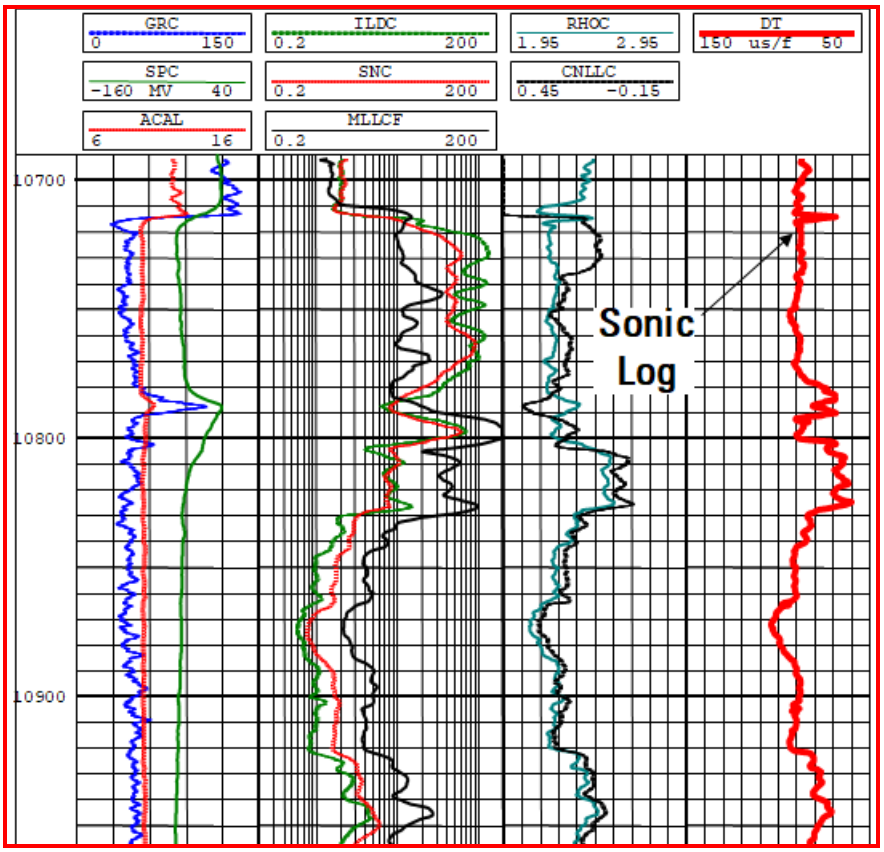

Figure 2.12: Acoustic Logging Modified from (Tang et al., 2007)

2.3.4 Reservoir Characterization

Reservoir characterization is the process of evaluating reservoir qualities (such as thickness, depth, pore fluid, porosity, shale volume, water saturation, and permeability) to determine its producibility effectively (Munyithya et al., 2020). In general, there are two types of reservoir characterizations, namely static characterization and dynamic characterization. Static characterization determines reservoir rocks' properties in a given area and therefore improves the understanding of the spatial reservoir layer parameters distribution and their environments. On the other hand, Dynamic characterization deals with the analysis of the evolution of reservoir properties in evaluating existing fluids over time (Oumarou et al., 2021).

Petroleum reservoirs may contain oil, natural gas, or both. Their important properties include pay zone thickness, lithology, rock porosity, rock total compressibility, and rock permeability. These properties affect fluid flow within the reservoir and thus well productivity. Some of the key properties studied in petrophysics are lithology,

porosity, water saturation, permeability, and density. A key aspect of petrophysics is measuring and evaluating these rock properties by acquiring well-log measurements (in which a string of measurement tools are inserted in the borehole), core measurements (in which rock samples are retrieved from the subsurface), and seismic measurements. These studies are then combined with geological and geophysical studies and reservoir engineering to give a complete picture of the reservoir (Naseer & Asim, 2018).

2.3.4.1 Reservoir Identification

The most reliable indicator of reservoir rock will be from the behaviour of the density-neutron logs, with the density moving to the left (lower density) and touching or crossing the neutron curve. In the clastic reservoirs in nearly all cases, this will correspond to a fall in the GR log. However, in a few reservoirs, the GR is not a reliable indicator of sand, due to the presence in sands of radioactive minerals. Shales can be identified as zones where the density lies to the right of the neutron, typically by 6 or more neutron porosity units. The greater the crossover between the density and the neutron logs, the better the quality of the reservoir. Generally, gas zones exhibit a greater crossover for a given porosity than oil or water zones (Darling, 2005).

2.3.4.2 Formation Evaluation

Formation evaluation (FE) is the process of interpreting a combination of measurements taken inside a wellbore to detect and quantify oil and gas reserves in the rock adjacent to the well. Formation evaluation data can be gathered with wireline logging instruments or logging-while-drilling tools. Data organized and interpreted by the depth and represented on a graph called a log is used in the study of the physical properties of rocks and their fluid content (Welte & Tissot, 1984).

2.3.4.3 Petrophysical Analysis

The petrophysical analysis is carried out to determine the various parameters such as the formation temperature, water resistivity, volume of shale, effective porosity,

water saturation, and hydrocarbon saturation using empirical petrophysical relations (Avseth, Mukerji, & Mavko, 2010). The separation in the combined Neutron-Density logs indicates the lithology, whereas the average indicates porosity (Ijasan et al., 2013). Crossing over of Neutron-Density logs with high resistivity responses concurrently indicate hydrocarbon bearing zones at low gamma-ray section. The separation in a reservoir zone indicates the presence of a gas (gas effect) (Oladele et al., 2019).

2.3.4.3.1 Formation Temperature

Different regions have different specific temperature gradients that are determined by either the regional tectonic or geologic activity. The amount of activity is directly proportional to the geothermal gradient. The common unit of expressing geothermal gradients is degrees Celsius per kilometre (^{0}C/km). Where the geothermal gradient is unknown, a chart or formula can be used in determining it as shown in equation 2.14.

$$g_G = \left(BHT - \frac{T_{ms}}{TD} x100\right) \qquad 2.14$$

Where g_G is the geothermal gradient, BHT is the bottom hole temperature (from the header), TD is total depth (Depth-Logger from the header), and T_{ms} the mean surface temperature.

Once the geothermal gradient (g_G) has been established, it is possible to determine the temperature for a particular depth. This is often referred to as formation temperature (T_f) as in equation 2.15.

$$T_f = T_{ms} + \left[g_G \left(\frac{D}{100}\right)\right] \qquad 2.15$$

Where T_{ms} is the mean surface temperature, g_G the geothermal gradient, and D the depth at which temperature is desired.

2.3.4.3.2 Water Resistivity

Equations 2.16, 2.17, and 2.18 shows the formulae for estimating the water resistivity, water resistivity at room temperature, and water resistivity at formation temperature respectively.

$$R_w = \phi^m R_t \tag{2.16}$$

At room temperature,

$$R_{wT} = 0.123 + \frac{3647.5}{S^{0.995}} \tag{2.17}$$

At a given formation temperature,

$$R_{wT_2} = R_{wT}\left(\frac{T+6.77}{T_2+6.77}\right) \tag{2.18}$$

Where R_w is water resistivity, R_t formation resistivity, ϕ^m porosity, R_{wT} water resistivity at room temperature, R_{wT_2} water resistivity at formation temperature, S salinity in ppm, T room temperature, and T_2 formation temperature.

2.3.4.3.3 Shale Volume

This second step could be done by using a gamma ray log, Larionov proposed two formulae to calculate the shale volume (Larionov, 1969), and they include:

Larionov (1969) for tertiary rocks (Equation 2.19):

Unconsolidated rocks,

$$V_{sh} = 0.083(2^{3.7 \times I_{GR}} - 1.0) \tag{2.19}$$

Larionov (1969) for older rocks (Equation 2.20):

Consolidated rocks,

$$V_{sh} = 0.33(2^{2\times I_{GR}} - 1.0) \quad 2.20$$

The gamma-ray index can be determined using Equation 2.21

$$I_{GR} = \frac{GR_{log} - GR_{min}}{GR_{max} - GR_{min}} \quad 2.21$$

Where I_{GR} is the gamma-ray index, GR_{log} the actual borehole corrected GR response in a zone of interest, GR_{min} the minimum borehole corrected GR response against clean zones, and GR_{max} the maximum borehole-corrected GR response against shale zones.

Calculating shale volume is an important thing to do because, it can be useful to calculate the water saturation, if the reservoir has shale within its body (shaly) such as in the delta, that reservoir may have higher water saturation because shale can bound together with water which will increase the water saturation. Shale volume could also be used as an indicator of the zone of interest or not, many users usually will not classify a formation with high shale volume as a reservoir.

2.3.4.3.4 Porosity

Porosity, being the space or void inside the rock, is very useful to store geophysical fluids such as water, gas, and oil. Permeability transmits the fluids due to pressure difference i.e. from high to low pressure. Porosity calculation is correctly done if the first step (lithology interpretation) is correct. Porosity calculation can be done using many methods including neutron log, sonic log, density log, or a combination of any two, the most common one being combining neutron-density log (Minigalieva et al., 2018).

Some of the formulae that may be used include equations 2.22 and 2.23.

$$\emptyset_{T_{sh}} = \frac{\rho_{ma} - \rho_{sh}}{\rho_{ma} - \rho_f} \qquad 2.22$$

$$\emptyset_E = \emptyset_T - \left(\emptyset_{T_{sh}} \times V_{sh}\right) \qquad 2.23$$

Where $\emptyset_{T_{sh}}$ is the shale-derived porosity, $\emptyset_E$ the effective porosity, $\emptyset_T$ the total porosity, ρ_{ma} the matrix density, ρ_{sh} the bulk density (density log reading in the zone of interest), ρ_f the fluid density (density log reading in 100% water), and V_{sh} the volume of shale.

The average of neutron and density porosities gives the correct actual porosity regardless of lithology. The cross-plot porosity is the average neutron-density porosity. The advantage of the limestone scale is that the separation tells you the lithology and the average tells the porosity.

2.3.4.3.5 Water Saturation

Water saturation would be estimated from Archie's equation (Equation 2.24). To estimate water saturation from this method, Formation water resistivity (Rw) and True formation resistivity (Rt) need to be estimated. Rw is usually estimated in a clean water-bearing interval (water log) while Rt is estimated in hydrocarbon-bearing zones using deep resistivity reading. Hydrocarbon saturation is obtained from the determined water saturation using equation 2.25.

$$S_W = \left(\frac{a \times R_W}{R_t \times \emptyset_t^m}\right)^{\frac{1}{n}} \qquad 2.24$$

$$S_H = 1 - S_W \quad 2.25$$

Where S_H is the hydrocarbon saturation, S_W the water saturation, a the tortuosity factor, m the cementation exponent, n the saturation exponent, R_w the formation water resistivity, R_t the formation resistivity, and $\emptyset_t^m$ the calculated porosity.

2.3.5 Rock Physics Analysis

Rock physics creates a link between geophysical observable to geological parameters which is an important part of reservoir characterization (Golyan, 2012). For a successful exploration and production of hydrocarbons, it is imperative to characterize the hydrocarbon reservoir accurately in terms of its fluid properties and lithology. Various rock physics models have their benefits and limitations (Rasaq et al., 2015). Rock Physics models are important for quantitative seismic interpretation and reservoir characterization which increases the chances of success in hydrocarbon exploration. One of the most powerful uses of rock physics is extrapolation. The seismic reflections are physically explained by contrasts in elastic properties, and rock physics models allow us to link seismic properties to geologic properties. Hence, the application of rock physics models can guide and improve qualitative interpretation (Avseth et al., 2010). A disturbance of the earth generates shear and compressional waves whose velocity of travel depends on the rock's elastic properties. The compressional (Vp) and shear (V_s) propagation velocities are determined from equations 2.26 and 2.27.

$$V_p = \sqrt{\frac{\lambda+2\mu}{\rho}} \quad 2.26$$

$$V_s = \sqrt{\frac{\mu}{\rho}} \quad 2.27$$

Where ρ is the density, μ is the rigidity, and λ is the incompressibility of the medium of the wave propagation. Equations 2.26 and 2.27 above indicate that the reservoir rock propagation velocities are affected by the rock matrix, fluid saturation, and porosity. The secondary velocity (Vs) can also be generated using Greenberg and Castagna relation for sandstones as shown in equation 2.28 (Castagna, Batzle, & Eastwood, 1985).

$$V_s = 0.8042V_p - 0.8559 \qquad 2.28$$

The derived rock attributes such as velocity ratio, lambda-rho, acoustic impedance, and mu-rho, can be computed using standard rock physics equations (Rider, 1986). The use of the ratio of compressional wave velocity to shear wave velocity, Vp/Vs, is a good tool for identifying the fluid type. The fact that compressional wave velocity decreases and shear wave velocity increases with the increase of light hydrocarbon saturation, makes the ratio of Vp/Vs more sensitive to the change of fluid type than the use of Vp or Vs separately (Hamada, 2004). The velocity ratio, V_p/V_s, is expressed as shown in equation 2.29.

$$\frac{V_p}{V_s} = \sqrt{\frac{\lambda+2\mu}{\mu}} \qquad 2.29$$

The P-Impedance (ρV_p) and the S-Impedance (ρV_s) are useful in deriving the Lambda-rho ($\lambda\rho$) and Mu-rho ($\mu\rho$) as shown in equations 2.30 and 2.31.

Lambda-Rho ($\lambda\rho$) is derived from squaring both sides of equation 2.26 to obtain

$$\lambda\rho = (\rho V_p)^2 - 2(\rho V_s)^2 \qquad 2.30$$

Mu-rho is derived from squaring both sides of equation 2.27 to obtain

$$\mu\rho = (\rho V_s)^2 \qquad 2.31$$

The rock physics cross-plots are utilized in delineating lithology and fluid prediction and also to give an insight into the degree of cementation within the reservoirs. Cross plots are visual representations of the relationship between two or more variables, and they are used to visually identify or detect anomalies that could be interpreted as the presence of hydrocarbon or other fluids and lithologies (Bodunde & Enikanselu, 2019);(Rasaq et al., 2015). Lambda-Rho is a measure of incompressibility; therefore, low values indicate hydrocarbon-saturated zones since hydrocarbon density and velocities are lower than other geofluids such as water. Mu-Rho is a measure of rigidity; therefore, it will be higher in reservoir zones since sands that make up reservoirs have generally higher acoustic impedance than lithologies such as shale (Oladele et al., 2019).

2.3.6 Fluid Substitution

Fluid substitution is used to estimate changes in the elastic properties of porous media caused by changes in pore fluids. The fluid substitution process employs Gassmann's relations (1951) in predicting saturated rock properties from dry rock properties (Azeem et al., 2017), which gives the relationship between bulk modulus of saturated rock, dry rock modulus, pore fluid, and solid matrix (Mavko, Mukerji, & Dvorkin, 2020).

$$\frac{K_{sat}}{K_{min}-K_{sat}} = \frac{K_{dry}}{K_{min}-K_{dry}} + \frac{K_{fluid}}{\emptyset(K_{min}-K_{fluid})} \qquad 2.3.2$$

$$\mu_{sat} = \mu_{dry} \qquad 2.3.3$$

Where;

K_{sat} – Effective bulk modulus of the porous rock with fluid (oil, gas, or water)

K_{dry} – Effective bulk modulus of the dry porous rock

K_{min} – Bulk modulus of the minerals which compose the rock

K_{fluid}– Effective bulk modulus of the fluids contained in the porous rock

$\emptyset$ – Rock porosity

μ_{sat} – Effective shear modulus of the porous rock with fluid (oil, gas, or water)

μ_{dry} – Effective shear modulus of the dry porous rock

Gassmann's equation is applied on the assumption that the rock is isotropic and homogenous with a complete pore system connection (Smith, Sondergeld, & Rai, 2003). Its results are reliable when applied in the clean sand zone with high effective porosity. The model requires the acoustic properties (Vp, Vs, and bulk density) as the input parameters while the rock shear modulus (μ), frame, or dry rock modulus (K_{dry}), and the matrix bulk modulus (K_{min}) remain constant during the fluid substitution modelling process (Magoba & Opuwari, 2020).

2.3.7 Basin and Petroleum System Modelling

2.3.7.1 Basin Modelling

Basin modelling is constituted by the modelling of the various geological processes over a long period, in the geological time scale, within a given sedimentary basin (Hantschel & Kauerauf, 2009). Through basin modelling, petroleum systems can effectively be investigated in a given sedimentary basin (Poelchau *et al.*, 1997). This can be achieved with the help of computer software whereby the thermal and burial evolution history of a sedimentary basin and the geodynamic processes can be simulated and reconstructed. Examples of geodynamic processes include the maturation and generation of organic matter, expulsion from source rocks, migration through pathways, accumulation in the reservoir, and preservation of hydrocarbons within the traps (Waples, 1994).

In hydrocarbon exploration preliminaries, risks in exploration can be effectively assessed through basin modelling by simulating petroleum system geodynamic processes linking it to the evolution of basins which is complex (Figure 2.13) (Poelchau, Baker, Hantschel, Horsfield, & Wygrala, 1997). Basin modelling has had a previous successful application in building velocity models because of its ability to simulate the impact of geohistory on petroleum systems over time (Brevik *et al.*, 2014). A basin model in existence is a representation of an already-made investment and can be utilized to translate a given velocity model to geohistory (Szydlik *et al.*, 2015).

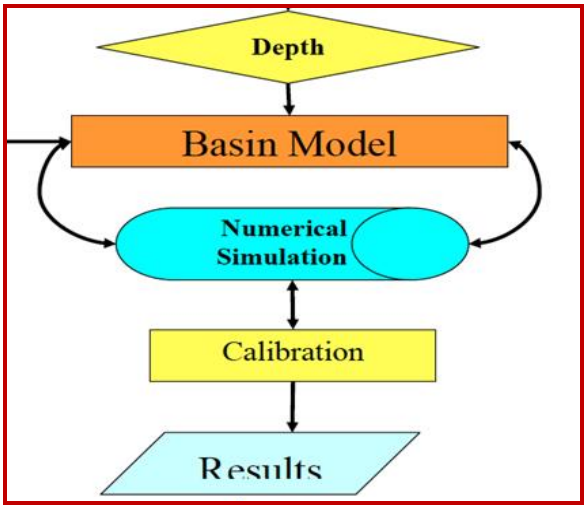

Figure 2.13: Modelling Workflow (Ben-Awuah et al., 2013)

In petroleum exploration, the highly effective technique is the integration of seismo-tectonics and seismic stratigraphy (Martinelli, 2010). This helps in coming up with a tectonostratigraphic template useful in petroleum system modelling. Modelling helps in the evaluation of the potential of the elements of a petroleum system (Nanda, 2016).

2.3.7.2 Petroleum System Modelling

A network of mature source rocks, migration channels, reservoir rocks, and trapping and seal rocks in a geologic system constitute petroleum system elements. The combination of petroleum system elements and geologic processes such as hydrocarbon generation, migration, and accumulation defines a petroleum system

and determines the existence of accumulated hydrocarbon in a given geologic environment (Figure 2.13) (Magoon & Dow, 1994). In petroleum systems model simulation of a network of processes and the related outcome is done to have an understanding and prediction of the various scenarios (Hantschel & Kauerauf, 2009). A petroleum systems model may be built in one, two, or three dimensions (Higley, Lewan, Roberts, & Henry, 2006).

Petroleum system models require geochemical and petrophysical characterization of the sedimentary formations in conjunction with boundary conditions that include basal heat flow, sediment-water interface temperature, and Paleo-water depth. Petroleum systems modelling software is used to integrate all the information at hand to yield a range of scenarios in which the conditions of the petroleum system could have evolved in the past. The final phase of the BPSM is the forward modelling that simulates the history of burial, temperature and pressure variations, maturation of Kerogen, the expulsion of hydrocarbons, hydrocarbon migration, and accumulation over time by performing model calculations. To run the forward modelling simulation, a combined Darcy/ Flow path is selected (Busanello et al., 2017).

Model building and forward modelling are the two stages in modelling Basin and petroleum systems. In the Model building stage, structural models are constructed, deposition chronology identified and layer properties noted. In the forward modelling stage, simulation of sediment burial, temperature and pressure variations, maturation of Kerogen, the expulsion of hydrocarbons, and migration and accumulation of hydrocarbons is achieved through model calculations. The model is refined through calibration whereby model results are compared with standard measurements. BPSM, which can reduce risk in exploration, incorporates a wide range of geoscience data and therefore has gained popularity among integrated exploration companies and can be used to predict the presence, types, and volumes of hydrocarbons (Peters *et al.*, 2009).

Petroleum System Analysis is the evaluation and understanding of all the necessary geological elements (Source Rock, Reservoir Rock, Cap Rock (Seal), and Overburden Rock) and processes (Trap Formation, Generation, Migration &

Accumulation of hydrocarbons) comprehensively for petroleum accumulation, and preservation. For hydrocarbon to be accumulated and preserved petroleum system elements and processes must be prerequisites and both trap formation and seal capacity acquirement must be completed before hydrocarbon expulsion and migration. Petroleum system modelling addresses questions of source rock maturity, expected hydrocarbon quality, expected hydrocarbon type, the effect of uncertainties, future investments as well as constraining geological conditions necessary for a successful charge. The critical moment of the petroleum system is the time that best depicts the generation, migration, and accumulation of hydrocarbon in a petroleum system. Prerequisite to the critical moment, the source, reservoir, seal, and sufficient amount of overburdened rocks must be in place (Saputra & Ohara, 2016);(Higley et al., 2006);(Neumaier, 2016).

In Figure 2.14 (a) favourable timing for the accumulation of generated hydrocarbons is indicated. It is evident that by the time hydrocarbons were migrating in the middle of the Cretaceous (K), many traps had formed and were available to capture fluids. (Al-Hajeri *et al.*, 2009).

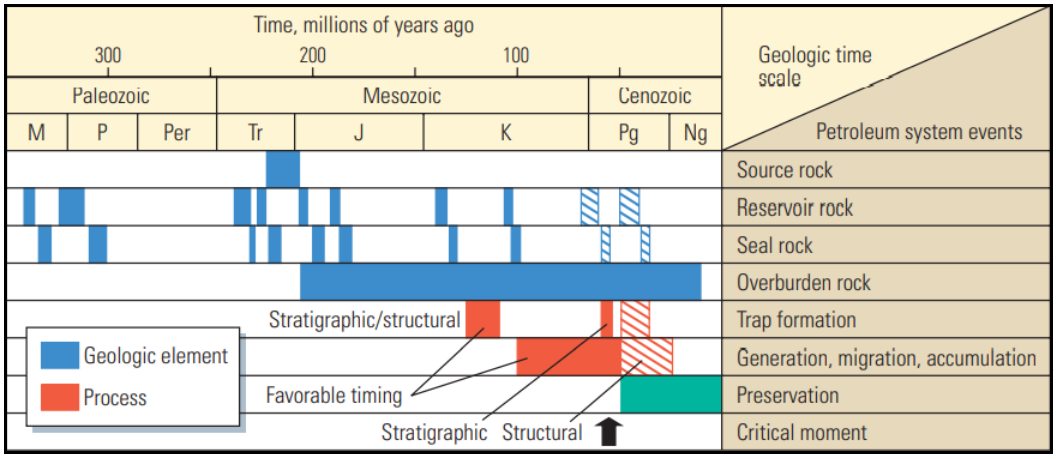

(a)

In Figure 2.14 (b) events were not as favourably timed. Although traps may have formed too late to contain oil and gas generated in the Cretaceous, they might have formed in time to hold remigrating fluids, or those displaced from other areas (hatched).

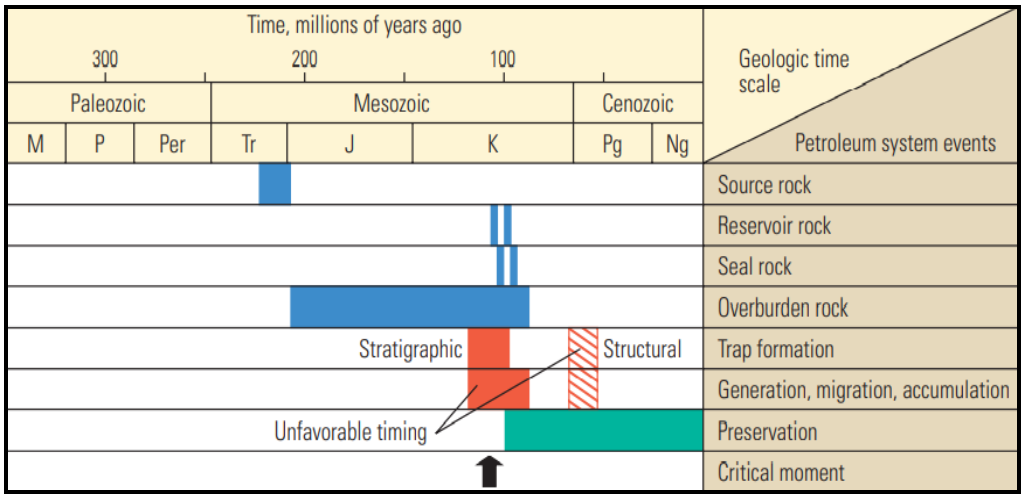

(b)

Figure 2.1: Event Chart Comparison (Al-Hajeri et al., 2009).

Figure 2.15 shows the basin and petroleum system workflow starting from geophysical interpretation of the gravity and seismic data, well log analysis, using geochemical data in developing the petroleum system model, model calibration, and finally the output.

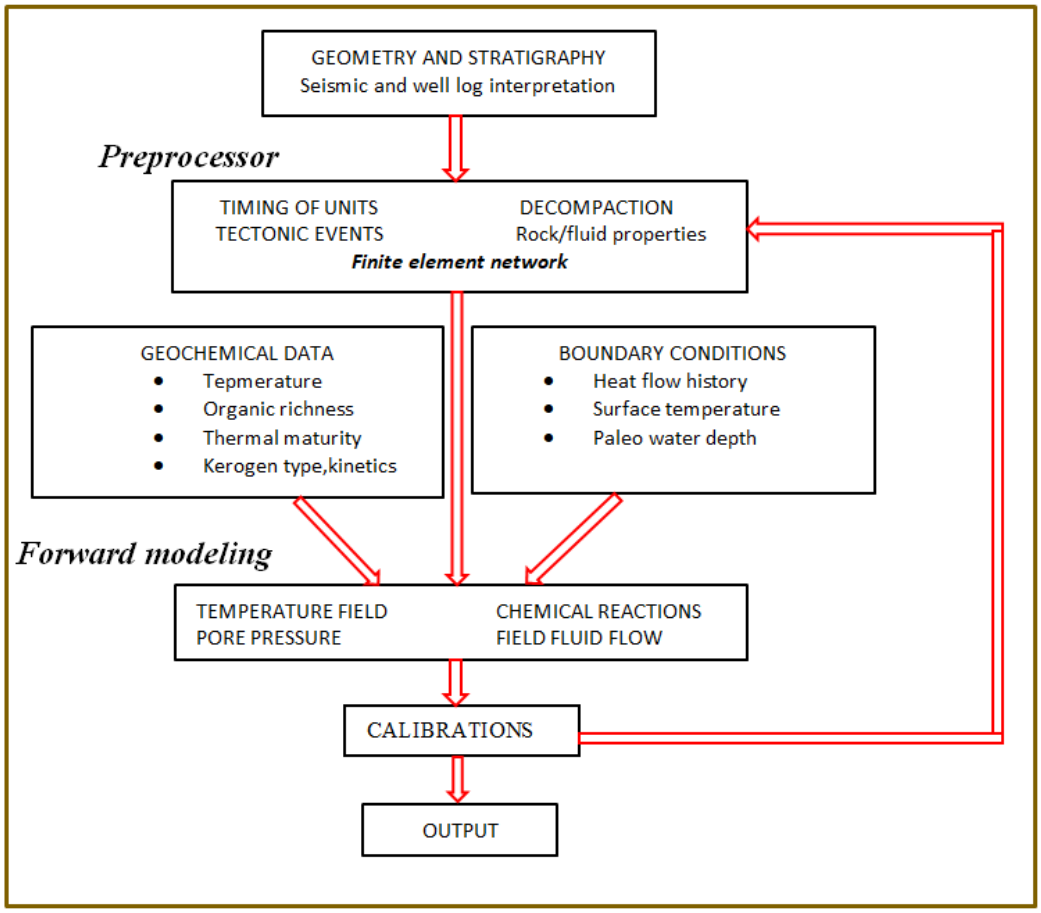

Figure 2.15: Process Workflow Diagram for Basin and Petroleum System Modelling (Modified from Peters *et al.*, 2009)

CHAPTER THREE

MATERIALS AND METHODS

Geophysical methods complement each other, for instance, Gravity and Seismics as seen in Figure 3.1. Figure 3.1(a) shows how uniquely potential field methods (gravity and magnetics) can pick horizontal variations of subsurface formations. The vertical layers cannot be effectively imaged using the seismic method. The limitation of the potential field methods is indicated in Figure 3.1(b) which also depicts the unique applicability of the seismic method in picking vertical variations and hence imaging the anomalies.

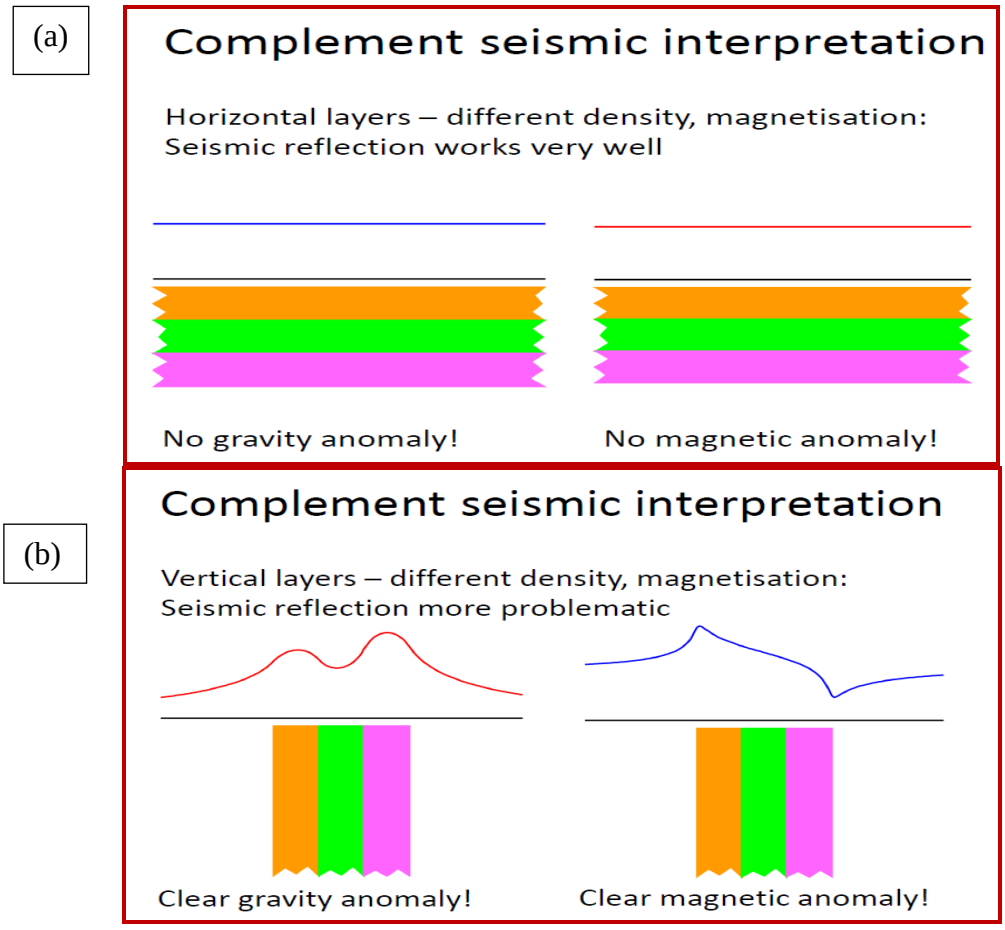

Figure 3.1: The Unique Application of the Geophysical Methods (Fairhead, 2016)

3.1 Materials

This research project used the following Data and software

a) Gravity data
b) 2D Seismic Data
c) Four vertical wells (Kubwa-1, Mbawa-1, Pomboo-1, and Simba-1)
d) Well logs (Triple combo)
e) Specified reports on data acquisition, well completion, and area geology
f) Geochemical data
g) Softwares (Oasis Montaj, Petrel, Techlog, Petromod)

3.1.1 Gravity Data

The data used in this study were sourced from the International Gravity Bureau (BGI), National Oil Corporation of Kenya digital data courtesy of companies like Woodside Energy, Anadarko Kenya Limited, and Total Exploration and Production companies. In the reduction of the data, the Global relief model (ETOP01) and the geopotential model (EGM2008) were applied. Included in the geopotential model (EGM2008) are measurements from satellite gravimetry (GRACE mission), satellite altimetry, and surface gravity (from land, marine, or airborne surveys). The topography and bathymetry data (elevation data) used are from the Global relief model (ETOP01) (Bonvalot *et al.*, 2012) and (Balmino *et al.*, 2012). The data given was numerical reduced data. The various datasets were merged within the Oasis Montaj software.

The computation of all the gravity anomaly grids and maps was done at the atmosphere's lower limit (earth's surface) with a resolution of 1'×1' (meaning one pixel on the image equals one pixel on the screen). The Bouguer and Isostatic anomaly maps' reference density used is 2670 Kg/m^3. The spherical harmonic gravity coefficients for the compensation of all relief components for the Airy-Heiskanen Isostatic model with a constant compensation depth of T_c=30km were applied (Balmino *et al.*, 2012).

3.1.2 Seismic Data

The data used in this study were sourced from the National Oil Corporation of Kenya digital data centre. During the acquisition of 2D seismic data, a 6000 m long streamer with 480 channels having a group interval of 12.5 m and a shot point interval of 25 m was used at an operating depth of 8m. The source depth was 6 m with an operating pressure of 2000 psi and data was recorded at a sample rate of 2 ms with a record length of 8000 ms. In the 3D marine acquisition, a single vessel, dual source, and multiple streamers (8) technique was employed maintaining a source separation of 50 m operating at a depth of 6 m with an air pressure of 2000 psi hence generating a signal at a sample rate of 2 ms with a recording length of 6000 ms. The data set includes a total of 9 lines (7 2D lines by Woodside Energy (Woodside, 2007) and 2 extracted from 3D by Origin Energy (Origin, 2009) covering a total length of approximately 1042 km (Figure 3.2). The quality of the 2D seismic data is fair and the seismic data extracted from the 3D cube is fairly good.

3.1.3 Well Log Data

Well-log measurements were done to give information on the likely type and amount of available hydrocarbon in a geological environment. This can be applied in fracture detection, determination of reservoir pressure, distribution of pore sizes and porosity, and reservoir fluid movement monitoring. Information from four offshore wells (Kubwa-1, Mbawa-1, Pomboo-1, and Simba-1) (Figure 3.2) was received and quality checked. It was noted that Simba-1 well lacked the log information and therefore could not be considered for characterization. The quality check shows that the rest of the four wells have data with the basic required logs (Triple/Quad Combo), necessary for formation evaluation and reservoir characterization. The logs include Gamma Ray (GR) in API units, Resistivity (RT) in Ohm-m, Sonic (Vp) in m/s, Density (RHOB) in g/cm^3, and neutron log (NPHI) in fraction. All the wells are vertical wells separated by huge distances (up to 100 km) and having depths ranging from 3150 m-5887 m.

3.1.4 Reservoir Characterization

Reservoir characterization involved reservoir identification, formation evaluation, petrophysical analysis, and rock physics analysis. Identification of reservoirs combined the GM SYS gravity models, interpreted seismic sections, and well logs inspection. Reservoir properties were obtained from the formation evaluation and petrophysical analysis results. The lithology and fluid content discrimination was achieved through rock physics analysis.

3.1.5 Geochemical Data

The geochemical characteristics of the petroleum source rocks analyzed include TOC (Appendix IV), Vitrinite reflectance (R_0), Kerogen Macerals analysis, visual Kerogen, and hydrocarbon content. Geochemical analyses of Kubwa-1(Appendix VII) and Mbawa-1 (Appendix VI) samples were done by Weatherford laboratories. Geotech laboratories carried out the analysis for Pomboo-1 (Appendix VIII) samples and Core laboratories analyzed samples from Simba-1 well. Rock–Eval pyrolysis was performed for 254 samples consisting of 52 from Mbawa-1 (Appendix VI), 107 from Simba-1, 64 from Kubwa-1 (Appendix VII), and 31 from Pomboo-1 (Appendix VIII).

3.1.6 Petroleum System Modelling Data

The purpose of the model and the dimension determines the types of data used in building a model. The main input data for the model building include the Chronostratigraphy, lithology, and source rock properties. The boundary conditions at the model building stage used are the paleo water depth, sediment-water interface temperature, and heat flow. In the study of properties through geologic time at a well location, well data was used to give the timing of play elements at a specific location such as a well. Interpreted seismic surfaces were used in the study of properties at present-day and represented as a map to show the spatial distribution of play elements.

3.1.7 Softwares Used

Three softwares employed for this study, with the specific tasks, were Geosoft Oasis Montaj version 6.4.2 for gravity data analysis and modelling, Schlumberger's Petrel 2017 for Seismic interpretation and BPSM modelling, and Schlumberger's Techlog 2015 for Reservoir characterization (petrophysical analysis and rock physics analysis). Gassmann fluid substitution was achieved through the use of both Petrel and Techlog software.

3.1.8 Wells Considered

Figure 3.2 shows the wells considered in this study and their corresponding closest seismic lines. Mbawa-1 well is located in block L8 about 90 km offshore Kenya and it targeted the upper cretaceous deep water turbidite sand reservoirs. The Kubwa project is 84.4 km south of the Pomboo-1 well and 265 km northwest of Mombasa and is located in block L7. The primary target of Kubwa-1 is a series of stacked Upper Cretaceous (Maastrichtian) turbidite channels and fans deposited within lows created by tensional faulting in the deeper Campanian section. Pomboo-1 well located in block L5, approximately 60 km from the coast, and Simba-1 well located in block L9 were primarily structural test wells of the upper Cretaceous section.

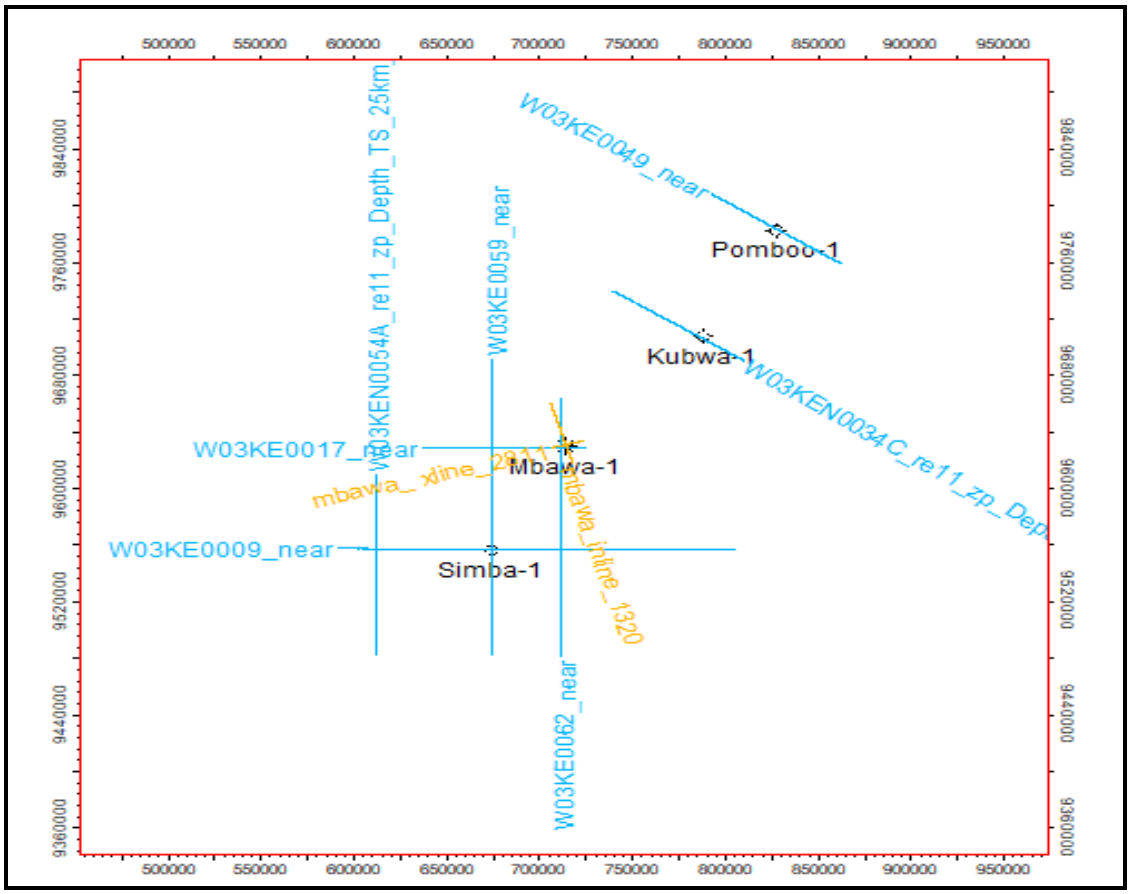

Figure 3.2: Base Map with the Wells Used and their Closest Seismic Lines

3.2 Methods of Study

The main methods in this study include gravity and seismic methods for regional structural interpretation, petrophysics and rock physics for reservoir delineation and characterization, and petroleum system modelling for source rock characterization and understanding the occurrence of the petroleum system elements and processes necessary for hydrocarbon accumulation as seen in the schematic diagrams in Figures 3.3 (a), (b), (c), and (d). Data presence and quality are checked, converted to software-compatible formats, and then imported into the respective software.

3.2.1 Gravity Maps, Spectral Analysis, and Models

Obtained reduced data was converted into comma separated value (CSV) format and imported into the Oasis Montaj database (Figure 3.3 (a)). The data was then gridded to produce the anomaly grids (Free air, Bouguer and Isostacy) which were

consequently plotted into maps as shown in the analysis and discussions of the result (section 4.1.1). The Isostacy anomaly map was then subjected to spectral analysis as a guide in the residualization process. This resulted in a residual map and a regional map showing residual and regional features respectively (section 4.1.2).

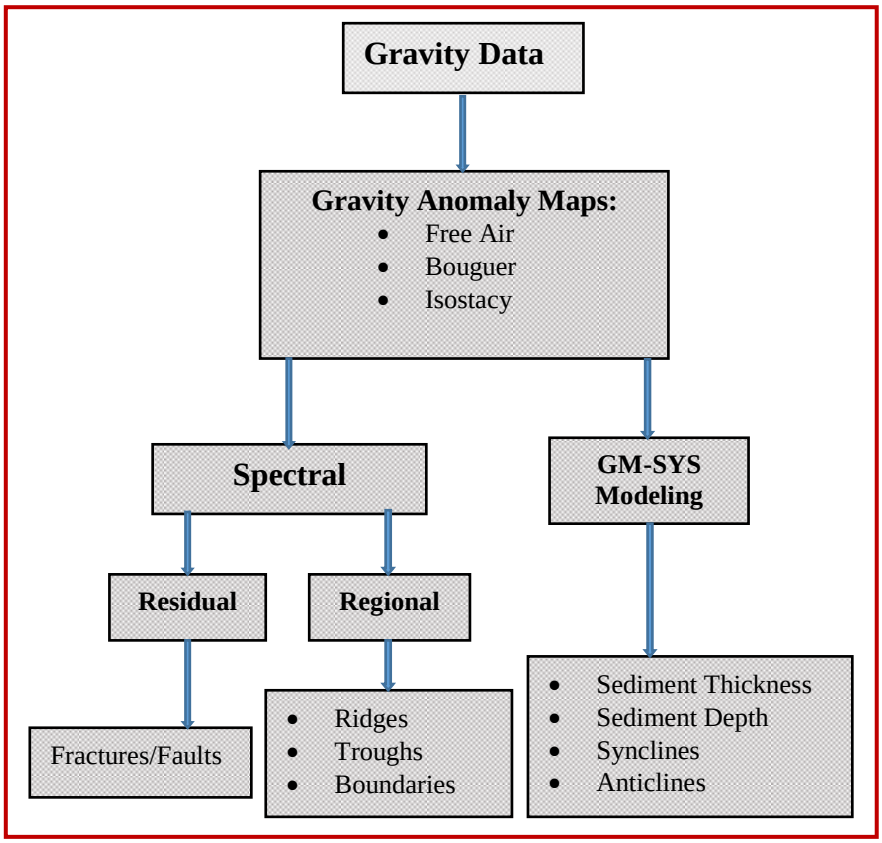

Figure 3.3 (a): Schematic Workflow for Gravity Data Interpretation

3.2.2 Seismic Sections, Well to Seismic Tie, Faults, and Horizons

In seismic interpretation, maps were made that provided geologic information and correlated the known elements of geology with the seismic data worked features. It involved the transformation of seismic data presented on seismic sections into geological information. The major steps involved in the interpretation workflow include a well-to-seismic tie, fault, and horizon interpretation, making surfaces and zonation, seismic attribute analysis, and petroleum system element identification (Figure 3.3(b)). Well-seismic ties allowed well data, measured in units of depth, to be compared to seismic data, measured in units of time hence relating horizon tops

identified in a well with specific reflections on the seismic sections. Sonic and density well logs were used to generate a synthetic seismic trace. The synthetic trace was compared to the real seismic data collected near the well location hence providing a link between geological and geophysical information.

Guided by the termination of reflections, offset in stratigraphic markers, and abrupt changes in seismic patterns, the faults were marked. Then Horizons, being surfaces that separate two rock layers that give rise to a seismic reflection according to the acoustic impedance contrast were traced. Horizons were correlated by recognizing and tracking continuous or changing patterns of reflection. From the interpreted faults and horizons, surfaces were made and zones marked.

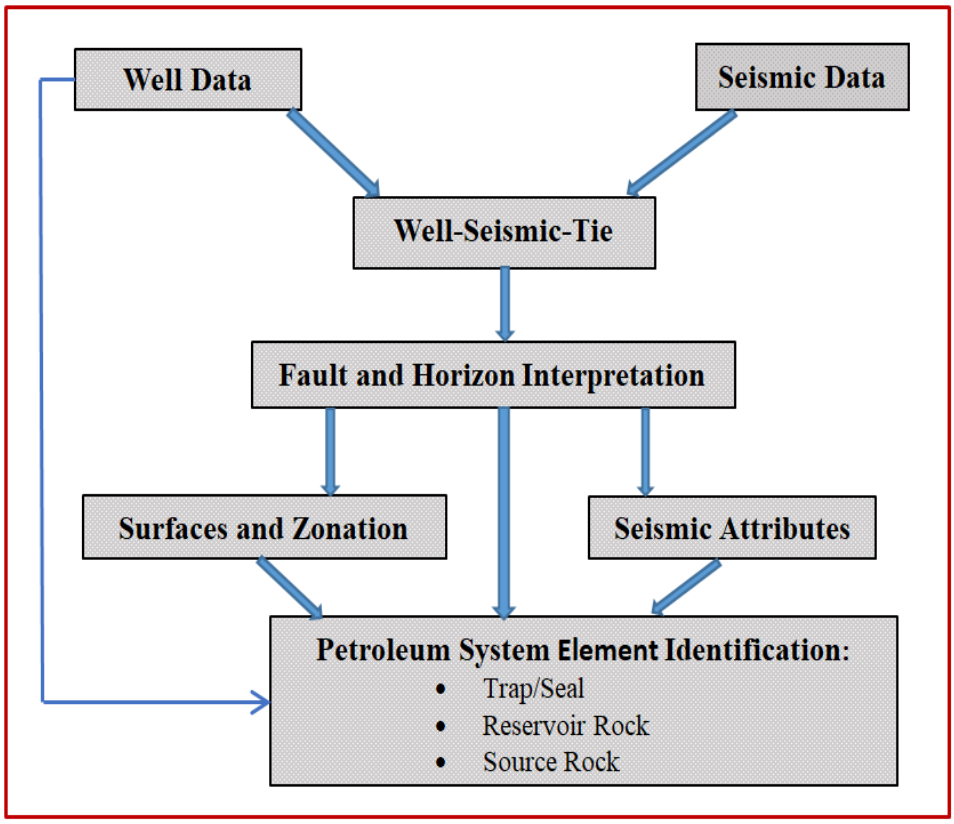

Figure 3.3 (b): Schematic Workflow for Seismic Data Interpretation

3.2.3 Seismic Attribute Analysis

Appropriate seismic attributes were used. Seismic attributes are mathematical descriptions of the shape or other characteristics of a seismic trace over specific time

intervals that enable interpreters to extract more information from the seismic data. Finally, the identification of petroleum system elements such as the traps/seal, reservoir, and source rock was done on the interpreted seismic sections.

3.2.4 Reservoir Characterization

Well logs consisting of G.R. in API units, Resistivity (R.T.) in Ohm-m, Sonic (V_p) in m/s, Density (RHOB) in g/cm^3, and Neutron log (NPHI) in fraction were used in the formation evaluation. Reservoir zones were delineated using both petrophysical and rock physics analyses. A reservoir was selected for analysis in each of the three wells from the delineated zones. Petrophysical properties (shale volume, effective porosity, water saturation, and net thickness) and rock physics model analysis contributed to characterizing the reservoir (Figure 3.3(c)). Integrating petrophysical and rock physics analyses improved the reservoir characterization whereby petrophysical analysis was leveraged to obtain the petrophysical parameters and identify lithology and the rock physics data cluster analysis aided in delineating lithology and discriminating reservoir fluids.

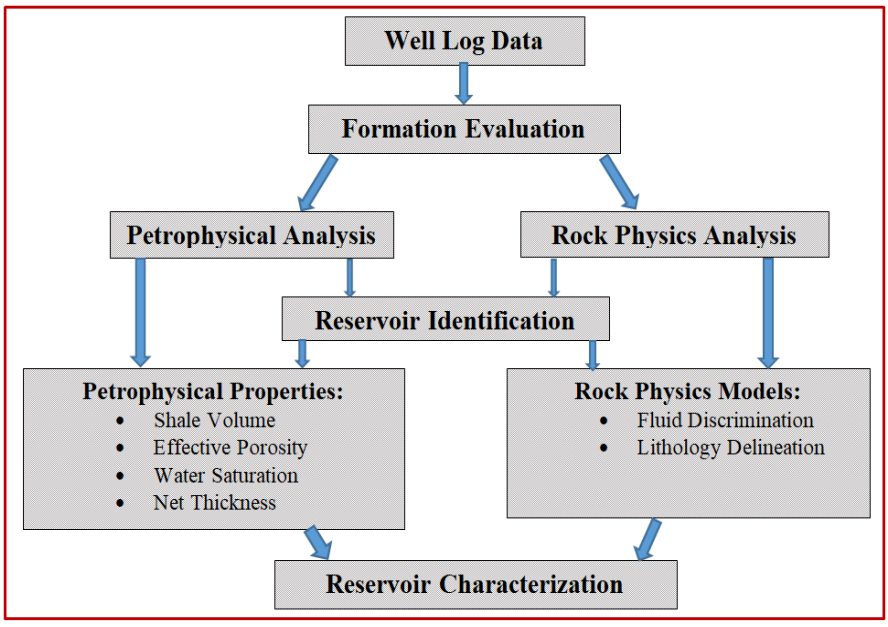

Figure 3. 3 (c): Schematic Workflow for Petrophysics and Rock Physics Analysis

3.2.5 Rock Physics Models

Quantitative analysis and interpretation of seismic data employed various rock physics models. This study employed some of the empirical models. The most commonly used empirical rock physics models include Gardner's relation which uses compressional velocity and density, Wyllie's equation relating compressional velocity and porosity, Han's relation which relates compressional velocity, porosity, and clay content, Greenberg–Castagna relation that uses compressional and shear velocity and finally Faust's relation relating resistivity and compressional velocity (Simm et al., 2014). The models were achieved through the use of cross plots. Cross plots are visual representations of the relationship between two or more variables, and they are used to visually identify or detect anomalies that could be interpreted as the presence of hydrocarbon or other fluids and lithologies (Rasaq et al., 2015).

3.2.6 Fluid Substitution

Gassmann fluid substitution was performed on the shallow marine reservoirs in the three studied wells to model the seismic velocity and density at different water saturation levels. Equations 2.3.2 and 2.3.3 were used within Petrel software under the advanced geophysics perspective, quantitative interpretation tab, and rock physics group to calculate the effects of fluid substitution on seismic elastic properties using the rock frame properties. The input parameters such as the dry porous rock frame's bulk modulus (K_{dry}), the pore fluid's bulk modulus (K_{fluid}), the mineral matrix's bulk modulus (K_{min}), and the porosity of the rock ($\emptyset$), were determined from the well log data and remained constant during the fluid substitution process. Porosity was determined from both well-log data and core data analyses. The primary inputs consisting of the compressional slowness ($1/V_p$), shear slowness ($1/V_s$), and bulk density (ρ) represented the saturated rock properties. In Techlog software, the Geophysics tab, rock physics group, Gassmann fluid substitution option, bulk density, total porosity, compressional slowness, and shear slowness logs were used as the input.

The measured elastic rock properties (compressional velocity, shear velocity and density) were used in the Schlumberger's software to determine the elastic moduli (K_{sat} and μ) according to the relations shown in equations 3.1 and 3.2.

$$K_{sat} = \rho\left(v^2{}_p - \frac{4}{3}v^2{}_s\right) \qquad 3.1$$

$$\mu = \rho v^2{}_s \qquad 3.2$$

The initial effective fluid properties (K_{fluid}) are computed according to the percentage mixing of the fluids (scenarios) calculated from petrophysical analysis. The software then transforms the elastic moduli (K_{sat}) from the initial fluid saturation to the dry state (K_{dry}) for each of the scenarios. New fluid properties are calculated when water saturation is set at 100 % (water as the only fluid in the pores). Shear modulus remains unchanged but density is transformed since the substituted fluid saturations affect it. Finally the new compressional and shear velocities are computed that give information about the seismic wave propagation response of various media.

3.2.7 Petroleum System Modelling (PSM)

Petroleum system modelling was applied in evaluating geological conditions necessary for a successful charge. The three major stages involved in petroleum system modelling include the making model stage, the numerical simulation stage, and the calibration/inferences stage (Figure 3.3(d)). Petrel software 2017 was used to integrate all the available information to produce a set of possible scenarios in which the conditions of the petroleum system could have evolved in the last 200 Myrs. Chronostratigraphy was set up and defined in the chronostratigraphic column

indicating the geological ages. Geological ages in million years were attached to events whereby two events build the frame for one period. The defined Chronostratigraphy and Facies were attached to a well. The definition of facies, constrained by period, was done in terms of lithological parameters. Source rock kinetics and properties (TOC and HI) were assigned (Appendix IV). Model boundary conditions including the paleo-water depth, sediment-water interface temperature, and heat flow were created. The paleo water depth (PWD) is the geometric boundary condition while the sediment-water interface temperature (SWIT) and the basal heat flow (HF) are the thermal boundary conditions. The petroleum system 1D model and the three types of time trends previously created were combined. Calibration of the models was done using Vitrinite reflectance (R_o), maximum temperature (T_{max}), and bottom hole temperature (BHT). The customizable output in the form of burial histories, depth curves, and/or time curves was set. The reaction kinetics used is the Sweeney and Burnham (1990) easy% R_o (Sweeney & Burnham, 1990) and the T_{max} model used is the pepper and Corvi (1995) _TIII (Pepper & Corvi, 1995). To run the forward modelling simulation, Darcy Flowpath was selected (Ombati, John, & K'Orowe, 2023).

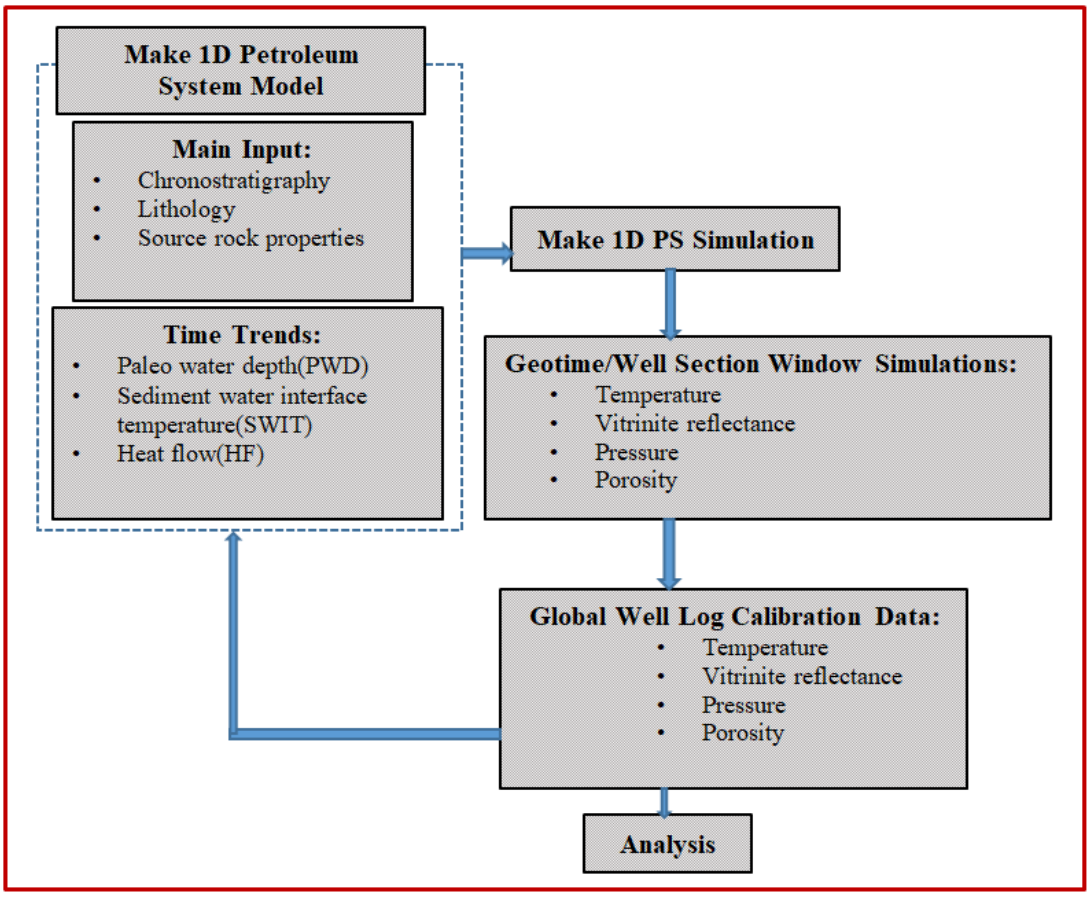

Figure 3.3 (d): Schematic Workflow for 1D Petroleum System Modelling.

CHAPTER FOUR

RESULTS ANALYSIS AND DISCUSSIONS

4.1 Gravity Results and Discussion

4.1.1 Gravity Anomaly Maps

The anomaly maps show regions of gravity highs (positive) and lows (negative) as shown in figures 4.1 (a), (b), and (c)

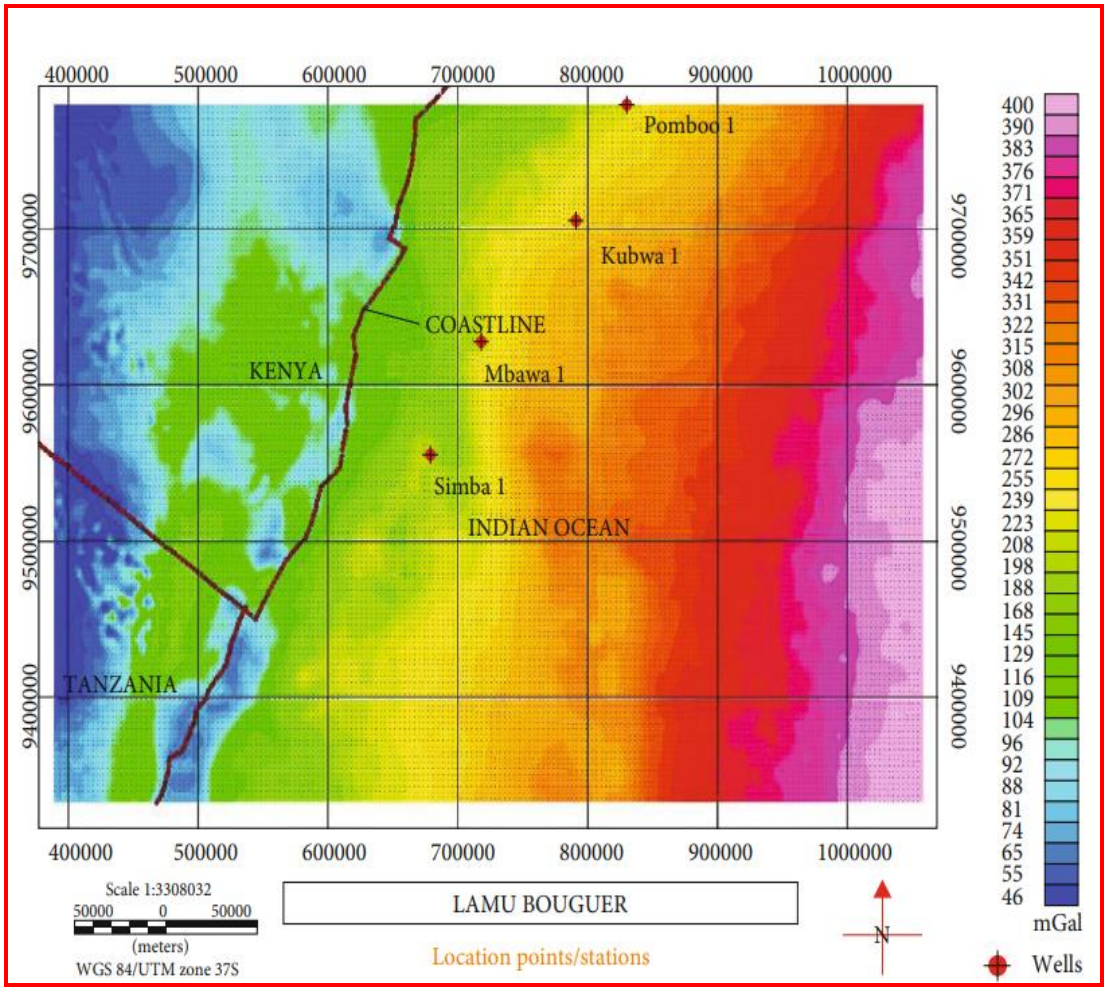

Figure 4.1 (a): Bouguer Anomaly Map

Notable from Figure 4.1 (a) is the increase in the Complete Bouguer Anomaly (CBA*)* values as you move from onshore to offshore. This is the regional effect that reflects the effects of the denser oceanic crust relative to the continental crust (Ekinci

& Yiğitbaş, 2015). Here the bathymetry-sourced anomalies have been removed but not Moho-sourced anomalies. Because of the effect of thick continental crust and thin oceanic crust, the gravity anomalies show negative and positive gravity signatures respectively (Ombati et al., 2022).

Similarly, from Figure 4.1(a), the Bouguer gravity anomaly map indicates that towards the land areas are low amplitude (negative) gravity anomalies while high amplitude (positive) gravity anomalies are seen to be dominating towards the deep sea. There is a high amplitude gravity anomaly as you go eastwardly with remarkable gravity value increasing trend in the same direction ranging from about 45.4 mGals to about 399.9 mGals due to the effects of the denser oceanic crust compared to the continental crust.

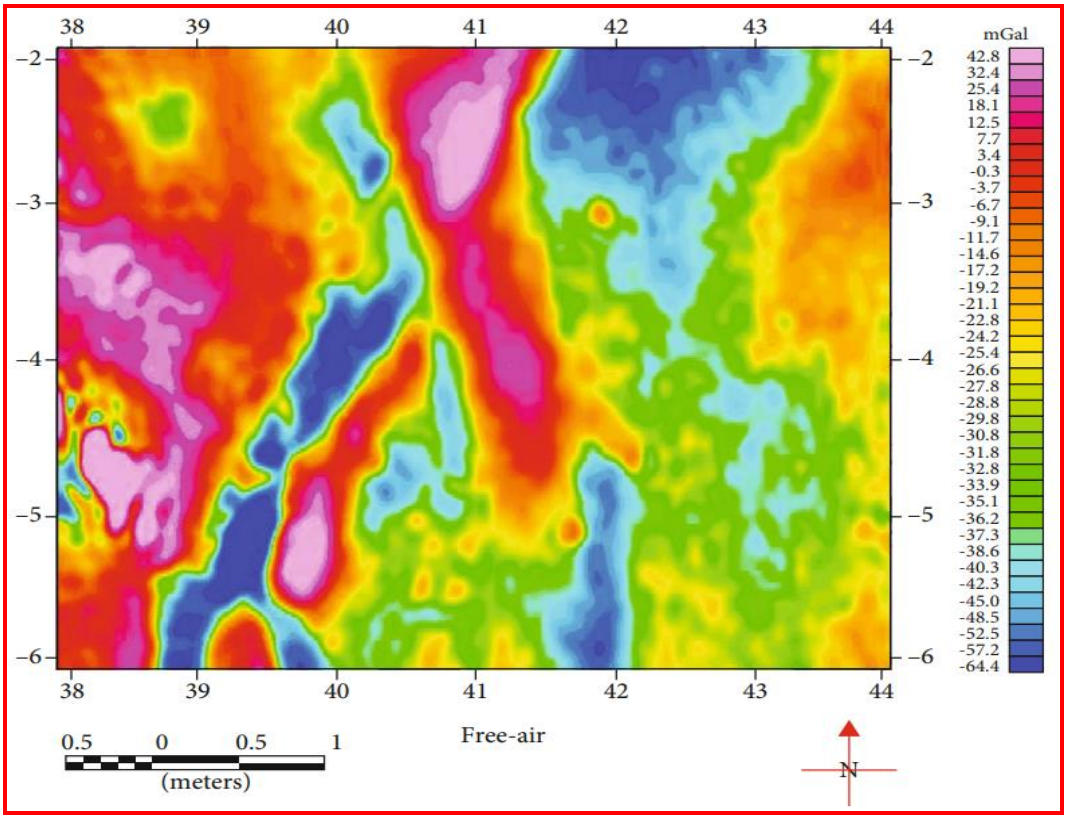

Figure 4.1 (b): Free-Air Anomaly Map (Ombati et al., 2022)

Figure 4.1(b) represents gravity observed data after being subjected to free air correction. This correction reduces the effects of elevation differences between measuring points and the geoid. It can be noticed from Figure 4.1(b) above that there is a variation of gravity anomaly amplitude across the study area with the central part of the figure showing promising features such as the troughs, faults/fractures, and ridges. The gravity lows and highs between 39^0 E and 43^0E are separated by N-S and NE-SW trending sharp density contrast lineaments. These can be inferred to be the major fracture zones or faults. The range of the gravity values within the study area is -64.4 mGals to 42.8 mGals. The change in gravity due to elevation change is rated by 0.3086 mGals/meter. Thus to reduce the change in gravity to sea level, a gravity value measured at elevation (h) meter must be done by increasing the observed gravity by 0.3086h mGals (Alsadi & Baban, 2014).

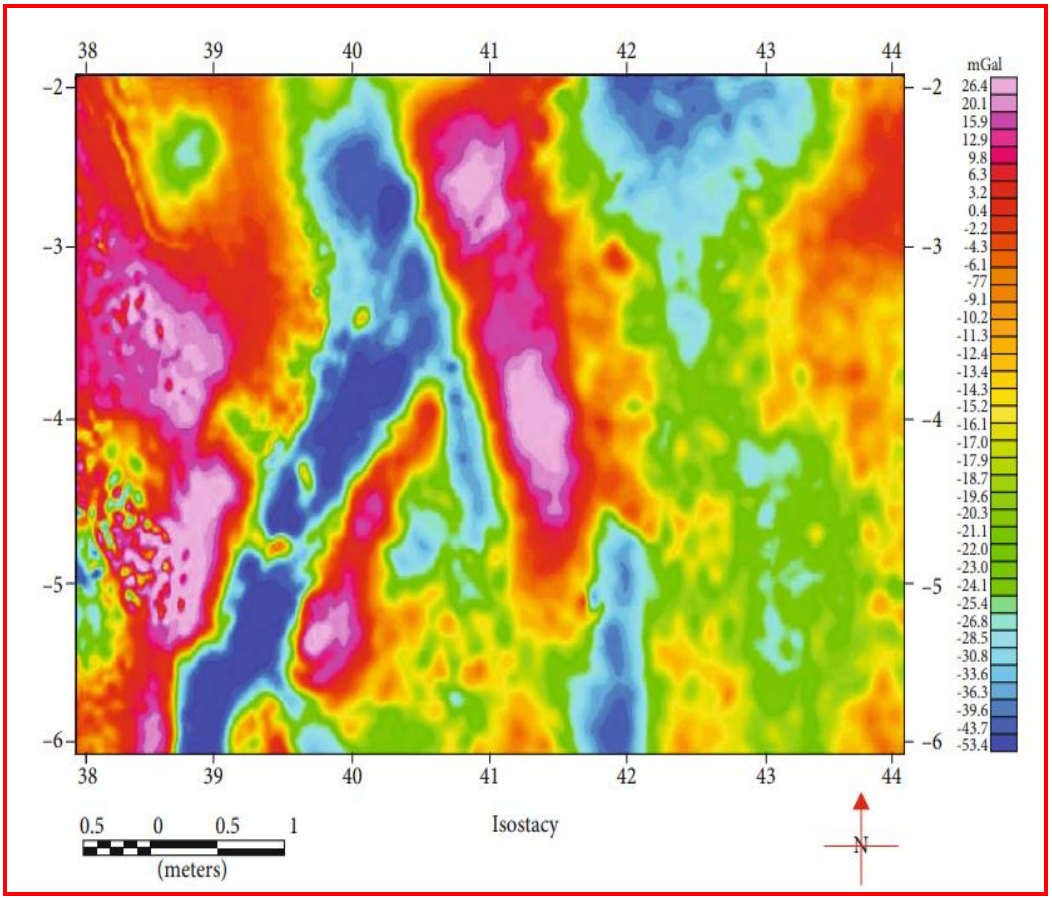

Figure 4.1 (c): Isostacy Anomaly Map

Figure 4.1(c) is a representation of data devoid of water effects and the masking or distortion of the anomalies by the Moho effect. The greatest value for interpretation is provided by Isostatic anomalies since it accounts for most of the effects that may affect the measured gravity data. The gravity values from the Isostatic anomaly map range between -53.4 mGals to 26.4 mGals. The Isostatic anomaly map was then subjected to Spectral Analysis which was consequently used to estimate the depth of shallow sources and deep sources as shown in Figures 4.2(a) and 4.2(b). These depths were used to set filters for residual (Figure 4.3(a)) separation using the Gaussian filter and regional. First Horizontal Derivative (FHD) was applied to the regional Isostatic anomaly map which yielded features that were inferred as the intrasediment fractures/faults trending in NW-SE and NE-SW directions (Figure 4.3(c)).

Discernable from the regional map, Figure 4.4, are features like the; ridges, troughs, and faults mainly trending in the NW-SE direction. These features are similar to the ones interpreted in a related study (Masinde, 2019). Selected profiles, cutting across the Isostatic anomaly map through the ridges, troughs, faults, drilled wells and along some seismic lines, were used to develop models using GM-SYS software within the Oasis Montaj platform.

4.1.2 Spectral Analysis

The decay slope of the radially averaged power spectral curve (RAPS) describes the various depths of a source ensemble. The deep source ensemble is described at a lower frequency (low wavenumber) and the shallow source ensemble at a higher frequency (high wavenumber) (Figure 4.2). The depth of a source ensemble was computed from the slope of a tangent fitted to any linear segment of the curve using equation 2.3. The plot of the log of the power versus wavenumber illustrates a typical reduction in energy with increasing wavenumber.

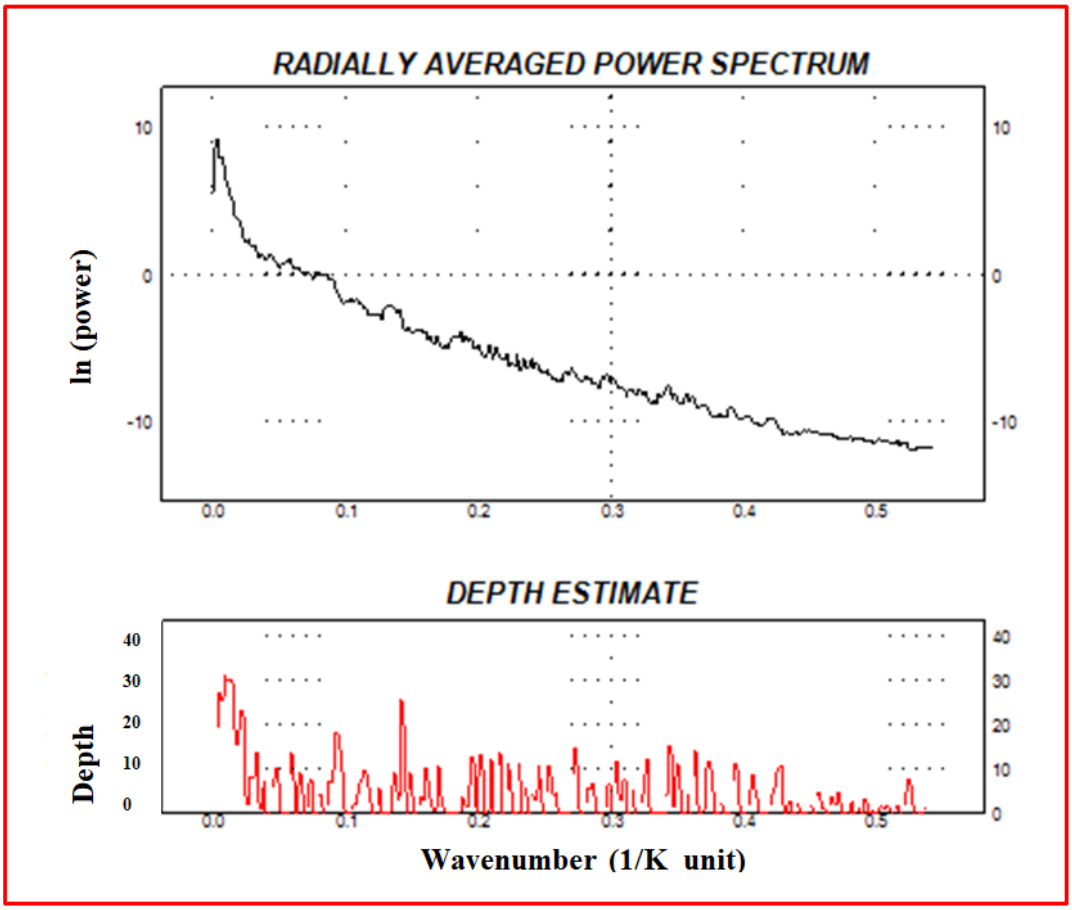

Figure 4.2 (a): Illustration of the Typical Reduction in Energy with Increasing Wavenumber.

The depth estimate is a plot of the 5-point depth data from the spectrum file.

Figure 4.2: (b) shows three principal slopes: Slope 1, Slope 2, and Slope 3. Their respective depths are calculated using the formula in equation 2.3,

$$h = -\frac{S}{4\pi}$$

Slope 1:

Depth, h= 16820 m

Slope 2:

Depth, h =5598 m

Slope 3:

Depth, h =1756 m

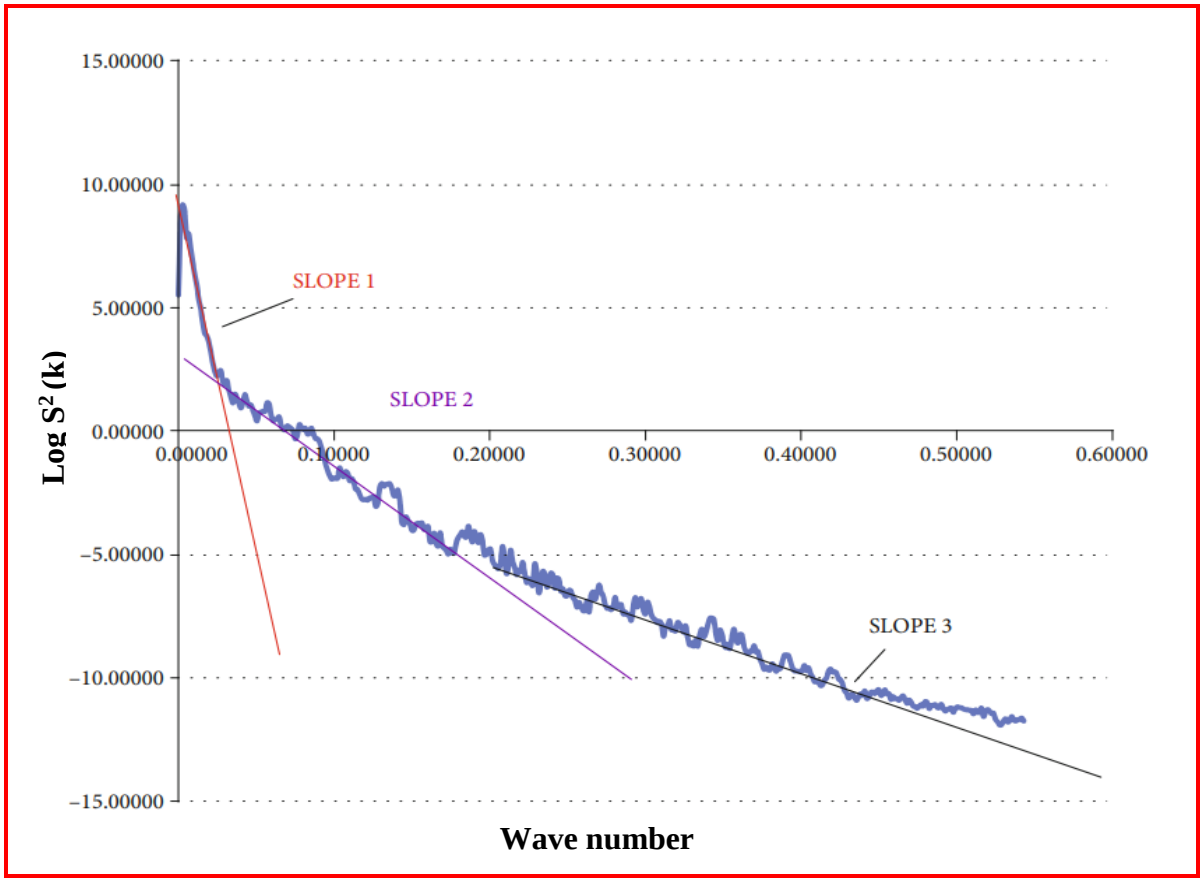

Figure 4.2 (b): RAPS Showing Three Principal Slopes

So depth is related to wavenumber but not with a simple relationship where one wavenumber represents one depth (Fairhead, 2016). The power spectrum method was used to estimate the depth and consequently design filters for deeper source and shallow source separation.

Figure 4.3 (a) and (b) compares FHD and Gaussian high pass filters to show residual features within the study area. In Figure 4.3 (c) the possible faults and/or fractures have been highlighted.

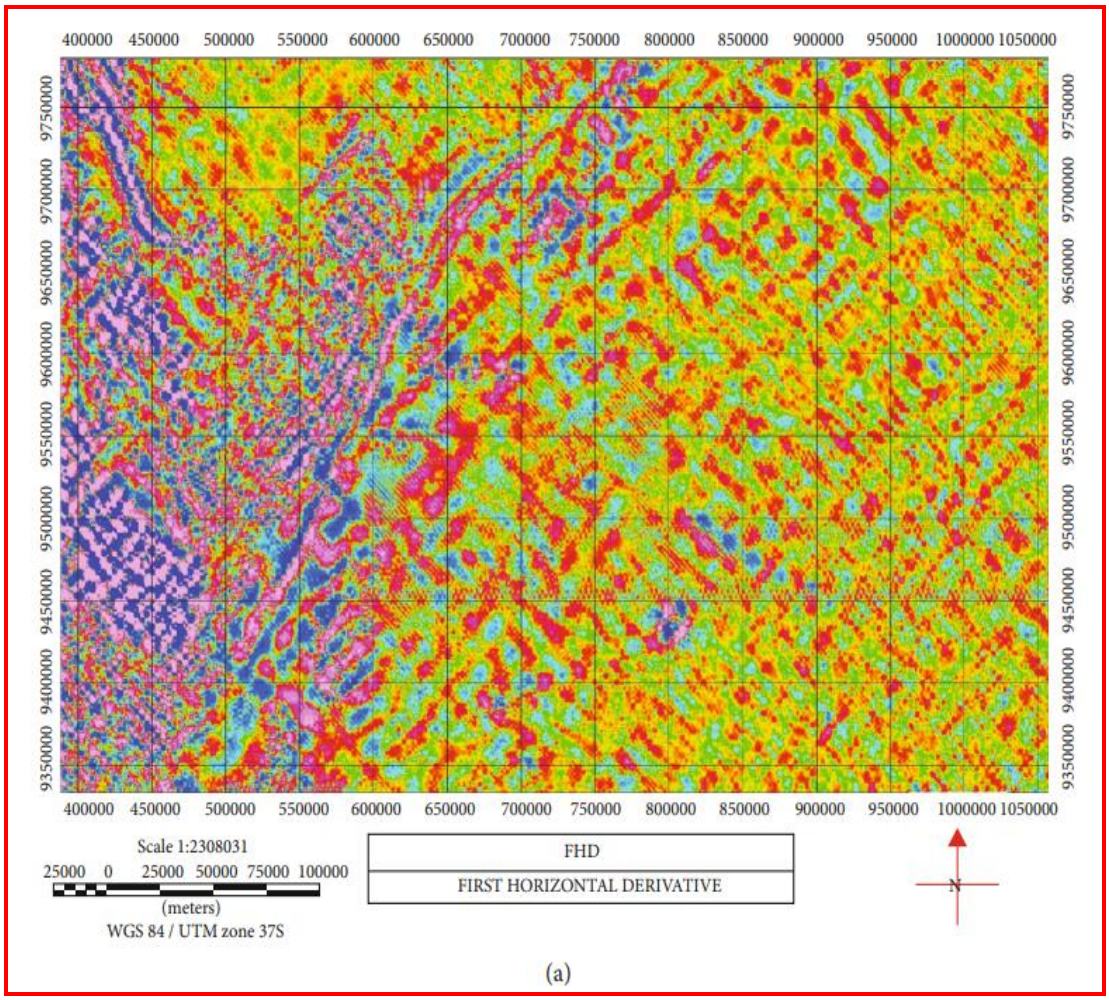

Figure 4.3 (a): First Horizontal Derivative

Figure 4.3 (b) is a first horizontal derivative map that is derived from the root sum square of horizontal x first derivative and horizontal y first derivative. This filter helps outline areas of sharp contrast in density between vertical blocks. From this figure, possible fracture zones have been highlighted as shown with discontinuous lines in Figure 4.3 (c). The total horizontal derivatives or Horizontal Gradient Magnitude (HGM) is commonly used to enhance the anomalous source's boundaries. It is computed using equation 4.1 (Blakely, 1996),(Ombati et al., 2022).

$$\mathrm{FHD} = \sqrt{\left(\frac{\partial g}{\partial x}\right)^2 + \left(\frac{\partial g}{\partial y}\right)^2} \qquad 4.1$$

Where FHD is the first horizontal derivative, $\frac{\partial g}{\partial x}$ is the derivative component in the x-direction and $\frac{\partial g}{\partial y}$ the derivative component in the y -direction. This is embedded in the Oasis Montaj software.

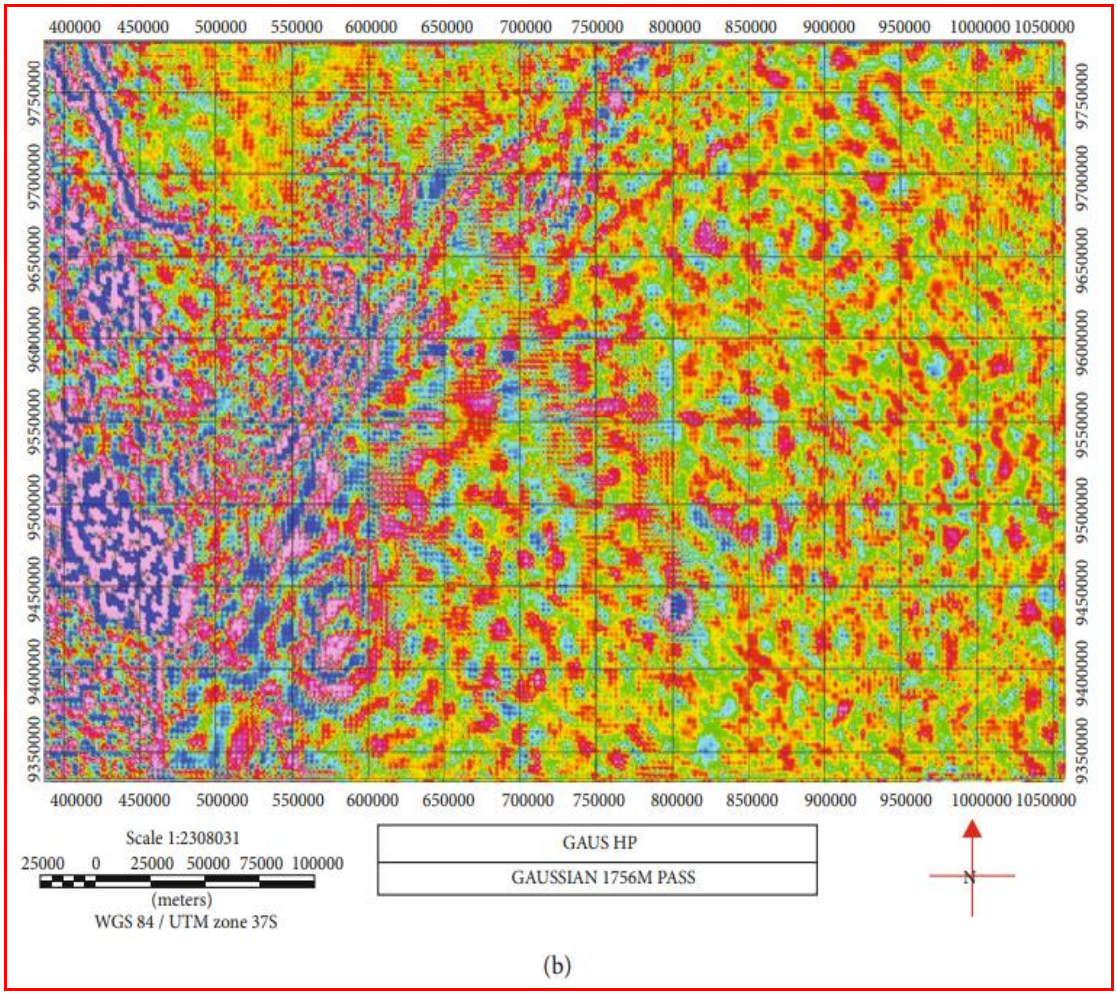

Figure 4.3 (b): The Gaussian HP (1756)

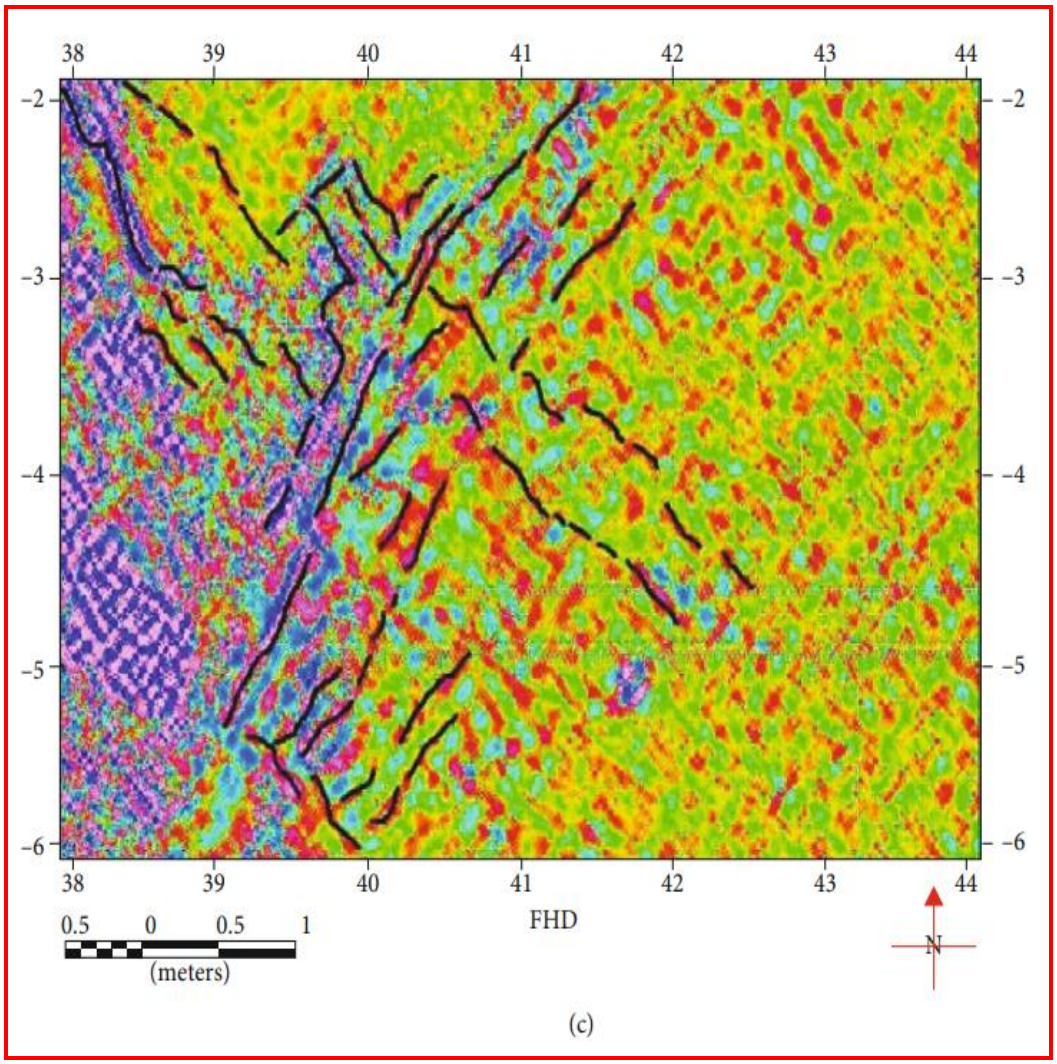

Figure 4.3 (c): FHD with Highlighted Faults

The horizontal derivative (FHD) was applied to the regional Isostatic anomaly map, which yielded features that were inferred as intrasediment fractures/faults trending in NW-SE and NE-SW directions (Figure 4.3 (c)). Discernable from the regional map, are features like the ridges, troughs, and faults mainly trending in the NW-SE direction (Figure 4.4). Selected profiles, cutting across the Isostatic anomaly map through ridges, troughs, faults, and drilled wells and along some seismic lines, were used to develop models.

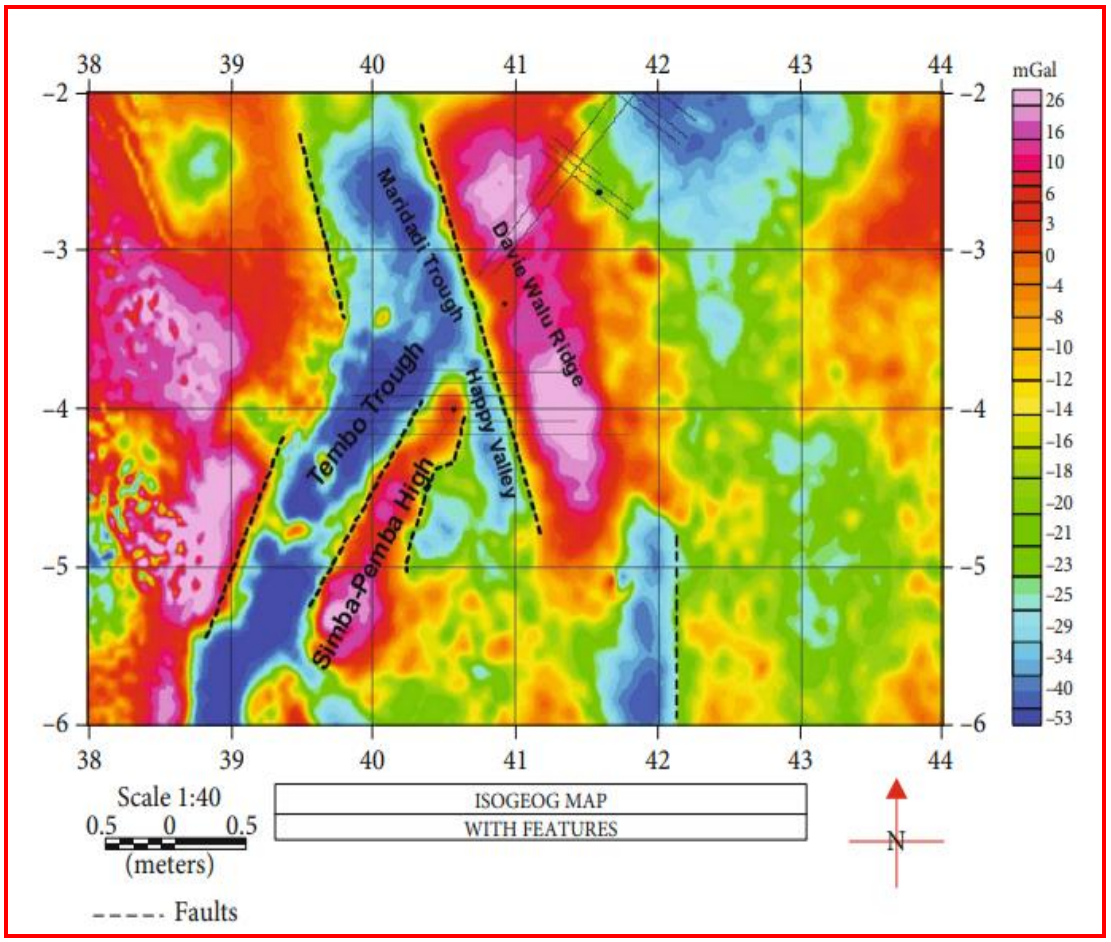

Figure 4.4: Regional Anomaly Map Showing Inferred Ridges, Troughs, and Faults.

4.2 Seismic Results and Discussion

4.2.1 Seismic to Well Tie

Mbawa-1 well is located in block L8 about 90 km offshore Kenya and it targeted the upper cretaceous deep water turbidite sand reservoirs. Figure 4.5 shows the generated synthetic trace using Mbawa-1 sonic and density logs together with the Mbawa-1 check shot data (Appendix IX). The generated synthetic seismogram is then tied to the seismic sections from both inline_1320 and xline_2811 to confidently relate the horizon tops identified in Mbawa-1 well with the specific reflections on the seismic sections (Figure 4.6).

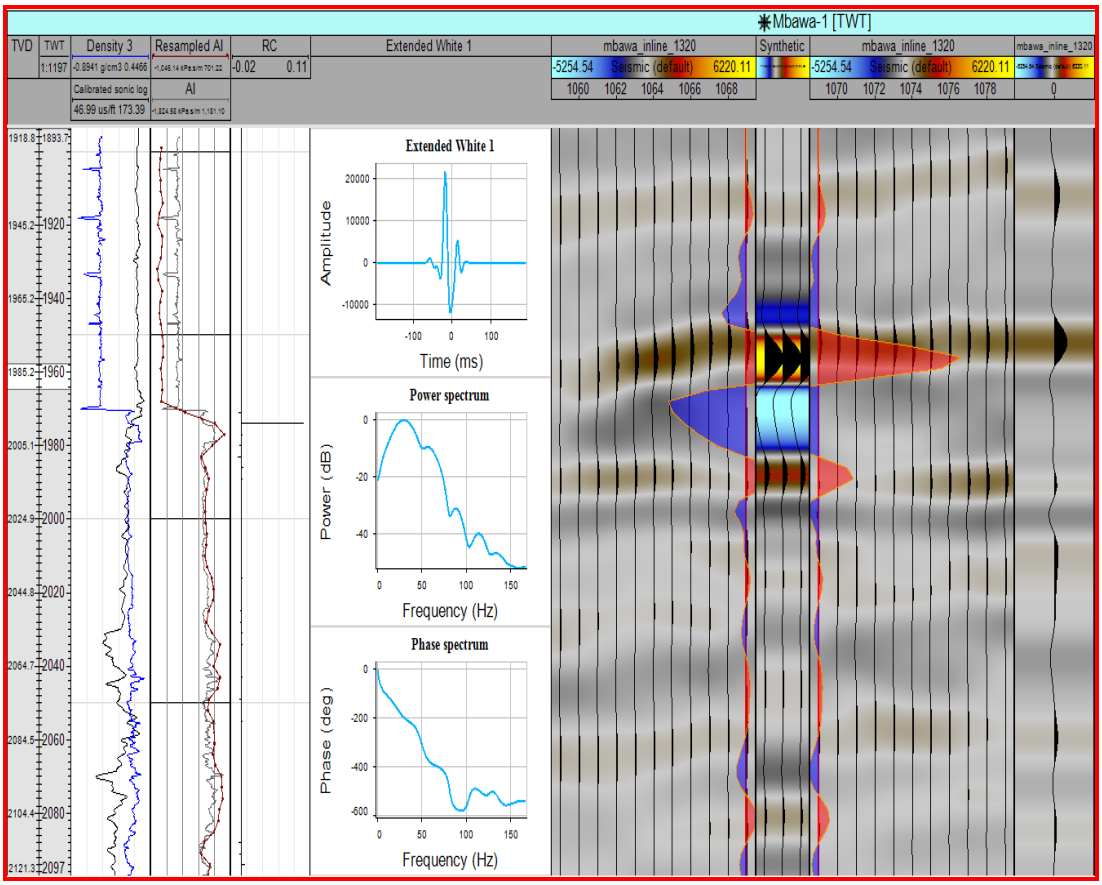

Figure 4.5: Typical Generation of Synthetic Trace and Seismic-to-Well Tie (Mbawa-1 well)

The main formations intercepted during the drilling of the Mbawa-1 well at different depths include the Miocene, Eocene, Paleocene, and Cretaceous. Drilled to a depth of 3150m, into the Albian, the well was plugged and abandoned with non-commercial gas shows in the upper cretaceous sandstones at a depth of about 2.4 km, and no observed oil shows in either the cuttings or sidewall cores, save for the reported mineral fluorescence. The well penetrated through the Simba shales, Lamu reefs, Oligocene and Paleocene unconformities, Hargaso carbonates, and finally through the Walu shales. The wellbore also intersected what appears to be a direct hydrocarbon indicator (DHI) at the crest of the visible anticline from the seismic sections (Figure 4.7 (a)).

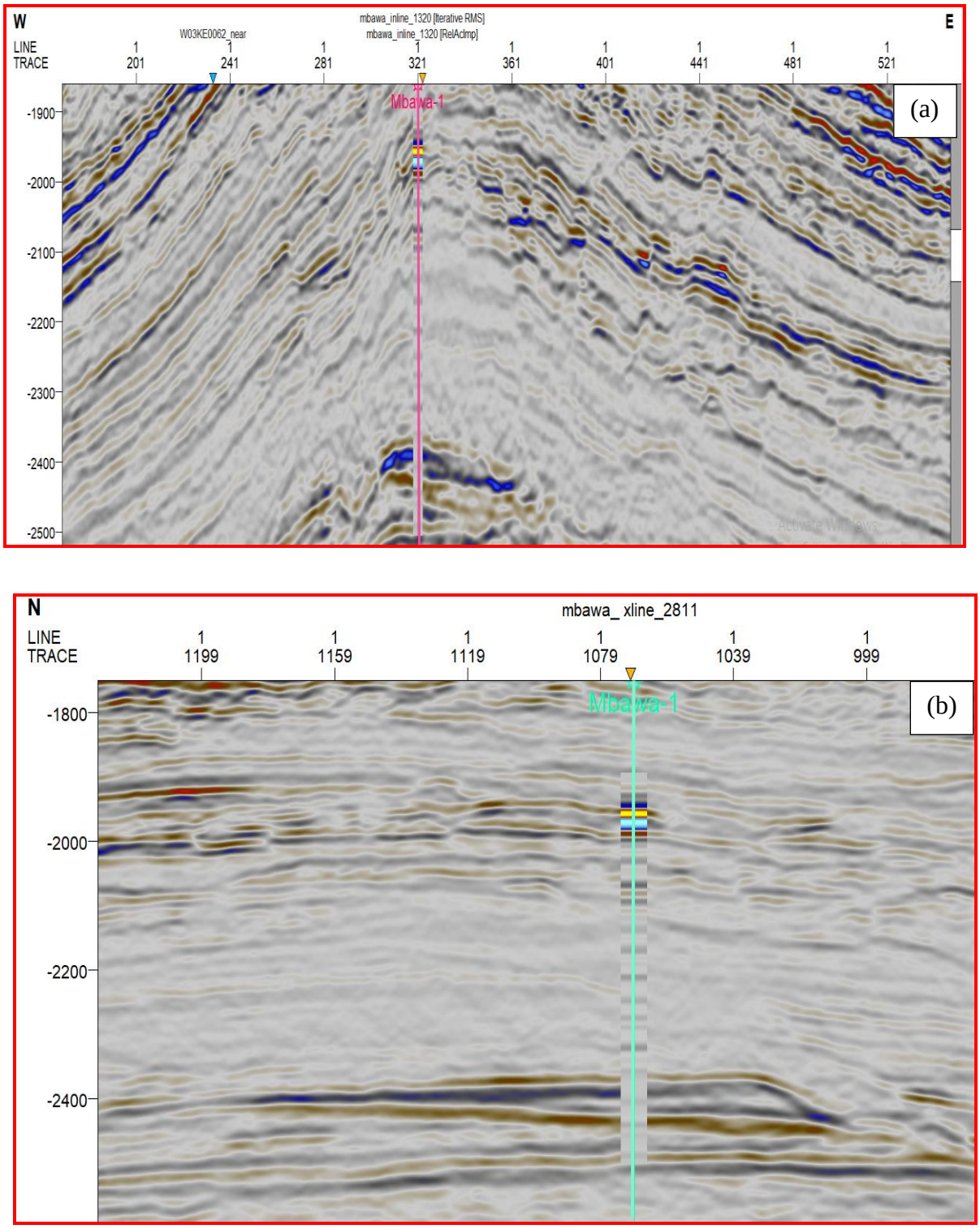

Figure 4. 6: Well Tops Identified and Matched on a Seismic Section ((a) and (b))

4.2.2 Seismic Sections

Figure 4.7 shows seismic sections through which Mbawa-1, Pomboo-1, and Simba-1 wells have traversed and a seismic section near the Kubwa-1 well pathway. From the figures, it is evident that the location of the wells is in sections where there seem to be potential structures such as the antiforms (Anabwani, 2012). Mbawa-1 well cuts through various sedimentary layers to reach a maximum depth of 3150 m and Pomboo-1 to a depth of 4887 m. Simba-1 well reached a total depth of 3604 m while Kubwa-1 was drilled to a total depth of 5860 m and it is therefore the deepest in this consideration. All these four wells are vertical exploration wells (Appendix II). Mbawa–1 (Apache, 2012) was a non-commercial gas discovery (52 m net pay in 3 zones of Upper Cretaceous Sands) drilled on the axis of the Davy Walu inverted graben feature just west of the partnership's block L12.

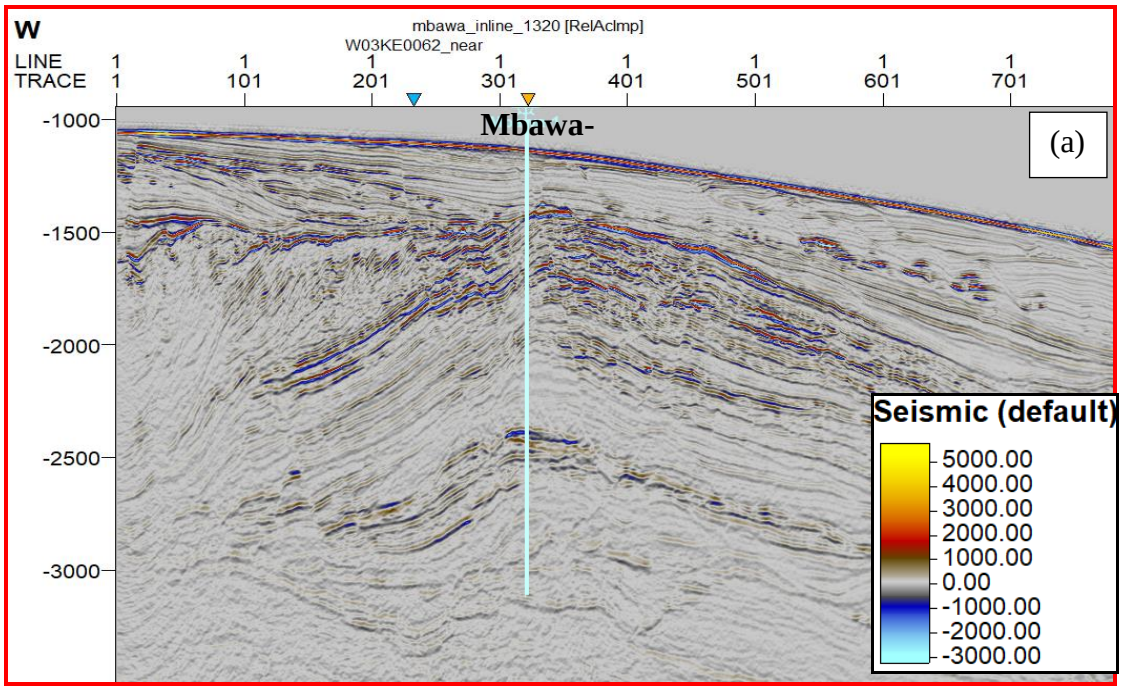

Figure 4.7 (a): Seismic Section Showing Mbawa-1 well

Pomboo-1 was drilled to a depth of 4887 m in block L5, intersecting three main seismic markers: the Paleocene, the Maastrichtian, and the Campanian. Pomboo–1 (Woodside, 2007) was a dry hole drilled within a regional gravitational fold and thrust system to the Campanian.

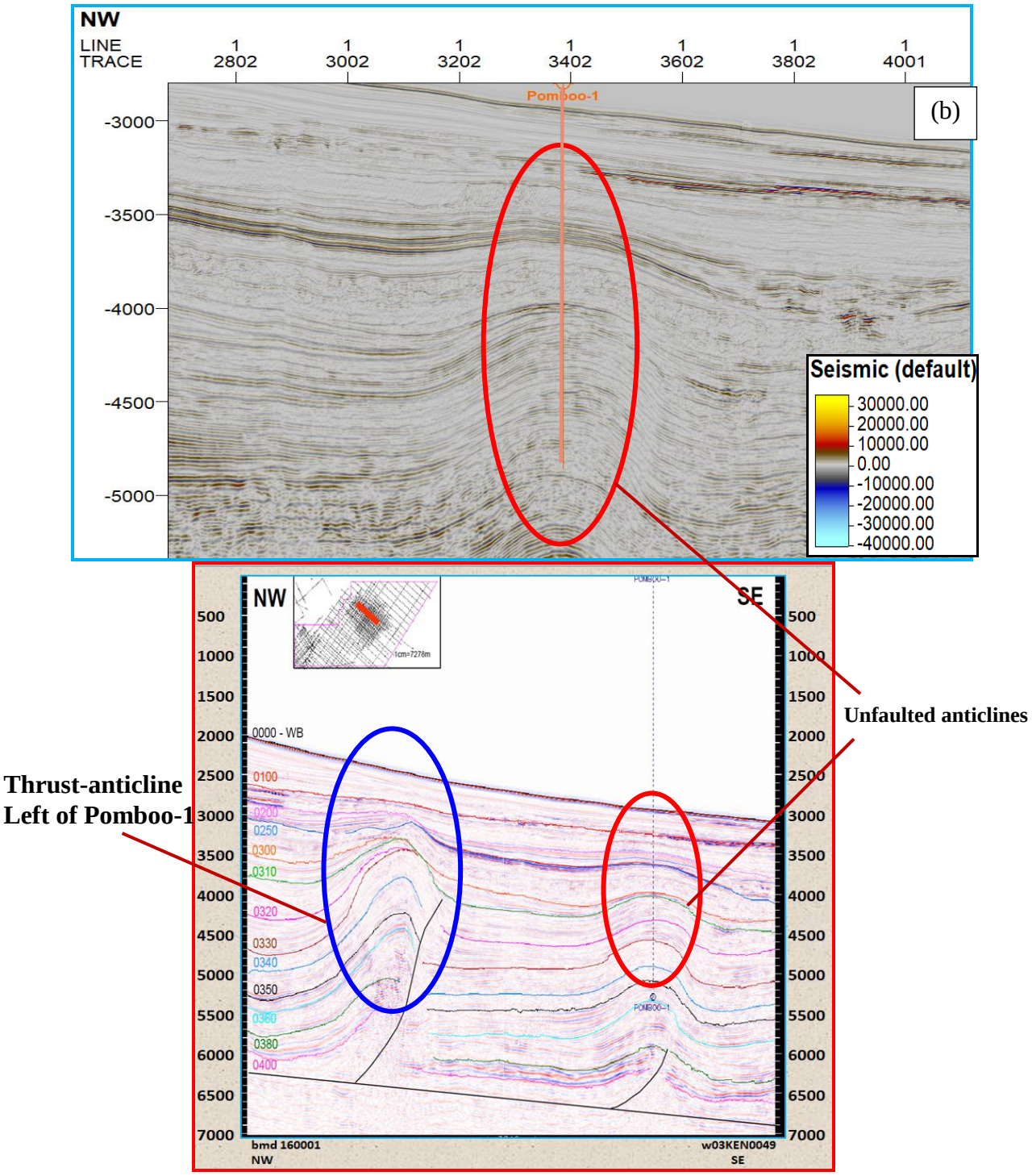

Figure 4.7 (b): Seismic Section Showing Pomboo-1 Well

The Pomboo anticline is sandwiched between two other thrust-anticline structures. The Pomboo trap structure is said to be well-constrained to accommodate hydrocarbons. The Pomboo structure was selected for drilling based on its perceived higher structural integrity due to its unfaulted nature relative to the other structures

(Figure 4.7 (b)). The discrepancies between the predicted depths and the actual depths could be attributed to the limited offset well data pre-drill since the nearest shelfal, coastal, and deep water drilled wells are the likes of Simba (275 km SSW), DSDP 241(300 km E), and Kofia-1 (129 km WSW). Pomboo-1 was drilled on an anticline (fault propagation fold) overlying a thrust that splays from a basal detachment.

Several thick shale packages which could act as top seals were intersected in the well. A complete dataset was obtained from the well, including good-quality logs, RFT pressure and sample data, isotubes, and sidewall cores. Despite the good data set obtained from the drilling of the Pomboo-1 well, no significant gas or oil shows were encountered. Nevertheless, exceptionally fresh formation waters were encountered in the Pomboo-1 well which is believed to be due to the liberation of fresh water during the process of smectite diagenesis to illite.

Located across a major structural high (the DWR), that separates the Southern Lamu Basin from the Northern Lamu Basin, Simba-1 well was drilled to a total depth of 3604 m in block L9 as shown at the intersection of the seismic lines in the seismic section in Figure 4.7(c). Simba-1 (Total, 1978) was a dry hole with gas shows drilled to the Campanian on a large, long-lived structural high.

Furthermore, in Simba-1 there is also poor biostratigraphic control below the base of the Tertiary hence making it problematic to correlate the seismic stratigraphic events dates with other wells like Pomboo-1 since Simba-1 is in the southern Lamu basin and Pomboo-1 is in the northern Lamu basin.

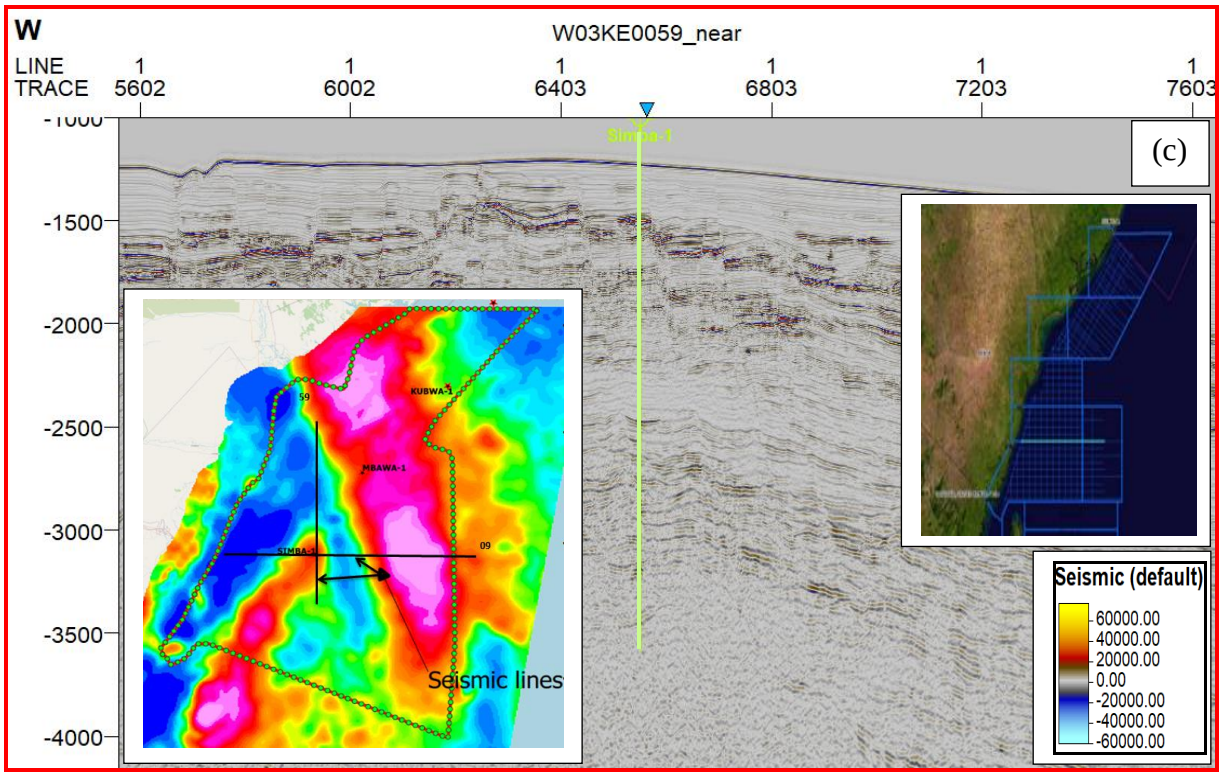

Figure 4.7 (c): Seismic Section Showing Simba-1 Well

Kubwa-1 well was drilled to a total depth of 5860 m in block L7, 84.4 km south of Pomboo well and 265 km northwest of Mombasa. It was drilled primarily to test the Upper Cretaceous (Mass-Campanian) sloe and toe-of-slope fans systems and the source-prone intervals in the Upper Cretaceous (Anadarko, 2013). Figure 4.7(d) shows a seismic section close to the Kubwa-1 well drill point. Before this drilling program, three offshore wells (Simba-1, Pomboo-1, and Mbawa-1) were drilled in the offshore Lamu Basin. They were primarily structural tests of the upper Cretaceous section.

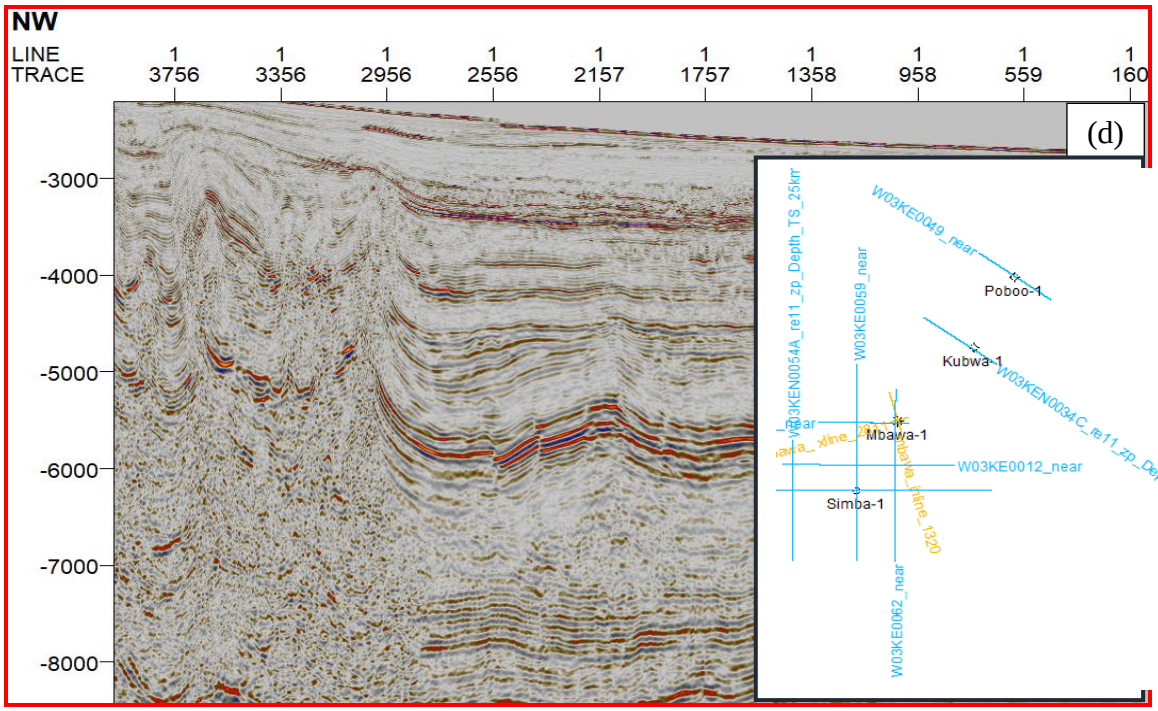

Figure 4.7 (d): Closest Seismic Section to Kubwa-1 Well Path

4.2.3 Fault and Horizon Interpretation

With the help of termination of reflections, offset in stratigraphic markers and abrupt changes in seismic patterns, the faults were marked. Horizons, being surfaces that separate two rock layers that give rise to a seismic reflection according to the acoustic impedance contrast were traced (Figure 4.8). Horizons were correlated by recognizing and tracking continuous or changing patterns of reflection. The main horizons interpreted include Horizon A, Horizon B, Horizon C, and Horizon D which corresponded to the available well tops. The said horizons match with the possible petroleum system elements (source rock, reservoir, and seal). Horizon A would be the much-needed trap/seal, Horizons B, and C could be the potential reservoirs, and Horizon D the source rock. Figure 4.8(a) shows a possible closed structure that could enable the accumulation of hydrocarbons. The seemingly closed structure could be fault assisted.

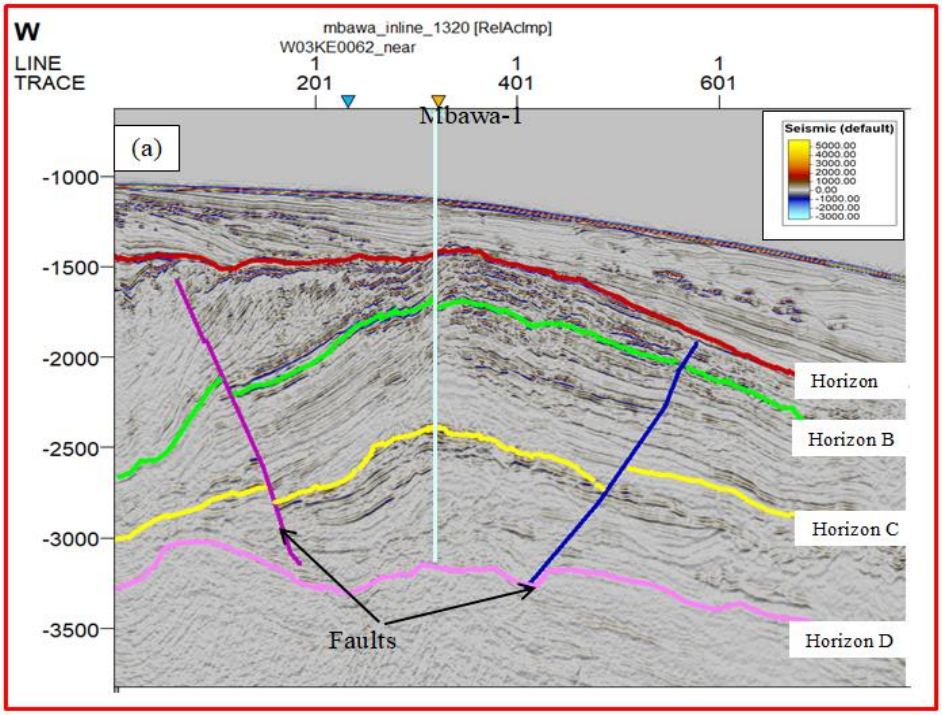

Figure 4.8 (a): Interpreted Faults and Horizons Around Mbawa-1 Well

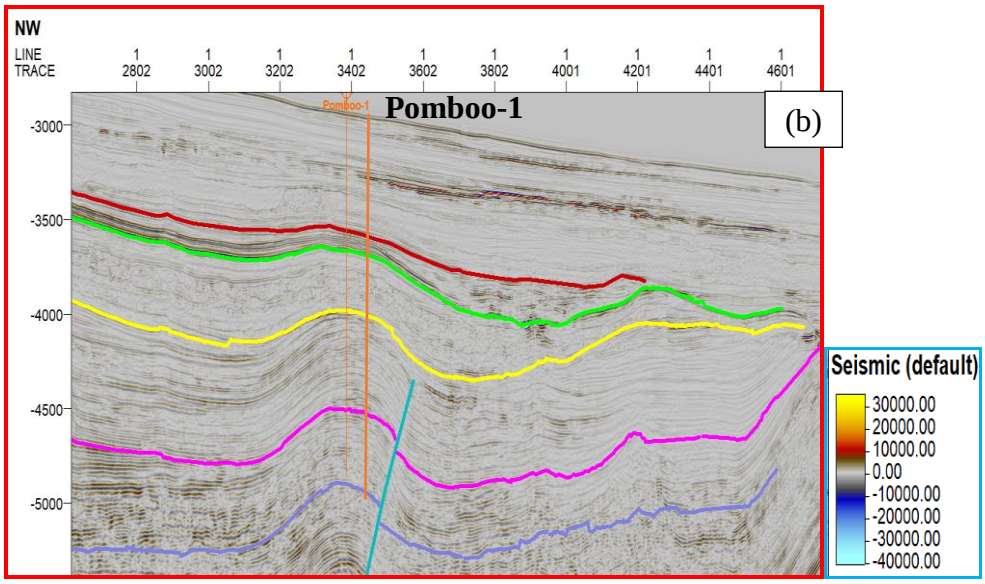

Figure 4.8 (b): Interpreted Fault and Horizons Around Pomboo-1 Well

As evidenced by Figure 4.8, the target points for drilling must have been at the anticline where there are likely to be hydrocarbon traps. There have been no major periods of compression in the Lamu Basin, although small N and NNE trending anticlines suggests some compressive stress. The presence of the interpreted faults

suggests the availability of closed structures and possible migration pathways. The Lamu Basin underwent extensive faulting in the Jurassic (Syn-rift), forming typically tilted fault blocks, downthrown to the east. The major transform faults in the region include the Davie Fracture Zone, which terminates in the Davie-Walu Ridge in the Lamu Basin. An inversion axis is also found just to the southwest of the Davie-Walu ridge, suggesting compression that reactivated normal faults as thrust faults.

From the gravity data interpretation, regional basement faults depicted a mainly coast-parallel NE-SW trend arising from the rifting of Madagascar in the Jurassic (Figure 4.3 (c)). This contrasts with the dominant orientation south of the Davie-Walu ridge, which is NW-SE, a trend shared with the onshore Anza rift faults (Figure 4.4). This is because of the transition from a rifted transform margin setting to the south of the Davie-Walu ridge to a purely rifted margin to the north. These faults may act as good seals forming part of the necessary closed structures needed in hydrocarbon exploration as can be seen in Figure 4.8(a). On the other hand, faults may be migration pathways and act as hydrocarbon conduits within the sedimentary structures allowing the movement of hydrocarbons from the source rock right to the reservoirs. In certain cases, faults can be problematic in that they may cause the generated hydrocarbons to leak away and therefore adversely affect the accumulation within the interpreted structures.

According to the lithology/LWD log report (Apache, 2012), during the drilling of the Mbawa-1 well, at a depth of between 2800 m and 2900 m, three faults were intersected in the late cretaceous (Appendix XI). These faults may have acted as either the necessary conduits or the problematic hydrocarbon leak pathways that may explain the reason for the non-commercial accumulation of the hydrocarbons in the Mbawa-1 well. From the Kubwa-1 lithology by Anardako Company Limited (Anadarko, 2013) and Pomboo-1 lithology by Woodside Energy (Woodside, 2007), there are no visible intersected faults. In fact from the seismic section in Figure 4.8(b), showing the drilled Pomboo-1 well is visibly unfaulted.

4.2.4 Surface Slicing

Surface slicing is a novel approach to interpreting seismic horizons. This technique involves visualizing and interpreting finite portions of horizons on time-slice slabs of the data (Stark, 1991). The contour lines in the surfaces imply the shape of the terrain and the nature of the structures inferred. Figure 4.9 (a to d) shows seismic surfaces derived from the time slices at different depths. The surfaces were generated by the Petrel software under the geology and geophysics perspective, seismic interpretation tab, utilities group, and make surfaces option using the interpreted horizons as the input.

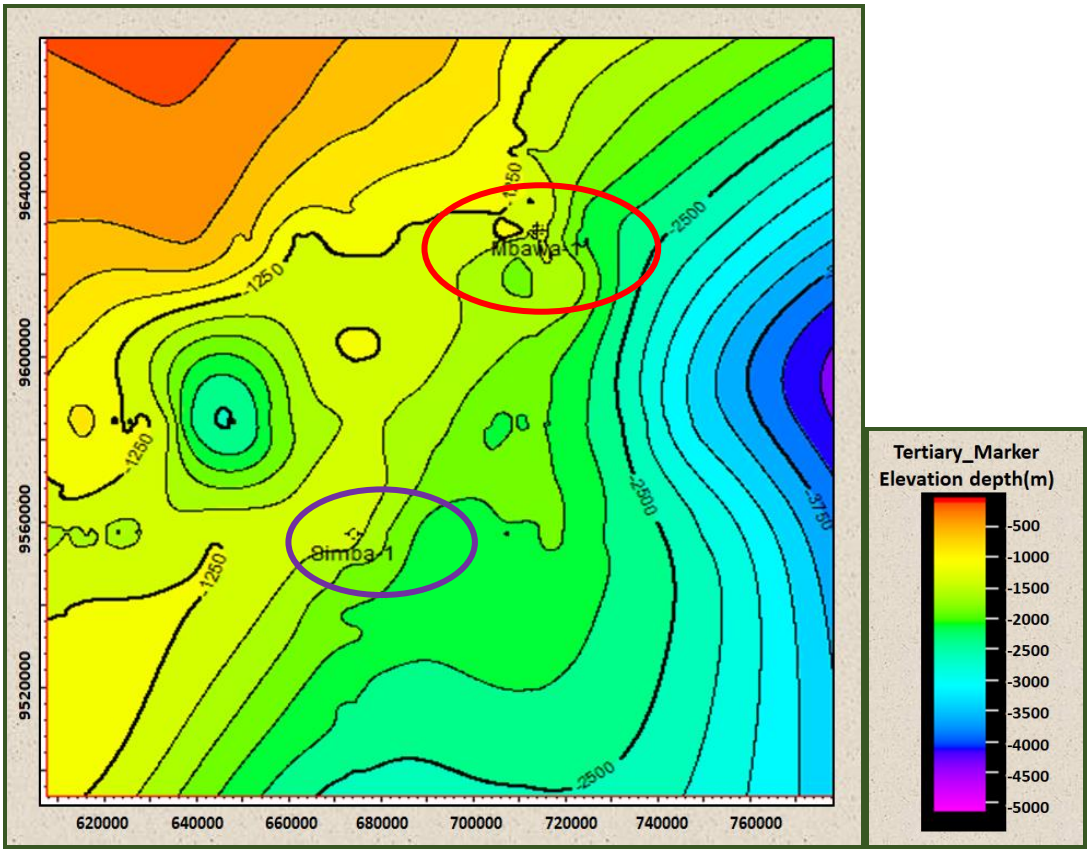

Figure 4.9 (a): Seismic Slice with Structural Properties During the Quaternary

In the seismic surfaces are indicated two wells whose location structural properties are compared from quaternary in the tertiary period through to the lower cretaceous. Figure 4.9(a) shows a surface in the quaternary whereby both the Mbawa-1 and Simba-1 wells traversed open structures following the nature of the contouring. The

two wells are drilled from a depth of about 1000 m below sea level. Around Mbawa-1 (area circled in red) there are two small isolated closed contours and there is none around Simba-1 (area circled in purple). Trap sealing at these points therefore cannot be relied upon since the contours are not closed at the well path. The western part of the slice North West of the Simba-1 well shows a closed structure.

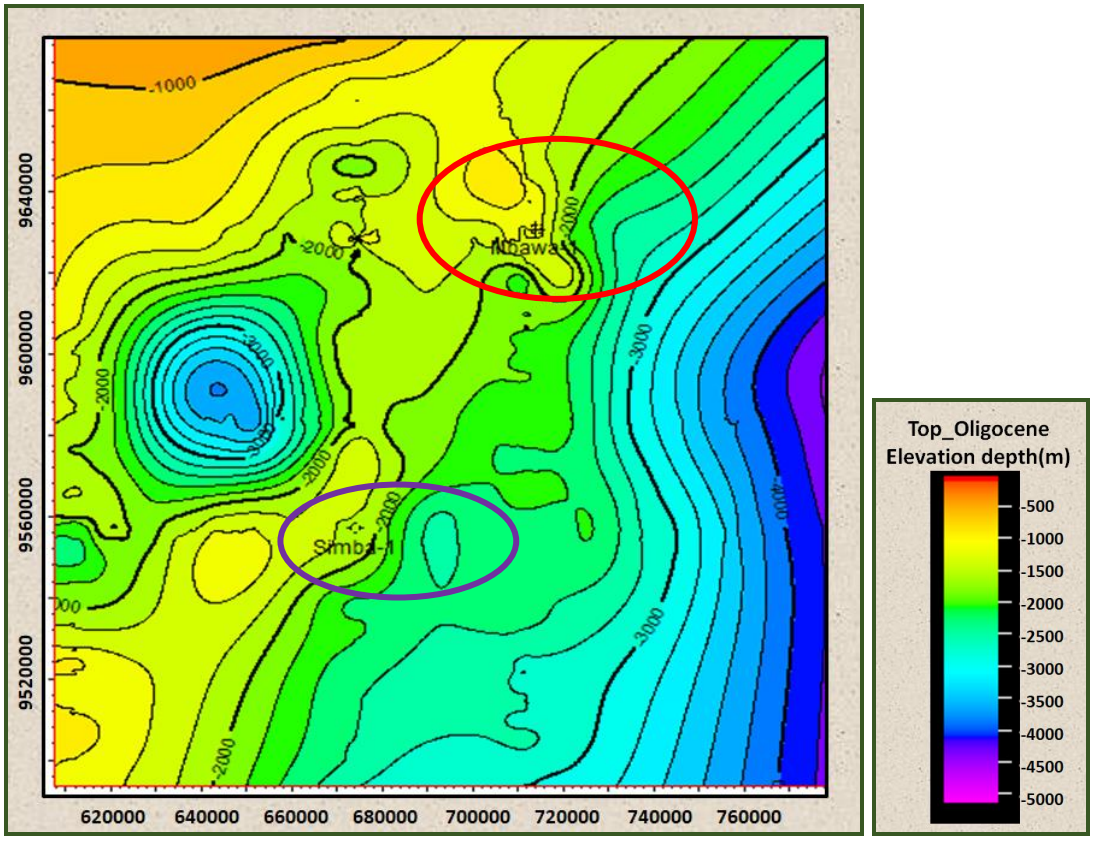

Figure 4.9 (b): Seismic Slice with Structural Properties During the Top Oligocene

In Figure 4.9(b) a similar scenario as in Figure 4.9(a) is seen considering the surface picked representing the top Oligocene. This equally means that the trapping at this surface is compromised at the well path.

However, from the western part of the section, there is an evident good structure given the closed nature of the contours which is relatively deep to a depth of up to 4000 m below sea level than the well locations and that could serve as the hydrocarbon kitchen.

The upper cretaceous seismic surface shown in Figure 4.9(c) portrays deeper sections westerly with visible closed structures at two nearby troughs. However, as it is visible from red and purple circled areas, the location of wells is at the crests (using the elevation depth scale) which are lacking closed structures.

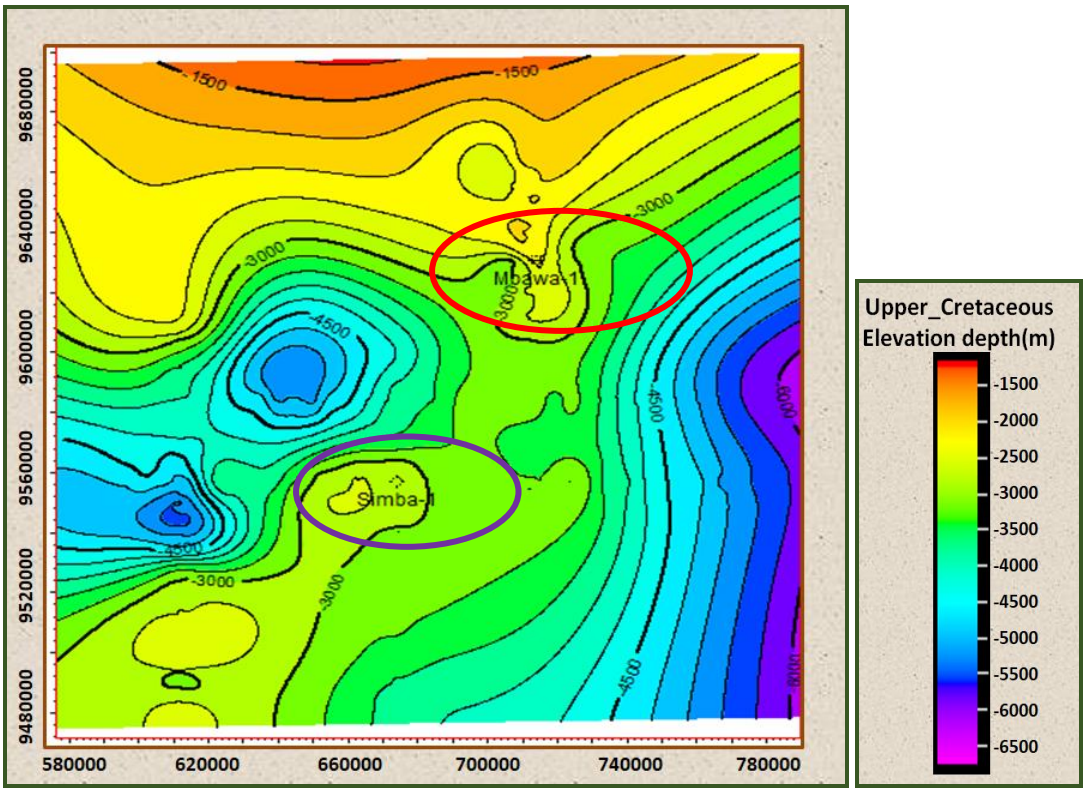

Figure 4.9 (c): Seismic Slice with Structural Properties During the Upper Cretaceous

Simba-1 well in Figure 4.9(d) seems to be within a closed structure at the lower cretaceous (a depth of about 3500 m) if the trap were to be located at that depth. From the nature of the contouring, Mbawa-1 well is still located at the crest, and the structure at the depth is still open. The two troughs seem to be interconnected at a depth of about 6000 m.

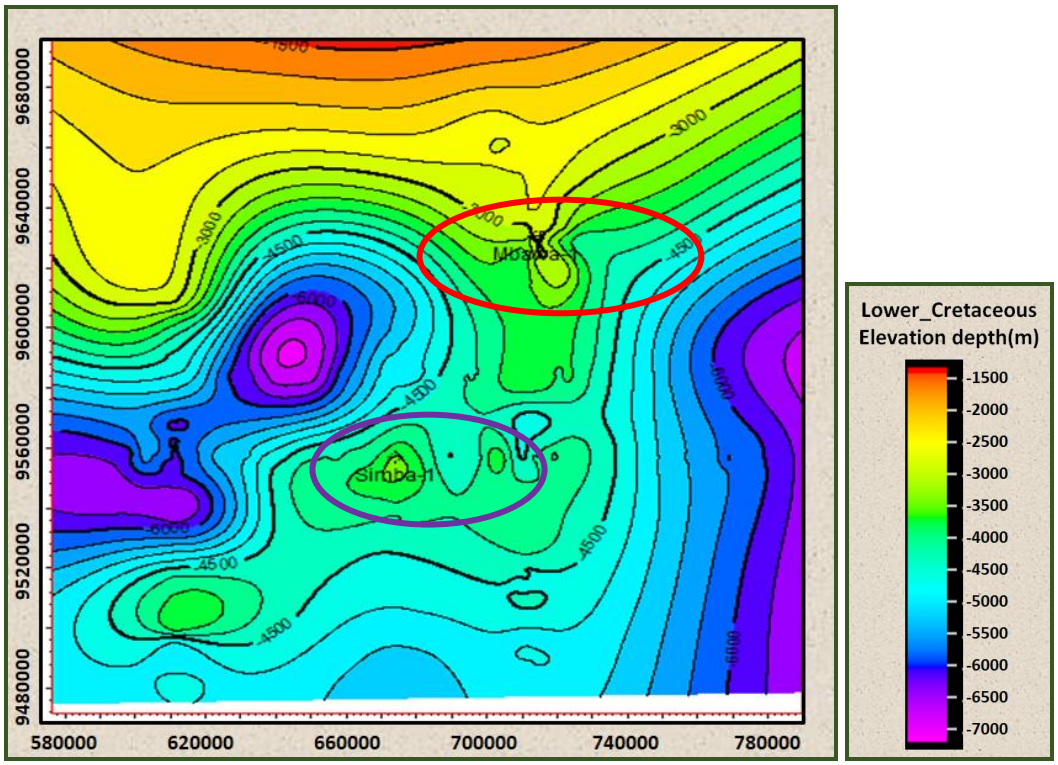

Figure 4.9 (d): Seismic Slice with Structural Properties During the Lower Cretaceous

From the analysis of the seismic surfaces, it is inferred that although the westerly part of the section shown with lower elevation depths (troughs) is indicative of closed structures, they were not the target points for drilling and therefore considered as the possible hydrocarbon source kitchens. The target drilling points for the two wells, Simba-1 and Mbawa-1 were the crests with higher elevation depths but missing out closed structures down through the quaternary, Oligocene, upper cretaceous, and lower cretaceous seismic surfaces safe for some closed structure possible for Simba-1 at the lower cretaceous seismic surface.

4.2.5 Seismic Attributes

Seismic attributes are very useful in enhancing the visualization of information from seismic data that would be otherwise subtle to discern conventionally. Figure 4.10 (a to f) shows the results of running the volume attributes such as envelope, sweetness, variance edge, RMS amplitude, and relative acoustic impedance on the 2D seismic data from part of the study area alongside the interpreted horizons and faults.

The envelope attribute shows lithological changes that seem subtle in conventional seismic data. From Figure 4.10 (a) and (b) bright spots are visible signifying gas accumulations, and major lithological changes that are caused by strong energy reflections and sequence boundaries. The advantage of using envelop attribute over the conventional vertical seismic profile (seismic section) is that it does not depend on either the phase or the polarity of the seismic data since phase and polarity affect a reflection's apparent brightness (Oumarou et al., 2021). The Variance edge attribute was used to isolate edges (discontinuities in the horizontal continuity of amplitude) from the input data set.

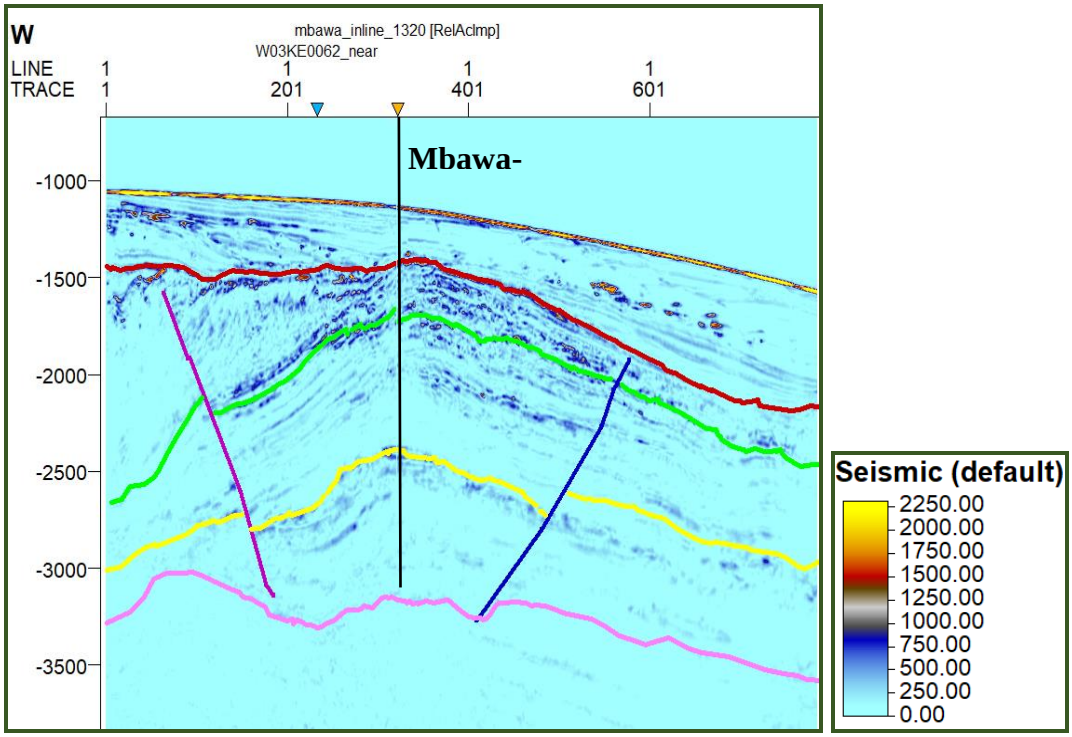

Figure 4.10 (a): Seismic Volume Attributes: Mbawa-1 Envelope Attribute

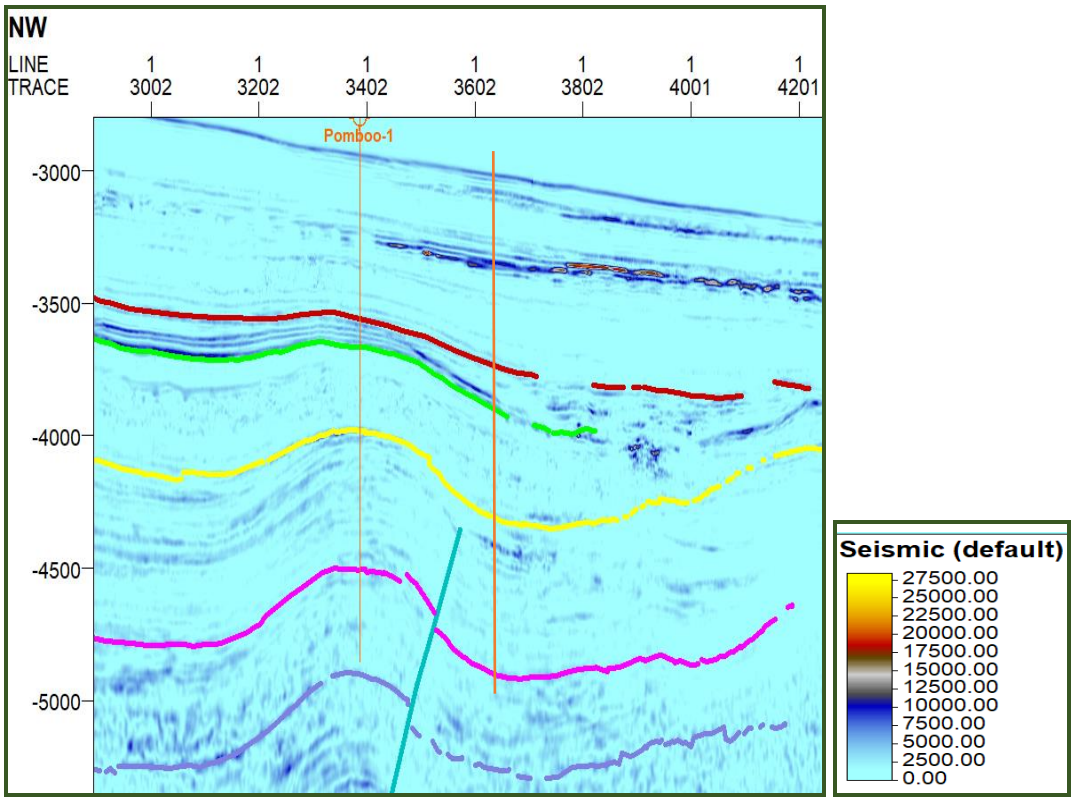

Figure 4.10 (b): Seismic Volume Attributes: Pomboo-1 Envelope Attribute

Figure 4.10 (c), has been used as a stratigraphic attribute whereby the highest value lies in the western part of the interval between horizon A and horizon B. The darkest vertical strips may represent fracture zones while the horizontal dark regions could be the unconformity or major sequence boundaries. Also, the stratal laminated beds are more pronounced using this attribute than when the conventional seismic sections are used. In Figure 4.10 (d) one of the darkest vertical strips coincides with the green fault interpreted from the seismic section. This increases our confidence in the interpretations since the variance edge attribute enhances the visibility of the structures that could otherwise be subtle or unclear to visualize conventionally (Adero et al., 2017).

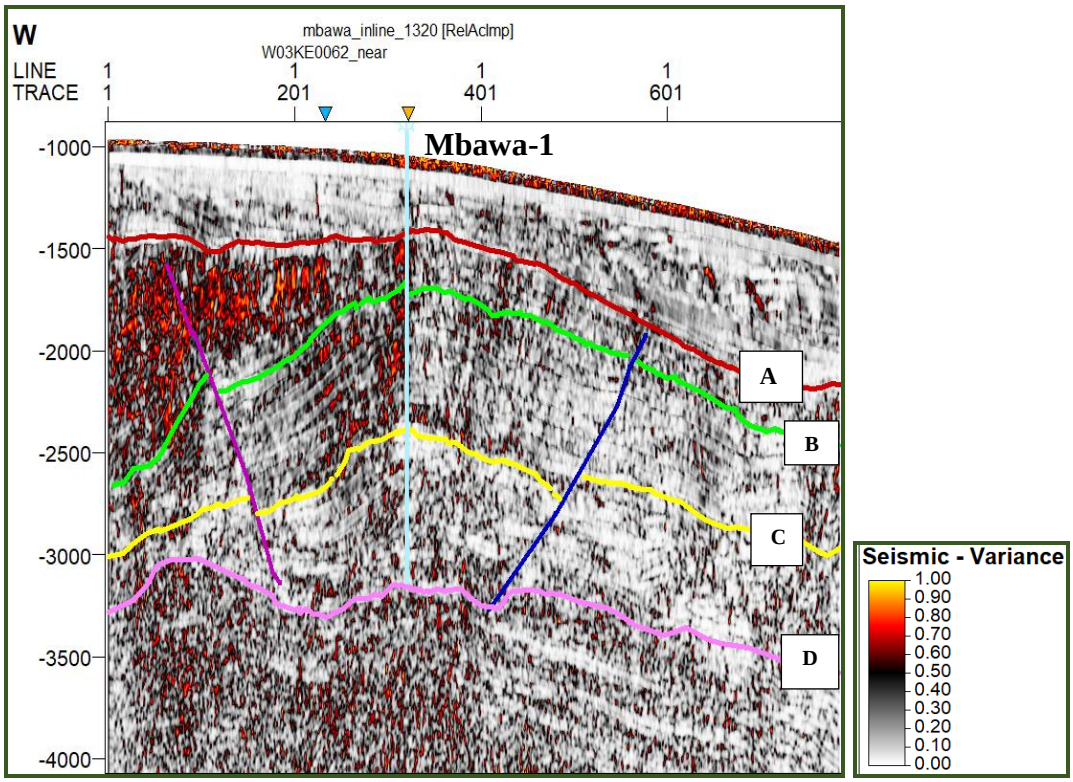

Figure 4. 10 (c): Seismic Volume Attributes: Mbawa-1 Variance Attribute

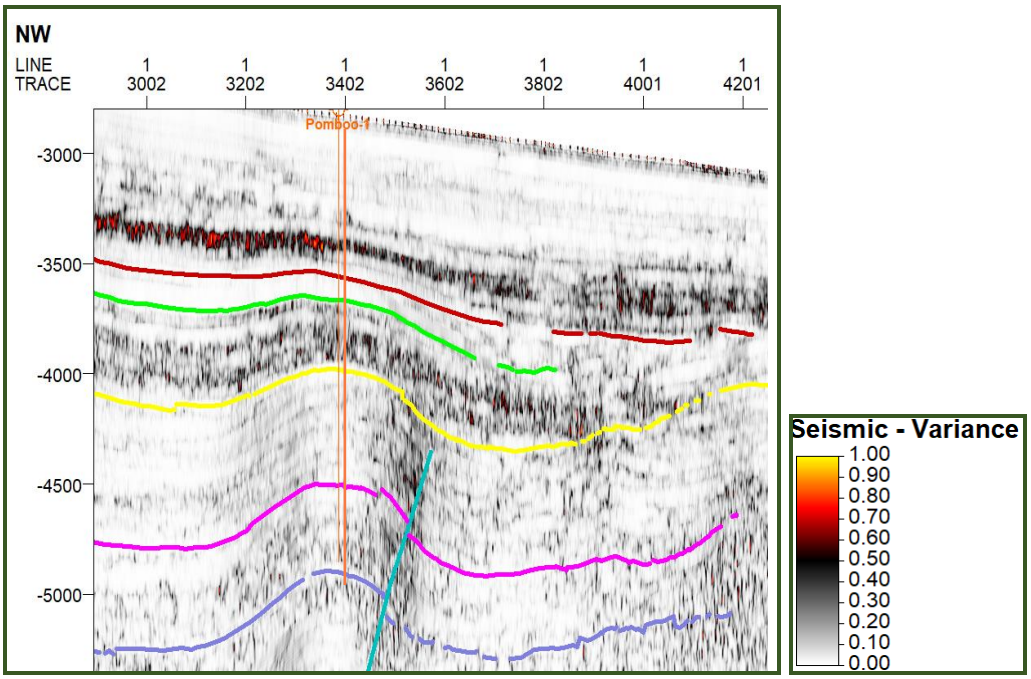

Figure 4.10 (d): Seismic Volume Attributes: Pomboo-1 Variance Attribute

Figure 4.10 (e and f) shows the root mean square (RMS) amplitude attribute as applied in revealing the bright spots and related amplitude anomalies thus highlighting facies with coarser grains, effects related to compaction, and unconformities. From both (e) and (f), traces of bright spots are visible but may not be suggesting the presence of hydrocarbons given their distribution. High seismic signatures are evident in both and are more pronounced at the crests. This has significance in telling about the seal integrity, indicating that the structures along which the wells were drilled may have had trapping mechanisms with uncompromised seals.

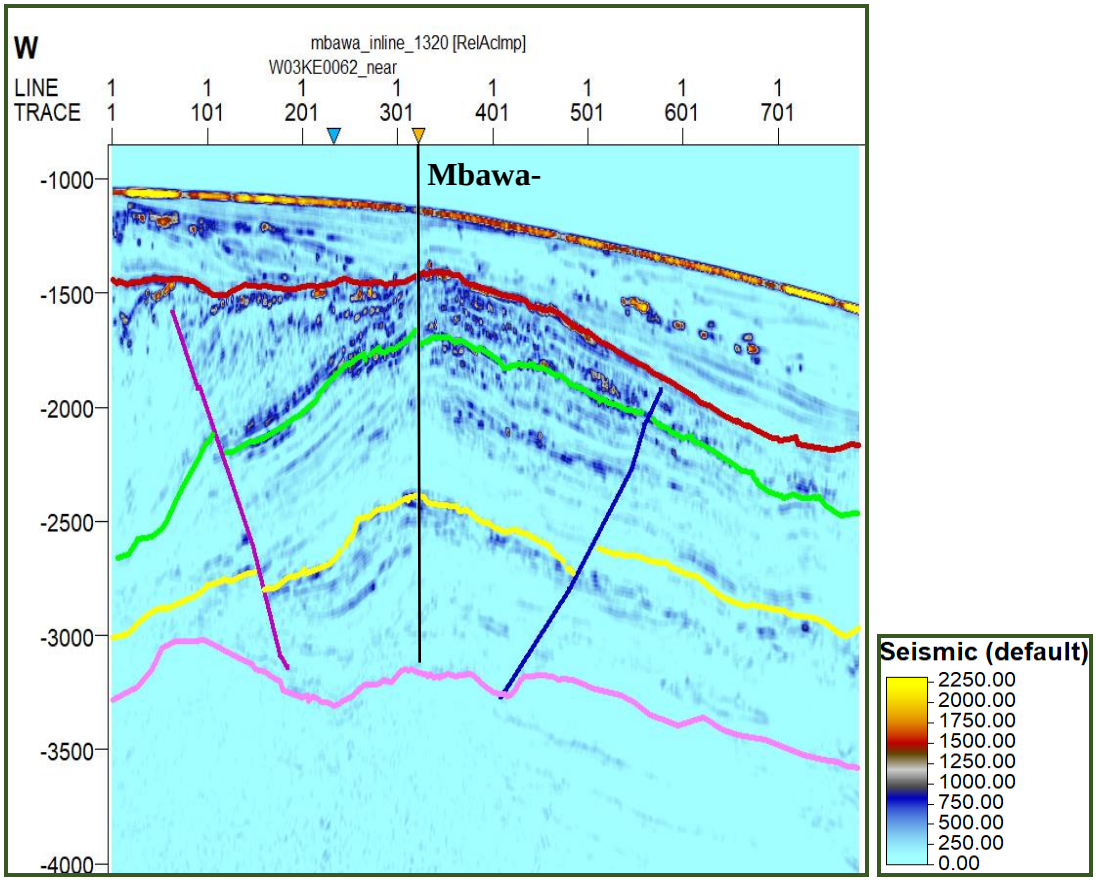

Figure 4.10 (e): Seismic Volume Attributes: Mbawa-1 RMS Amplitude

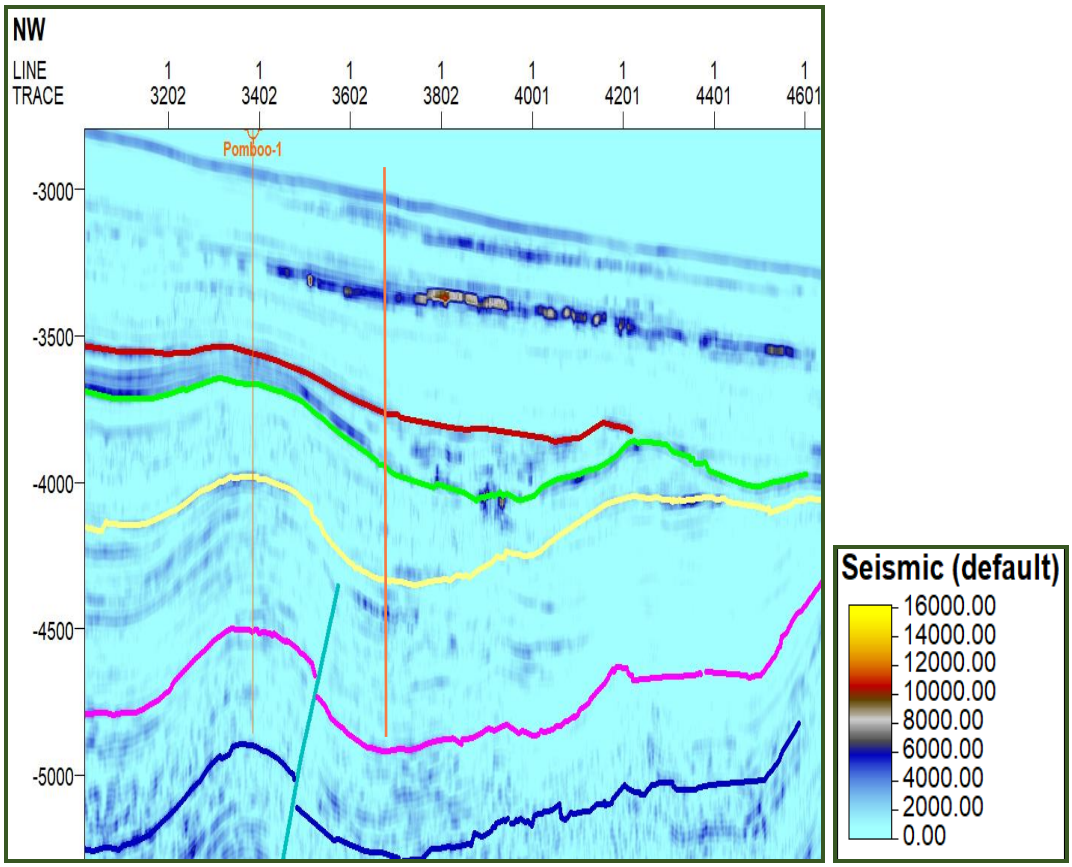

Figure 4.10 (f): Seismic Volume Attributes: Pomboo-1 RMS Amplitude

4.3 Reservoir Characterization Results

4.3.1 Formation Evaluation

This involves checking the quality of the data, determining the zones from the logs, and identifying the lithologies from the cross plots. The presence and quality of logs, their families, and units were checked and displayed in the log view as can be seen in Figure 4.11. The logs were qualitatively and quantitatively analyzed. Neutron-Density cross plots resulted in delineating lithology in situ.

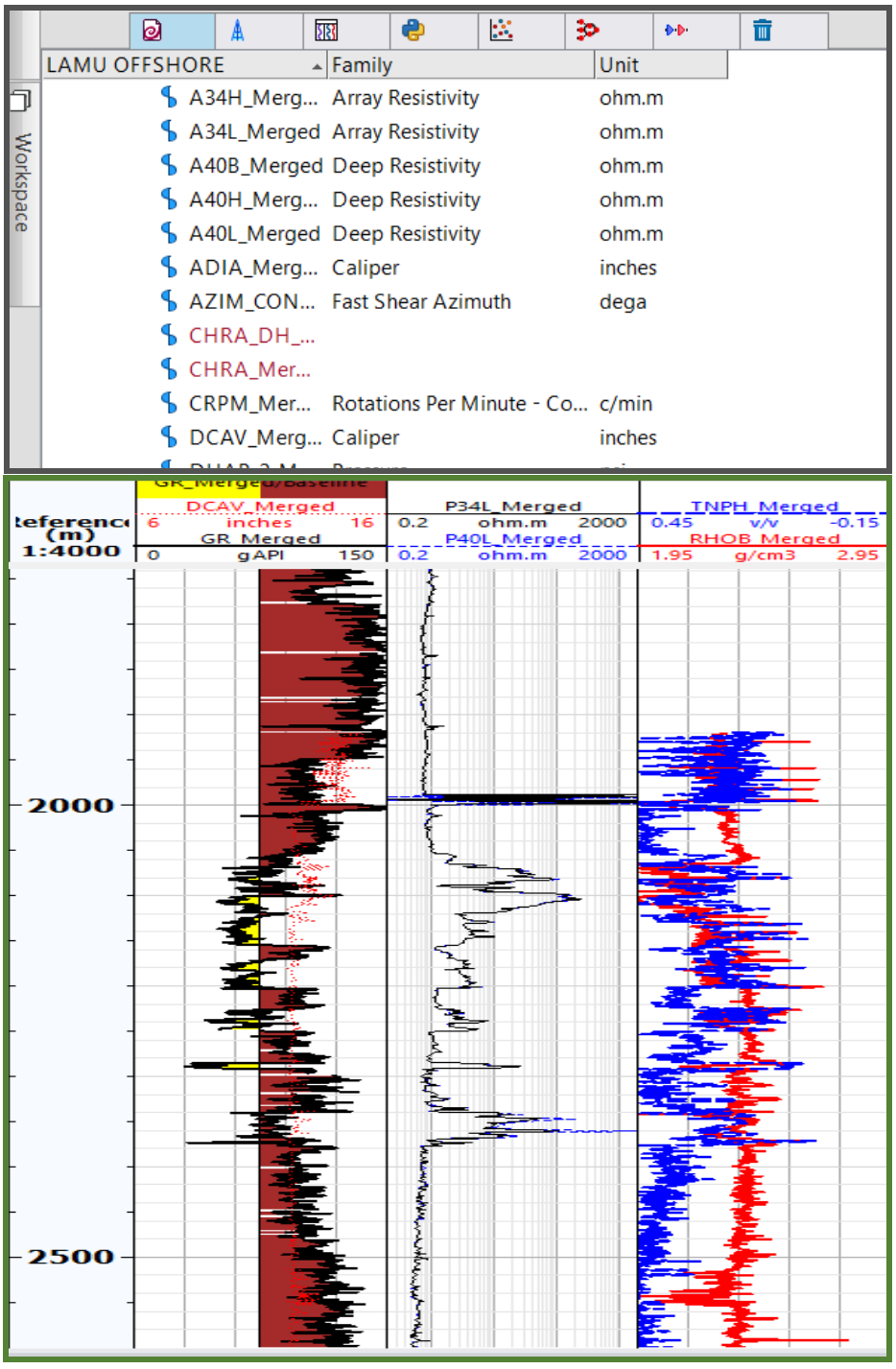

Figure 4.11: Data Quality Check in Terms of Family and Unit.

The main lithologies identified from the cross plots include sandstones, limestones, dolomites, shales, and a blend of the combinations at the interfaces. In Figure 4.12(a) at the depth range 5741.86 m – 5806.28 m the main lithology identified from the cross plot is sandstone with traces of limestone and dolomite.

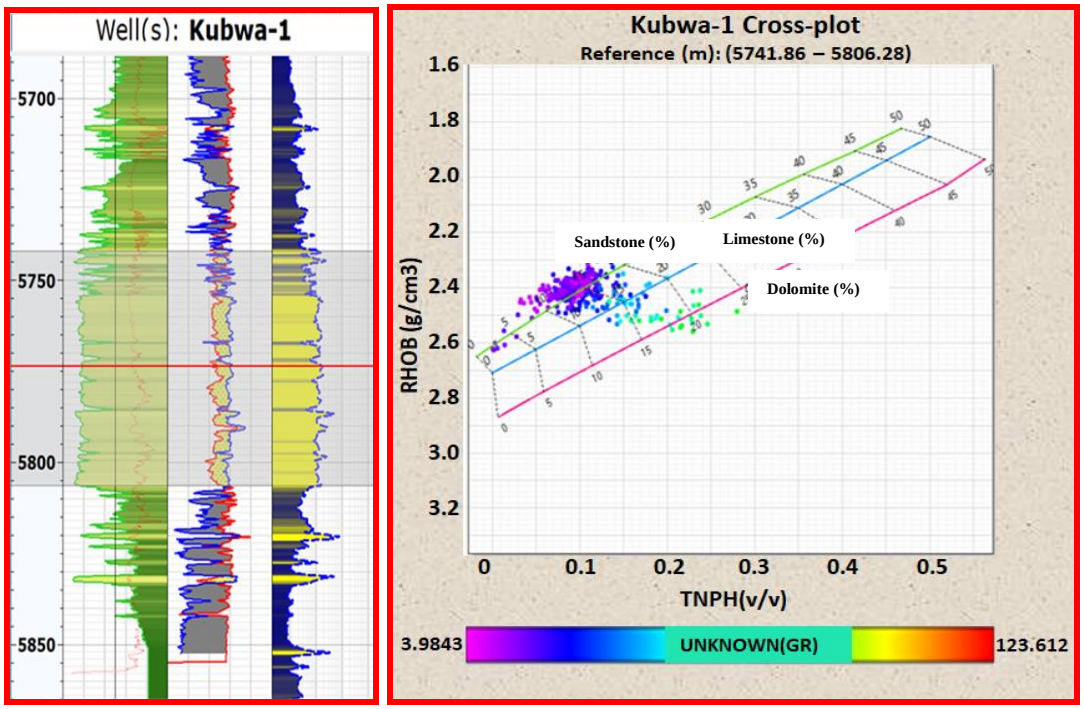

Figure 4.12 (a): Interactive Selection Mode Log View Highlighting Sandstone with Traces of Calcareous Dolomite Lithology in the Cross-Plot

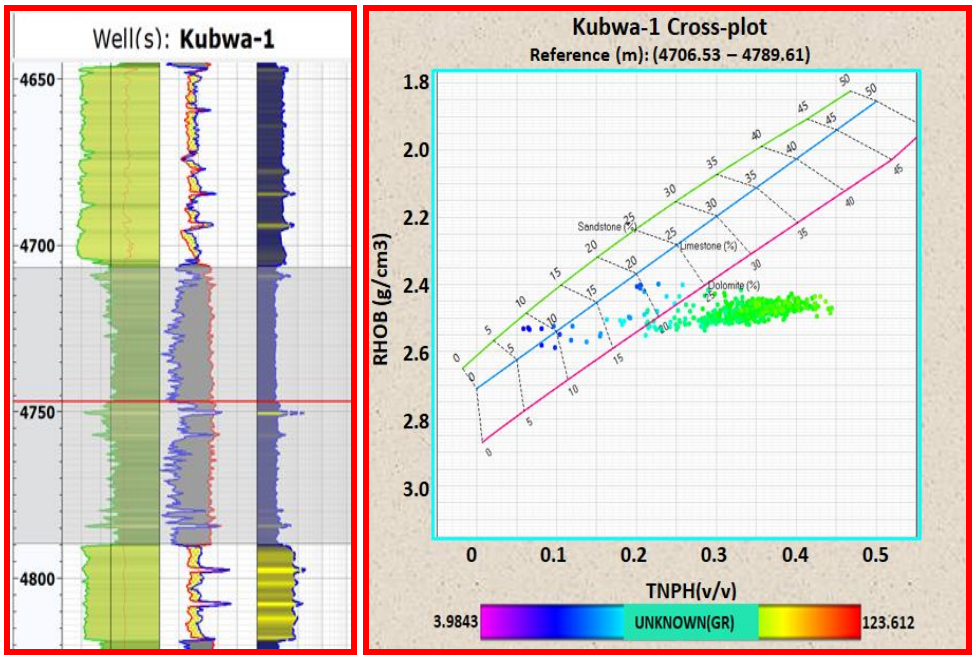

Figure 4.12 (b): Interactive Selection Mode Log View Highlighting Shale Lithology in the Cross-Plot

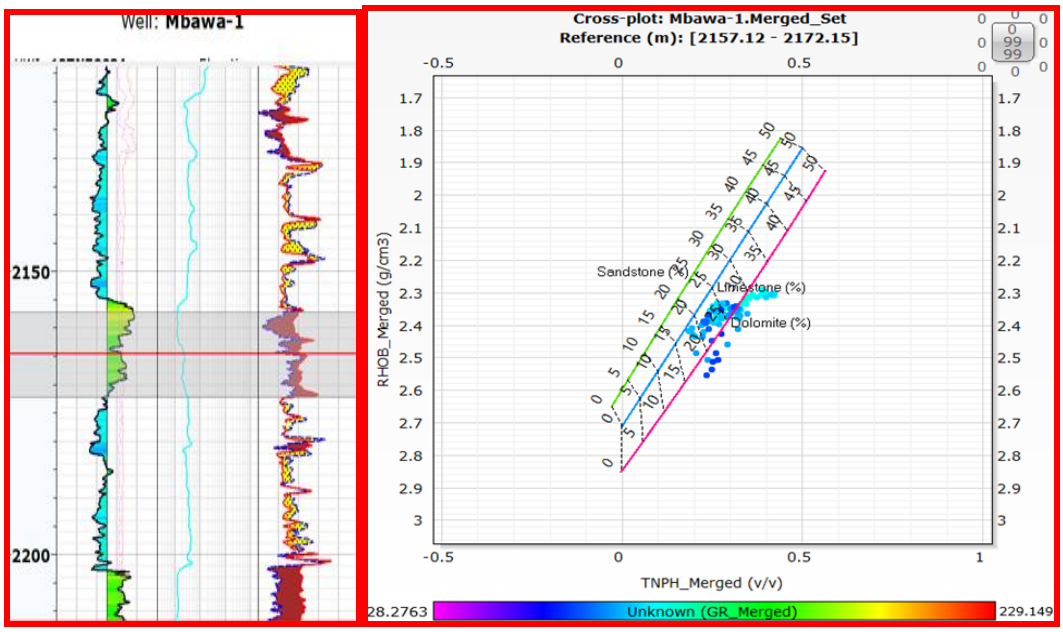

Figure 4. 13 (a): Dolomitic Limestone Lithology Identified from the Density Versus Neutron Porosity Cross Plot

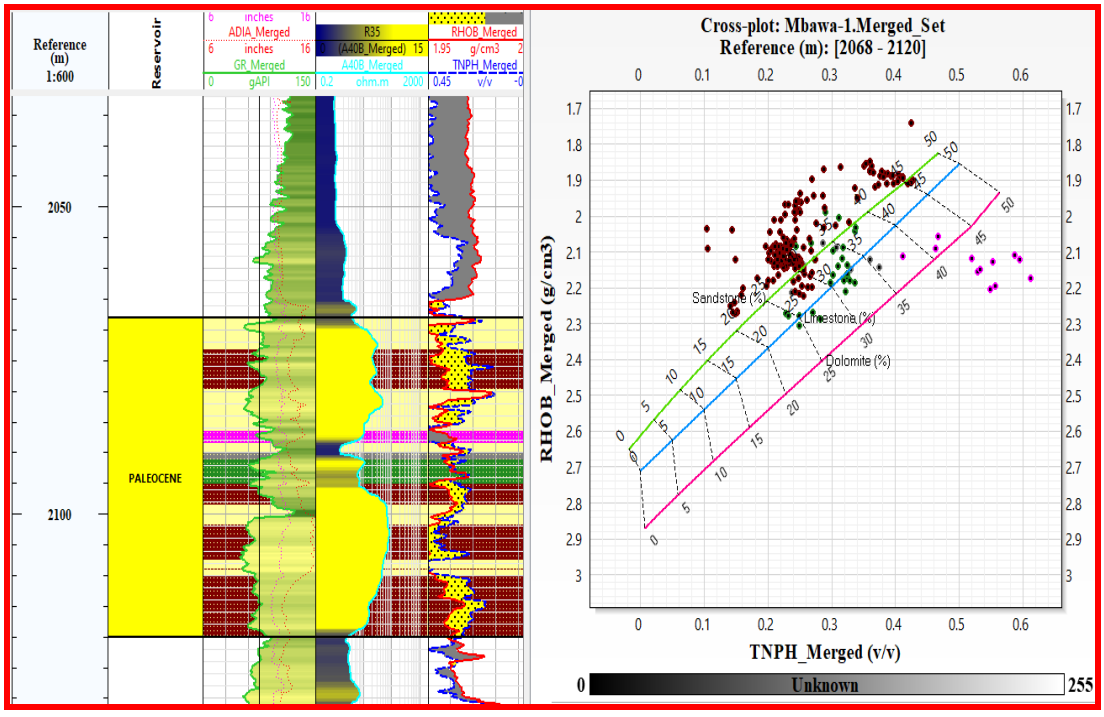

Figure 4.13 (b): Intercalations of Sandstone with a Possible Gas Sand(Brown), Limestone(Green), Dolomite(Purple), and Shale.

At a depth range of 4706.53 m – 4789.61 m, the dominant lithology implied is shale. In Figure 4.13(a) dolomitic lithology is inferred at the depth range of 2157.12 m-2172.15 m. In Figure 4.13(b) intercalations of sandstone, limestone, dolomite, and shale are possible at a depth range of 2068 m – 2120 m. At this depth range gas sand can be inferred especially from the cluster points well above the sandstone line and shale below the dolomite line according to the model in Figure 4.13(b).

The result from the cross plots compares to the lithologies according to the well completion reports (Woodside, 2007). From the identified lithologies, reservoir and non-reservoir were distinguished, hydrocarbon and water-bearing lithologies were marked, and oil-bearing and gas-bearing sections were mapped from the well logs. Qualitatively, reservoir rocks were identified as regions with low gamma rays using the log view display of the well logs (Darling, 2005). Hydrocarbon-bearing zones were mapped out at regions with low gamma rays combined with high resistivity values (Figure 4.14 a to c).

In distinguishing oil from gas-bearing zones, the separation between the density and the Neutron logs at the crossover region was employed alongside the low gamma ray and high resistivity values. Water-bearing zones were identified as regions with low gamma ray and low resistivity values. Reliably, the reservoir rock is indicated from the neutron/density logs behaviour whereby the density curve moves to lower density (towards the left) to touch or cross the neutron curve (crossover). This corresponded to low gamma ray log readings implying a clastic reservoir. The greater the separation between the neutron and density curves (crossover), the better the reservoir quality (Ijasan et al., 2013). Gas zones will generally depict greater crossovers compared to oil and water zones at the same porosity consideration. Shales correspond to zones where the neutron curve lies to the left of the density curve by at least 6 neutron porosity units with relatively high gamma ray readings and low resistivity.

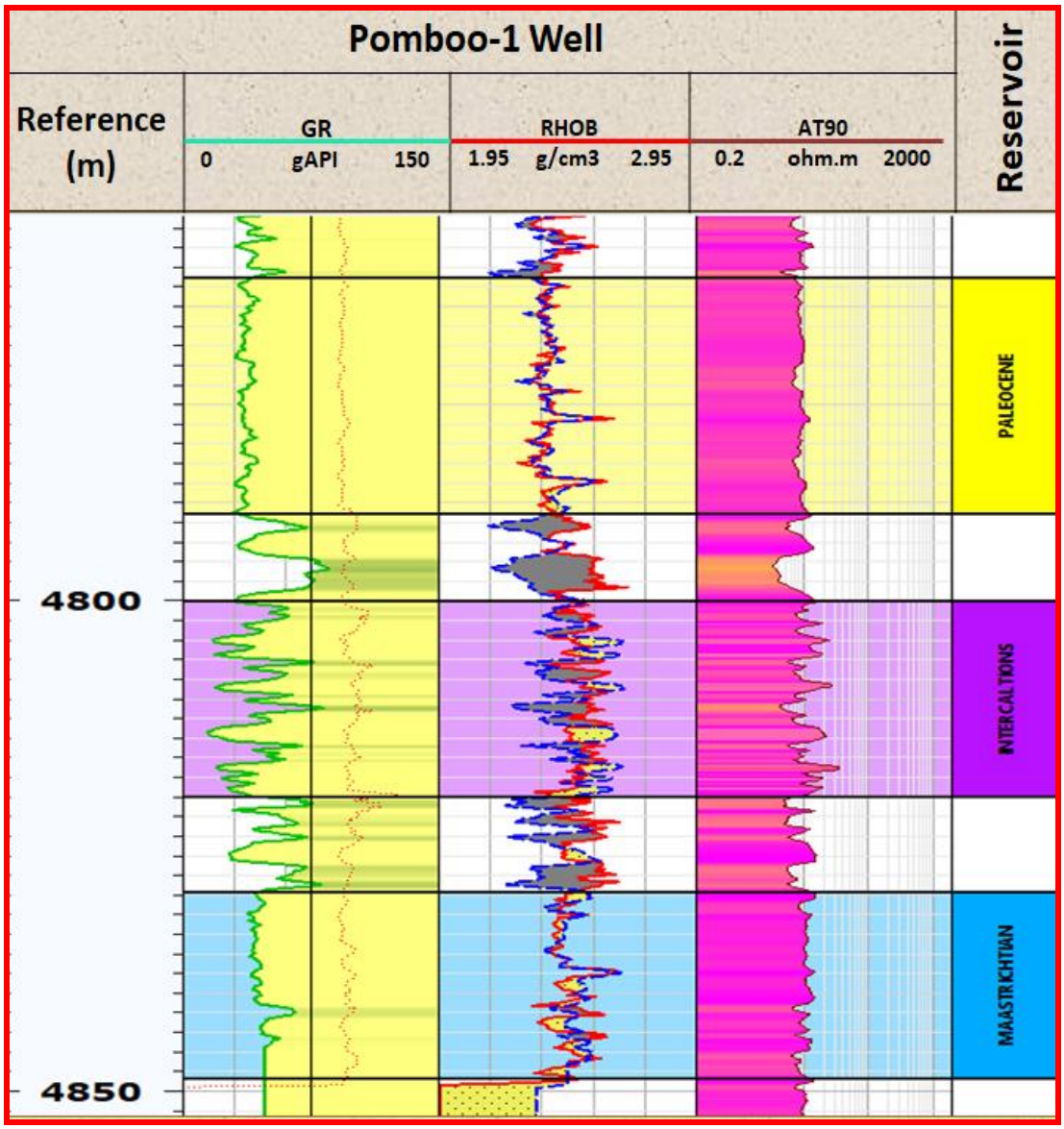

Figure 4.141 (a): Possible Reservoir Zones in Pomboo-1 Well

Kubwa-1 well

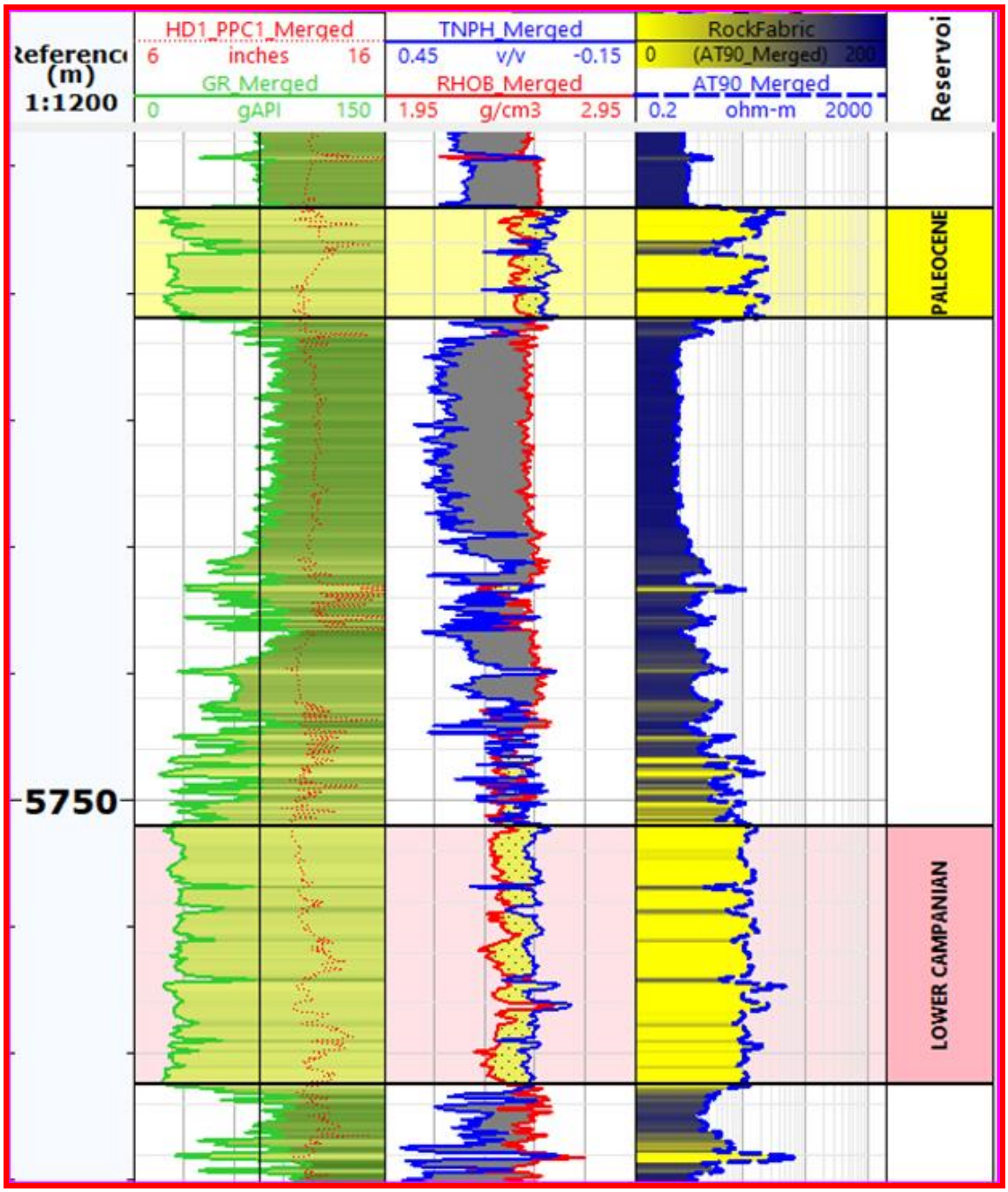

Figure 4.14 (b): Possible Reservoir Zones in Kubwa-1 Well

Mbawa-1 Well

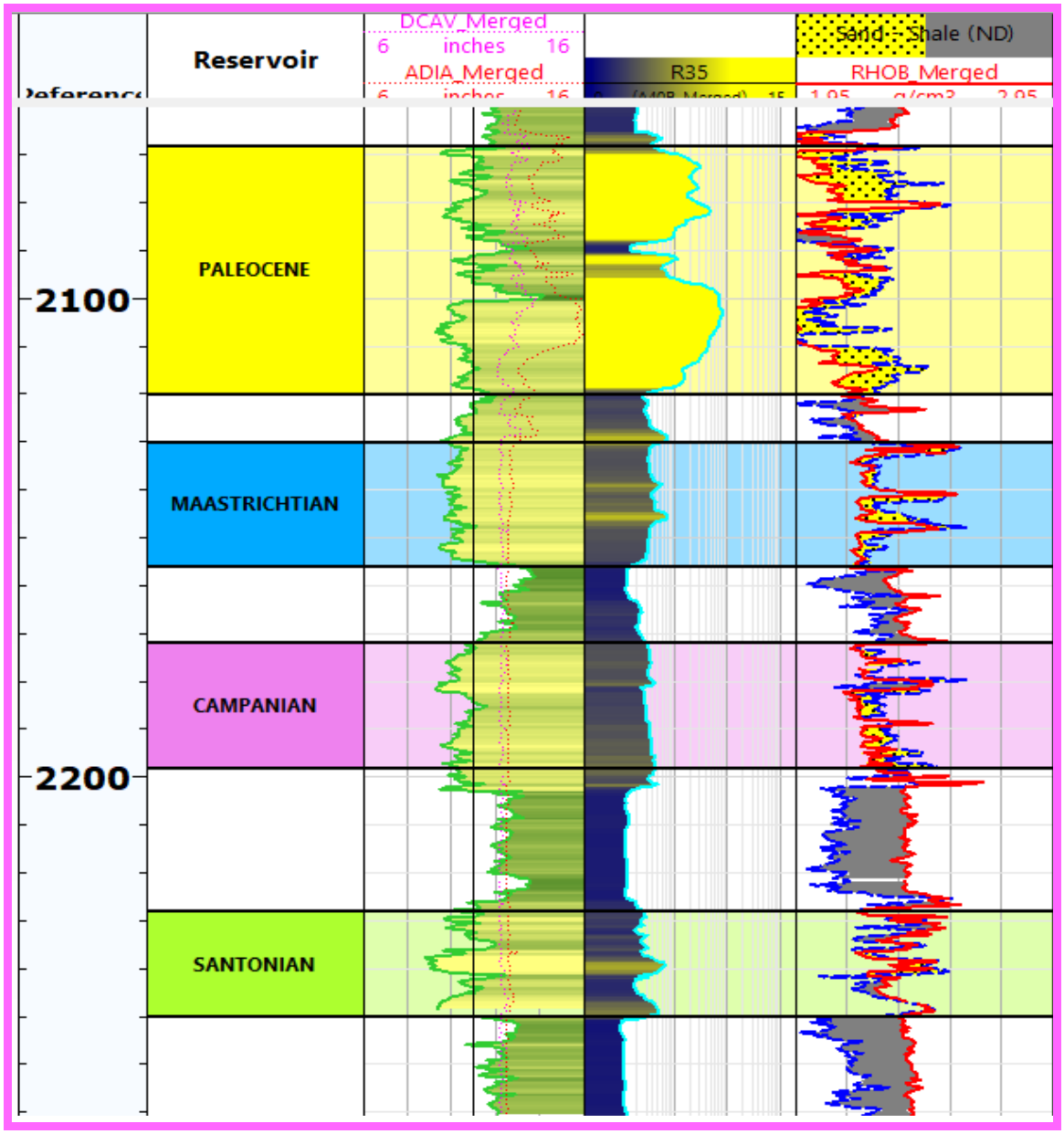

Figure 4.14 (c): Possible Reservoir Zones in Mbawa-1 Well

Quantitatively, the reservoirs' hydrocarbon potential was estimated through the determination of the petrophysical parameters like the effective porosity, permeability, water saturation, hydrocarbon saturation, shale volume, and net pay depth and thickness. The evaluation of the petrophysical parameters was achieved through the application of the formulae, (discussed in section 2.5.3), within Schlumberger's Techlog software. Porosity was estimated using a combined neutron-density log applying equations 2.22 and 2.23. Water saturation was determined using

equation 2.24 which is Archie's method within the software and hydrocarbon saturation was estimated through equation 2.25. Shale volume was determined through equation 2.20. The depth of the net pay and its thickness was obtained from the petrophysical analysis summaries from the software. The qualitative and quantitative formation evaluation was constrained by the lithological and stratigraphic reports and related publications of the well-completion reports. Details of the petrophysical properties are tabulated in section 4.3.3 under petrophysical analysis.

4.3.2 Reservoir Identification

Various regions were identified as possible reservoir zones in the three wells based on the curve behaviour of the gamma-ray, neutron, density, and resistivity logs (Figures 4.14 and 4.15). Well, log analysis for Kubwa-1 well resulted in the identification of five possible reservoir zones in the depths between 4650-4704 m (Miocene), 4884-4910 m (Oligocene), 5444-5484 m (Eocene), 5633-5655 m (Paleocene), and 5755-5806 m (Campanian). In Mbawa-1 well log analysis six potential reservoir zones were identified. In the Paleocene (2068-2120 m), Maastrichtian (2130-2156 m), Campanian (2172-2198 m), Santonian (2228-2250 m), and Albian (2340-2376 m). For Pomboo-1 well log evaluation, three probable zones were marked. They include the Paleocene (4767-4791 m), Intercalations (4800-4820 m), and Maastrichtian (4830-4849 m) (Appendix III).

In Figures 4.14 (a to c), the Paleocene zone was compared for the three wells. It was found that for Pomboo-1 well at this zone the lithology was a carbonate, both from the neutron-density curve behaviour and from the stratigraphic information (Appendix V). For both the Kubwa-1 and Mbawa-1 wells, the lithology was sandstone as could also be confirmed from the stratigraphic information and well completion reports. The qualified zones from each well and particular depth were subjected to petrophysical analysis.

Regarding the various petrophysical properties obtained for all the identified zones, a zone was picked from each well whose petrophysical properties were best compared to other zone properties. The petrophysical properties used as criteria for picking the

best reservoir zones include the reservoir thickness, shale volume, effective porosity, and water saturation. The best zone would have the highest thickness, highest effective porosity, least shale volume, and least water saturation. Picked from each well was the 4884-4910 m (Oligocene) for Kubwa-1, Paleocene (2068-2120 m) for Mbawa-1, and Paleocene (4767-4791 m) for Pomboo-1, as seen in figures 4.15 (a to c), for further analysis and comparison.

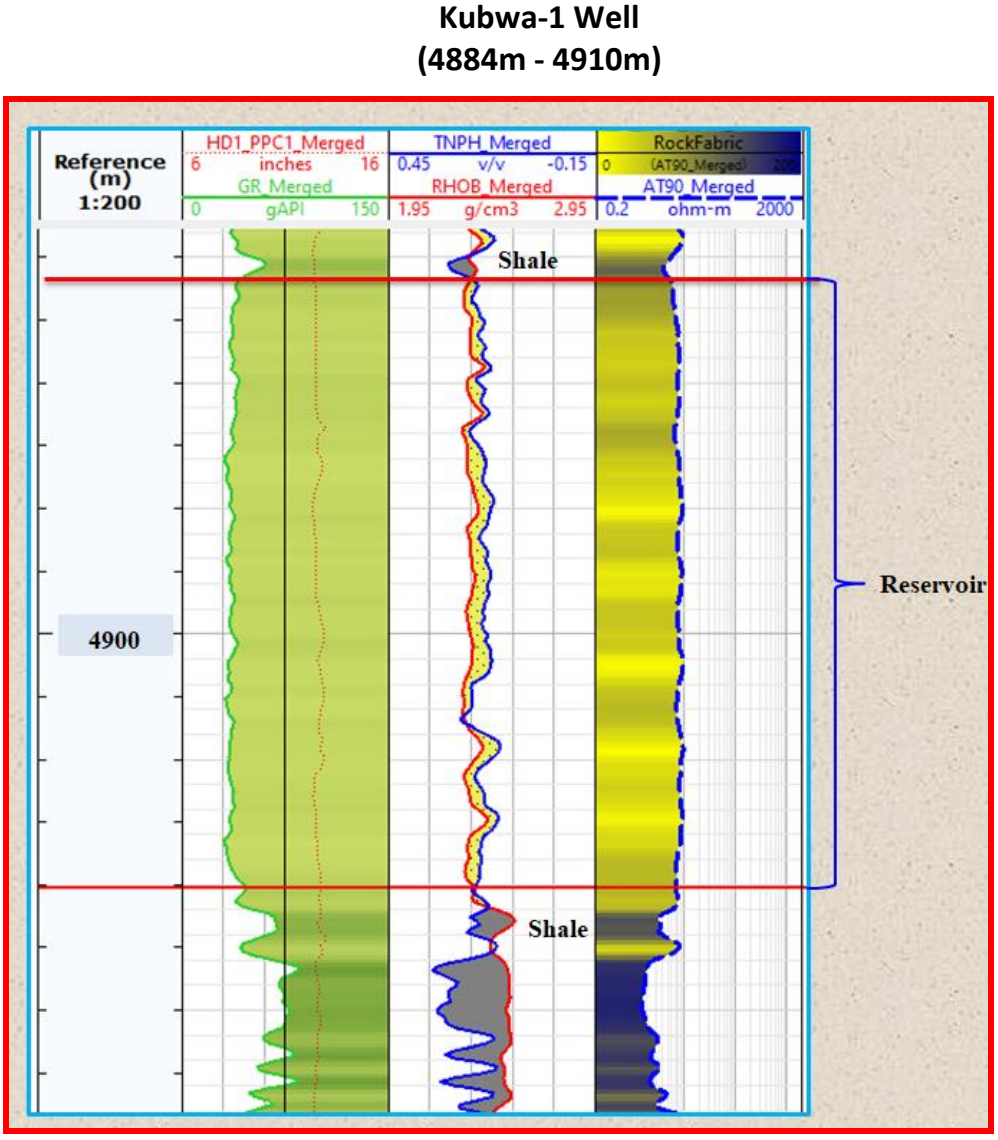

Figure 4.15 (a): Reservoir Identified in the Kubwa-1 Well for Analysis

Mbawa-1 Well
(2068m-2120m)

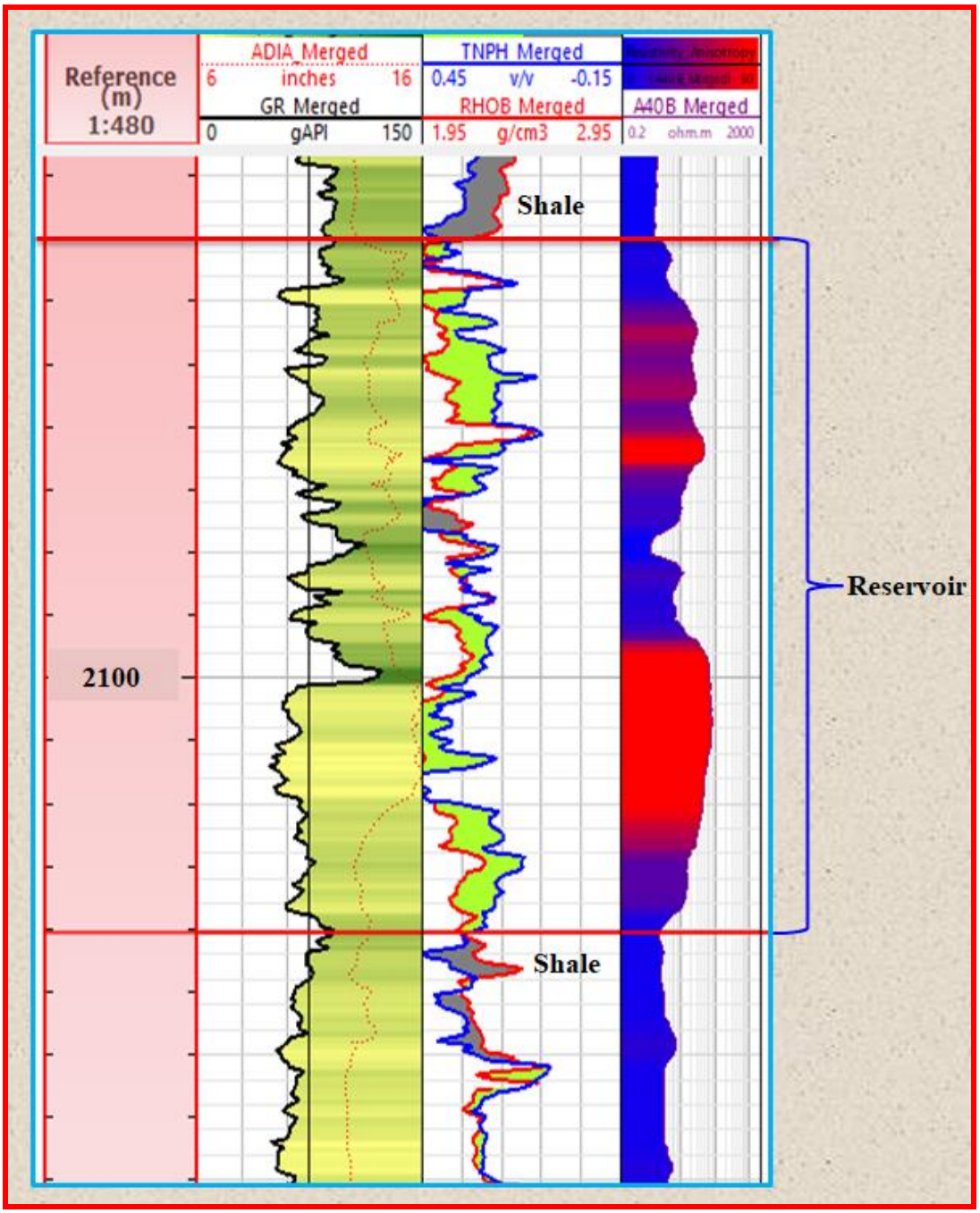

Figure 4.15 (b): Reservoir Identified in the Mbawa-1 Well for Analysis

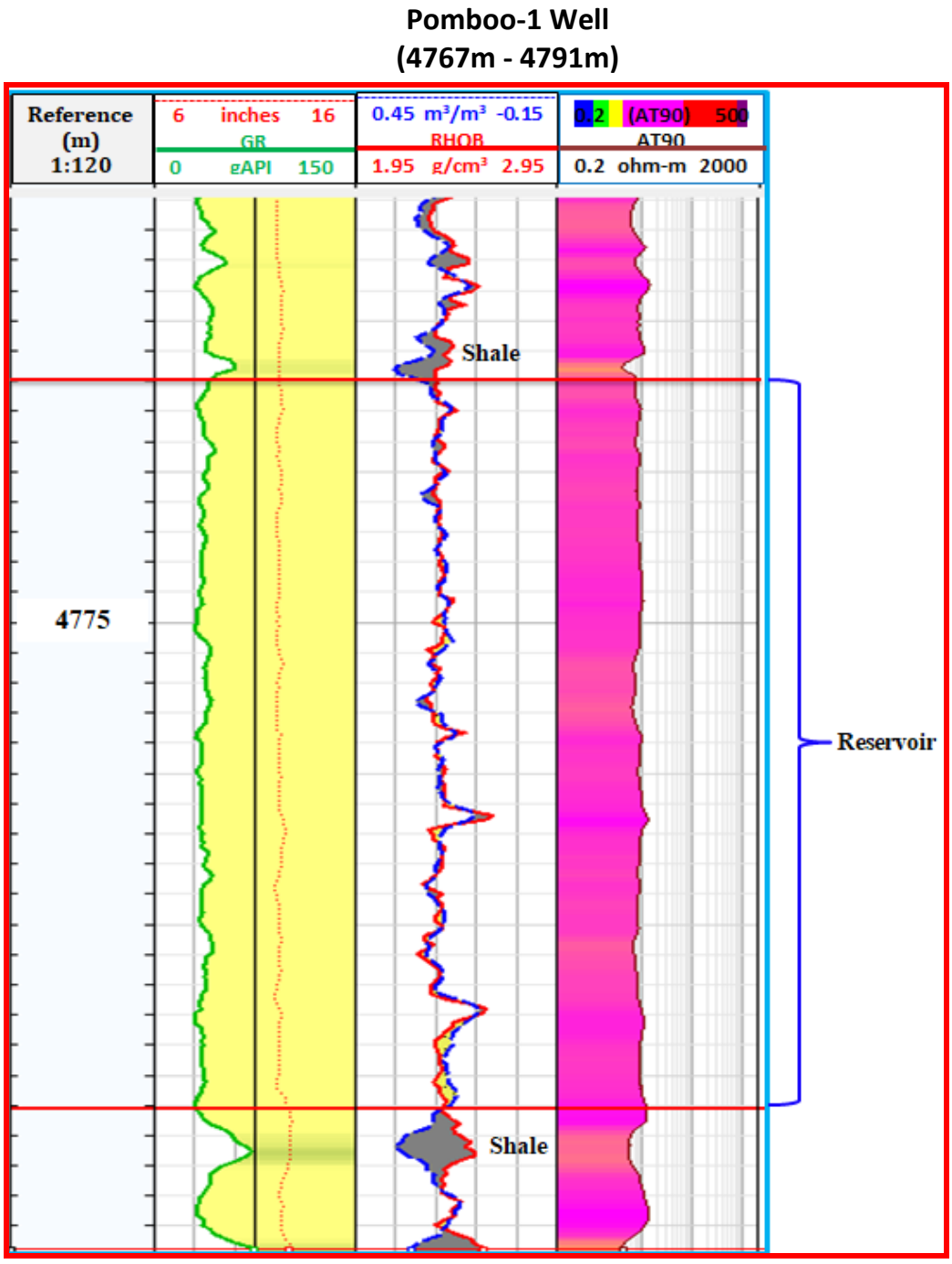

Figure 4.15 (c): Reservoir Identified in the Pomboo-1 Well for Analysis

The reservoir lithologies for the identified zones include the sandstones (Paleocene and Top Campanian) for the Kubwa-1 well, calcareous sand (Base Paleocene) and turbidite sandstones (Top Cretaceous) for Mbawa-1 well, and carbonate (Base Maastrichtian) and sandstone (Base Campanian) for Pomboo-1 well.

4.3.3 Petrophysical Analysis

Delineation of lithology and fluid discrimination was achieved by analyzing the Gamma Ray and Resistivity logs. High Gamma Ray values with Low Resistivity values signified shale lithology. Conversely, Low Gamma Ray values with high Resistivity values indicated a hydrocarbon-bearing zone. Quantitative analysis of the well logs shows a high porosity hydrocarbon reservoir with moderate thickness, low shale volume, and water saturation, as seen in Table 4.1.

Table 4.1: Reservoir Petrophysical Properties Summary of the Three Wells

Well	Top (m)	Bottom (m)	Thickness (m)	V_{Shale} (%)	Φ_{Eff} (%)	S_w (%)
Kubwa-1	4884	4910	25.38	7.1	18.8	43.6
Mbawa-1	2068	2120	43.22	22.2	25.2	22.8
Pomboo-1	4767	4791	18.95	26.4	11.8	55.7

The hydrocarbon bearing zone reflects possibly coarse-grained friable sandstone in Kubwa-1 and Mbawa-1 and calcareous sand in Pomboo-1 having low shale volume and water saturation with high porosity (Figure 4.16).

Figure 4.16(a) shows the log view of the calculated petrophysical properties for Kubwa-1. The details shown include the depth of the reservoir, the shale volume, porosity, and the water saturation. At a depth of 5764.18 m in Kubwa-1, the petrophysical properties obtained such as the shale volume (0.1%), effective porosity (13.39%), water saturation (41.85%), and pay thickness (10.66 m) signify a possible reservoir.

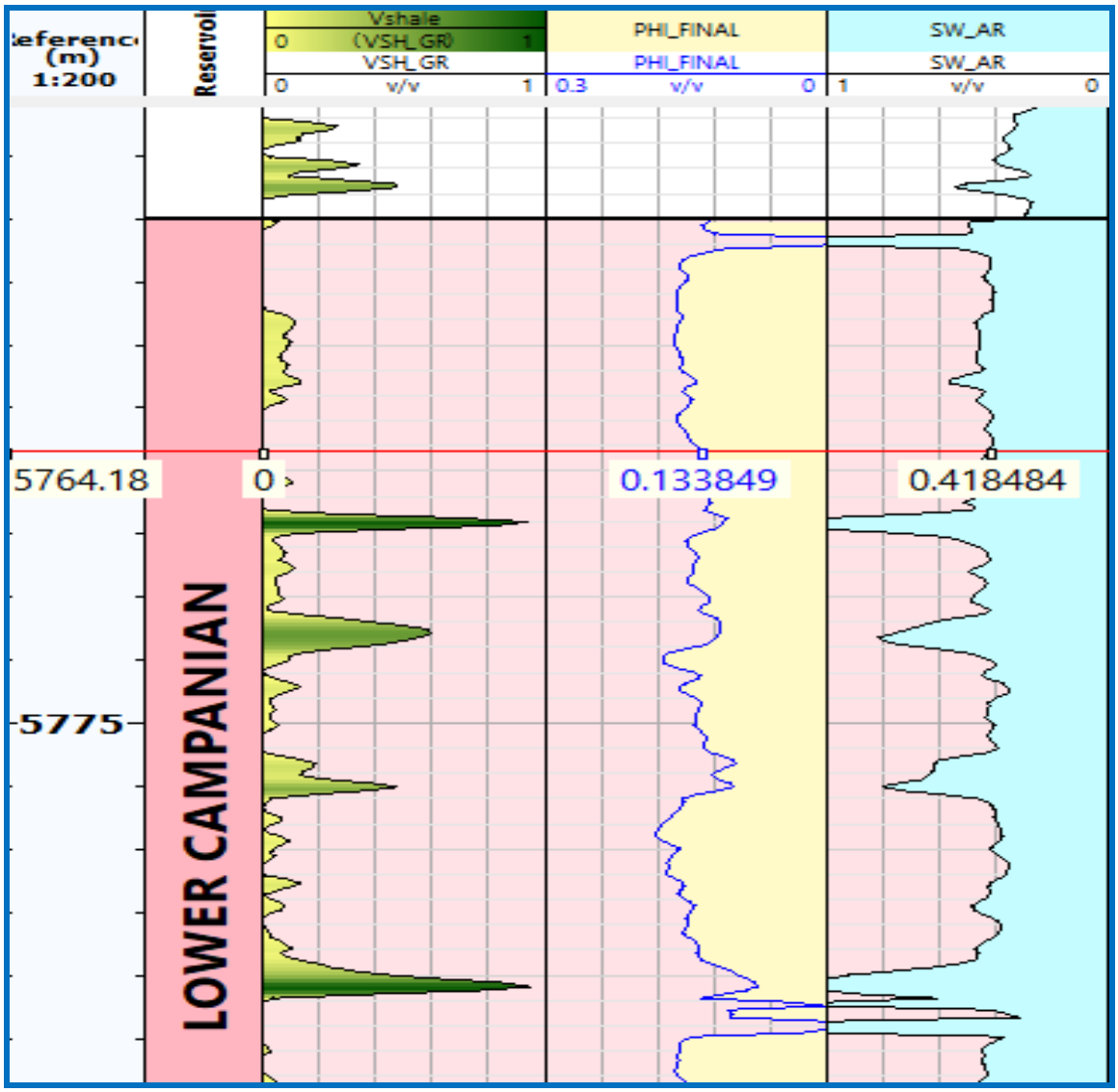

Figure 4.16 (a): Calculated Petrophysical Properties for Kubwa-1

Figure 4.16(b) shows the log view of the calculated petrophysical properties for Mbawa-1. The details shown include the depth of the reservoir, GR response, resistivity response, neutron density, the shale volume, porosity, and the water saturation. In Figure 4.16 (b), the shale volume (4.0%), porosity (25.66%), water saturation (14.40%), resistivity (47.15 Ωm), and less than half gamma ray reading (56.50 gAPI) were registered at a depth of 2081.29 m in Mbawa-1 well implying a reservoir with good characteristics.

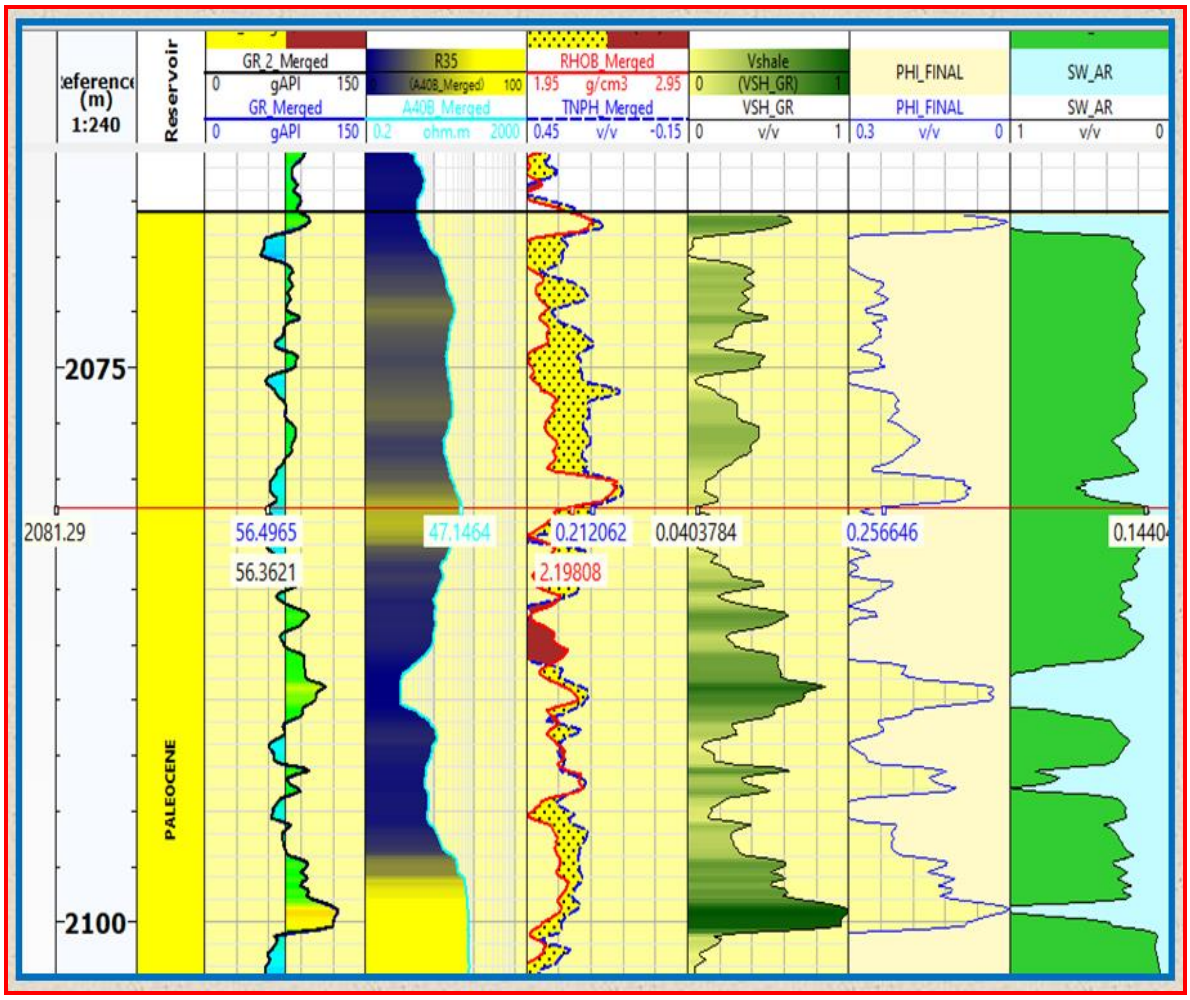

Figure 4.16 (b): Calculated Petrophysical Properties for Mbawa-1

Figure 4.16(c) shows the log view of the calculated petrophysical properties for Pomboo-1. The details shown include the depth of the reservoir, GR response, resistivity response, neutron density, the shale volume, porosity, and the water saturation. Figure 4.16 (c) shows the results of the calculated Pomboo-1 well petrophysical properties indicating a suitable reservoir whose properties at a depth of 4839.44 m include 5.8% shale volume, 11.99% porosity, 48.14% water saturation, and 3.15 m pay thickness.

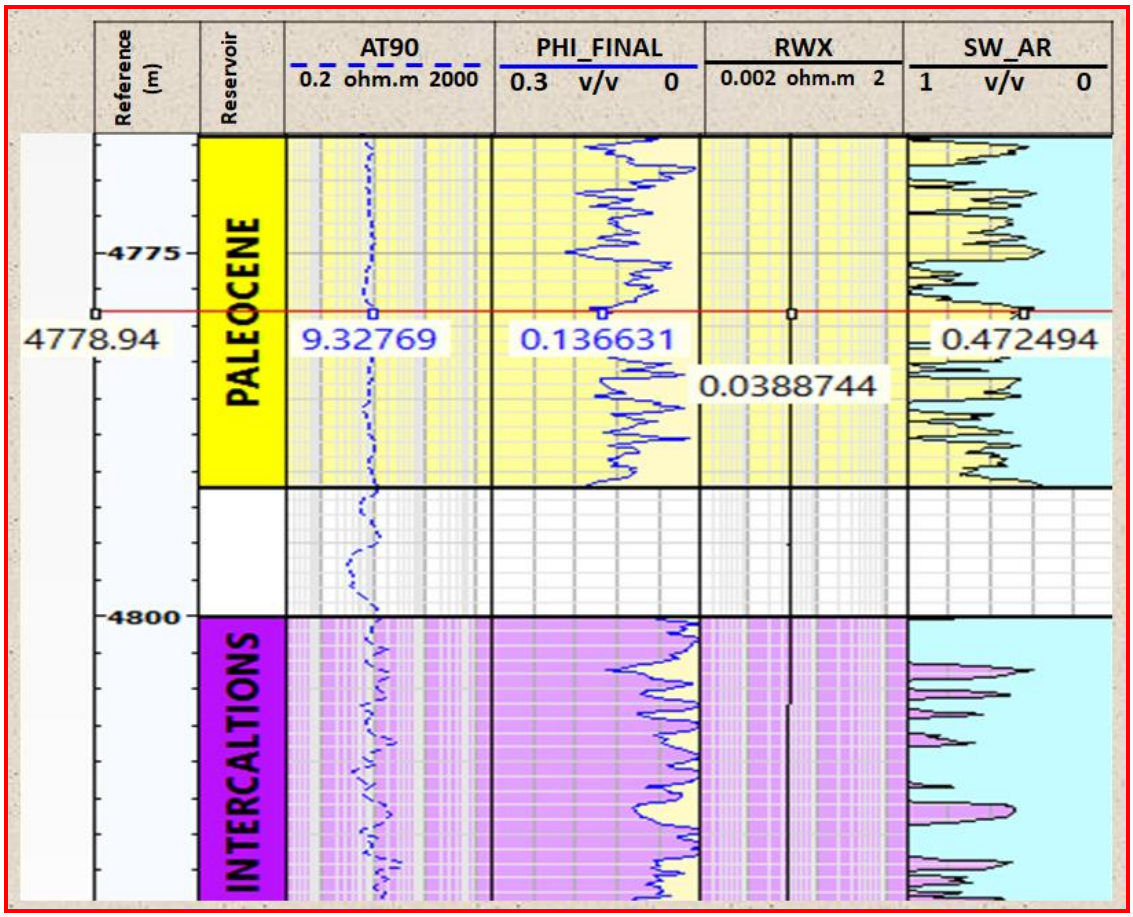

Figure 4.16 (c): Calculated Petrophysical Properties for Pomboo-1

Following the exploration companies' reports within the National oil cooperation of Kenya (NOCK) library, the cutoff value of shale in the Lamu basin is 50%, meaning rocks with more than 50% shale content were considered non-reservoirs, while those with less than 50% of shale content were regarded as a reservoir. The minimum cutoff for effective porosity was set at 5% to delineate porous sand intervals that could allow the flow of reservoir fluids and non-porous ones that could not. A maximum 60% water saturation cutoff was set to distinguish pay zone with less than 60% water saturation from non-pay zones with more than 60% water saturation. The petrophysical properties obtained at the specific depths indicated above in the three wells lie within the range of the cutoffs. Constrained with the petrophysical properties calculated based on the core analysis, the properties above indicate potential reservoirs in the respective wells. The summary of the petrophysical properties of the identified reservoir intervals across the wells is shown in Table 4.1.

4.3.4 Rock Physics Analysis

Whereas petrophysics is focused on log interpretation for formation evaluation, rock physics concentrates on linking rock properties with geophysical measurements. The integrated approach of applying both the petrophysics analysis and the rock physics technique is a powerful tool in subsurface imaging. The petrophysics properties (such as the shale volume, effective porosity, and water saturation) were used as the necessary input to rock physics modelling and calibration. The geophysical measurements such as the bulk density, compressional slowness, and shear slowness were used in the rock physics toolbox group under the geophysics tab of Schlumberger's Techlog software in generating the acoustic impedance, Mu-rho, Lambda-Rho, Compressional velocity, and shear velocity. Appropriate pairs were then cross-plotted and suitably Colour coded to delineate the various lithologies and fluid types. The output of the models is a representation of the changes in the elastic properties due to lithological, fluid, and pressure variations at the well location.

In rock physics analysis as shown in Figures 4.17 (a) to (f) selected color codes were used. The cross-plotted petrophysical parameters and pairs of rock properties reflected the various litho-units and fluid types with varied sensitivity. This is because elastic parameters such as shear and bulk modulus, density, P-wave impedance, and S-wave impedance are routinely used to discriminate lithology since they are sensitive to lithological changes. Conversely, V_p/V_s ratio, Lamé constants, elastic wave velocity, and Poisson's ratio are leveraged in discriminating fluids in hydrocarbon reservoirs since they are sensitive to fluid changes. The best property pairs were preferred for the present study analysis. Cross-plotting Mu-rho against density separated the data clusters into three zones (hydrocarbon sand, brine sand, and shale) since shale has a higher density than sand and brine is denser than hydrocarbon. Mu-rho and density are good at discriminating lithology, with density being good at discriminating fluids as well.

Therefore, the orange ellipse indicates shale, the red shows brine-saturated sand, and the green represents the hydrocarbon-bearing zone (Figure 4.17 (a)).

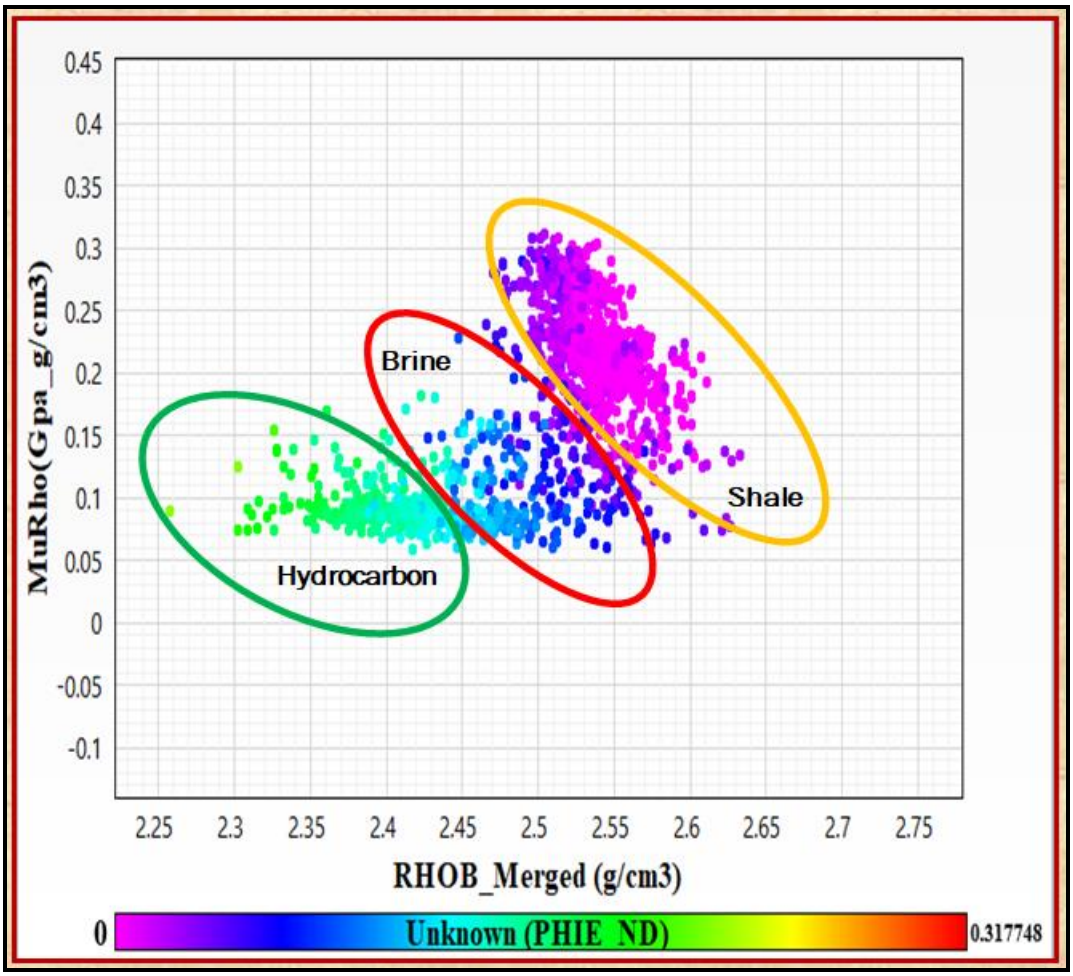

Figure 4.17 (a): Mu-Rho Against Density Rock Physics Model

From the cross plot of acoustic impedance against Lambda-Rho, the hydrocarbon zone shows high acoustic impedance and low Lambda-Rho compared to brine-saturated sand and shale regions, as confirmed by the effective porosity colour code (Figure 4.17(b)).

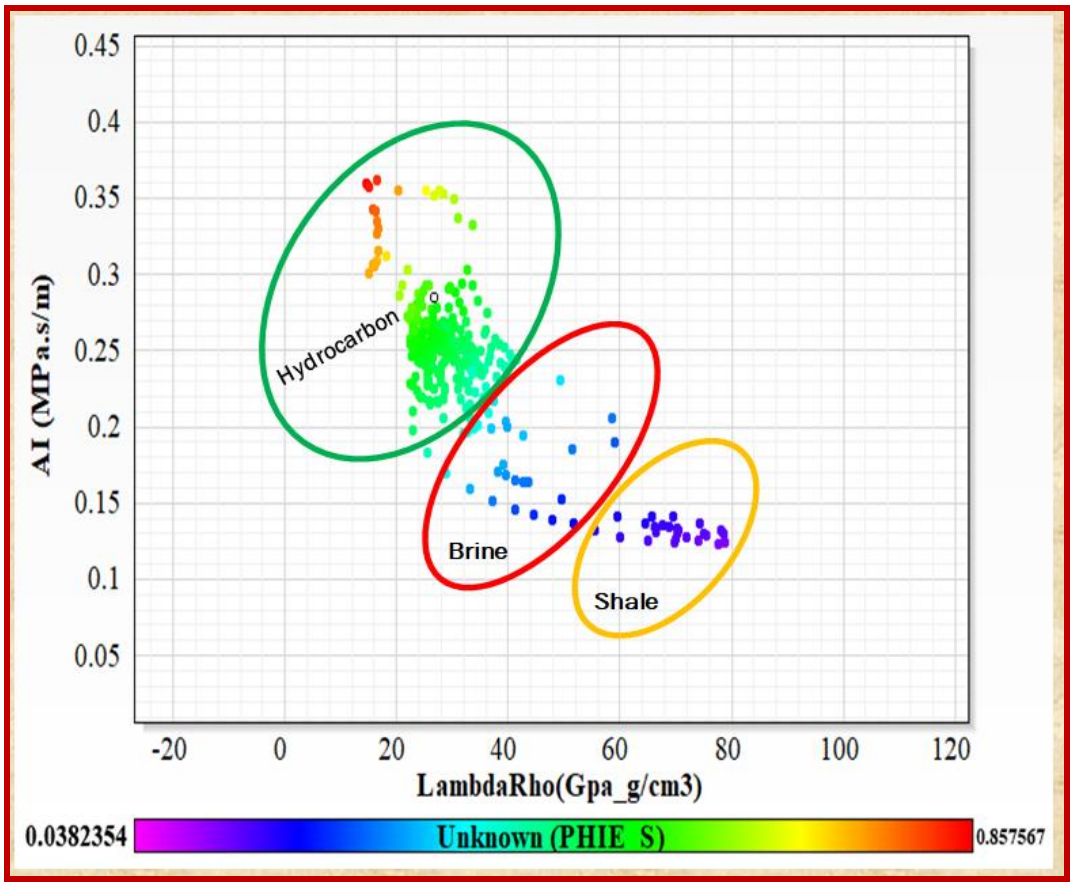

Figure 4.17 (b): Acoustic Impedance Against Lambda-Rho Rock Physics Model

Data cluster analysis in the Lambda-Rho against Mu-Rho cross plot suggests the presence of gas-saturated sand as it occupies the lower values of Lambda-Rho, a measure of incompressibility. It is also evident from the cross plot that Lambda-Rho is more robust to use in fluid discrimination than Mu-Rho (Figure 4.17(c)). Lambda-Rho against V_p/V_s cross plot signifies that Lambda-Rho is a better fluid type and lithology discriminator than the velocity ratio. The hydrocarbon zone likely to be gas is shown by low values of lambda-rho (Figure 4.17(d)).

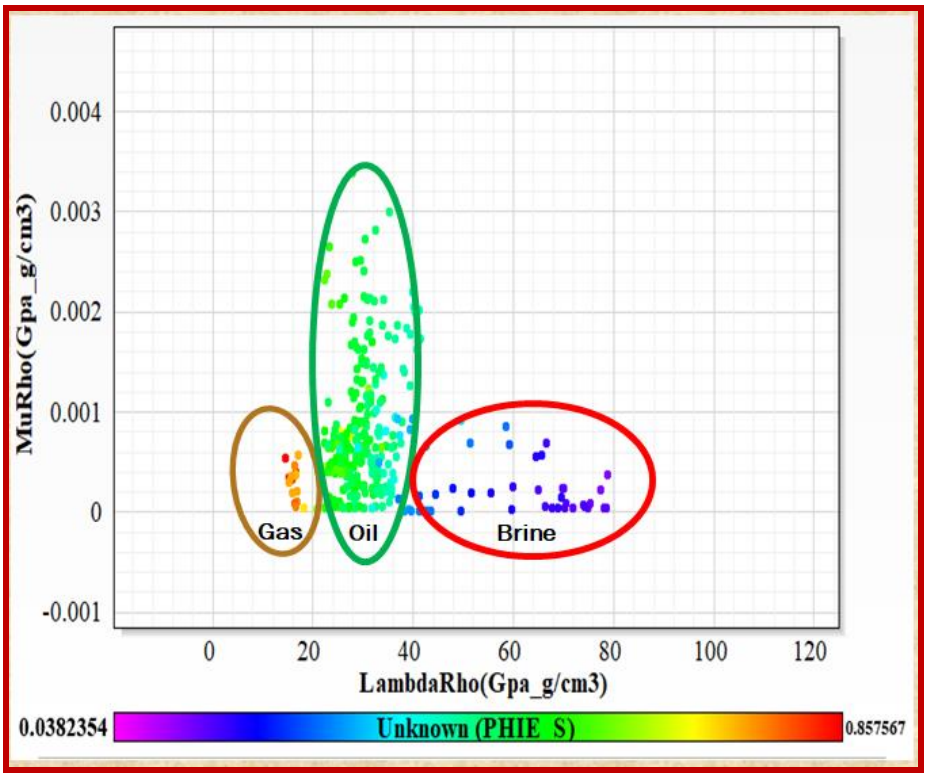

Figure 4.17 (c): Mu-Rho Against Lambda-Rho Rock Physics Model

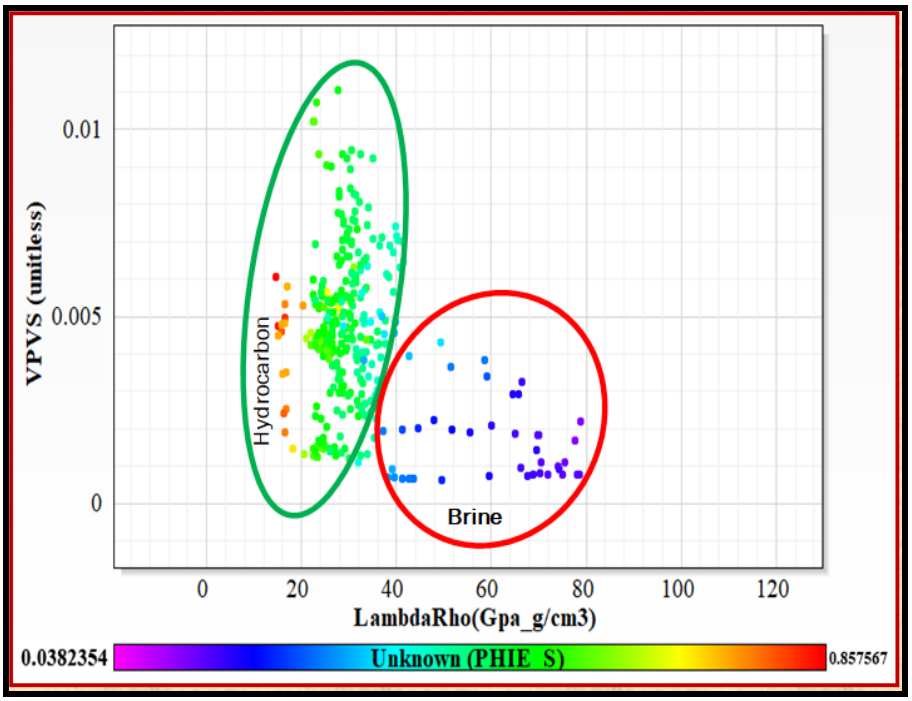

Figure 4.17 (d): Vp/Vs Against Lambda-Rho Rock Physics Model

The V_p/V_s ratio against the Acoustic impedance cross-plot distinguished the reservoir into three zones: hydrocarbon sand (green ellipse), brine sand (red ellipse), and shale (orange ellipse), especially along the acoustic impedance axis. The acoustic impedance value is highest in the shale zone and lowest in the hydrocarbon-bearing sand region, with the lowest and highest effective porosity values, respectively (Figure 4.17(e)).

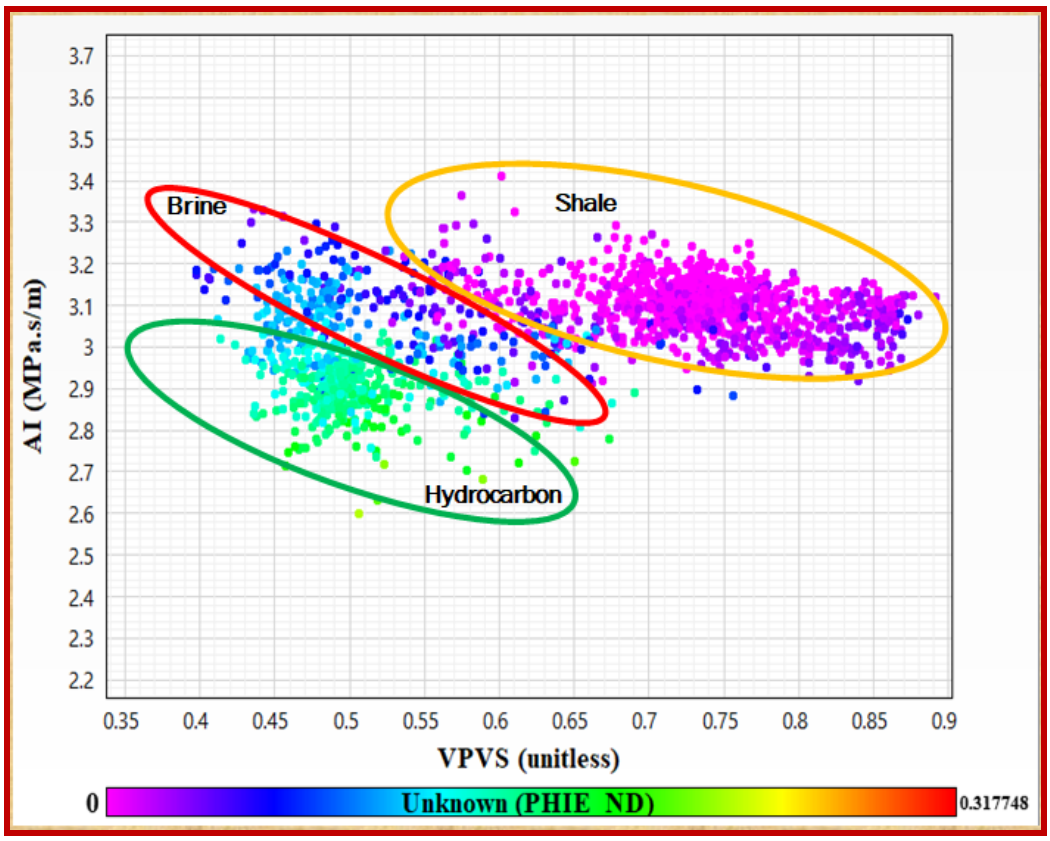

Figure 4.17 (e): Acoustic Impedance Against Vp/Vs Rock Physics Model

Cross-plotting velocity against porosity indicates that the reservoir consists of friable sandstones given the velocity and final effective porosity range values (Figure 4.17(f)). In Figure 4.17(f) the sediments lie on and close to the Reuss lower bound, which implies that they are weak and unconsolidated. Their porosity values majorly ranging from 0.1 to 0.5 support this. The Sediments are also aligning to the steeper part of the Reuss bound which indicates that they are fractured. These sediments observed lie below the friable sand model, indicating that they are less cemented.

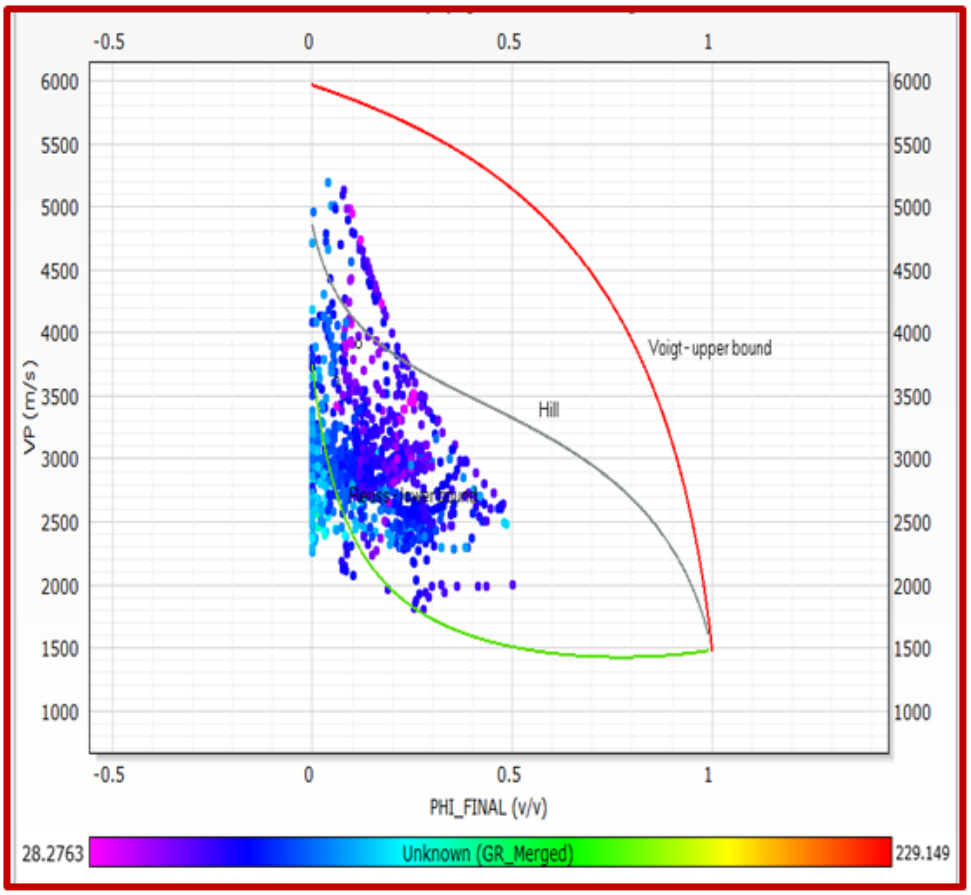

Figure 4.17 (f): Velocity Against Porosity Rock Physics Model

From the data cluster analyses of the models, it can be noted that, generally, hydrocarbon-saturated zones have low density, acoustic impedance, Mu-rho, and Lambda-rho. Brine-saturated regions are associated with low acoustic impedance and Mu-rho values and relatively higher Lambda-rho values.

Shale zones are indicated at high values of density, acoustic impedance, Mu-rho, and Lambda-rho. When the reservoir properties; S_w, Φ, and G.R. response are used as colour codes in the cross-plots, hydrocarbon-bearing zones indicate relatively low S_w and G.R. with high porosity values compared to brine saturated regions and shale zones.

4.3.5 Fluid Substitution Results

Rock frame properties were obtained from the well log data using the Petrel software and were kept constant during the fluid substitution process. The properties for the three wells (Kubwa-1, Mbawa-1, and Pomboo-1 respectively) are summarized in table 4.2. Porosity was determined from both well log data and core data analyses.

Table 4.2: Rock Frame Properties from Kubwa-1, Mbawa-1, and Pomboo-1 Wells

WELL NAME	RESERVOIR ZONE		K_{dry}(Gpa))	K_{min} (Mpa)		K_{fluid}(Gpa)	Φ (%)
	Top(m)	Bottom(m)		Quartz	Clay		
Kubwa-1	4884	4910	14.56	35981	35000	2.39	18.8
Mbawa-1	2068	2120	13.85	35981	35000	2.26	25.2
Pomboo-1	4767	4791	15.13	35981	35000	2.87	55.7

The rock frame properties were used as input in the Petrel software to calculate the effects of fluid substitution on seismic elastic properties in the three wells when subjected to the various model scenarios as displayed in table 4.3(Kubwa-1), 4.4(Mbawa-1), and 4.5(Pomboo-1). In the oil case, 70% oil, 25% water, and 5% gas saturations were used. For the gas case, 70% gas, 25% water, and 5% oil saturations were used. In the water scenario, 100% water and 0% oil and gas were used.

From the analysis of the model results, compressional velocity (V_p) was higher when the rock was water saturated than when dry or saturated with gas in Kubwa-1 and Pomboo-1 while in Mbawa-1 it was highest in dry rock. Conversely, shear velocity, with slight changes, indicated a higher value in the dry or gas-saturated case than in the oil-saturated or water-saturated case in Kubwa-1 and Mbawa-1.

Table 4.3: Gassmann Fluid Substitution Parameters and Results for Kubwa-1 Well

INPUT		SCENARIOS	OUTPUT			
Elastic Rock Properties			**Elastic Rock Properties**			
V_P (m/s)	3511			**Oil**	**Gas**	**Brine**
V_S (m/s)	2084		$V_{P(m/s)}$	3763	3640	3740
$\rho\ (g/cm3)$	2.42		$V_{S\ (m/s)}$	2040	2052	2017
			$\rho\ (g/cm3)$	2.32	2.29	2.37

Mineral Data

Mineral	**%**	**K_{min}(Mpa)**	ρ(kg/m^3)
Quartz	93	35981	2640
Clay	7	35000	2680

Initial Fluid Data		**Final Fluid Data**		
	%	%	Oil	Gas
Water	44	S_w	25	25
Oil	28	S_o	70	5
Gas	28	S_g	5	70
		The water scenario is always 100%		

Table 4.4: Gassmann Fluid Substitution Parameters and Results for Mbawa-1 Well

INPUT		SCENARIOS	OUTPUT		
Elastic Rock Properties			**Elastic Rock Properties**		
V_P (m/s)	2462			**Oil**	**Gas**	**Brine**
V_S (m/s)	1488		V_P (m/s)	1883	1606	2152
$\rho\ (g/cm3)$	2.58		V_S (m/s)	1463	1476	1452
			$\rho\ (g/cm3)$	2.34	2.26	2.49

Mineral Data

Mineral	**%**	**K_{min}(Mpa)**	ρ(kg/m^3)
Quartz	77	35981	2640
Clay	23	35000	2680

Initial Fluid Data		**Final Fluid Data**		
	%	%	Oil	Gas
Water	22	S_w	25	25
Oil	39	S_o	70	5
Gas	39	S_g	5	70
		The water scenario is always 100%		

Table 4.5: Gassmann Fluid Substitution Parameters and Results for Pomboo-1 Well

INPUT		SCENARIOS	OUTPUT			
Elastic Rock Properties			**Elastic Rock Properties**			
V_P (m/s)	3274			**Oil**	**Gas**	**Brine**
V_S (m/s)	2292		V_P (m/s)	3560	3480	3654
$\rho\ (g/cm3)$	2.46		V_S (m/s)	2202	2240	2160
			$\rho\ (g/cm3)$	2.32	2.24	2.38

Mineral Data

Mineral	**%**	**K_{min}(Mpa)**	ρ(kg/m^3)
Quartz	73	35981	2640
Clay	27	35000	2680

Initial Fluid Data		**Final Fluid Data**		
	%	%	Oil	Gas
Water	56	S_w	25	25
Oil	22	S_o	70	5
Gas	22	S_g	5	70
		The water scenario is always 100%		

Generally, there is a notable decrease in compressional velocity in Mbawa-1 and a notable increase in Kubwa-1 and Pomboo-1 when brine saturation increases. The density was reduced in the three wells when saturation was increased. Shear velocity in the three wells indicated slight changes with the highest values seen when the rock is dry than when fluid was saturated in all the wells.

4.4 Integrating Gravity, Seismic, Petrophysics, and Rock Physics Analysis

Gravity modelling utilized Geosoft's Oasis Montaj software which provided a platform on which GM-SYS software operates and this makes it possible to integrate well data, gravity, and seismic data. This enhanced concurrent visualization within the same software. Oasis Montaj is designed to meet specific needs on geophysical

data. It can process data of various dimensions, filter data using various techniques and generate maps of various dimensions to make interpretation easier.

Figure 4.18 (a) and (b) are cross-sections of gravity profiles cutting across the major features, namely: Troughs and Ridges and passing through Wells. These cross-sections were constrained with a 2D seismic section (Figure 4.19), stratigraphic information (Appendix X) from drilled wells' completion reports like the Pomboo-1 well completion report and published papers like; (Nyagah, 1995), (Cruciani & Barchi, 2016), (Bosellini, 1986), and (Masinde, 2019) on the geology of the area.

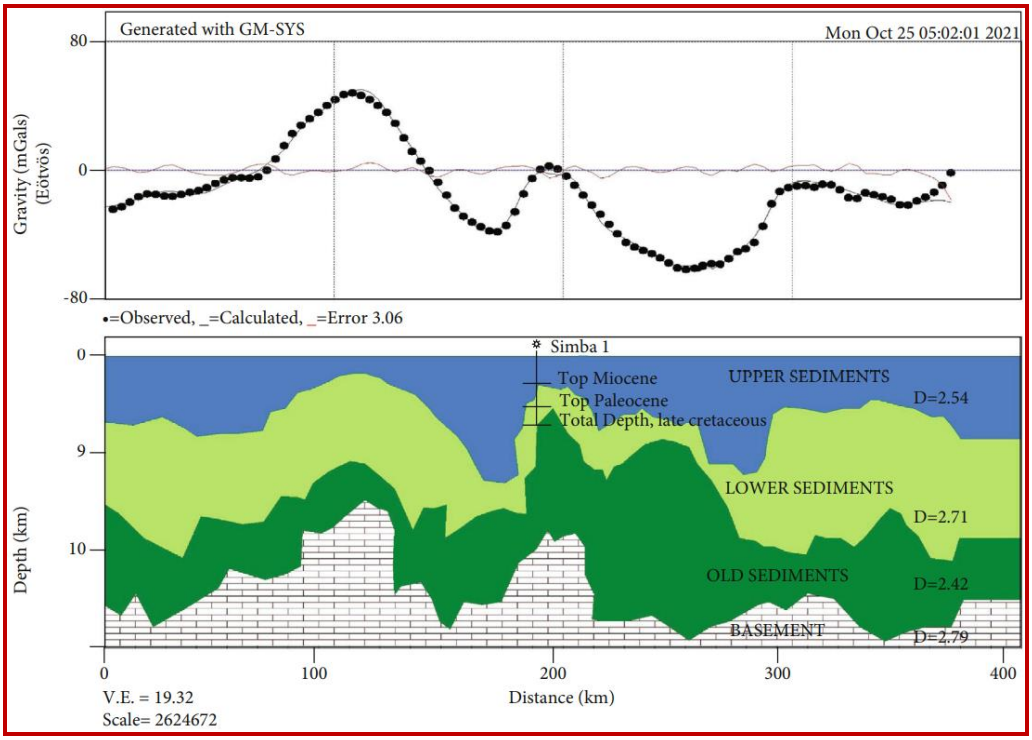

Figure 4.18 (a): GM-SYS Gravity Model from a Profile Cutting Through Simba-1 Well in the EW Direction

From the models in Figures 4.18 (a) and (b), it is observed that the three wells; Simba-1, Kubwa-1, and Mbawa-1 penetrated through the upper sediments, lower sediments, and the old sediments that could be the equivalents of the Miocene, Paleocene, and the Cretaceous that was the target for investigations. There are basement highs at the point of location of the wells and possible anticlinal and synclinal structures as depicted by the undulations of the four layers seen in the

models. The anticlinal structures are the possible trapping structures necessary for the accumulation of hydrocarbons while the synclinal structures would form the desired source kitchens.

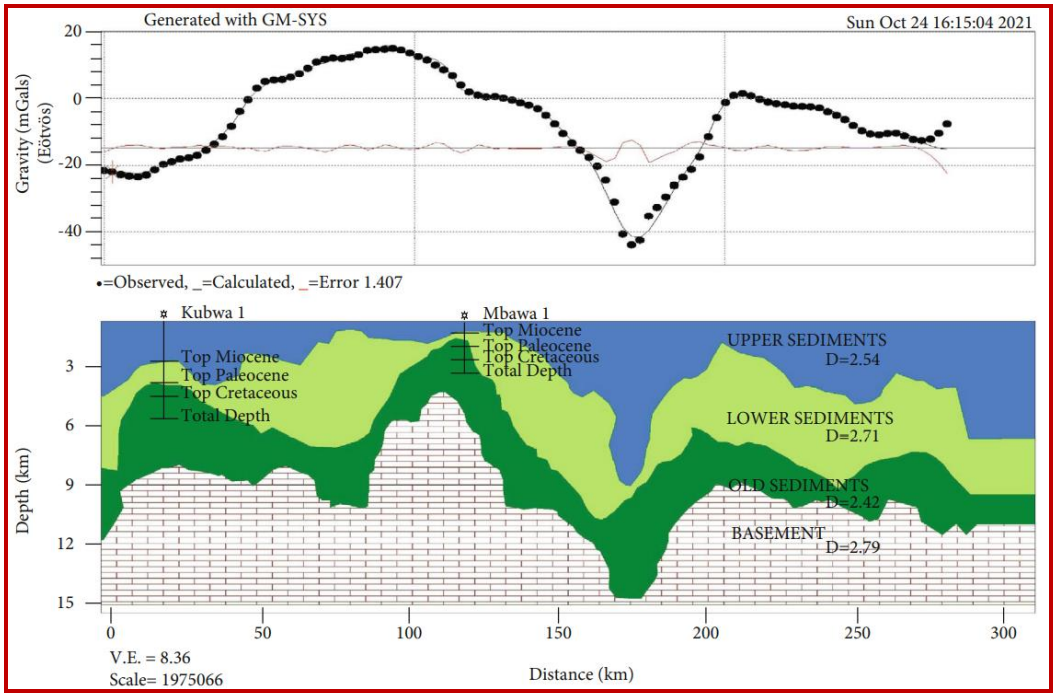

Figure 4.18 (b): GM-SYS Gravity Model from a Profile Cutting Through Kubwa-1 and Mbawa-1 (Ombati et al., 2022)

Seismic sections tied with well stratigraphy were used to estimate the number of possible layers and in estimating the approximate depth of the deepest point of interest. The Well completion reports were used in identifying possible layers and their stratification. The depths obtained from the spectral analysis were used to estimate the shallow source and deep sources in the range (of 1800 m to 15000 m) and this correlates well with the depths from the seismic model in Figure 4.19. The sections go to a maximum depth of fifteen kilometres and show four major layers, namely: upper sediments, lower sediments, old sediments, and the basement layer. The undulations of the layers forming the basement highs beneath the upper sediments would form the best oil reservoir entrapment that would then migrate upwards following lines of weakness. The zones of contact between the troughs and the ridge are the most likely candidates for fracture areas which would form possible migration paths. The possibility of having significant oil and gas source kitchens is

represented by the presence of the said troughs signified by the thick sedimentary succession and basement lows.

Figure 4.19 is a 2D seismic section showing sedimentary layers. The blue layer indicates immature, green the oil window, and red the gas window. The most interesting point to note is that within a column of 9 km from the seabed, are strata within which intercalations of shale, sand, and carbonate beds were identified. Shales form good seals and can as well be good source rocks, sandstone makes good oil reservoirs, and carbonates can be good as reservoirs and source rocks. Therefore, the hope for the presence of these petroleum system elements in the Lamu basin lies within these rocks.

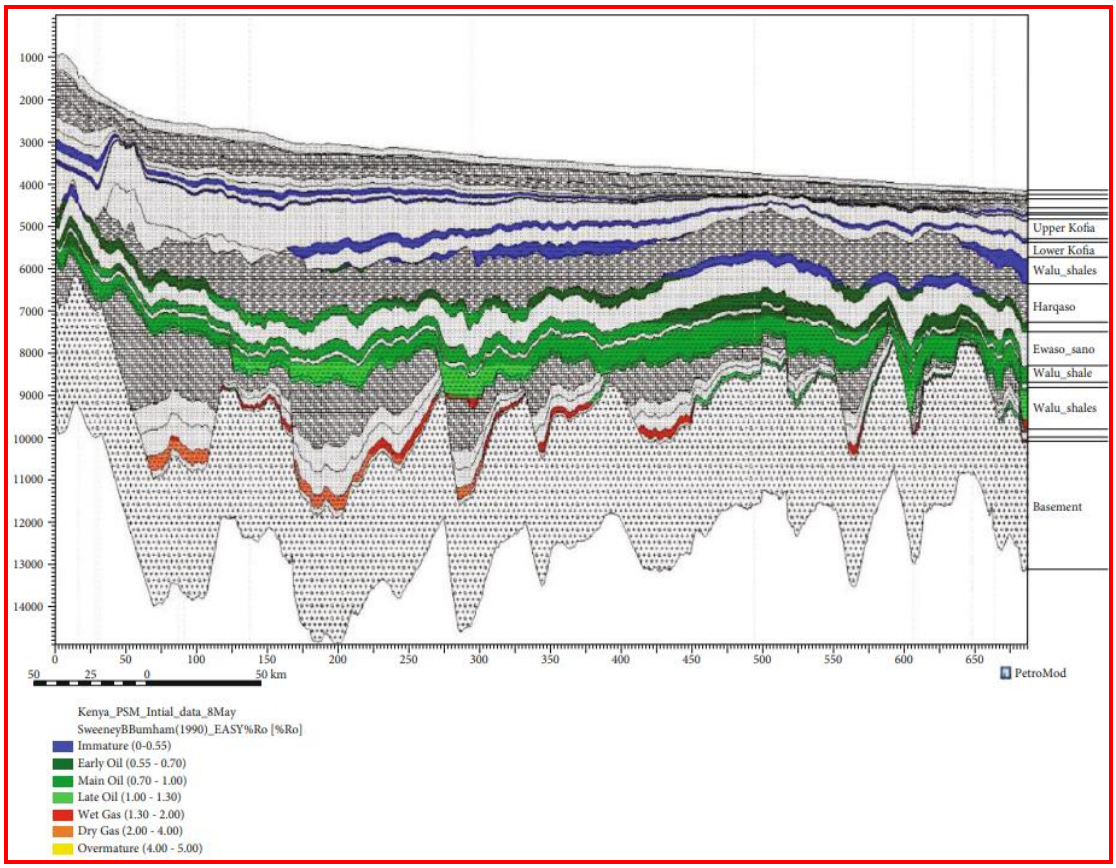

Figure 4.19: 2D Seismic Section (Ombati et al., 2022).

Based on the Sweeney and Burnham scale (Sweeney & Burnham, 1990), the modelled present-day source rock maturity is highlighted by the regional line (Osicki et al., 2015).

Figure 4.20 shows Simba-1 well and Mbawa-1 well at both the upper and lower cretaceous surfaces. The location of these wells in this 3D seismic model surface is similar to the location of the same in the GM-SYS gravity model and hence the models can be applied in this study. It is observed that the wells are located at an anticline (basement high) while the synclines (troughs) are visible to the western part of the surfaces. These crests would be forming the traps and the troughs forming the sources of the hydrocarbons.

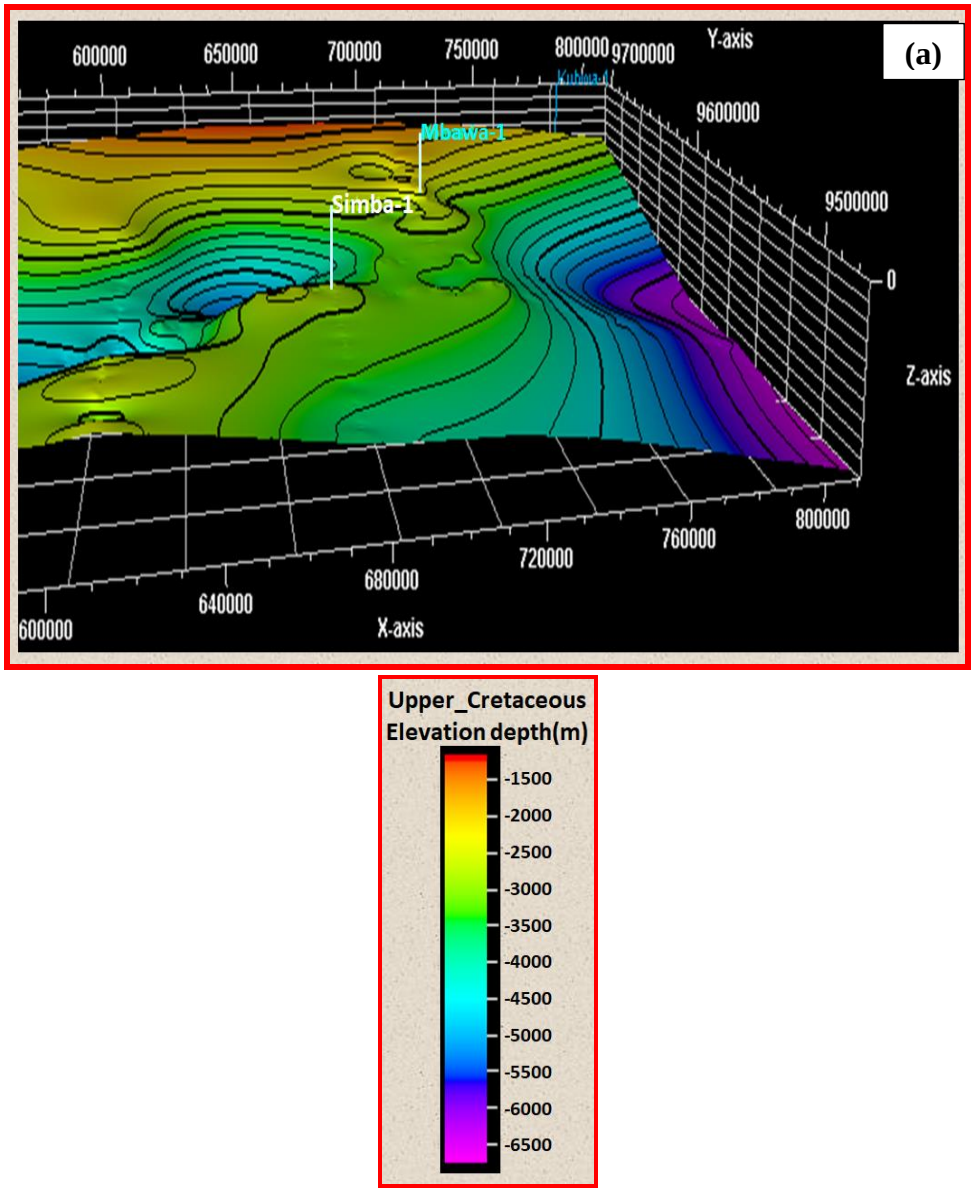

Figure 4.20 (a): 3D Well Location at Upper Cretaceous Surface

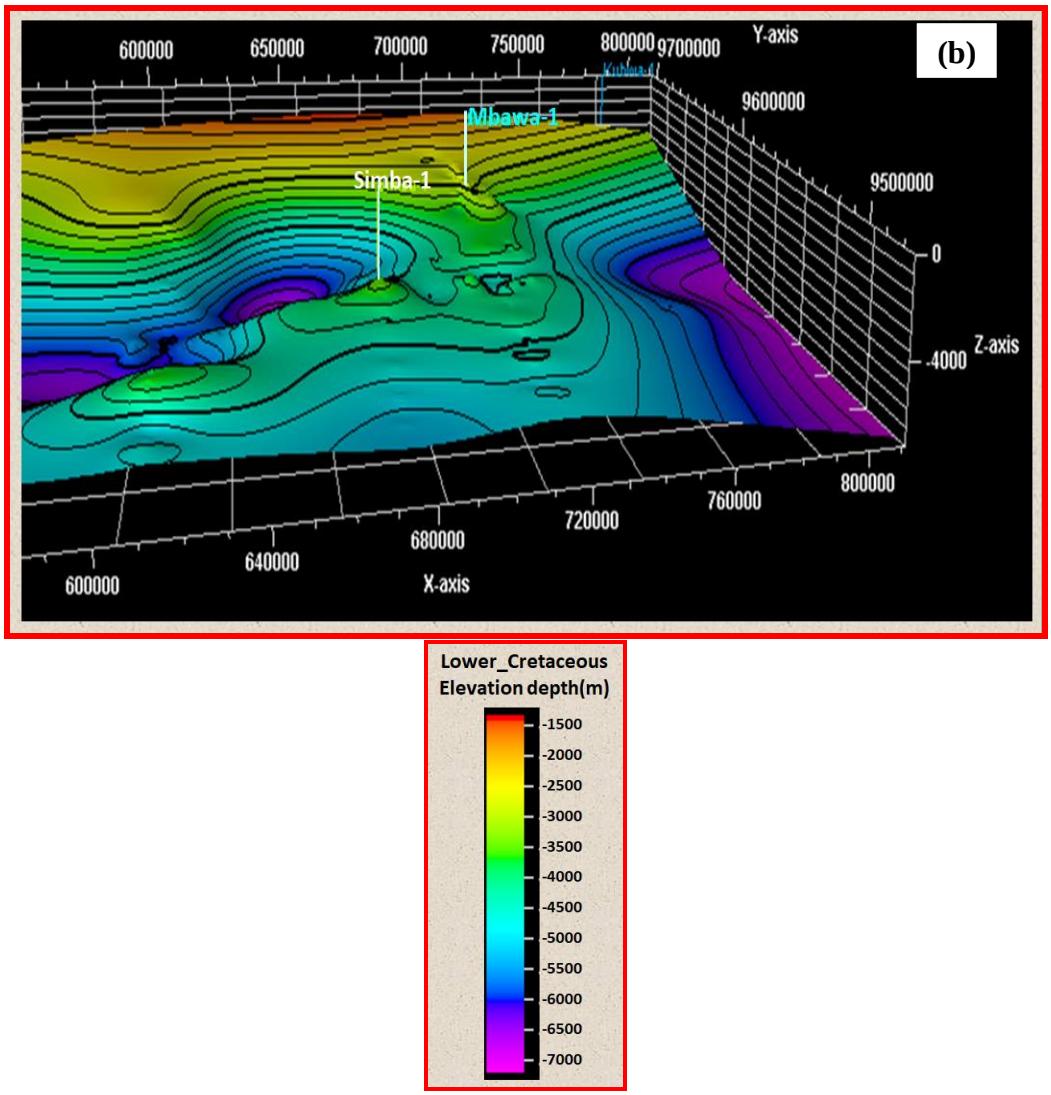

Figure 4.20 (b): 3D Well Location at Lower Cretaceous Surface

The advantage of the seismic surfaces is that besides showing the location of the well bores, it is also possible to tell more about the penetrated structures as to whether they are closed or not depending on the behaviour of the contours shown at the well location point (details discussed in section 4.2.4).

Rock physics models were utilized to quality-check the seismic interpretation results obtained qualitatively and quantitatively. Qualitatively, seismic properties were linked to geologic properties hence guiding and improving the seismic qualitative interpretation. Quantitatively, the seismic amplitude, as postulated in the seismic reflections, was related to the changes in the rock properties. In utilizing rock

physics models in reservoir characterization, the tool created a bridge between elastic properties such as p and s-waves, impedance, density, and V_P/V_S ratio, and the reservoir properties such as the formation water saturation, shale volume, and porosity. The integration guided the identification of litho facies and discrimination of the fluid fills thus minimizing the exploration risk by suggesting possible production zones for future wells in the shallow offshore basin. Linking the rock physics models to other geological information like seismic interpretation, geochemical analysis, and geology, validated the model for extrapolated use away from the well location.

Figures 4.21 (a to c) show Mbawa-1 well intersecting through the various layers in 4.21 (a) to reach the total depth at the old sediments. In 4.21 (b), the well cuts through the interpreted horizons within the probable fault-assisted or fault-dependent closure.

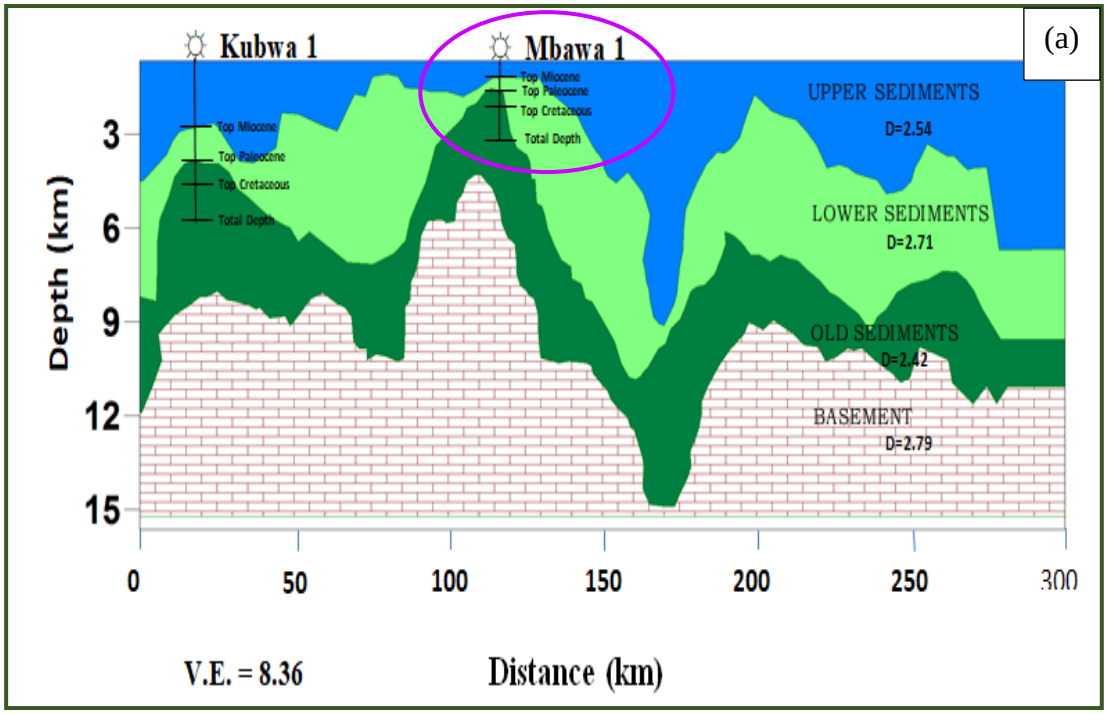

Figure 4.21 (a): Shows Mbawa-1 Well Through Gravity GM-SYS Model

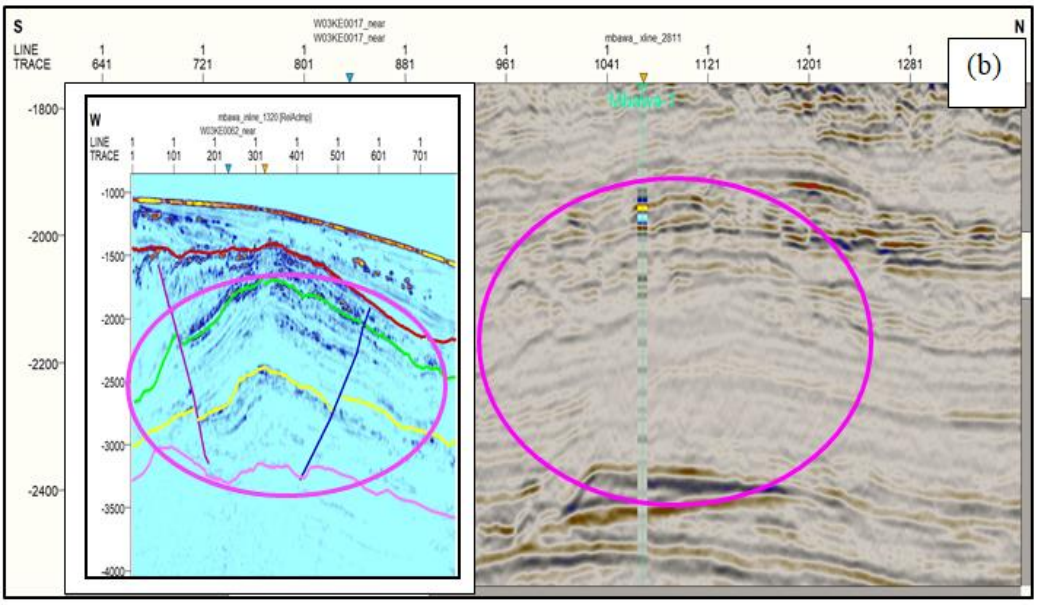

Figure 4.21 (b): Shows Mbawa-1 Well Through Seismic Section and RMS Amplitude Attribute Section

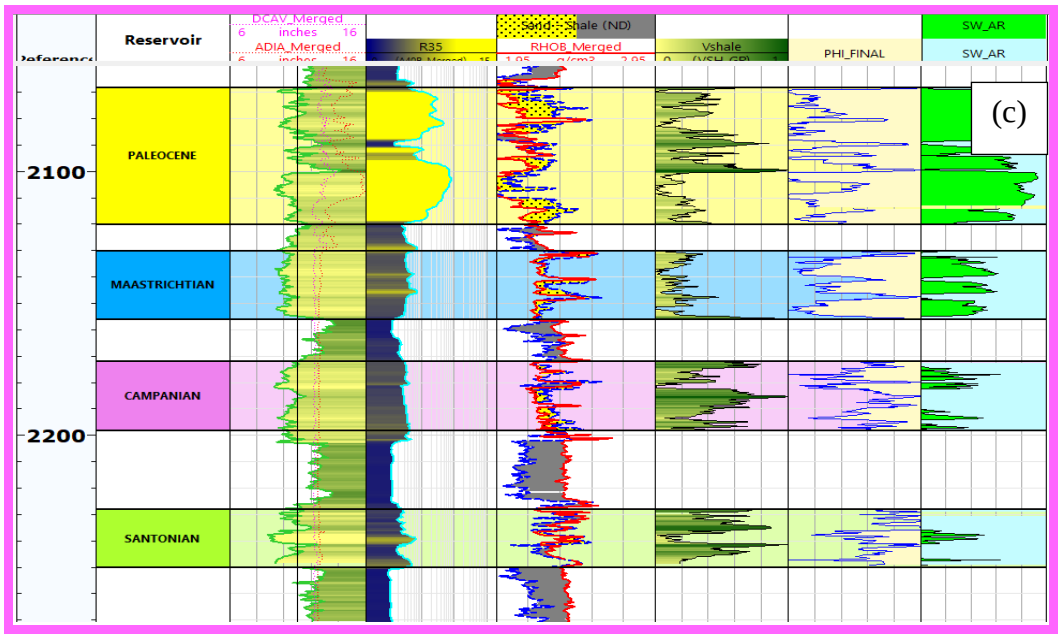

Figure 4.21 (c): Shows Mbawa-1 Well Through Petrophysical Analysis

In 4.21 (c), the petrophysical analysis result of the identified section is shown. The possible reservoir sections in the Paleocene through to Santonian together with their petrophysical properties are highlighted in different shades. It is at the depth of about

2200 m that non-commercial gas shows were intercepted in the upper cretaceous Kofia sandstones of the Mbawa-1 well during drilling (see also Appendix V). This depth corresponds to the old sediment section in Figure 4.26 (a), the region between Horizon B and Horizon C in Figure 4.21 (b), and the Campanian reservoir in Figure 4.21 (c).

4.5 Petroleum System Modelling Results

In the geology and geophysics perspective of Schlumberger's Petrel 2017 software, under the exploration geology tab and 1D model group, a model was created for each of the three wells. The input data to the model including the Chronostratigraphy, lithology, and source rock kinetics and properties were loaded. A simulation case was set for each well by setting the geometric and thermal boundary conditions (time trends), simulation options (Darcy flow), and output parameters (burial history, depth, and time curves) before running the 1D simulation. The results indicating the properties through geologic time at the well location were observed in the Geotime window (Figures 4.22, 4.23 and 4.24). The charge properties (i.e. Temperature, transformation ratio, and Vitrinite reflectance) over geologic time at each of the three wells were estimated and their spatial variation was mapped as seen from the burial history and depth curves overlayed with temperature, transformation ratio, and Vitrinite reflectance respectively.

The highest temperature (246.56 ^{0}c), transformation ratio (99.19 %), and Vitrinite reflectance (3.0) in Kubwa-1 is achieved at the Cretaceous (Maastrichtian) time at a depth of about 4500 m. The transformation ratio curve indicates both mature and immature source rocks where generation with/without expulsion has occurred in the cretaceous and no generation in the rest of the time. The Vitrinite reflectance curve indicates Overmature Cretaceous (Maastrichtian), gas generation in Paleocene, and oil window during the Miocene.

Mbawa-1 highest temperature achieved is 109.81 ^{0}c between the base Campanian and base Paleocene at a depth of between 1800 m and 2300 m. The maximum transformation ratio value is 47.94 % which signifies a possible oil generation at the

base Campanian but without an expulsion. The Vitrinite reflectance (0.7) curve implies an early oil window at the base Paleocene and base Campanian.

In Pomboo-1 well, 158.13 ^{0}c was achieved as the highest temperature during the base Campanian at a depth of over 2600 m. The transformation ratio overlay indicates, at a depth of between 2500 m to 4000 m, an implied oil generation and expulsion during the base Campanian with more than 50% value and the rest of the periods indicating no hydrocarbon generation. The Vitrinite reflectance curve suggests a possible gas generation window during the base Campanian and an oil window between the base Eocene and the base Campanian.

Generally, a transformation ratio of <10% indicates the presence of immature source rocks and that generation of hydrocarbons has not occurred. When the range of the transformation ratio is 10%-50% it suggests oil generation but without an expulsion. With more than 50% (>50%) transformation ratio, both oil generation and expulsion occur (Figure 4.23).

The prediction of the timing of the hydrocarbon generation and expulsion was necessitated by the subsidence (burial) histories overlayed with the Vitrinite reflectance of the respective three wells (Figure 4.24). The thermal maturity history of the Upper Cretaceous source rocks was calculated based on the Sweeney and Burnham Easy% Ro routine (Sweeney & Burnham, 1990) using single well 1D modelling. Detailed source rock maturity history of the Upper Cretaceous source rocks was modelled for the three wells (Figure 4.24) (Appendix I). From the models, different hydrocarbon generation levels were identified.

In the Kubwa-1 model, the unit reached the early oil window (0.5 - 0.7%) from about 70 Ma at a depth of 1500 m, the main oil window (0.7 – 1.3%) from about 66 Ma at a depth of 2000 m, gas generation (1.3-2.0%) from about 30 Ma at a depth of 3000 m, and Overmature stage (>2.0%) from about 20 Ma at a depth of 4000 m (Figure 4.28(a)).

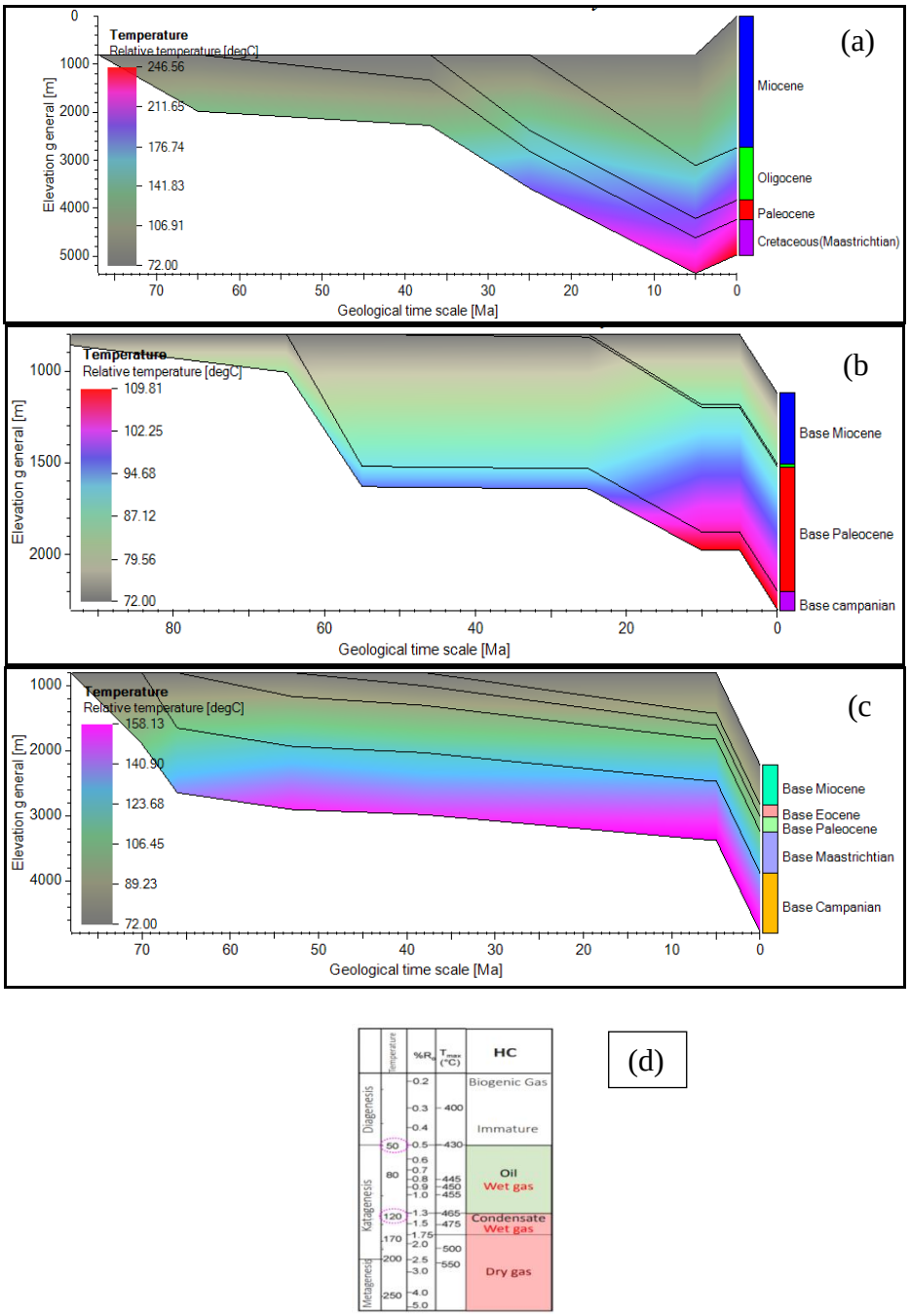

Figure 4. 22: Burial Curve Overlayed with the Relative Temperature for (a) Kubwa-1 (b) Mbawa-1 (c) Pomboo-1 (d) Interpretation Scale

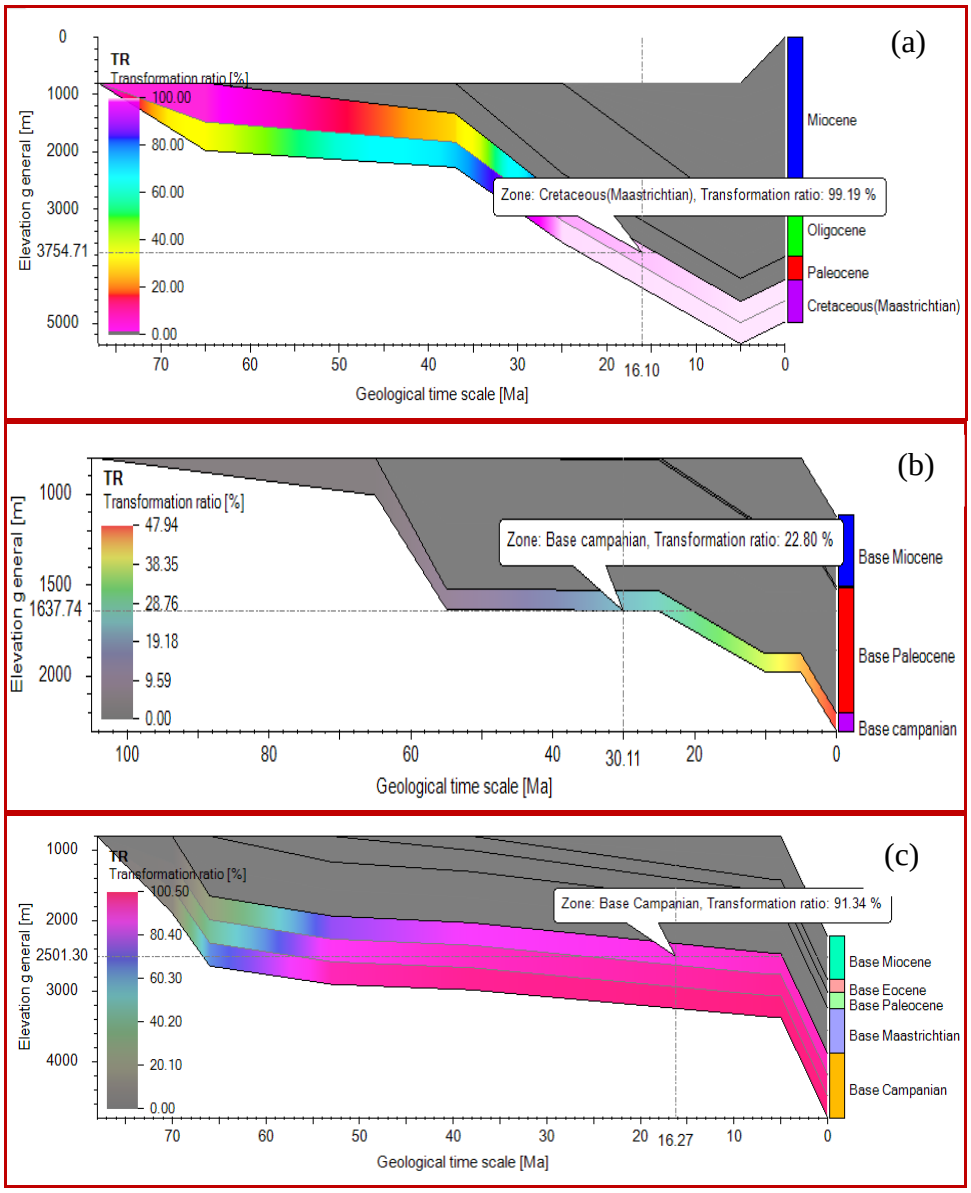

Figure 4. 23: Burial Curve Overlayed with the Transformation Ratio for (a) Kubwa-1 (b) Mbawa-1 (c) Pomboo-1 (d) Interpretation scale

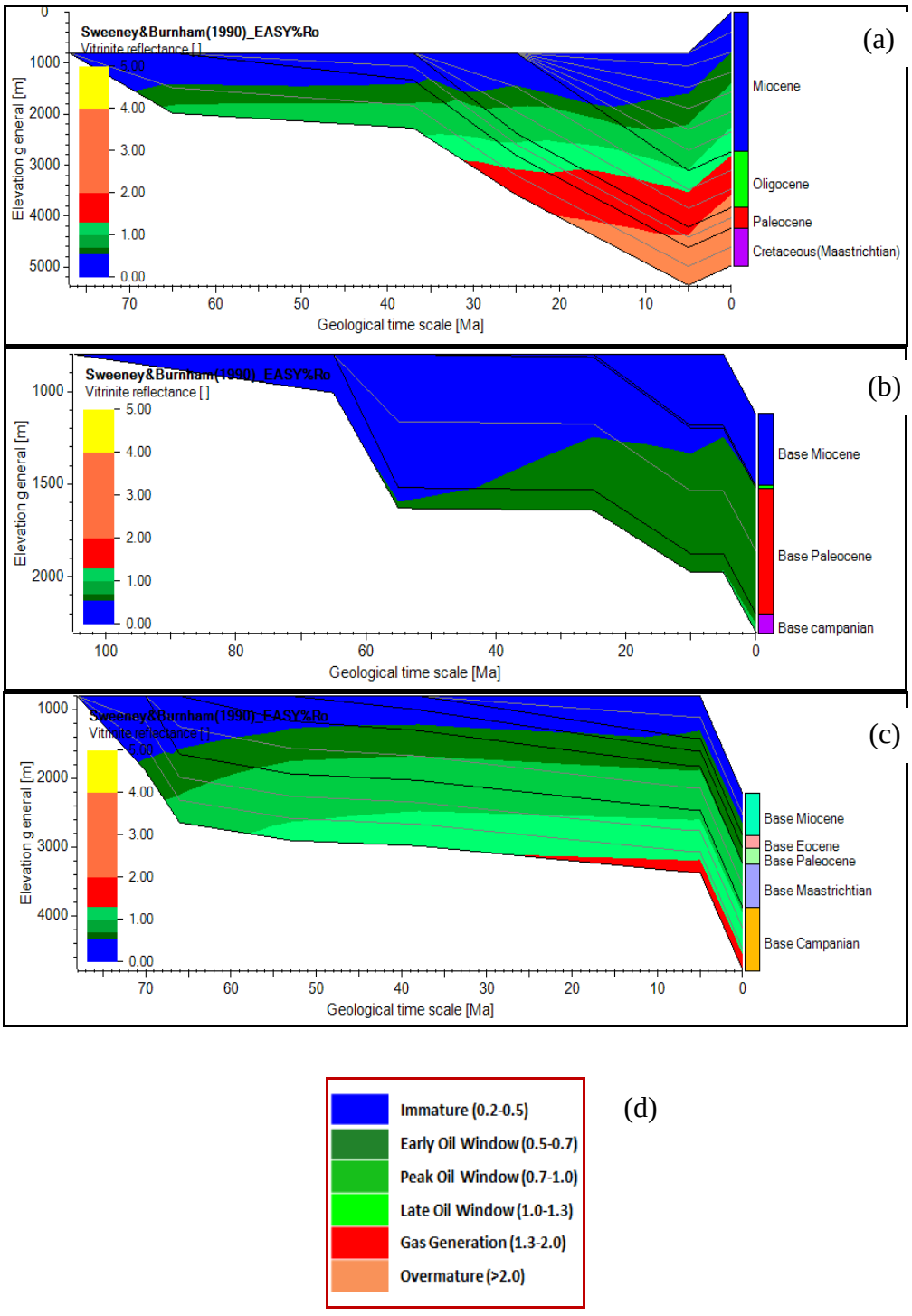

Figure 4.24: Burial Curve Overlayed with the Vitrinite Reflectance for (a) Kubwa-1 (b) Mbawa-1 (c) Pomboo-1 (d) Interpretation scale

In the Mbawa-1 model, the unit reached only the early oil window (0.5 – 0.7%) from about 58 Ma at a depth of about 1500 m with a negligible show of the main window from about 2 Ma. This indicates that the Mbawa-1 formation may have not reached the required levels of maturity to begin generating. In the Pomboo-1 model, the unit reached the early oil window (0.5 - 0.7%) from about 72 Ma at a depth of 1800 m, the main oil window (0.7 – 1.3%) from about 68 Ma at a depth of 2100 m, gas generation (1.3-2.0%) from about 25 Ma at a depth of 3000 m.

Based on the detailed subsidence and thermal history models, the hydrocarbon generation levels of the probable source rocks are different because of the varying thermal and burial histories. Generally, there are better levels of transformation ratios and maturity with increased depth and temperature over an extended period of burial.

In the geology and geophysics perspective of Schlumberger's Petrel 2017 software, under the exploration geology tab, quick look group, and generation-related attributes to the source rock depth map were created. The input data from seismic data interpretation included the bathymetry surface, top source surface, base source surface and age. The geochemistry input data included the Kerogen type, percentage of total organic carbon, and hydrogen index value. Thermal parameters such as the sediment surface temperature and the heat flow created from the 1D petroleum system modelling processes were entered. Output parameters were appropriately set. The results indicated the present-day spatial distribution of source rock generation properties represented as a map (Figures 4.25 and 4.26).

The Upper Cretaceous temperature and Vitrinite reflectance maps show that both temperature and Ro maturity favours near coastal regions. These results may explain why Pomboo-1, Kubwa-1, and Simba-1 wells were dry, although the Mbawa-1 well had gas shows in the late cretaceous sandstones.

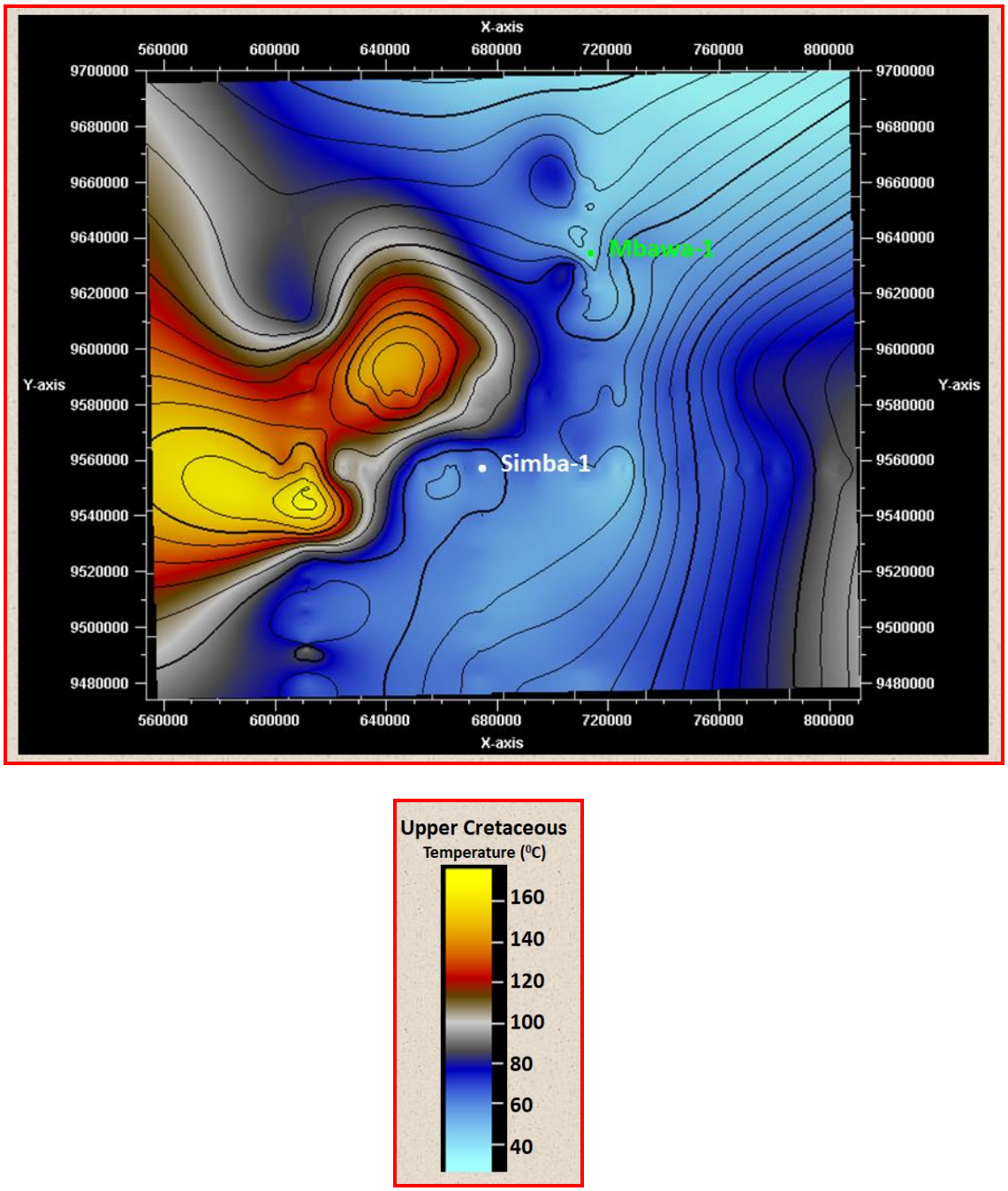

Figure 4.25: Temperature Map

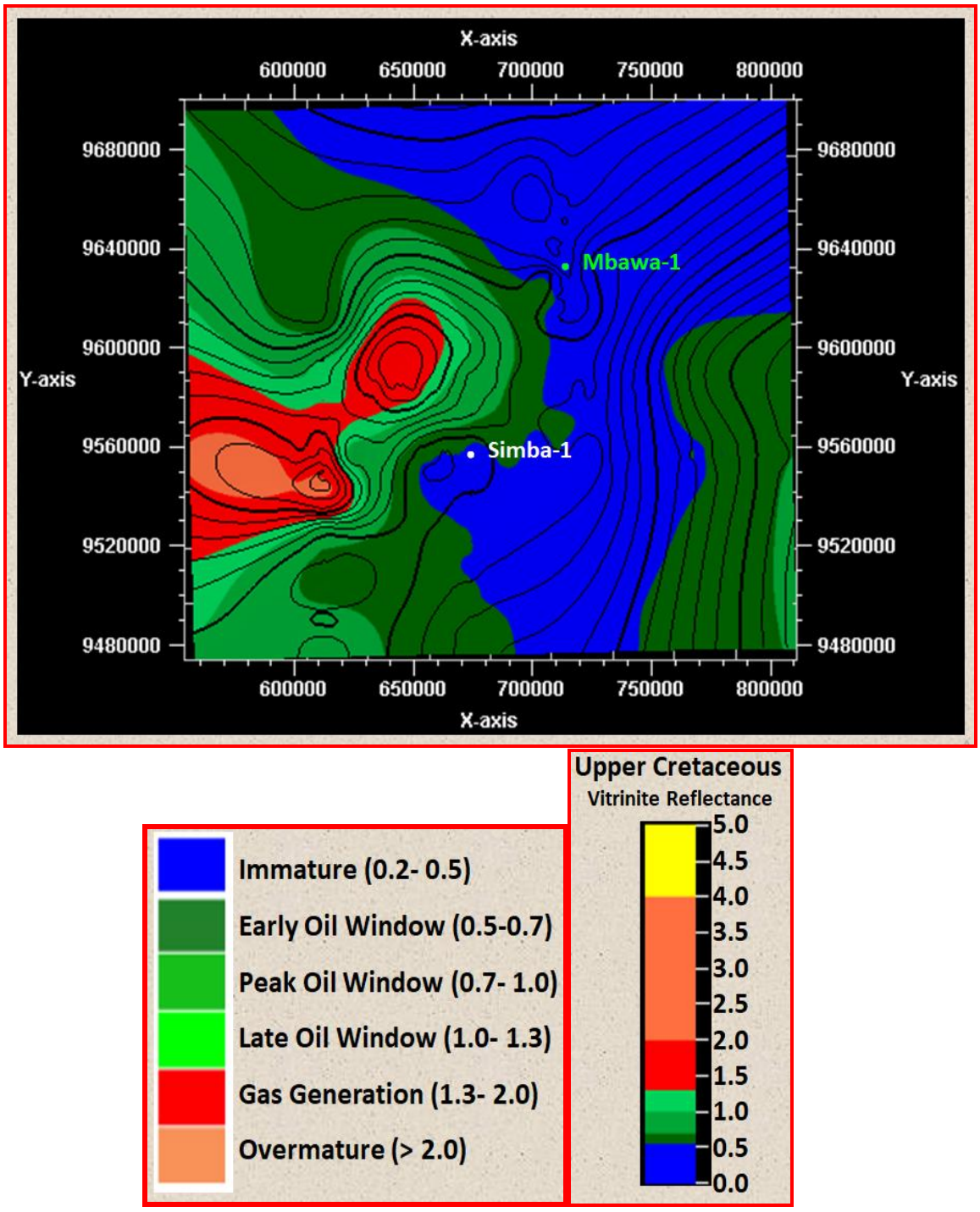

Figure 4.26: Vitrinite Reflectance Map

4.6 Summary of Findings

The increasing demand for oil and gas and the decrease in conventional hydrocarbon sources have driven exploration to extreme and adverse areas with geological complexities thus compounding the exploration risks. This necessitated an integrated

approach of using gravity and seismic geophysical methods, petrophysics and rock physics analyses, and the petroleum system modelling technique to suggest proper possible well location thus minimizing the risks associated.

Gravity results and discussion section (4.1), adequately addressed the first objective. In this case, Spectral analysis was used to estimate the depth to shallow sources (approx. 1800m) and deep sources (approx. 16800m). These depths were used to set filters for regional and residual separation using the Gaussian filter. FHD applied to the regional Isostatic anomaly yielded features that were inferred as the intrasediment fractures/faults trending in NW-SE and NE-SW directions. The regional map has discernable features like; ridges, troughs, and faults mainly trending in the NW-SE direction. The ridges are identified as DWR and the Pemba-Simba ridge. The troughs are identified as the; Maridadi, Tembo, and Happy Valley. From the models are seen the basement highs and lows with a possibility of anticlinal and synclinal structures.

Pomboo-1 was drilled on an anticline (fault propagation fold) overlying a thrust that splays from a basal detachment. The Pomboo anticline is sandwiched between two other thrust-anticline structures. The Pomboo trap structure is said to be well-constrained to accommodate hydrocarbons. The Pomboo structure was selected for drilling based on its perceived higher structural integrity due to its unfaulted nature relative to the other structures. The Lamu Basin underwent extensive faulting in the Jurassic (Syn-rift), forming typically tilted fault blocks, downthrown to the east. The major transform faults in the region include the Davie Fracture Zone, which terminates in the Davie-Walu Ridge in the Lamu Basin. An inversion axis is also found just to the southwest of the Davie-Walu ridge, suggesting compression that reactivated normal faults as thrust faults.

From the gravity data interpretation, regional basement faults depicted a mainly coast-parallel NE-SW trend arising from the rifting of Madagascar in the Jurassic. This contrasts with the dominant orientation south of the Davie-Walu ridge, which is NW-SE, a trend shared with the onshore Anza rift faults. This is because of the transition from a rifted transform margin setting to the south of the Davie-Walu ridge

to a purely rifted margin to the north. These faults may act as good seals forming part of the necessary closed structures needed in hydrocarbon exploration.

Section 4.2, on Seismic results and discussion, the results that were leveraged towards the achievement of the second objective of the study were presented, analyzed and discussed. From the analysis of the seismic surfaces, it is possible that although the westerly part of the section shown with lower elevation depths (troughs) is indicative of closed structures, they were not the target points for drilling and therefore considered the possible hydrocarbon source kitchens. The target drilling points for the two wells, Simba-1 and Mbawa-1 at the crests with higher elevation depths but missing out closed structures down through the quaternary, Oligocene, upper cretaceous, and lower cretaceous seismic surfaces save for some closed structure possible for Simba-1 at the lower cretaceous seismic surface.

Volume attributes such as envelop, sweetness, variance edge, RMS amplitude, and relative acoustic impedance were run on the 2D seismic data from part of the study area alongside the interpreted horizons and faults. The envelope attribute postulated lithological changes that could otherwise be subtle in conventional seismic data whereby the bright spots signified gas accumulations and strong reflections suggesting major lithological changes and sequence boundaries. The Variance edge attribute was used to isolate edges (discontinuities in the horizontal continuity of amplitude) from the input data set with the darkest vertical strips postulating fracture zones while the horizontal dark regions depicting possible unconformity or major sequence boundaries. RMS amplitude attribute revealed bright spots and related amplitude anomalies thus highlighting facies with coarser grains suggesting the compaction levels and the unconformities.

The reservoir characterization results presented, analyzed and discussed at section 4.3 substantively addressed the third objective of the study. Whereas petrophysics is focused on log interpretation for formation evaluation, rock physics concentrates on linking rock properties with geophysical measurements. The integrated approach of applying both the petrophysics analysis and the rock physics technique is a powerful tool in subsurface imaging. The petrophysics properties (such as the shale volume,

effective porosity, and water saturation) were used as the necessary input to rock physics modelling and calibration. The output of the models is a representation of the changes in the elastic properties due to lithological, fluid, and pressure variations at the well location.

Integrated petrophysical analysis with rock physics analysis has been leveraged in characterizing identified reservoirs in the shallow offshore, Lamu basin, Kenya, using a suite of well log data from Kubwa-1, Mbawa-1, and Pomboo-1 wells within the field. Qualitatively, reservoir rocks were identified as regions with low gamma rays using the log view display of the well logs. Hydrocarbon-bearing zones were mapped out at regions with low gamma rays combined with high resistivity values. Water-bearing zones were identified as regions with low gamma ray and low resistivity values.

The greater the separation between the neutron and density curves (crossover), the better the reservoir quality. Gas zones will generally depict greater crossovers compared to oil and water zones at the same porosity consideration. Quantitatively, the reservoirs' hydrocarbon potential was estimated through the determination of the petrophysical parameters like the effective porosity, water saturation, hydrocarbon saturation, shale volume, and net pay depth and thickness. Petrophysical interpretations of mainly sand, calcareous sand, and turbidite sand reservoirs indicated 7.1-26.4% shale content, 22.8-55.7% water saturation, and 11.8-25.2% effective porosity.

Cross-plotting Mu-rho against density separated the data clusters into three zones (hydrocarbon sand, brine sand, and shale) since shale has a higher density than sand and brine is denser than hydrocarbon. From the cross plot of acoustic impedance against Lambda-Rho, the hydrocarbon zone shows low acoustic impedance and low Lambda-Rho compared to brine-saturated sand and shale regions. Data cluster analysis in the Lambda-Rho against Mu-Rho cross plot suggests the presence of gas-saturated sand as it occupies the lower values of Lambda-Rho, a measure of incompressibility. The hydrocarbon zone likely to be gas is shown by low values of lambda-rho and V_p/V_s in the Lambda-Rho against V_p/V_s cross plot.

The V_p/V_s ratio against the Acoustic impedance cross-plot discriminates the lithology, especially along the acoustic impedance axis. The acoustic impedance value is highest in the shale zone and lowest in the hydrocarbon-bearing sand region, with the lowest and highest effective porosity values, respectively. Cross-plotting velocity against porosity indicates that the reservoir consists of friable sandstones given the velocity and final effective porosity range values. From the data cluster analyses of the models, it can be noted that, generally, hydrocarbon-saturated zones have low density, acoustic impedance, Mu-rho, and Lambda-rho.

Brine-saturated regions are associated with low acoustic impedance and Mu-rho values and relatively higher Lambda-rho values. Shale zones are indicated at high values of density, acoustic impedance, Mu-rho, and Lambda-rho. It has been demonstrated in this study how the petrophysical properties obtained at the specific depths indicated above in the three wells lie within the range of the cutoffs. Constrained with the petrophysical properties calculated based on the core analysis, the petrophysical properties indicate potential reservoirs in the respective wells. Reservoir lithology and fluid content can be predicted using rock physics.

Rock physics is a tool that could help with more accurate subsurface modelling, though coupled with enough challenges and uncertainties creating more gaps for more study and research. The rock physics models increased the possibility of finding reservoir sand and mitigating the risk involved in finding hydrocarbons. Linking the models to other geological information like seismic interpretation, geochemical analysis, and geology, validated the model for extrapolated use away from the well location.

The petroleum system modelling results covered in section 4.5 were utilized in the achievement of the fourth objective of the study. The Upper Cretaceous temperature and Vitrinite reflectance maps show that both temperature and Ro maturity favours shelfal and near the coastal region. These results may explain why Pomboo-1, Kubwa-1, and Simba-1 wells were dry though the Mbawa-1 well had gas shows in the late cretaceous sandstones. Generally, a transformation ratio of <10% indicates the presence of immature source rocks and that generation of hydrocarbons has not

occurred. When the range of the transformation ratio is 10%-50% it suggests oil generation but without an expulsion. With more than 50% (>50%) transformation ratio, both oil generation and expulsion occur.

The temperature, transformation ratio, and Vitrinite reflectance as the charge properties, over geologic time, at each of the three wells have been estimated and their spatial variation mapped as seen from the burial history and depth curves overlayed with temperature, transformation ratio, and Vitrinite reflectance respectively.

Detailed source rock maturity history of the Upper Cretaceous source rocks was modelled for the three wells. In the Kubwa-1 model, the unit reached the early oil window (0.5 - 0.7%) from about 70 Ma at a depth of 1500 m, the main oil window (0.7 – 1.3%) from about 66 Ma at a depth of 2000 m, gas generation (1.3-2.0%) from about 30 Ma at a depth of 3000 m, and Overmature stage (>2.0%) from about 20 Ma at a depth of 4000 m. In the Mbawa-1 model, the unit reached only the early oil window (0.5 – 0.7%) from about 58 Ma at a depth of about 1500 m with a negligible show of the main window from about 2 Ma. In the Pomboo-1 model, the unit reached the early oil window (0.5 - 0.7%) from about 72 Ma at a depth of 1800 m, the main oil window (0.7 – 1.3%) from about 68 Ma at a depth of 2100 m, gas generation (1.3-2.0%) from about 25 Ma at a depth of 3000 m.

CHAPTER FIVE

CONCLUSIONS AND RECOMMENDATIONS

5.1 Conclusion

The Isostatic gravity map yielded both the regional and residual maps upon application of the Gaussian filter set on the depths derived from spectral analysis. Fractures and faults trending in NW-SE and NE-SW directions were inferred from the first horizontal derivative (FHD) map obtained from the regional Isostatic anomaly map. The regional map has discernable features like; ridges, troughs, and faults mainly trending in the NW-SE direction. The ridges are identified as DWR and the Pemba-Simba ridge. The troughs are identified as the; Maridadi, Tembo, and Happy Valley. From the models are seen the basement highs and lows with anticlinal and synclinal structures that would possibly form the necessary traps and hydrocarbon sources.

The seismic surfaces and volume attribute analyses indicated possible structures that would generate, transport, and store hydrocarbons. It is observed that the wells are located at an anticline (basement high) while the synclines (troughs) are visible to the western part of the surfaces. These crests would be forming the traps and the troughs forming the sources of the hydrocarbons. The advantage of the seismic surfaces is that besides showing the location of the well bores, it also gives details about the penetrated structures as to whether they are closed or not depending on the behaviour of the contours shown at the well location point. A scan through the seismic surfaces shows that Mbawa-1 well was drilled off the structure while the Simba-1 well displays a possible closed structure at the lower cretaceous seismic surface. The faults identified in the FHD map, seismic surfaces, and the seismic volume attributes sections form part of the needed closed structures. The inferred faults provide the necessary migration pathways within the sedimentary structures. However, there is a possibility that the interpreted faults may have compromised the closed structures leading to a possible leaking away of hydrocarbons hindering commercial accumulations.

The integrated petrophysical analysis with rock physics analysis has been leveraged in characterizing identified potential reservoirs in the shallow offshore, Lamu basin, Kenya. An integrated approach is a powerful tool in subsurface imaging whereby the petrophysics properties were used as the necessary input to rock physics modelling and calibration. Qualitatively, potential reservoir rocks were identified as regions with low gamma rays, hydrocarbon-bearing zones that showed low gamma rays with high resistivity values, and low gamma rays with low resistivity values for water-bearing zones. Quantitatively, the petrophysical parameters of the potential reservoirs (sand, calcareous sand, and turbidite sand reservoirs) were in the range of 7.1-26.4% shale content, 22.8-55.7% water saturation, and 11.8-25.2% effective porosity. From the data cluster analyses of the models, it can be noted that, generally, hydrocarbon-saturated zones have low density, acoustic impedance, Mu-rho, and Lambda-rho. Brine-saturated regions are associated with low acoustic impedance and Mu-rho values and relatively higher Lambda-rho values. Shale zones are indicated at high values of density, acoustic impedance, Mu-rho, and Lambda-rho.

Gassmann fluid substitution was used to calculate the fluid effect on elastic rock properties from the rock frame properties. The behaviour of clean reservoir zone saturation scenarios resulting from the brine, oil, and gas fluid substitution models was measured. The values indicate that fluid substitution has a greater effect on compressional velocity than on shear velocity and density (ρ) significantly decreased

when hydrocarbons replaced water saturation in the wells. Shear wave velocity (V_s)

indicated a slight change in all the wells.

The temperature, transformation ratio, and Vitrinite reflectance as the charge properties, over geologic time, at each of the three wells have been estimated and their spatial variation mapped as seen from the burial history and depth curves overlayed with temperature, transformation ratio, and Vitrinite reflectance respectively. From the upper cretaceous maturity maps, the results seem to favour near coastal regions where average TOC is about 1.4 wt%, Vitrinite reflectance is more than 0.5%, transformation ratio is more than 10%, and temperatures range from

80^0c to 160^0c. For instance, the result implies that Mbawa-1 formation may have not reached the required levels of maturity to begin generating. However, greater uncertainty rests on the source rock's presence and viability tending toward the deep offshore.

Combining gravity and seismic methods for regional structural interpretation, petrophysics and rock physics for reservoir delineation and characterization, and petroleum system modelling for source rock characterization improved the understanding of the occurrence of the petroleum system elements and processes necessary for hydrocarbon accumulation. Appropriate points where wells may be drilled with reduced exploration risk have been suggested.

5.2 Recommendations

This study recommends an increase in the number of drilled exploration wells per 5000 km^2 to upgrade the exploration status and improve the success rate by providing the necessary offset data needed for well correlation. The study further recommends an investigation of the contribution of the faults on the closed structures to determine whether the structures are fault assisted or fault dependent or both.

An intensified study on the availability, maturity and distribution of the source rocks regionally is paramount. This study, therefore, recommends comparative source rock characterization in offshore basins of East Africa where excellent source rocks have been inferred or discovered in some basins.

The quality of the 2D seismic data used in this study was fair and the seismic data extracted from the 3D was fairly good. This study then recommends more seismic surveys to cater for the distance between the seismic lines and improve the quality of the seismic sections to ease future seismic interpretations.

REFERENCES

AAPG (Producer). (2022). Quick look at lithology from logs. Retrieved from https://wiki.aapg.org/Quick-look_lithology_from_logs

Abdul Fattah, R., Meekes, J., Colella, S., Bouman, J., Schmidt, M., & Ebbing, J. (2013). The application of GOCE satellite gravity data for basin and petroleum system modelling: a case study from the Arabian Peninsula. *Search and Discovery Article, 120130*.

Adero, B., Masinde, A., & Osukuku, G. (2017). *Using seismic attributes for reservoir characterization.* Paper presented at the Oil, Gas and Mines Africa, Exhibition and Conference (OGMA), Nairobi, Kenya P.

Al-Areeq, N. M. (2018). Petroleum source rocks characterization and hydrocarbon generation. *Recent Insights in Petroleum Science and Engineering, 1*.

Albakr, M. A., Abd, N., Hasan, S., & Al-Sharaa, G. H. (2022). Reservoir characterization and density–velocity analysis using rock physics and integrated multi-types post-stack inversion to identify hydrocarbon possibility and litho-prediction of Mishrif formation in the Kumaite and Dhafriyah oil fields, Southern Iraq. *Geophysical Prospecting*, 1886-1913.

Al-Hajeri, M. M., Al Saeed, M., Derks, J., Fuchs, T., Hantschel, T., Kauerauf, A., . . . & Tessen, N. (2009). Basin and petroleum system modelling. *Oilfield Review, 21*(2), 14-29.

Alsadi, H. N. (2017). Seismic Hydrocarbon Exploration. *2D and 3D Techniques, Seismic waves*. Germany: Springer.

Alsadi, H. N., & Baban, E. N. (2014). *Gravity Exploration Method*. Sulaimaniyah: University of Sulaimani.

Anabwani, J. K. (2012). *Stratigraphic and structural interpretation of seismic sections in Lokichar Basin.* Unpublished PhD thesis, Nairobi: The University of Nairobi.

Anadarko, K. C. L. (2013). *Kubwa well site lithology log: National Oil Corporation of Kenya.* Nairobi: National Oil Corporation of Kenya.

Apache, K. C. L. (2012). L*ithology/LWD LOG for Mbawa-1 well: National Oil Corporation of Kenya (NOCK).* Nairobi: National Oil Corporation of Kenya.

Avseth, P., Mukerji, T., & Mavko, G. (2010). *Quantitative seismic interpretation: Applying rock physics tools to reduce interpretation risk*: Cambridge: Cambridge university press.

AWEMAC, I. (2016). *Strategic environmental and social assessment (SESA).* Lamu: AWEMAC.

Azeem, T., Chun, W. Y., Khalid, P., Qing, L. X., Ehsan, M. I., Munawar, M. J., & Wei, X. (2017). An integrated petrophysical and rock physics analysis to improve reservoir characterization of Cretaceous sand intervals in the Middle Indus Basin, Pakistan. *Journal of Geophysics and Engineering*, *14*(2), 212-225.

Baker, H. (1992). Advanced wireline and MWD procedures manual. *Houston, TX: Baker Hughes INTEQ Technical Publications Group*.

Balmino, G., Vales, N., Bonvalot, S., & Briais, A. (2012). Spherical harmonic modelling to ultra-high degree of Bouguer and isostatic anomalies. *Journal of Geodesy*, *86*(7), 499-520.

Beicip-Franlab. (2020). *Kenya exploration potential play-based resource assessment: National oil corporation of Kenya (NOCK)*. Nairobi: National Oil Corporation of Kenya.

Ben-Awuah, J., Adda, G., Mijinyawa, A., Andriamihaja, S., & Siddiqui, N. (2013). 2D Basin modelling and petroleum system analysis of the Triassic play in the Hammerfest basin of the Norwegian Barents Sea. *Research Journal of Applied Sciences, Engineering, and Technology, 6*(17), 3137-3150.

Bjorlykke, K. (2010). *Petroleum geoscience: From sedimentary environments to rock physics*: London: Springer Science & Business Media.

Blakely, R. J. (1996). *Potential theory in gravity and magnetic applications*: Cambridge: Cambridge University press.

Bodunde, S., & Enikanselu, P. (2019). Integration of 3D-seismic and petrophysical analysis with rock physics analysis in the characterization of SOKAB field, Niger delta, Nigeria. *Journal of Petroleum Exploration and Production Technology, 9*(2), 899-909.

Bonvalot, S., Balmino, G., Briais, A., Kuhn, M., Peyrefitte, A., Vales, N., . . .& Reinquin, F. (2012). *World Gravity Map., Bureau Gravimetrique International* (BGI), map: CGMW-BGI-CNES-IRD Ed., Paris: CGMW-BGI-CNES-IRD Ed.

Bosellini, A. (1986). East Africa continental margins. *Geology, 14*(1), 76-78.

Brevik, I., Szydlik, T., Corver, M. P., De Prisco, G., Stadtler, C., & Helgesen, H. K. (2014). Geophysical basin modelling: Generation of high-quality velocity and density cubes for seismic imaging and gravity field monitoring in complex geology settings *SEG Technical Program Expanded Abstracts 2014* (pp. 4733-4737): Society of Exploration Geophysicists.

Bryant, I. D., Stabell, C. B., & Neumaier, M. (2013). *Evaluation of unconventional resources using a petroleum system modelling approach.* Paper presented at the Unconventional Resources Technology Conference.

Busanello, G., Del Ben, A., & Pipan, M. (2017). Petroleum systems modelling as an exploration tool: from surface seismic acquisition to basin modelling: a case study from a periplatform basin in Northern Adriatic. *First Break, 35*(3).

Castagna, J. P., Batzle, M. L., & Eastwood, R. L. (1985). Relationships between compressional-wave and shear-wave velocities in clastic silicate rocks. *Geophysics, 50*(4), 571-581.

Chopra, S., & Marfurt, K. J. (2007). Volumetric curvature attributes for fault/fracture characterization. *first break, 25*(7).

Close, D. (2010). Isostasy and Gravity Modelling: Integrating Potential Field Data in Interpretation Workflows. *Official Publication of the Canadians Society of Exploration Geophysicists (CSEG RECORDER), 35*(6).

Coffin, M. F., & Rabinowitz, P. D. (1987). Reconstruction of Madagascar and Africa: evidence from the Davie fracture zone and western Somali basin. *Journal of Geophysical Research: Solid Earth, 92*(B9), 9385-9406.

Cruciani, F., & Barchi, M. R. (2016). The Lamu Basin deepwater fold-and-thrust belt: An example of a margin-scale, gravity-driven thrust belt along the continental passive margin of East Africa. *Tectonics, 35*(3), 491-510.

Dalley, R., GEVERS, E. A., Stampfli, G., Davies, D., & Gastaldi, C. (1989). Die and azimuth displays for 3D seismic interpretation. *First Break (Print), 7*(3), 86-95.

Darling, T. (2005). *Well logging and formation evaluation*: New York: Elsevier.

Ekinci, Y. L., & Yiğitbaş, E. (2015). Interpretation of gravity anomalies to delineate some structural features of Biga and Gelibolu peninsulas, and their surroundings (north-west Turkey). *Geodinamica Acta, 27*(4), 300-319.

Ellis, D. V., Case, C. R., & Chiaramonte, J. M. (2003). Tutorial-porosity from neutron logs I-Measurement. *Petrophysics-The SPWLA Journal of Formation Evaluation and Reservoir Description, 44*(06).

Ellis, D. V., & Singer, J. M. (2007). *Well logging for earth scientists* (Vol. 692): New York: Springer.

Fairhead, J. D. (2016). *Advances in gravity and magnetic processing and interpretation*: London: EAGE Publications.

Farfour, M., Yoon, W. J., & Kim, J. (2015). Seismic attributes and acoustic impedance inversion in the interpretation of complex hydrocarbon reservoirs. *Journal of Applied Geophysics, 114*, 68-80.

Fiduk, J. C., Weimer, P., Trudgill, B. D., Rowan, M. G., Gale, P. E., Phair, R. L., . . . Lowe, R. S. (1999). The Perdido fold belt, northwestern deep Gulf of Mexico, part 2: seismic stratigraphy and petroleum systems. *AAPG Bulletin, 83*(4), 578-612.

Gadallah, M. R., & Fisher, R. (2009). Seismic Interpretation *Exploration Geophysics* (pp. 149-221): New York: Springer.

Golyan, M. F. (2012). *Compaction, rock property evolution and rock physics diagnostics of Askeladd discovery, Norwegian Barents Sea.*

Green, C. M., Fairhead, J. D., & Maus, S. (1998). Satellite-derived gravity: Where we are and what's next. *The Leading Edge, 17*(1), 77-79.

Hamada, G. (2004). Reservoir fluids identification using Vp/Vs ratio? *Oil & Gas Science and Technology, 59*(6), 649-654.

Hantschel, T., & Kauerauf, A. I. (2009). *Fundamentals of basin and petroleum systems modelling*: Springer Science & Business Media.

Hesthammer, J., Landrø, M., & Fossen, H. (2001). Use and abuse of seismic data in reservoir characterization. *Marine and petroleum geology, 18*(5), 635-655.

Higley, D. K., Lewan, M., Roberts, L. N., & Henry, M. E. (2006). Petroleum system modelling capabilities for use in oil and gas resource assessments. *US Geological Survey Open-File Report, 1024*, 18.

Ijasan, O., Torres-Verdín, C., & Preeg, W. E. (2013). Interpretation of porosity and fluid constituents from well logs using an interactive neutron-density matrix scale. *Interpretation, 1*(2), T143-T155.

Johansen, S., Ostisty, B., Fedorovsky, Y., Martirosjan, V., Christensen, O. B., Cheredeev, S., . . . & Margulis, L. (1993). Hydrocarbon potential in the Barents Sea region: play distribution and potential *Norwegian Petroleum Society Special Publications* (Vol. 2, pp. 273-320): Elsevier.

Larionov, V. (1969). Radioactivity by Well log. *Nedra, Moscow (in Russian).*

Likkason, O. (2011). Spectral analysis of geophysical data. *Advances in Data Methods, Models and Their Application in Geoscience*.

Liner, C. L., & McGilvery, T. A. (2019). *The art and science of seismic interpretation*: Springer.

Liu, H. (2017). *Principles and applications of well logging*: Springer.

Loke, M. H. (1999). Electrical imaging surveys for environmental and engineering studies. *A practical guide to, 2*, 70.

Lowrie, W., & Fichtner, A. (2019). *Fundamentals of geophysics*, Cambridge: Cambridge University press.

Magoba, M., & Opuwari, M. (2020). Petrophysical interpretation and fluid substitution modelling of the upper shallow marine sandstone reservoirs in the Bredasdorp Basin, offshore South Africa. *Journal of Petroleum Exploration and Production Technology, 10*, 783-803.

Magoon, L., & Dow, W. (1994). The petroleum system: From source to trap: AAPG Memoir 60. *American Association of Petroleum Geologists, Tulsa*, 25-49.

Mahanjane, E. S. (2014). The Davie Fracture Zone and adjacent basins in the offshore Mozambique Margin–A new insight for the hydrocarbon potential. *Marine and petroleum geology*, *57*, 561-571.

Mahanjane, E. S., & Franke, D. (2014). The Rovuma Delta deep-water fold-and-thrust belt, offshore Mozambique. *Tectonophysics*, *614*, 91-99.

Mariita, N. O. (2007). The gravity method. *Short course II on surface exploration for geothermal resources*, *1*.

Martinelli, G. (2010). Basin and petroleum system modelling. Retrieved from *http://www. math. ntnu. no/~ gabriele/PetroModPres. pdf*

Masinde, A. (2019). Petroleum prospectivity of offshore Lamu basin, Kenya: Davie Walu Fracture Zone.

Maurya, S., Singh, N., & Singh, K. H. (2020). *Seismic Inversion Methods: A Practical Approach*: Springer.

Mavko, G., Mukerji, T., & Dvorkin, J. (2020). *The rock physics handbook*: Cambridge university press.

Milligan, M. (2004). What are seismic surveys and how much shaking do they create? *Utah Geological Survey Notes*, *36*, 10-11.

Minigalieva, G., Nigmatzyanova, A., Burikova, T., Privalova, O., Akhmetzyanov, R., & Kinzikeeva, A. (2018). *Well-log analysis for reservoir characterization of famenian carbonates with the criterion of texture heterogeneity.* Paper presented at the SPE Russian Petroleum Technology Conference.

Mondol, N. H. (2010). Seismic exploration. *Petroleum Geoscience*, 375-402.

Munyithya, J., Ehirim, C., & Dagogo, T. (2020). Reflectivity and spectral attribute-based reservoir characterization: a case study from" MUN" onshore Niger delta field, Nigeria. *Journal of Petroleum Exploration and Production Technology*, *10*(6), 2195-2205.

Murray, A., & Tracey, R. (2001). Best practices in gravity surveying; *Geoscience Australia*, *3*(5).

Nabighian, M. N., Ander, M., Grauch, V., Hansen, R., LaFehr, T., Li, Y., . . . Ruder, M. (2005). Historical development of the gravity method in exploration. *Geophysics*, *70*(6), 63ND-89ND.

Nanda, N. C. (2016). *Seismic data interpretation and evaluation for hydrocarbon exploration and production: A practitioner's guide,* London: Springer.

Naseer, M. T., & Asim, S. (2018). Characterization of shallow-marine reservoirs of Lower Eocene carbonates, Pakistan: Continuous wavelet transforms-based spectral decomposition. *Journal of Natural Gas Science and Engineering*, *56*, 629-649.

Neumaier, M. (2016). *Structural Restoration and Basin and Petroleum Systems Modelling: Case Studies from the Monagas Fold and Thrust Belt, Venezuela, and the Moroccan Atlantic Margin.* Universitätsbibliothek der RWTH Aachen.

Ngechu, J. M. (2012). *Assessment of source rock maturity in the Lamu Basin based on well distribution, hydrocarbon shows, Total Organic Carbon (TOC) levels, Kerogen type, and Vitrinite reflectance.* Unpublished PhD Desertation, Nairobi: University of Nairobi.

NOCK. (1995). *Hydrocarbon potential of the coastal onshore and offshore Lamu Basin of southeast Kenya* (pp. 97). Nairobi: NOCK.

NOCK. (2009). *Oil exploration booklet*. Nairobi: NOCK.

Nyaberi, M. D., & Rop, B. K. (2014). Petroleum prospects of Lamu Basin, South-Eastern Kenya. *Journal of the Geological Society of India, 83*(4), 414-422.

Nyagah, K. (1995). Stratigraphy, depositional history and environments of deposition of Cretaceous through Tertiary strata in the Lamu Basin, southeast Kenya and

implications for reservoirs for hydrocarbon exploration. *Sedimentary Geology, 96*(1-2), 43-71.

Ombati, D., Githiri, J., K'Orowe, M., & Nyakundi, E. (2022). Delineation of Subsurface Structures Using Gravity Data of the Shallow Offshore, Lamu Basin, Kenya. *International Journal of Geophysics, 2022*.

Ombati, D., John, G., & K'Orowe, M. (2023). Evaluation of Source Rock Potential for Hydrocarbon Generation in Shallow Offshore, Lamu Basin, Kenya. *Journal of Geoscience and Environment Protection, 11*(5), 60-85.

Oladele, S., Salami, R., & Adeyemi, O. B. (2019). Petrophysical and rock physics analyses for characterization of complex sands in deepwater Niger delta, Nigeria. *GeoScience Engineering, 65*(2), 24-35.

Oraby, M. (2021). Evaluation of the fluids saturation in a multi-layered heterogeneous carbonate reservoir using the non-Archie water saturation model. *Journal of Petroleum Science and Engineering, 201*, 108495.

Origin, e. K. l. (2009). *3D Seismic Survey in Lamu Offshore Basin.* Nairobi: NOCK.

Osicki, O., Schenk, O., & Kornpihl, D. (2015). Prospectivity and petroleum systems modelling of the offshore Lamu Basin, Kenya: Implications for an Emerging Hydrocarbon Province. *AAPG Search and Discovery Article, 10700*.

Osukuku, G., Osinowo, O., Sonibare, W., Makhanu, E., Rono, S., & Omar, A. (2022). Assessment of Hydrocarbon Generation Potential and Thermal Maturity of the Deep Offshore Lamu Basin, Kenya. *Energy Geoscience, 4*, 100133.

Othman, I. M., Abdeldayem, A., Soliman, M., & El-Qady, G. (2022). Petrophysical Evaluation Using Well logging of the Alam El-Beuib Reservoirs, Shushan Basin, Northern Western Desert, Egypt. *Delta Journal of Science, 43*(2), 63-80.

Oumarou, S., Mabrouk, D., Tabod, T. C., Marcel, J., Ngos III, S., Essi, J. M. A., & Kamguia, J. (2021). Seismic attributes in reservoir characterization: an overview. *Arabian Journal of Geosciences, 14*(5), 1-15.

Oyeyemi, K. D., & Aizebeokhai, A. P. (2015). Seismic attributes analysis for reservoir characterization; offshore Niger Delta. *Petroleum & Coal, 57*(6), 619-628.

Pepper, A. S., & Corvi, P. J. (1995). Simple kinetic models of petroleum formation. Part I: oil and gas generation from kerogen. *Marine and Petroleum Geology, 12*(3), 291-319.

Peters, C. K., Schenck, O., & Wygrala, B. (2009). Exploration paradigm shift: the dynamic petroleum system. *Swiss Bulletin Angew Geology, 14*(1), 2.

Poelchau, H., Baker, D., Hantschel, T., Horsfield, B., & Wygrala, B. (1997). Basin simulation and the design of the conceptual basin model *Petroleum and basin evolution* (pp. 3-70), New York: Springer.

Rasaq, B., Igwenagu, C. L., & Onifade, Y. (2015). Cross plotting of rock properties for fluid and lithology discrimination using well data in a Niger Delta oil field. *Journal of Applied Sciences and Environmental Management, 19*(3), 539-546.

Reeves, C., Karanja, F., & MacLeod, I. (1987). Geophysical evidence for a failed Jurassic rift and triple junction in Kenya. *Earth and Planetary Science Letters, 81*(2-3), 299-311.

Rider, M. H. (1986). *The geological interpretation of well logs*. United States: Office of Scientific and Technical Information.

Roy, L. E., Hay, P. J., & Martin, R. L. (2008). Revised basis sets for the LANL effective core potentials. *Journal of chemical theory and computation, 4*(7), 1029-1031.

Saibi, H., Nishijima, J., Ehara, S., & Aboud, E. (2006). Integrated gradient interpretation techniques for 2D and 3D gravity data interpretation. *Earth, planets and space, 58*(7), 815-821.

Saleh, A. A., & Castagna, J. P. (2004). Revisiting the Wyllie time average equation in the case of near-spherical pores. *Geophysics, 69*(1), 45-55.

Saputra, A., & Ohara, M. (2016). *Basin and Petroleum System Modelling of Offshore Tanimbar Region: Implications of Structural Development History*. Indonesian:The AAPG/Datapages Combined Publications Database

Sheriff, R. E. (2002). *Encyclopedic Dictionary of Applied Geophysics*: Society of exploration geophysicists. Retrieved from library.seg.org

Sheriff, R. E., & Geldart, L. P. (1995). *Exploration seismology*: Cambridge: Cambridge university press.

Simm, R., Bacon, M., & Bacon, M. (2014). *Seismic Amplitude: An interpreter's handbook*: Cambridge: Cambridge University Press.

Smith, T. M., Sondergeld, C. H., & Rai, C. S. (2003). Gassmann fluid substitutions: A tutorial. *Geophysics, 68*(2), 430-440.

Spector, A., & Grant, F. (1970). Statistical models for interpreting aeromagnetic data. *Geophysics, 35*(2), 293-302.

Stark, T. J. (1991). *Surface slices: Interpretation using surface segments instead of line segments.* Paper presented at the 1991 SEG Annual Meeting.

Sweeney, J. J., & Burnham, A. K. (1990). Evaluation of a simple model of vitrinite reflectance based on chemical kinetics. *AAPG Bulletin, 74*(10), 1559-1570.

Szydlik, T., Helgesen, H. K., Brevik, I., De Prisco, G., Clark, S. A., Leirfall, O. K., . . . & Cogan, M. (2015). Geophysical basin modelling: Methodology and application in the deepwater Gulf of Mexico. *Interpretation, 3*(3), SZ49-SZ58.

Tang, X., Zheng, Y., & Patterson, D. (2007). Processing array acoustic-logging data to image near-borehole geologic structures. *Geophysics, 72*(2), E87-E97.

Telford, W. M., Telford, W., Geldart, L., Sheriff, R. E., & Sheriff, R. (1990). *Applied geophysics* (Vol. 1): Cambridge: Cambridge university press.

Tong, Y. (2016). *Basin and Petroleum System Modelling with Uncertainty Quantification: A Case Study on the Piceance Basin,* Colorado: Stanford University.

Total, K. c. l. (1978). *Simba formation evaluation,* Nairobi: National Oil Corporation of Kenya.

Waples, D. W. (1994). *Maturity Modelling: Thermal Indicators, Hydrocarbon Generation, and Oil Cracking*: Chapter 17: Part IV. Identification and Characterization. The AAPG/Datapages Combined Publications Database

Watts, A. B. (2001). *Isostasy and Flexure of the Lithosphere*: Cambridge: Cambridge University Press.

Welte, D., & Tissot, P. (1984). *Petroleum formation and occurrence,* London: Springer.

Woodside, E. (2007). Formation evaluation log, Pomboo Wildcat: National oil corporation of Kenya, Nairobi: NOCK.

Yilmaz. (2001). *Seismic data analysis: Processing, inversion, and interpretation of seismic data*, Tulsa: Society of exploration geophysicists.

Zongying, Z., Ye, T., Shujun, L., & Wenlong, D. (2013). Hydrocarbon potential in the key basins in the East Coast of Africa. *Petroleum exploration and development, 40*(5), 582-591.

APPENDICES

Appendix I: HC Generation Windows Scheme and Source Rock Evaluation Parameters

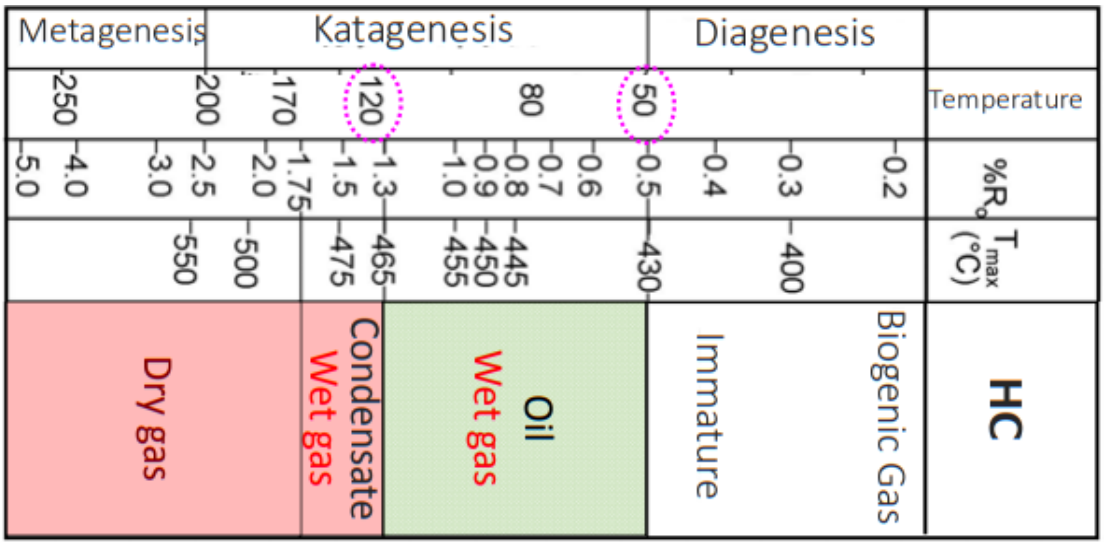

Maturity	R_o (%)	immature	0.5	oil zone	1.3	gas zone
	T_{max} (°C)	immature	430	oil zone	465	gas zone
Kerogen Type	HI (mgHC/g TOC)	III(gas-prone)	200	II/III(oil/gas)	300	II(oil-prone)
Organic richness	TOC (%)	Poor	0.5	Fair	1	Good
	S_2(mgHC/gRock)	Poor	1	Fair	3	Good

Appendix II: Map of Kenya Showing the Drilled Wells (AWEMAC, 2016)

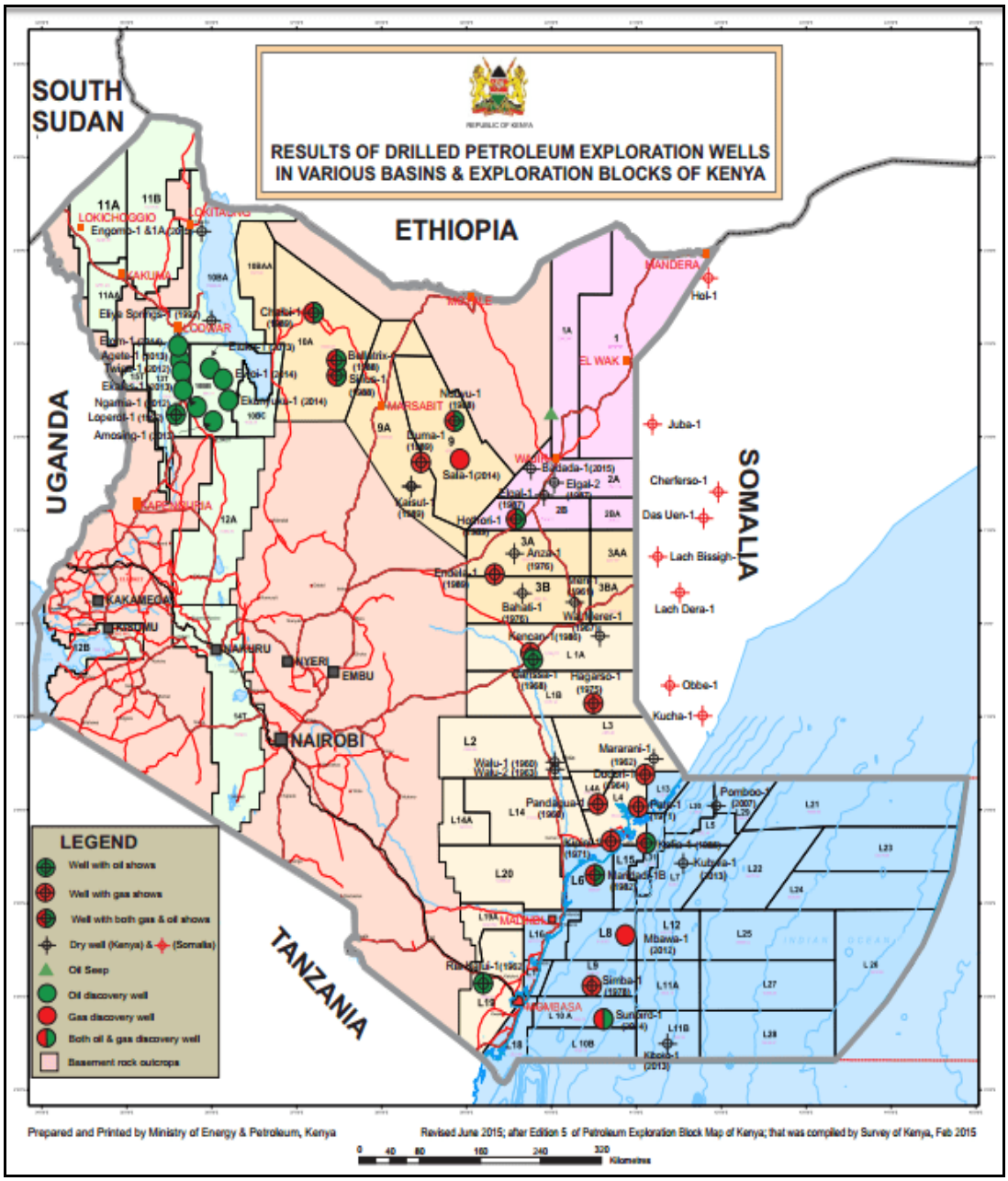

Appendix III: Petroleum System Elements' Properties in the Three Wells

Petroleum system element	Kubwa-1(2013,B 7)			Mbawa-1(2012,B 8)			Pomboo-1(2007,B 5or29)		
	Age (ma)	**Depth (m)**	**Thick (m)**	**Age (ma)**	**Depth (m)**	**Thick (m)**	**Age (ma)**	**Depth (m)**	**Thick (m)**
Source Rock	Upper Cretaceous (Campanian)	5140 - 5410	270	Upper Cretaceous (Turonian)	2383-2610	227	Upper Campanian	4520-4610	90
Reservoir Rock	Upper Cretaceous (Campanian)	4800 - 4990	190	Upper Cretaceous (Campanian)	2050-2250	200	Early Maastrichtian	4040-4210	170
Trap								4767-4791	19
Seal	Upper Cretaceous (Maastrichtian)	4250 - 4440	190	Upper Campanian	2000-2075	75	Upper Maastrichtian	3520-3690	170
	Paleocene	3770 - 3870	100						

Appendix IV: Average TOC Values for Source Rock from Four Offshore Wells

Age	Kubwa-1	Mbawa-1	Pomboo-1	Simba-1	Average
Paleogene	0.51	0.94	1.01	0.78	0.81
Late Cretaceous	0.38	1.13	1.38	1.04	0.98
Early Cretaceous		0.43			
Average	0.45	1.04	1.20	0.91	0.89

Appendix V: Lamu Basin Stratigraphic Intervals Modified from

(BEICIP-FRANLAB, 2020)

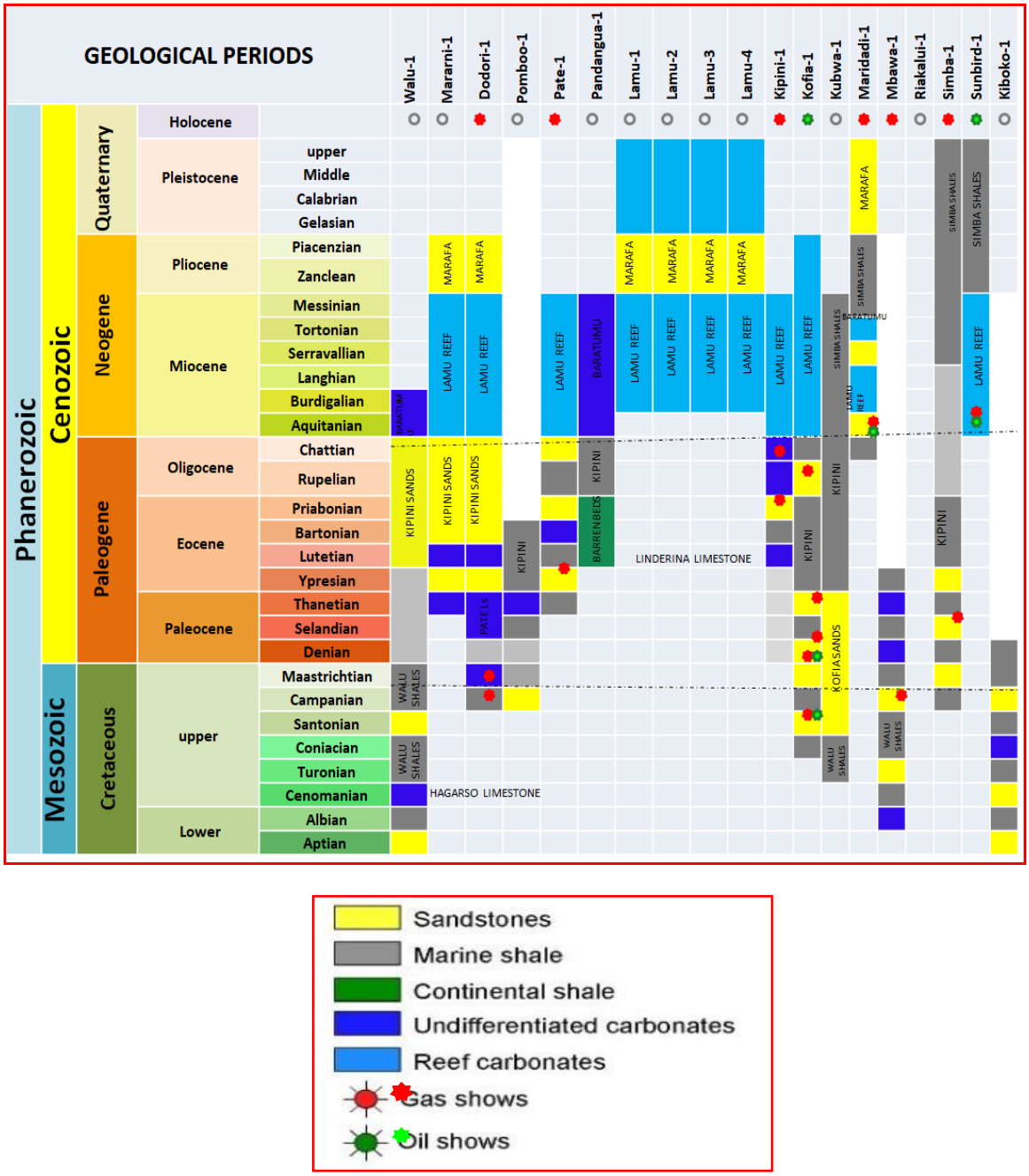

Appendix VI: Mbawa- 1 Geochemical and Rock-Eval Pyrolysis Data Parameters

Depth (m)		Formation	Tmax	Leco	RE			(S1/TOC) *100	S2/S3	HI	OI	PI	Ro,%
Top	Bottom		(°C)	TOC	S1	S2	S3						
1519	1520	Lower Eocene	-1	0.2	0.02	0.01	0.46	10	0.0	5	232	0.67	
1520	1530	Lower Eocene	-1	0.3	0.01	0.01	0.41	3	0.0	3	136	0.50	
1530	1550	Lower Eocene	353	0.7	0.06	0.32	1.94	9	0.2	49	298	0.16	
1550	1580	Upper Paleocene	-1	0.4	0.02	0.04	0.49	5	0.1	10	124	0.33	
1580	1610	Middle Paleocene	-1	0.2	0.02	0.06	0.57	9	0.1	28	263	0.25	
1610	1640	Middle Paleocene	-1	1.2	0.01	0.04	0.59	1	0.1	3	51	0.20	
1640	1670	Lower Paleocene	422	0.8	0.02	0.04	0.54	2	0.1	5	68	0.33	
1670	1700	Upper Maastrichtian	334	0.6	0.01	0.03	0.58	2	0.1	5	101	0.25	
1700	1730	Upper Maastrichtian	422	0.7	0.02	0.07	0.49	3	0.1	10	70	0.22	
1730	1760	Lower Maastrichtian	359	0.8	0.04	0.08	0.47	5	0.2	9	55	0.33	
1760	1790	Lower Maastrichtian	-1	0.6	0.03	0.05	0.47	5	0.1	8	76	0.38	
1790	1820	Upper Campanian	316	0.9	0.04	0.13	0.36	4	0.4	14	40	0.23	
1820	1850	Upper Campanian	364	0.7	0.10	0.11	0.67	14	0.2	15	91	0.48	
1850	1880	Upper Campanian	327	0.9	0.04	0.17	0.27	5	0.6	20	31	0.19	
1880	1910	Upper Campanian	428	1.1	0.05	0.26	0.51	5	0.5	24	47	0.16	
1910	1940	Upper Campanian	435	1.5	0.05	0.42	0.52	3	0.8	28	34	0.11	
1940	1970	Upper Campanian	426	1.5	0.06	0.45	0.5	4	0.9	30	33	0.12	
1970	2000	Upper Campanian	431	1.5	0.05	0.44	0.34	3	1.3	29	23	0.10	
2000	2006	Upper Campanian	427	1.2	0.04	0.3	0.25	3	1.2	25	21	0.12	
2006	2030	Upper Campanian	426	1.0	0.05	0.33	0.34	5	1.0	33	34	0.14	
2030	2060	Upper Campanian	425	0.8	0.04	0.18	0.36	5	0.5	22	44	0.18	
2060	2083	Upper Campanian	361	0.3	0.02	0.07	0.38	6	0.2	20	111	0.22	
2083	2086	Upper Campanian	-1	0.3	0.04	0.07	0.48	12	0.1	22	148	0.37	
2086	2089	Upper Campanian	429	0.8	0.10	0.33	0.7	12	0.5	39	83	0.23	
2089	2092	Upper Campanian	318	0.3	0.07	0.07	0.32	21	0.2	21	94	0.51	
2092	2095	Upper Campanian	304	0.4	0.06	0.16	0.22	14	0.7	36	50	0.27	
2095	2098	Upper Campanian	-1	0.2	0.00	0.01	0.11	-1	0.1	6	61	-1.00	
2098	2101	Upper Campanian	338	0.2	0.05	0.03	0.47	30	0.1	18	281	0.63	
2101	2104	Upper Campanian	361	0.4	0.14	0.29	1.07	37	0.3	75	278	0.33	
2104	2107	Upper Campanian	423	0.5	0.24	0.71	1.05	49	0.7	141	209	0.26	
2107	2110	Upper Campanian	324	0.5	0.06	0.16	0.3	11	0.5	31	58	0.27	
2110	2113	Upper Campanian	-1	0.3	0.06	0.05	0.33	24	0.2	20	129	0.55	
2113	2116	Upper Campanian	422	0.2	0.04	0.07	0.57	19	0.1	32	263	0.37	
2116	2119	Upper Campanian	-1	0.3	0.04	0.04	0.62	14	0.1	14	219	0.50	
2119	2122	Upper Campanian	423	0.3	0.06	0.13	0.72	21	0.2	47	259	0.31	
2122	2125	Upper Campanian	366	0.4	0.09	0.15	0.74	21	0.2	35	172	0.37	
2125	2128	Upper Campanian	346	0.4	0.06	0.12	0.76	15	0.2	30	190	0.34	
2128	2131	Middle Campanian	-1	0.2	0.10	0.04	0.75	54	0.1	22	410	0.71	
2131	2134	Middle Campanian	-1	0.1	0.06	0.04	0.56	79	0.1	53	747	0.60	
2134	2137	Middle Campanian	-1	0.1	0.02	0.01	0.41	29	0.0	14	577	0.67	
2137	2140	Middle Campanian	-1	0.0	0.02	0.01	0.36	69	0.0	34	1241	0.67	
2140	2143	Middle Campanian	-1	0.1	0.01	0.01	0.26	16	0.0	16	413	0.51	
2143	2146	Middle Campanian	-1	0.3	0.02	0.02	0.42	8	0.0	8	167	0.51	
2146	2149	Middle Campanian	-1	0.0	0.02	0.01	0.38	49	0.0	24	927	0.67	
2149	2152	Middle Campanian	-1	0.1	0.00	0.01	0.68	-1	0.0	7	493	-1.00	
2152	2155	Lower Campanian	366	0.2	0.18	0.06	1.12	111	0.1	36	675	0.75	
2155	2158	Lower Campanian	-1	0.1	0.10	0.04	0.84	99	0.0	40	848	0.71	
2158	2161	Lower Campanian	338	0.4	0.13	0.1	0.89	37	0.1	29	254	0.56	
2161	2164	Lower Campanian	428	0.6	0.10	0.24	0.63	18	0.4	42	109	0.30	
2164	2167	Lower Campanian	422	0.7	0.17	0.5	1.23	25	0.4	74	182	0.25	
2167	2173	Lower Campanian	422	0.3	0.10	0.15	0.74	40	0.2	58	287	0.41	
2173	2179	Lower Campanian	320	0.3	0.09	0.1	0.73	30	0.1	32	235	0.48	
2179	2185	Lower Campanian	-1	0.2	0.07	0.05	0.84	32	0.1	23	378	0.59	
2185	2191	Lower Campanian	426	0.6	0.09	0.18	0.58	16	0.3	32	104	0.33	
2191	2197	Lower Campanian	314	0.1	0.07	0.04	0.67	100	0.1	57	957	0.64	

2197	2203	Lower Campanian	353	0.3	0.13	0.13	0.83	43	0.2	42	269	0.50	
2203	2227	Upper Santonian	-1	0.1	0.00	0.02	0.46	-1	0.0	19	434	-1.00	
2227	2260	Upper Santonian	-1	0.2	0.04	0.04	0.56	23	0.1	23	316	0.50	
2260	2290	Middle Santonian	407	0.1	0.05	0.04	0.68	35	0.1	28	476	0.56	
2290	2323	Lower Santonian	-1	0.2	0.05	0.04	0.64	31	0.1	25	398	0.56	
2323	2353	Lower Santonian	-1	0.2	0.06	0.05	0.79	31	0.1	26	409	0.54	
2353	2383	Upper Turonian	-1	0.2	0.07	0.11	0.64	40	0.2	62	364	0.39	
2383	2413	Middle Turonian	318	0.1	0.05	0.04	0.55	41	0.1	32	444	0.56	
2413	2443	Middle Turonian	315	0.2	0.05	0.04	0.58	33	0.1	26	379	0.56	
2443	2475	Middle Turonian	422	0.2	0.07	0.07	0.68	42	0.1	41	400	0.51	
2475	2505	Middle Turonian	345	0.2	0.08	0.06	0.68	33	0.1	25	282	0.57	
2505	2535	Lower Turonian	-1	0.2	0.07	0.04	0.78	33	0.1	18	358	0.64	
2535	2553	Lower Turonian	-1	0.3	0.06	0.07	0.58	20	0.1	22	184	0.47	
2553	2580	Lower Turonian	-1	0.4	0.09	0.07	0.58	21	0.1	17	137	0.56	
2580	2610	Lower Turonian	-1	0.5	0.12	0.07	0.54	25	0.1	15	113	0.63	
2610	2640	Upper Cenomanian	-1	0.5	0.18	0.12	0.59	37	0.2	24	118	0.61	
2640	2670	Upper Cenomanian	-1	0.3	0.07	0.07	0.52	28	0.1	27	202	0.50	
2670	2700	Middle Cenomanian	-1	0.4	0.10	0.07	0.67	26	0.1	18	171	0.59	
2700	2730	Middle Cenomanian	-1	0.2	0.04	0.02	0.57	25	0.0	12	341	0.67	
2730	2760	Middle Cenomanian	-1	0.2	0.13	0.19	0.66	64	0.3	93	324	0.41	
2760	2790	Middle Cenomanian	-1	0.2	0.09	0.14	0.72	52	0.2	81	419	0.39	
2790	2820	Middle Cenomanian	423	0.2	0.08	0.16	0.66	44	0.2	86	357	0.34	
2820	2850	Middle Cenomanian	311	0.3	0.11	0.21	0.72	42	0.3	80	274	0.34	
2850	2880	Upper Albian	422	0.3	0.09	0.13	1.03	26	0.1	38	299	0.41	
2880	2910	Upper Albian	351	0.4	0.12	0.16	1.27	27	0.1	36	286	0.43	
2910	2940	Upper Albian	413	0.3	0.12	0.24	0.95	40	0.3	80	317	0.34	
2940	2970	Upper Albian	-1	0.3	0.10	0.15	0.76	31	0.2	46	231	0.41	
2970	3000	Upper Albian	-1	0.2	0.11	0.16	0.72	48	0.2	70	317	0.41	
3000	3030	Upper Albian	355	0.3	0.31	0.36	0.46	95	0.8	112	143	0.46	
3030	3060	Upper Albian	-1	0.2	0.13	0.15	0.68	53	0.2	62	280	0.46	
3060	3090	Middle Albian	-1	0.3	0.13	0.11	0.7	45	0.2	38	241	0.54	
3090	3120	Middle Albian	-1	0.2	0.10	0.11	0.67	41	0.2	45	272	0.48	
3120	3150	Middle Albian	-1	0.2	0.05	0.06	0.86	29	0.1	34	494	0.45	

Appendix VII: Kubwa-1 Geochemical and Rock-Eval Pyrolysis Data Parameters

Depth(m)	Formation	Tmax(0C)	S1	S2	S3	S1+S2	S2/S3	PI	TOC	HI	OI	Ro
3330	Miocene	396	0.26	1.01	2.4	1.27	0.4	0.20	0.7	140	333	0.5
3340	Miocene	389	0.12	0.71	1.74	0.83	0.4	0.14	0.8	92	226	0.5
3770	Paleocene	375	0.18	0.77	0.64	0.95	1.2	0.19	1	81	67	0.5
4000	Paleocene	331	0.56	0.72	0.47	1.28	1.5	0.44	1	76	49	0.6
4020	Paleocene		0.51	0.54	0.41	1.05	1.3	0.49	0.9	59	45	0.6
4300	Maastrichtian		0.44	0.59	0.37	1.03	1.6	0.43	0.8	73	46	0.6
4350	Maastrichtian	419	0.54	0.95	1.01	1.49	0.9	0.36	1.1	87	93	0.7
4354	Maastrichtian	437	0.13	0.74	0.33	0.87	2.2	0.15	1.1	66	29	0.7
4400	Maastrichtian	418	0.29	0.66	0.77	0.95	0.9	0.31	1.3	52	61	0.7
4790	Maastrichtian	428	0.17	0.68	0.35	0.85	1.9	0.20	0.8	88	45	0.7

Appendix VIII: Pomboo-1 Geochemical and Rock-Eval pyrolysis data parameters

Depth (m)	Formation	Tmax	Leco	RE			S1+S2	1/TOC)*10	S2/S3	HI	OI	PI	Ro,%
		(°C)	TOC	S1	S2	S3							
2950	Middle Eocene	441	0.82	1.47	3.93	2.91	5.4	1.79	1.35	479	355	0.27	
3040	Middle-early Eocene	419	0.89	1.06	3.17	2.23	4.23	1.19	1.42	356	251	0.25	
3140	Middle-early Eocene	367	0.94	2.39	3.47	2.16	5.86	2.54	1.61	369	230	0.41	
3170	Early Eocene	360	1.07	3.92	3.64	1.93	7.56	3.66	1.89	340	180	0.52	
3270	Late Paleocene	426	1.3	3.16	4.42	2.22	7.58	2.43	1.99	340	171	0.42	
3340	Late Maastrichtian	427	2.02	9.16	8.08	2.16	17.24	4.53	3.74	400	107	0.53	
3420	Late Maastrichtian	388	1.13	3.87	2.76	1.76	6.63	3.42	1.57	244	156	0.58	
3480	Late Maastrichtian	428	1.47	5.29	4.88	1.62	10.17	3.60	3.01	332	110	0.52	
3530	Late Maastrichtian	430	1.32	3.23	5.22	1.4	8.45	2.45	3.73	395	106	0.38	
3650	Late Maastrichtian	426	1.13	1.4	4.84	1.66	6.24	1.24	2.92	428	147	0.22	
3690	Late Maastrichtian	426	1.15	2.75	4.97	1.59	7.72	2.39	3.13	432	138	0.36	
3830	Late Maastrichtian	428	1.3	2.8	5.44	1.37	8.24	2.15	3.97	418	105	0.34	
3900	Early Maastrichtian	425	1.88	6.28	6.16	1.95	12.44	3.34	3.16	328	104	0.50	
3990	Early Maastrichtian	429	1.6	4.65	7.02	1.82	11.67	2.91	3.86	439	114	0.40	
4040	Early Maastrichtian	430	0.92	1.52	2.72	1.7	4.24	1.65	1.60	296	185	0.36	
4140	Early Maastrichtian	431	1.44	3.69	6.08	2.04	9.77	2.56	2.98	422	142	0.38	
4190	Early Maastrichtian	426	1.53	6.04	5.32	1.59	11.36	3.95	3.35	348	104	0.53	0.58
4210	Early Maastrichtian	429	1.23	1.98	4.44	1.6	6.42	1.61	2.78	361	130	0.31	
4230	Early Maastrichtian	428	1.45	5.58	6.78	1.94	12.36	3.85	3.49	468	134	0.45	
4270	Early Maastrichtian	425	1.69	7.64	6.16	1.6	13.8	4.52	3.85	364	95	0.55	
4300	Early Maastrichtian	424	1.33	4.44	4.23	1.92	8.67	3.34	2.20	318	144	0.51	
4320	Early Maastrichtian	428	1.43	5.16	4.72	1.77	9.88	3.61	2.67	330	124	0.52	0.6
4390	Early Maastrichtian	429	1.64	5.7	6.08	1.95	11.78	3.48	3.12	371	119	0.48	
4420	Early Maastrichtian	430	1.74	4.9	7.22	2.18	12.12	2.82	3.31	415	125	0.40	
4430	Early Maastrichtian	419	1.65	6.62	5	1.85	11.62	4.01	2.70	303	112	0.57	
4470	Early Maastrichtian	426	1.66	5.8	6.26	2.05	12.06	3.49	3.05	377	123	0.48	
4490	Early Maastrichtian	424	0.99	1.31	4.04	1.95	5.35	1.32	2.07	408	197	0.24	0.61
4520	Late Campanian	426	1.02	1	4.22	1.91	5.22	0.98	2.21	414	187	0.19	
4540	Late Campanian	422	0.84	1.72	4.28	1.8	6	2.05	2.38	510	214	0.29	
4590	Late Campanian	427	1.02	1.17	5.16	1.95	6.33	1.15	2.65	506	191	0.18	0.68
4610	Late Campanian	433	1.04	1.21	6.32	2.64	7.53	1.16	2.39	608	254	0.16	0.62

Notes:

"-1" – not measured or invalid value
TOC - Total Organic Carbon, wt. %
S1 - volatile hydrocarbon (HC) content, mg HC/ g rock
S2 - remaining HC generative potential, mg HC/ g rock
S3 - carbon dioxide content, mg CO_2/ g rock

* - Sample contaminated
** - low S2, Tmax is unreliable
Meas. %Ro - measured vitrinite reflectance
HI - Hydrogen index = S2 x 100 / TOC, mg HC/ g TOC
OI - Oxygen Index = S3 x 100 / TOC, mg CO_2/ g TOC
PI - Production Index = S1 / (S1+S2)

Pyrogram:
f - flat S2 peak
n - normal
ltS2sh - low temperature S2 shoulder
ltS2p - low temperature S2 peak
htS2p - high temperature S2 peak

LECO - TOC on LECO Instrument
SRA - Programmed Pyrolysis on SRA instrument
RE - Programmed Pyrolysis on Rock-Eval instrument
EXT - Extracted Rock
NOPR - Normal Preparation

Appendix IX: Mbawa-1 Check Shot Data

Stack Number	MD (m)	TVD (m)	MT (s)	One-way VT(s)	Two-way VT(s)	Interval V(m/s)	Average V(m/s)	RMS V(m/s)
	0	0	0	0	0			
						1507.8		
18	956.1	931.1	0.6152	0.6175	1.235		1507.8	1507.8
						1621.9		
17	1010.4	985.4	0.6486	0.651	1.302		1513.7	1513.9
						1628.7		
17	1025.6	1000.6	0.658	0.6604	1.3207		1515.3	1515.6
						1560.3		
17	1040.9	1015.9	0.6677	0.6701	1.3402		1516	1516.2
						1613.3		
17	1056.1	1031.1	0.6771	0.6796	1.3591		1517.3	1517.6
						1740		
16	1110.4	1085.4	0.7083	0.7108	1.4215		1527.1	1528.1
						1727.5		
16	1125.6	1100.6	0.7171	0.7196	1.4392		1529.5	1530.7
						2271.4		
16	1140.9	1115.9	0.7238	0.7263	1.4526		1536.4	1539.1
						1666.8		
16	1156.1	1131.1	0.7329	0.7354	1.4709		1538	1540.8
						1673.3		
15	1210.4	1185.4	0.7653	0.7679	1.5357		1543.7	1546.6
						1980.9		
15	1225.6	1200.6	0.773	0.7756	1.5511		1548.1	1551.5
						1734.8		
15	1240.9	1215.9	0.7818	0.7843	1.5687		1550.2	1553.7
						1669.6		
15	1256.1	1231.1	0.7909	0.7935	1.5869		1551.5	1555.1
						1951.8		
14	1310.4	1285.4	0.8186	0.8213	1.6426		1565.1	1570.2
						1723		
14	1325.7	1300.7	0.8275	0.8301	1.6603		1566.8	1571.9
						1919.9		
14	1340.9	1315.9	0.8354	0.8381	1.6762		1570.1	1575.5
						1714.9		
14	1356.1	1331.1	0.8443	0.847	1.6939		1571.6	1577.1
						2001.2		
13	1410.4	1385.3	0.8713	0.8741	1.7481		1585	1591.9
						2085.2		
13	1425.6	1400.6	0.8786	0.8814	1.7627		1589.1	1596.6

13	1440.9	1415.8	0.8863	0.8891	1.7782	1974.8	1592.4	1600.3
						2029.2		
13	1456.1	1431.1	0.8938	0.8966	1.7932		1596.1	1604.3
						1976.4		
11	1510.4	1485.3	0.9213	0.9241	1.8481		1607.4	1616.6
						1623.9		
11	1525.6	1500.6	0.9306	0.9334	1.8669		1607.6	1616.7
						2030.8		
11	1540.9	1515.8	0.9381	0.9409	1.8819		1610.9	1620.4
						1963.3		
11	1556.1	1531	0.9459	0.9487	1.8974		1613.8	1623.5
						1943.7		
10	1610.4	1585.3	0.9738	0.9766	1.9532		1623.3	1633.6
						2327.8		
10	1625.6	1600.6	0.9803	0.9832	1.9663		1628	1639.2
						2206.3		
10	1640.9	1615.8	0.9872	0.9901	1.9801		1632	1643.8
						2100.8		
10	1656.1	1631	0.9945	0.9973	1.9947		1635.4	1647.6
						2097.3		
9	1710.4	1685.3	1.0203	1.0232	2.0464		1647.1	1660.4
						2080.5		
9	1725.6	1700.5	1.0276	1.0305	2.0611		1650.2	1663.8
						2030.4		
9	1740.9	1715.8	1.0351	1.038	2.0761		1652.9	1666.7
						2061.1		
9	1756.1	1731	1.0425	1.0454	2.0908		1655.8	1669.9
						2233.5		
8	1771.4	1746.3	1.0493	1.0523	2.1045		1659.5	1674.1
						2153.9		
8	1786.6	1761.5	1.0564	1.0593	2.1187		1662.8	1677.8
						2045.4		
8	1801.9	1776.8	1.0639	1.0668	2.1336		1665.5	1680.6
						2025.3		
8	1817.1	1792	1.0714	1.0743	2.1486		1668	1683.3
						1968.6		
7	1832.4	1807.3	1.0791	1.0821	2.1642		1670.2	1685.5
						2087.6		
7	1847.6	1822.5	1.0864	1.0894	2.1788		1673	1688.5
						2082.5		
7	1862.9	1837.8	1.0937	1.0967	2.1934		1675.7	1691.5
						2069.8		
7	1878.1	1853	1.1011	1.1041	2.2081		1678.4	1694.3
						2141.1		

6	1893.3	1868.2	1.1082	1.1112	2.2223		1681.3	1697.5
						2127.7		
6	1908.6	1883.4	1.1153	1.1183	2.2366		1684.2	1700.6
						2094		
6	1923.8	1898.7	1.1226	1.1256	2.2512		1686.8	1703.4
						2239.1		
6	1939.1	1913.9	1.1294	1.1324	2.2648		1690.1	1707.1
						2210.1		
5	1954.3	1929.2	1.1363	1.1393	2.2786		1693.3	1710.6
						2127		
5	1969.6	1944.4	1.1435	1.1465	2.2929		1696	1713.6
						1997.8		
5	1984.8	1959.6	1.1511	1.1541	2.3082		1698	1715.6
						2231.3		
5	2000	1974.9	1.1579	1.1609	2.3218		1701.1	1719.1

Appendix X: Stratigraphic Information for Kubwa-1, Mbawa-1, and Pomboo-1 Wells

Kubwa-1

Surface/Horizon	Ma	Lithology	Measured Depth (m)	Petroleum System Element
Seabed	0		2438	Overburden
Top Miocene	6	Claystone	2738	Overburden
Top Oligocene	23	Claystone	3454	Overburden
Top Paleocene	53	Calcareous claystone	3832	Seal
Top Maastrichtian	65	Claystone Dolomite Limestone	4429	Seal
Top Campanian	70	sandstone	4971	Reservoir
Top Santonian	78	Calcareous shale	5705	Source

Mbawa-1

Surface/Horizon	Ma	Lithology	Measured Depth (m)	Petroleum System Element
Seabed	0		883	
Top Miocene	10	Simba shales	1123	Overburden
Tertiary Marker(middle Miocene)	15	Lamu reefs	1355	Overburden
Top Oligocene	25	Calcareous Shale	1508	Overburden
Top Paleocene	55	Unconformity	1522	Seal
Base Paleocene	64	Calcareous Sand	2120	Reservoir
Upper Cretaceous (Campanian)	65	Hargaso carbonates	2200	Underburden
Top Cretaceous (Albian)	105	Turbidite sandstones	2300	Reservoir
Base Cretaceous	120	Walu Shale	2940	Source

Pomboo-1

Surface/Horizon	Ma	Lithology	Measured Depth (m)	Petroleum System Element
Seabed			2219.4	Overburden
Base Miocene	23	Claystone	2831.6	Overburden
Base Eocene	53	Calcareous Claystone	3013.2	Overburden
Base Paleocene	65	Calcareous Claystone	3239.9	Seal
Base Maastrichtian	70	Carbonate	3879.6	Reservoir
Base Campanian	78	Sandstone	4788.8	Reservoir
Aptian	120	Shale	4887.4	Source

Appendix XI: Lithologies